

# VIBRATIONAL AND ELECTRONIC SPECTRA OF CERTAIN POLYATOMIC MOLECULES

A Thesis Submitted  
in partial Fulfilment of the Requirements  
for the Degree of  
DOCTOR OF PHILOSOPHY

By  
JITENDRA SINGH PARIHAR

to the

DEPARTMENT OF PHYSICS  
INDIAN INSTITUTE OF TECHNOLOGY KANPUR  
DECEMBER 1975

PHY-1975-D-PAR-VIB

CENTRAL LIBRARY

Acc. No. **A 46651**

24 JUL 1976



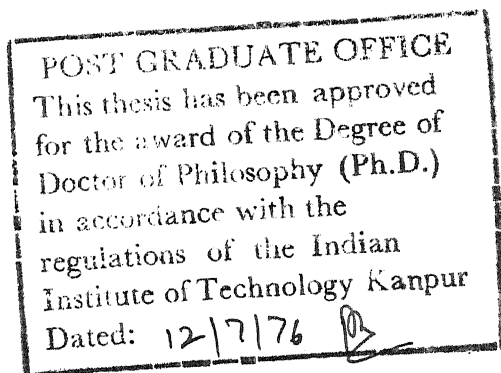
DEDICATED TO MY FATHER  
LAL VIJAI BAHADUR SINGH

CERTIFICATE

Certified that the work in this dissertation entitled  
"VIBRATIONAL AND ELECTRONIC SPECTRA OF CERTAIN POLYATOMIC  
MOLECULES" by Jitendra Singh Parihar has been carried out  
under my supervision and that this work has not been submitted  
elsewhere for any degree.

*H.D. Bist*  
12/12/75

H.D. Bist  
Assistant Professor  
Physics Department  
Indian Institute of Technology  
KANPUR - 16 (India)



### STATEMENT

I hereby declare that the work presented in this thesis is the result of investigations carried out by me in the Department of Physics, Indian Institute of Technology, Kanpur, India, under the supervision of Dr H.D. Bist.

In keeping with the general practice of reporting scientific observations, due acknowledgement has been made wherever the work described is based on the findings of other investigators.

J.S. Parihar  
(J.S. PARIHAR)

### ACKNOWLEDGEMENT

I would like to express my deep sense of gratitude and grateful regards to Dr H.D. Bist for inspiring and unfailing guidance during the course of this work.

I am highly indebted to Professor P. Venkateswarlu for his encouragement to carry out research under Quality Improvement Programme of Government of India. I am thankful to Professor T.M. Srinivasan for his interest in the progress of this project, and to Professor D. Ramachandra Rao for his encouragement.

I am also grateful to Dr V.N. Sarin for his unfailing interest in the successful completion of this thesis.

I gratefully thank Professor J.C.D. Brand (presently at London, Canada) for initiating the problem on Pyridine N-oxide and helpful communications.

Thanks are due to Drs (Mrs) S.A. Kuchadkar, Y.S. Jain, K.N.S. Rao and G.S. Pandey, Department of Chemistry, Govt. College of Engineering and Technology, Raipur (M.P.) and Messrs B.K. Srivastava, R.S. Saraswat, V.M. Malhotra, Nirbhaya Singh, R.K. Jain, S.S. Nigam and Miss Sunita Khandelwal for their help at various stages of this work.

Thanks are due to Education Department, Govt. of Madhya Pradesh for sponsoring me under Quality Improvement Programme and also to Principals Shri R.A. Deshpandey, Govt. College of Engineering and Technology, Raipur (M.P.) and Dr N.H. Harkare, Govt. Engineering College, Bilaspur (M.P.) for their interest in the progress of this work.

I am greatly indebted to my elder brother Shri Govind Pratap Singh for his profound affection and encouragement in my path of progress. I would like to express my most intimate thanks to my wife Smt Kamlesh Parihar for her understanding and son Dharmendra, daughters Rekha and Bindu for their love and affection which they kept intact during my busy time.

Finally, I thank Shri S L Rathore for typing the manuscript and to Shri H K Panda and Shri Lalloo Singh for cyclostyling the same.

JITENDRA SINGH PARIHAR

## CONTENTS

	Page
SYNOPSIS	i
LIST OF PUBLICATIONS	vi

### CHAPTER I

INTRODUCTION	1
--------------	---

1.0	GENERAL	1
1.1	ENERGY LEVELS OF A MOLECULE	3
1.2	ROTATIONAL ENERGY LEVELS	3
1.21	Asymmetric Top Molecules	4
1.22	Linear and Spherical Top Molecules	6
1.23	Symmetric Top Molecules	6
1.3	VIBRATIONAL ENERGY LEVELS	6
1.31	Diatomic Approximation	8
1.32	The Electric Dipolemoment	9
1.33	Evaluation of Anharmonicity Constants	9
1.34	Infrared Vibrational Spectra	10
1.35	Infrared Band Intensity	11
1.36	Spectra in Different Physical States	13
1.37	Raman Vibrational Spectra	16
1.38	Raman Band Intensity	18
1.39	Depolarization Ratios	19
1.4	VIBRATIONAL ROTATIONAL ENERGY LEVELS	20
1.41	Infrared Band Contours	21
1.42	The Band Types	22

## CONTENTS

	Page
1.43 The Molecular Parameters	22
1.44 The Symmetric Top Molecules	23
1.45 Asymmetric Top Molecules	26
1.46 Hybrid Bands	28
1.5 NORMAL COORDINATE ANALYSIS	29
1.51 Aim of the Normal Coordinate Analysis	29
1.52 Calculation Procedure	30
1.6 ELECTRONIC SPECTRA	34
1.61 Intensity of Electronic Transition	34
1.7 FERMION RESONANCE	35
1.8 THERMODYNAMIC PROPERTIES	37
1.81 Mathematical Relations	38
1.82 Entropy and Free Energy of Mixing	41
1.83 Heat, Free Energy and Equilibrium constant of formation	41
1.9 NUMBERING OF NORMAL MODES	41
REFERENCES	43
<u>CHAPTER II</u> EXPERIMENTAL DETAILS	49
2.1 PURIFICATION OF SAMPLES	49
2.11 Sublimation Apparatus	49
2.12 Vacuum System	50
2.2 SAMPLE HANDLING	51
2.21 Vapour Phase Filling of the Sample in the Multiple Reflection Cell	51

## CONTENTS

	Page
2.22 Adjustment of Path-length of Multiple Reflection Cell	52
2.23 Vapour Phase Filling of the Sample in UV Gas Cell	52
2.24 Liquid Phase Sample Preparation	53
2.25 Solid Phase Sample in Low Temperature Cell	54
2.26 Quartz Capillary and Pyrex Tube for Raman Spectra	54
2.3 RECORDING OF SPECTRA	55
2.31 Infrared Spectrophotometer	55
2.32 Raman Studies	57
2.33 Ultra Violet Spectrograph	58
2.4 GRANT COMPARATOR DENSITOMETER	59
 <u>CHAPTER III</u> THE 341 nm BAND SYSTEM OF PYRIDINE N-OXIDE	 71
ABSTRACT	71
3.0 INTRODUCTION	73
3.1 EXPERIMENTAL	75
3.2 SELECTION RULES AND NOTATION FOR PLANAR MODES OF PyO	77
3.21 Observed $\underline{B}_e$ and $\underline{A}_e$ Type Contours	77
3.22 Vibronic Analysis	79
3.23 The Shift of O-O Band	79
3.24 The $\underline{a}_1$ Modes in ${}^1\underline{A}_1$ State	80
3.25 The $\underline{a}_1$ Modes in ${}^1\underline{B}_2$ State	84
3.26 The $\underline{b}_2$ Modes in ${}^1\underline{A}_1$ and ${}^1\underline{B}_2$ States	85



## CONTENTS

	Page
3.27 Differences with Analogous Modes of Phenol and Chlorobenzene	86
3.28 Intensity Distribution and Principal Progressions	87
3.3 SELECTION RULES AND NOTATIONS FOR NON-PLANAR MODES OF PyO	88
3.31 Electronic Sequences and Cross Sequences	88
3.32 The $\underline{b}_1$ Modes in ${}^1\underline{A}_1$ and ${}^1\underline{B}_2$ States	89
3.33 The $\underline{a}_2$ Modes in ${}^1\underline{A}_1$ and ${}^1\underline{B}_2$ States	91
3.34 Differences with Analogous Modes of Phenol and Chlorobenzene	92
3.4 INFRARED SPECTRA OF PYRIDINE N-OXIDE IN SOLUTIONS	94
3.5 INTENSITIES OF INFRARED BANDS	94
3.6 LOW TEMPERATURE STUDIES	98
3.7 LATTICE MODES OF PYRIDINE N-OXIDE	100
3.8 MOLECULAR GEOMETRY	101
3.81 Theoretical Calculation of Fundamental Modes	102
3.9 CONCLUSION	103
REFERENCES	106
<u>CHAPTER IV</u> VIBRATIONAL SPECTRA OF $\alpha$ -, $\beta$ -, AND $\gamma$ -PICOLINES	176
4.0 ABSTRACT	176
4.0 INTRODUCTION	177
4.1 EXPERIMENTAL	178
4.2 SELECTION RULES AND NOTATIONS	179
4.3 VIBRONIC ANALYSIS	181

## CONTENTS

	Page
4.31 The Infrared Band Contours	182
4.4 FUNDAMENTAL VIBRATIONS	184
4.41 The $\underline{a}_1$ Fundamental Modes	184
4.42 The $\underline{b}_2$ Fundamental Modes	186
4.43 The $\underline{a}_1$ and $\underline{b}_2$ Modes from Electronic Spectral Studies	188
4.44 The $\underline{b}_1$ Fundamental Modes	189
4.45 The $\underline{a}_2$ Fundamental Modes	190
4.5 SOLID PHASE INFRARED SPECTRA	190
4.6 MOLECULAR GEOMETRY	191
4.7 THEORETICAL CALCULATION OF FUNDAMENTAL MODES	192
REFERENCES	194
 <u>CHAPTER V</u> VIBRATIONAL SPECTRA OF PARAFIUFOROPHENOL AND PARAFIUFORO BENZALDEHYDE	 236
ABSTRACT	236
5.0 INTRODUCTION	237
5.1 EXPERIMENTAL	238
5.2 SELECTION RULES AND NOTATIONS	239
5.3 VIBRONIC ANALYSIS	240
5.31 The Infrared Band Contours	240
5.4 FUNDAMENTAL VIBRATIONS	241
5.41 The $\underline{a}_1$ Fundamental Modes	242
5.42 The $\underline{b}_2$ Fundamental Modes	243
5.43 Hybrid Nature of $\underline{b}_2$ Bands	244

## CONTENTS

	Page
5.44      The $\underline{b}_1$ Fundamental Modes	244
5.45      The $\underline{a}_2$ Fundamental Modes	245
5.5        INFRARED SPECTRA OF PARAFLUOROPHENOL IN SOLUTIONS	246
5.6        LOW TEMPERATURE STUDIES	246
5.7        MOLECULAR GEOMETRY	247
5.8        THEORETICAL CALCULATION OF FUNDAMENTAL MODES	248
REFERENCES	249
 CHAPTER VI      THE IDEAL GAS THERMODYNAMIC PROPERTIES OF CERTAIN POLYATOMIC MOLECULES	 278
ABSTRACT	278
6.0        INTRODUCTION	279
6.1        PYRIDINE N-OXIDE	280
6.2 $\alpha$ -, $\beta$ -, AND $\gamma$ -PICOLINES	280
6.3        PARAFLUOROPHENOL AND PARAFLUOROBENZALDEHYDE	281
REFERENCES	282

## SYNOPSIS

Recent developments, both in the theoretical and the experimental aspects of spectroscopic techniques have provided several magnificent tools for the investigation of the energy structure of large polyatomic molecules. Accurate information about the rotational energy levels is deduced on the basis of the microwave and the far infrared (FIR) studies, the rotational Raman scattering experiments, the vibration-rotation spectra and the gyrovibronic studies in visible and ultraviolet regions both from the absorption and the emission techniques. For the energy structure of the electronically excited states, electronic absorption and emission (including fluorescence and phosphorescence) spectra are the only source of information. The recent advances in Raman spectroscopy using the laser sources (having the characteristics of coherence, high directionality, reliability, intense brightness, monochromaticity, modulation and polarization CHIRIMMP) have a major role in revealing the complex structure and dynamical behaviour of polyatomic molecules. Similarly the routine use of infrared spectroscopy with multiple reflection cells (which could be operated under low pressures) have helped in understanding the isolated polyatomic molecules in vapour phase.

In the present study, high resolution electronic spectra, the vapour phase infrared contours and laser-excited Raman spectra of Pyridine N-oxide,  $\alpha$ -,  $\beta$ -,  $\gamma$ -picolines, para-fluorophenol and para-fluorobenzaldehyde have been studied with a view to establish the fundamental normal modes of the molecules in isolated state. The theoretical (normal coordinate) analysis of vibrational data of the molecules provides a set of force constants as a representative of the potential energy for the system. The vibrational data have been used in ascertaining the degree of transferability of force-field and coupling between various modes. The thermodynamic constants and other observable properties derived from the spectroscopic data provide a feedback mechanism to test the reliability of vibrational assignments. Earlier available vibrational data for these molecules have been re-examined and suitable modifications are suggested on the basis of present more precise data. The thesis consists of six chapters. Related figures, tables, references and appendices have been inserted at the end of each chapter.

Various aspects of infrared, Raman and ultraviolet spectroscopy which are of relevance to the present investigations have been briefly reviewed in Chapter I.

Chapter II contains details of the experimental set-up and techniques used. This includes the description of the

purification of samples including the sublimation and fractional distillation techniques, the vacuum system used during vapour phase and low temperature studies, the different sample handling methods for vapour liquid and solid phase studies (including Hornig-type cell for studies at liquid nitrogen temperature and multiple reflection cell used for vapour phase IR studies); the PE 521 spectrophotometer; the methodology for laser Raman spectroscopy of samples along with the description of the Cary-82 and Spex-1400 spectrophotometers and the 3.4 meter Ebert spectrograph and Grant automatic comparator densitometer.

The vapour phase infrared and electronic band contours of pyridine N-oxide, its far- and ordinary infrared studies in solid and solution phases, laser-excited Raman studies in solid phase to obtain the reliable vibrational assignments form the basis of Chapter III. The  $A_e$ -type contours in high resolution electronic spectra have been identified for the first time. Accurate vibrational data for all the fundamental modes in both the ground ( ${}^1A_1$ ) and the first electronically excited singlet state ( ${}^1B_2$ ) of PyO, are based primarily on the identification of the  $A_e$  and  $B_e$ -type contours and observed sequences and combination bands in the high resolution electronic spectra. Other studies and comparison with other isovalence electronic molecules are

used for comparison purposes for the ground state. The main effort has been to establish all the fundamental modes for the  $^1\text{A}_1$  and  $^1\text{B}_2$  states. The vapour phase forbidden transition of PyO have been correlated with the solid phase spectra.

Special features of the IR band contours such as PR separation and relative intensity of Q-branch with respect to that of the whole band have been calculated and compared with the observed values in PyO. In most of the cases the agreement is good. The vibrational frequencies of the fundamental modes have further been used to obtain the most suited force field on the basis of normal coordinate analysis. From the observed overtones in the infrared, Raman and electronic spectra, the anharmonicities associated with the fundamental modes have been calculated. The ground and the excited state geometries of the compound have been discussed and it is shown that the excited state geometry is measurably different from that in the ground state. The information obtained both from rotational analysis and vibrational data is correlated qualitatively.

In Chapter IV, the assignments for  $\alpha$ -,  $\beta$ - and  $\gamma$ -picolines have been suggested on the basis of well resolved vapour phase infrared band contours, infrared spectra in liquid (at different thicknesses) and solid (at RT and INT) phases. The solid phase infrared spectra of  $\alpha$ -,  $\beta$ - and  $\gamma$ -picolines

have been studied at liquid nitrogen temperature. The observed changes in peak positions and intensities of infrared bands on going from vapour to liquid and then to solid phase at liquid nitrogen temperature have been discussed, as also splittings observed (for the first time) in the solid phase at low temperature. The anharmonicities associated with the fundamental bands have been calculated based on the observed overtones in the infrared spectra. The ground state geometry has been proposed for  $\alpha$ -,  $\beta$ - and  $\gamma$ -picolines and rotational constants for  $\alpha$ - and  $\beta$ -picolines have been theoretically calculated as the microwave data for these molecules are not available. The force constants and potential energy distribution between the different internal coordinates have been proposed for the best fit of the computed and observed frequencies based on normal coordinate analysis.

A similar analysis of infrared spectra in all phases of para-fluorophenol and para-fluorobenzaldehyde has been discussed in Chapter V.

Chapter VI deals with the thermodynamic properties like specific heat at constant pressure, enthalpy, Gibbs' energy, entropy, enthalpy of formation, Gibbs' energy of formation and logarithm of standard equilibrium constant of  $\text{PyO}$ ,  $\alpha$ -,  $\beta$ -,  $\gamma$ -picolines, para-fluorophenol and para-fluorobenzaldehyde based on vapour phase spectroscopic data.



List of Publications

1. H.D. Bist and J.S. Parihar, Chem. Phys. Lett. 32, 244 (1975).
2. J.C.D. Brand, H.D. Bist and J.S. Parihar, 30th Symposium on Molecular Structure and Spectroscopy; Columbus, Ohio 1975.
3. H.D. Bist, J.S. Parihar and J.C.D. Brand, J. Mol. Spectroscopy (in Press).
4. J.C.D. Brand, H.D. Bist, D. Liu and J.S. Parihar, CAP, DAMP, Meeting at Fredrickton, N.B., Canada.
5. J.S. Parihar, H.D. Bist, J.C.D. Brand and D. Liu (communicated).
6. J.S. Parihar, H.D. Bist and S.A. Kuchadkar (communicated).

## CHAPTER I

### INTRODUCTION

#### 1.0 General

Recent developments, both in the theoretical and the experimental aspects of spectroscopic techniques, have provided several magnificent tools for the investigation of the energy structure of large polyatomic molecules. Accurate information about the rotational energy levels is deduced on the basis of the microwave and the far infrared (FIR) studies, the rotational Raman scattering experiments, the vibrational-rotational spectra and the gyrovibronic studies in visible and ultraviolet regions using both the absorption and emission spectra. In addition to the above mentioned techniques, useful data on vibrational energies of a system could be obtained from the neutron inelastic scattering, the thermal diffuse scattering, and the proton magnetic resonance experiments. For the energy structure of the electronically excited states, electronic absorption and emission (including fluorescence and phosphorescence) spectra are the only source of information. A veritable renaissance seems evident in most of these branches of conventional spectroscopy, especially during the last two decades.

For determining the equilibrium atomic configurations, several modifications have also taken place in the diffraction techniques involving the X-rays, the electrons and the neutrons. Thus classical methods based on stereo chemistry, dipole moments and magnetic measurements etc are only of marginal importance to a spectroscopist involved in the correlation work of spectroscopic data with known or unknown structures.

In the present study, high resolution electronic spectra, the vapour phase infrared contours and laser excited Raman spectra of a few substituted aromatic compounds have been studied with a view to establish the fundamental normal modes of the molecules in isolated state.

The theoretical (normal coordinate) analysis of vibrational data of the molecules provides a set of force constants as a representative of the potential energy for the system. Once reliable vibrational assignments are achieved, the degree of the transferability of force-field and the coupling between various modes can be ascertained. The thermodynamic constants and other observable properties derived from such spectroscopic data could provide a feed back mechanism to test the reliability of vibrational assignments. If overtones and higher harmonics and combination bands could be established, the anharmonicities in the normal modes could be determined.

For determining the equilibrium atomic configurations, several modifications have also taken place in the diffraction techniques involving the X-rays, the electrons and the neutrons. Thus classical methods based on stereo chemistry, dipole moments and magnetic measurements etc are only of marginal importance to a spectroscopist involved in the correlation work of spectroscopic data with known or unknown structures.

In the present study, high resolution electronic spectra, the vapour phase infrared contours and laser excited Raman spectra of a few substituted aromatic compounds have been studied with a view to establish the fundamental normal modes of the molecules in isolated state.

The theoretical (normal coordinate) analysis of vibrational data of the molecules provides a set of force constants as a representative of the potential energy for the system. Once reliable vibrational assignments are achieved, the degree of the transferability of force-field and the coupling between various modes can be ascertained. The thermodynamic constants and other observable properties derived from such spectroscopic data could provide a feed back mechanism to test the reliability of vibrational assignments. If overtones and higher harmonics and combination bands could be established, the anharmonicities in the normal modes could be determined.

The geometrical structure in the electronically excited states could be attempted on the basis of electronic band contour analysis. Some prominent aspects of these methods, relevant to the present study, have been discussed in the following sections.

### 1.1 Energy Levels of a Molecule

The discrete energy  $T$  (in  $\text{cm}^{-1}$ ) in a molecular state neglecting the energies of the nuclear spins, the magnetic interactions and the translational motions and taking Born-Oppenheimer approximation (1) can be expressed as

$$T = T_e + G(v) + F(J, \tau) \quad (1)$$

where  $T_e$ ,  $G(v)$  and  $F(J, \tau)$  denote the pure electronic, the vibrational and the rotational term values, respectively.

### 1.2 Rotational Energy Levels

The rotational energy (in  $\text{cm}^{-1}$ ) for a rigid rotor may be written as (2)

$$E_r = -\frac{1}{h^2} (A P_a^2 + B P_b^2 + C P_c^2) \quad (2)$$

where  $P$ 's are angular momentum operators; and  $A$ ,  $B$  and  $C$  denote the rotational constants with  $A = \frac{h}{8\pi^2 I_A} \text{ cm}^{-1}$  etc,

where  $I_A$ ,  $I_B$  and  $I_C$  represent three principal moments of inertia of a molecule (3) with  $I_A \leq I_B \leq I_C$ . Depending on relative magnitudes of A, B and C all the molecules are classified into the following three categories from the viewpoint of rigid rotor energy levels:

### 1.21 Asymmetric Top Molecules

The asymmetric rotor is the most general case where

$$I_A \neq I_B \neq I_C \quad (3)$$

Introducing the scalar factors  $\sigma$  and  $\rho$  in equation (2) as change of variables, we have (2):

$$E_r(\sigma A + \rho, \sigma B + \rho, \sigma C + \rho) = \sigma E_r(A, B, C) + \rho J(J+1) \quad (4)$$

Here we choose

$$\sigma = \frac{2}{A-C} \quad \text{and} \quad \rho = -\frac{A+C}{A-C} \quad (5)$$

such that

$$\begin{aligned} \sigma A + \rho &= 1 \\ \sigma B + \rho &= \frac{2B - A - C}{A - C} = k \quad (\text{Asymmetry parameter}) \\ \sigma C + \rho &= -1 \end{aligned} \quad (6)$$

The asymmetry parameter  $k = -1$  or  $B = C$  (for prolate symmetric rotor) and  $k = +1$  or  $B = A$  (for oblate symmetric rotor).

Substituting relations (5) and (6) into the eqn (4) we have

$$E_r(1, k, -1) = E_r(k) = \frac{2}{A-C} E_r(A, B, C) - \frac{A+C}{A-C} J(J+1)$$

$$\text{or } E_r(A, B, C) = F(J) = \frac{A+C}{2} J(J+1) + \frac{A-C}{2} E_t(k) \quad (7)$$

For an oblate rotor  $B = A$ . The matrix elements of  $E(k)$  are

$$\langle J, K, M | E(k) | J, K, M \rangle = J(J+1) - 2k_1^2 \quad (8)$$

Substituting (8) into the equation (7) and  $B = A$  we have the energy term value for oblate symmetric top as:

$$F(J, K) = AJ(J+1) + (C-A)K_1^2 \quad (9)$$

Here  $C-A < 0$

and for prolate rotor  $B = C$  so the energy term value is

$$F(J, K) = CJ(J+1) + (A-C)K_{-1}^2 \quad (10)$$

Here

$$A-C > 0$$

### 1.22 Linear and Spherical Top Molecules

For linear molecules  $I_A = 0$ ,  $I_B = I_C$  and  $k = -1$  and for spherical top molecules  $I_A = I_B = I_C$ , the energy levels can be given as

$$F(J) = \frac{E_r}{hc} = BJ(J+1) \quad (11)$$

### 1.23 Symmetric Top Molecules

A symmetric rotor corresponds to one of the limits

$$A = B \quad (\text{Oblate rotor}).$$

$$B = C \quad (\text{Prolate rotor})$$

The corresponding term values are given in equations (9) and (10), respectively, where  $J$ ,  $K_1$  and  $K_{-1}$  are, respectively, the quantum numbers for total angular momentum and its components on the molecular figure axis.

### 1.3 Vibrational Energy Levels

A N-atomic non-linear molecule has  $3N$  degrees of freedom with  $3N-6$  vibrations ( $3N-5$  for linear molecules), 3 rotations (2 for linear molecules) and 3 translations of the center of mass (4). Thus, in general, there are  $3N-6$  (or  $3N-5$ ) normal modes of vibration describing the relative motions of the constituent nuclei.



In a normal or fundamental mode of a molecule its center of mass remains stationary and all the nuclei move in phase executing nearly simple harmonic motions with a common frequency about their equilibrium positions, yet the amplitudes may be different for the various nuclei.

In terms of the mass weighted displacement (or normal) coordinates the general expressions for the kinetic (T) and potential (V) energies is given as

$$T = \frac{1}{2} \sum_k^{3N} \dot{Q}_k^2 \quad (12)$$

and

$$V = \frac{1}{2} \sum_k^{3N} \lambda_k Q_k^2 + \text{higher terms} \quad (13)$$

where  $\lambda$ 's are related to the normal frequencies.

The higher terms or anharmonic terms in V affect the positions of overtone and combination levels (5) and the quadratic term which is predominant for small oscillations, gives the usual harmonic oscillator levels. The corresponding term values are given by (4)

$$\begin{aligned}
 G(v_1, v_2, v_3, \dots) = & \sum_i \omega_i \left(v_i + \frac{d_i}{2}\right) + \sum_i \sum_{k \geq i} x_{ik} \left(v_i + \frac{d_i}{2}\right) \\
 & \left(v_k + \frac{d_k}{2}\right) + \sum_i \sum_{k \geq i} g_{ik} l_i l_k + \dots
 \end{aligned}
 \tag{14}$$

Here  $v_i, v_k$  are the vibrational quantum numbers,  $\omega_i$  are the vibrational frequencies (in  $\text{cm}^{-1}$ ) for infinitesimal amplitudes,  $x_{ik}$  and  $g_{ik}$  are anharmonicity constants,  $d_i$  and  $d_k$  are degeneracies of the vibrations and  $l_i, l_k$  are angular momentum quantum numbers of degenerate vibrations

$$l_i, l_k = v_i, v_i-2, v_i-4, \dots, 1 \text{ or } 0$$

For non-degenerate vibrations  $l_i = 0$ ,  $g_{ik} = 0$ .  $d_i = 1$  or  $2$  depending whether  $i$  refers to a non-degenerate or doubly degenerate vibrations.

### 1.31 Diatomic Approximation

In case of diatomic molecules, the degeneracy  $d_i = 1$ ,  $l_i = 0$ ,  $g_{ik} = 0$  and  $W_e, x_e$  are the anharmonicity constants corresponding  $x_{ik}$ . Thus the equation (14) reduces to:

$$G(V) = W_e \left(V + \frac{1}{2}\right) - W_e x_e \left(V + \frac{1}{2}\right)^2 + W_e y_e \left(V + \frac{1}{2}\right)^3 + \dots
 \tag{15}$$

where  $W_e$  is the harmonic oscillator frequency and  $W_e X_e$  and  $W_e Y_e$  are the anharmonicity constants. However  $W_e Y_e \ll W_e X_e \ll W_e$ .

### 1.32 The Electric Dipole Moment

The electric dipole moment is not a linear function of the coordinates of the atoms. This can be expanded as a power series in the coordinates of atoms as:

$$M_i = M_i^0 + \sum_{k=1}^{3N-6} M_i^{(k)} Q_k + \text{higher terms} \quad (16)$$

The first term in the expansion gives the permanent dipole moment which is responsible for the pure rotational infrared spectrum; the second term is responsible for the appearance of vibrational infrared spectrum, while higher terms are effective in providing intensity to overtones and combination bands.

### 1.33 Evaluation of Anharmonicity Constants

From the expression (15) of diatomic approximation, we can calculate the separation of two successive vibrational levels:

$$\begin{aligned} \Delta G \left( V + \frac{1}{2} \right) &= G(V+1) - G(V) \\ &= W_e - 2 W_e X_e - 2 W_e X_e V \end{aligned} \quad (17)$$

Likewise the second difference is

$$\Delta^2 G(V+1) = \Delta G(V+3/2) - \Delta G(V+1/2) = -2 W_c X_0 \quad (18)$$

However, often we have situations where only the fundamental and the first overtone are available. In such cases the procedure is to express the vibrational term value in terms of the lowest level ( $V=0$ ) as zero, i.e.

$$G_0(V) = W_0 V - W_0 X_0 V^2 \quad (19)$$

Hence 
$$G_0(1) = W_0 - W_0 X_0 \quad (20)$$

and 
$$G_0(2) = 2W_0 - 4W_0 X_0 \quad (21)$$

Here  $G_0(1)$  and  $G_0(2)$  are the actual observed fundamental and the first overtone respectively. From these relations both  $W_0$  and  $W_0 X_0$  can be obtained.

### 1.34 Infrared Vibrational Spectra

The infrared absorption occurs through changes in electric dipole moment ( $\vec{M}$ ) of the molecular unit arising due to its excitation to a higher energy level. It may also occur through changes in electric moments of higher order, magnetic moments, etc; however, the absorption through such interactions is generally found to be negligibly weak. The vibrational energy intervals fall in the conventional IR region and hence informations about the vibrational energies is obtained from IR absorption spectra.

### 1.35 Infrared Band Intensity

The intensity of absorption line corresponding to a transition from the ground state  $m$  to an excited state  $n$  is defined as the energy absorbed from the incident beam per square cm cross section and expressed as:

$$\Delta I = hc W_{nm} B_{nm} c_{nm} N_m \Delta X \quad (22)$$

where  $C c_{nm} = I_o^{nm}$  gives the intensity of the incident beam,  $\Delta I$  is the amount absorbed in traversing a layer of thickness  $\Delta x$ ,  $N_m$  is the number of molecules per unit volume in the initial state  $m$ , and population  $N_n$  is considered negligibly small. The Einstein transition probability of absorption;  $B_{nm}$ , is related with the matrix element of the electric dipole moment by the relation

$$B_{nm} = \frac{8\pi^3}{3h^2 c} |R_{nm}|^2 \quad (23)$$

where

$$R_{nm} = \int \psi_n^* M_Q \psi_m d\tau \quad (24)$$

The matrix element  $R_{nm}$  is also called the transition moment between the given states  $m$  and  $n$ . For an allowed transition  $R_{nm}$  is non zero.

The formula (24) may be used to determine the interaction of electromagnetic wave with (a) electric dipole moment,

(b) magnetic dipole moment (c) quadrupole or higher moments, (d) induced dipole moment (in case of Raman scattering), etc by substituting appropriate moment in place of  $M_Q$ . In particular,  $R_{nm}$  turns out to be zero for all cases where the product of the two wavefunctions involved does not have the symmetry of one of the components of  $M_Q$ . When the electric dipole moment "M" given by the equation (16) is substituted in (24) the integral corresponding to the permanent dipole moment becomes zero in view of orthogonality of  $\psi$  functions, and  $R_{nm}$  comes out to be

$$R_{nm} = \frac{1}{\sqrt{2\alpha}} \left( \frac{dM}{dQ} \right)_{Q=0} \quad (25)$$

where

$$\alpha = \frac{2\pi (\mu \kappa)^{\frac{1}{2}}}{h} \quad (26)$$

$$\text{and} \quad \frac{1}{2\pi C} \left( \frac{\kappa}{\mu} \right)^{\frac{1}{2}} = W_{nm} \quad (27)$$

in this expression 'k' is the force constant,  $\mu$  is the reduced mass and  $W_{nm}$  is the frequency of vibration of the system.

The extinction coefficient  $A'$  is given by

$$A' = \frac{1}{\Delta x} \frac{\Delta I}{I} = h W_{nm} B_{nm} N_m \quad (28)$$

and using relations (22), (23) and (27) one gets

$$A' = \frac{\pi N}{30^2 \mu} \left( \frac{\partial M}{\partial Q} \right)_{Q=0}^2 \quad (29)$$

where  $N_m$  is put equal to  $N$  as a close approximation.

### 1.36 Spectra in Different Physical States

Vapour State: In the vapour phase spectra of simple light molecules the individual rotational lines can be identified in a rotation-vibration band. If the vapour pressure is small at ambient temperature better structure is obtained because of low pressure-broadening, but the path lengths have to be large. Often to overcome instrumental limitations pressure-broadening is induced by introducing a non-absorbing gas. This smears out the detailed structure, but the integrated intensity is not altered. On the other hand if the pressure of the absorbing gas itself is increased smaller path length may be used, but the structure will again be smeared out, until at large enough pressures when gas density approaches that of the liquid state, the rotational structure coalesces to give a broad band with a pronounced maximum at the band centre.

In the heavier polyatomic molecules, even at low pressures, only band contours with P, Q and R branch maxima are obtained, that too in favourable circumstances.

Liquid State: In the liquid state the molecules in general do not exhibit quantized free rotations. Consequently, the vibrational Raman and infrared bands do not show any rotational fine structure. In fact, in pure liquids and solutions the vibrational bands possess a comparatively simple form, usually consisting of a single maximum at the appropriate vibrational frequency. The shape of the curve may be approximated by a Lorentzian curve of the form

$$P = \frac{a}{(W - W_0)^2 + b^2} \quad (30)$$

where  $P$  is the value of absorbance at frequency  $W$  having its maximum value  $P_0$  equal to  $\frac{a}{b^2}$  at the band centre ( $W = W_0$ ); 'a' and 'b' are constants. The band half-width; defined as the full width of the absorption band at half the maximum absorbance value is given by

$$\Delta\nu_{1/2} = 2b. \quad (31)$$

The above formulae hold if the instrumental inadequacies are ignored. In practice the bands in the liquid state have half-width in the range of 5 to 10  $\text{cm}^{-1}$ .

In the condensed state some new bands which are not present in the vapour state may appear either due to the formation of new species (e.g. polymers or associated complexes) or due to resulting change of symmetry which allows



the vapour phase infrared or Raman inactive vibrations.

Solid State: In the solid phase, due to absence of rotations and homogeneity of environment the vibrational bands may be quite narrow. Some changes may also occur in the band positions and their relative intensities with respect to vapour phase values. The magnitude of frequency changes are small, usually not above 5 percent except in cases where hydrogen bonding is involved. It is noteworthy that different vibrations of a particular molecule may show very different relative shifts, which may be with opposite sign.

In crystalline state another important phenomenon is the splitting in the bands. The splittings may be classified as: (a) the site-symmetry splitting and (b) the factor-group splitting. The former type of splitting occurs simply because in several cases the site symmetry in the crystal may be lower than the molecular symmetry and the selection rules are altered to suit the crystal symmetry. Consequently, these equilibrium crystal field effects may result in the appearance of frequencies which are unexpected for free molecules. Further, the degenerate vibrations may also show splitting due to site symmetry effects. However, if a crystal contains 'n' molecules per unit cell, each non-degenerate vibration of the molecules may split into 'n' components due to the possible resonance interaction; and the phenomena is commonly known as factor-group or exciton

splitting (6-8). If the splittings are small only broadening of bands near peak positions will be observed.

In addition to the above two types of splittings, some new bands may also occur due to lattice vibrations. Combination of lattice vibrations with the fundamental internal modes of a molecule may lead to some additional bands in their vibrational finger print region.

Phase transformations resulting due to change of temperature in solid state may create additional complexities in the vibrational spectra. However, in molecules exhibiting rotational isomerism in free state the solid phase spectra are sometimes simpler than the gas phase spectra, if out of several possible conformations one isomer gets stabilized at low temperature.

### 1.37 Raman Vibrational Spectra

Inelastic scattering of electromagnetic radiations now known as Raman scattering was predicted theoretically by Smekal (9) in 1923. Sir C.V. Raman (10) observed it experimentally in 1928. The importance of the phenomenon lies in the fact that differences between the frequencies of scattered and incident radiations carry informations about the dynamics and structure of the scatterer.

The scattered radiations (excluding Rayleigh scattering) are found to have frequencies lower and higher than the

frequency of incident light. The phenomenon in the former case is known as Stokes Raman scattering while in the latter case anti-Stokes Raman scattering. An incident photon at  $W_e$  falls on the sample and a Stokes photon at  $W_s = W_e - W_v$  is emitted, simultaneously. To conserve energy the molecule is excited to a higher level, of energy  $h\nu W_v$ . If on the other hand, the molecule is initially in the excited state ( $E = h\nu W_v$ ), an anti-stokes photon at  $W_{AS} = W_e + W_v$  may be emitted along with de-excitation of the molecule from  $V=1$  to  $V=0$ . Since anti-Stokes emission depends on the number of molecules being in the initial excited state, it is weaker than Stokes emission.

Raman scattering is usually weak in intensity, hence a high intensity source is needed for its observation. For this reason, a stimulated interest in its studies and applications arose only in the past decade after the invention of high power and highly monochromatic continuous laser sources.

Raman effect is the result of interaction between electromagnetic waves and induced dipole moment ( $\vec{P}$ ) hence is fundamentally different from IR absorption. The two phenomena are complementary to each other in providing informations about the dynamics of a system. Whether a particular mode of vibration would appear in particular type of spectra is ascertained by the finite transition probability computed for it using appropriate transition moment.

### 1.38 Raman Band Intensity

The polarizability theory of Raman band intensity was developed by Placzek (11) in 1934 considering that Raman scattering arises from the ground state polarizability depending on molecular vibrations.

The transition probability for Raman scattering depends on the matrix element  $\alpha_{nm}$  of electric polarizability tensor ( $\tilde{\alpha}$ ). Thus

$$\alpha_{nm} = \int \psi_n^* \tilde{\alpha} \psi_m d\tau \quad (32)$$

The relationship between the induced dipole moment ( $\vec{P}$ ) and the electric field vector  $\vec{E}$  of the incident radiation is given by

$$\vec{P} = \alpha \vec{E} \quad (33)$$

In single crystal studies the intensity of Raman band is usually treated in terms of scattering efficiency's' defined as (12, 13)

$$S = \frac{N(W_s)}{N(W_e)} \quad (34)$$

where  $N(W_s)$  is the number of scattered photons of frequency  $W_s$  produced per unit time per unit cross sectional area of the crystal in the solid angle  $d\Omega$  about the direction of

observation and  $N(W_e)$  is the number of incident photons of frequency  $W_e$  per unit time per unit cross sectional area. For right angle scattering and unpolarized light, Smith (13)

$$S = \frac{3hId\Omega}{2\pi\sigma CW} \frac{(W_e - W)^4}{|a_{nm}|^2} [1 - \exp(-\frac{hCW}{kT})]^{-1} \quad (35)$$

where  $W = W_{nm} = \frac{E_n - E_m}{hC}$  and  $L$  is the effective length of crystal from which the scattered radiations are received at the slit of the spectrophotometer,  $\sigma$  is the density of the scattering centres,  $k$ , the Boltzmann's constant and  $T$ , the absolute temperature.

The experimentally observed Raman band intensity, which is proportional to the related value of  $s$ , as such can be of only relative importance. Here also the integrated intensity of the band may be considered to be of more significance than the peak intensity.

### 1.39 Depolarization Ratios

For the conventional right angle geometry for Raman studies, the depolarization ratio  $\rho$  is defined as the ratio of scattered intensity which is polarized perpendicular to the electric field vector  $\vec{E}$ , i.e. in the direction of propagation of the incident light, to the intensity parallel to  $E$ . If  $S_{\perp}$  and  $S_{\parallel}$  are the scattering efficiencies of a mode respectively in these two conditions then the depolarization ratio for the mode is given by

$$\rho = \frac{S}{S} \quad (36)$$

#### 1.4 Vibrational Rotational Energy Levels

In a free molecule, rotation can take place simultaneously with vibration which gives rise to the fine structure of infrared and Raman vibrational bands. This fine structure, when it is well resolved, leads to a very accurate and reliable information about the structure of a particular molecule. Also from this fine structure we can determine moments of inertia, internuclear distances and valence angles, in many cases with greater accuracy than by any other methods.

The total energy of vibration and rotation of a molecule (say for a linear molecule) is given by

$$\begin{aligned} T &= G(v_1, v_2, \dots) + F_{[v]}(J) \\ &= \sum_i W_i \left( v_i + \frac{d_i}{2} \right) + \sum_i \sum_k X_{ik} \left( v_i + \frac{d_i}{2} \right) \left( v_k + \frac{d_k}{2} \right) \\ &\quad + \sum_i g_{ik} l_i^2 + B_{[v]} J(J+1) - D_{[v]} J^2 (J+1)^2 \end{aligned} \quad (37)$$

For every vibrational state, there are a set of rotational levels, but with slightly different spacings. The details of rotational and vibrational energy levels have already been discussed under section 1.2 and 1.3, respectively.

#### 1.41 Infrared Band Contours

Infrared band contour analysis is one of the most powerful tools in the analysis of normal modes of vibration. The information about the rotational constants and the selection rules can be obtained from the shapes (A-, B-, C- or hybrid type) of band envelopes arising from the unresolved rotational transitions. This technique is very useful in identifying and ascertaining the location of some bands more accurately, particularly in regions overlapped by other bands. The observables involved are:

- (i) the separation of P and R branch peaks ( $\Delta\nu_{PR}$ )
- (ii) the relative intensity of the Q branch as compared to the integrated intensity of the whole band ( $I_Q/I_{total}$ ) and
- (iii) the actual shape of the band contour.

If explicit relations could be established between these observables and the molecular parameters, one could use band contour analysis to deduce these parameters. The situation is, however, quite complicated both from theoretical and experimental stand points. However, before reviewing the theoretical status in the field and presenting our data on substituted aromatic compounds it will be appropriate to clearly state the terminology used in the contour analysis.

#### 1.42 The Band Types

For infrared active modes the transition moment may be directed along any of the principal (a, b or c) axes or may have components along more than one principal axis. Resulting bands are termed A-type, B-type, C-type or hybrids, in that order. A band of a near symmetric top described as 'A-type' is of a parallel type in a prolate top and of perpendicular type in an oblate top; whereas a 'C-type' band is of the parallel type in an oblate top and of the perpendicular type in a prolate top. A 'B-type' band is of the perpendicular type in both prolate and oblate top molecules.

#### 1.43 The Molecular Parameters

The molecular parameters required for the calculations of the PR separations and the relative Q branch intensity with that of the whole band are either functions or simple ratios of the rotational constants A, B and C. The frequently used parameters are K,  $\beta$ ,  $\rho^*$  and  $S(\beta)$ . They are defined as

$$K = \frac{2B - A - C}{A - C} \quad (38)$$

$$\beta = \frac{A}{C} - 1 \text{ or } \frac{C}{B} - 1$$

for prolate or oblate molecules respectively.

And

$$\rho^* = \frac{A - C}{B} \quad (39)$$



The molecule is referred to as the oblate type for  $k = +1$  and for all values of  $\beta$  in the range  $-0.5 \leq \beta < 0$  whereas it is considered as prolate type for  $k = -1$  and for all values of  $\beta$  in the range  $0 < \beta < \infty$ . The constant  $\rho^*$  may have all values between 0 and  $\infty$  for prolate asymmetric top molecules but it can not exceed unity for oblate molecules. The constant  $\rho^*$  and  $\beta$  are identical for symmetric top molecules. The parameter  $S(\beta)$  is defined empirically as

$$\log_{10} S(\beta) = \frac{0.721}{(\beta + 4)^{1.13}} \quad (40)$$

which is found to hold good within 0.5 percent for  $\beta$  in the range  $-0.5$  to  $+100.00$ . The constant  $S(\beta)$  may have a fixed value or lie in a specific interval depending upon the type of the molecule.

#### 1.44 Symmetric Top Molecules

Gerhard and Dennison (14) have shown that for parallel bands

$$\frac{I_Q}{I_{\text{Total}}} = [\log_e (\sqrt{\beta} + \sqrt{\beta+1}) - \sqrt{\beta/(\beta+1)}] / \beta \sqrt{\beta/(\beta+1)},$$

for  $\beta > 0$ ;

(41)

$$\frac{I_Q}{I_{\text{Total}}} = \frac{1}{3}, \text{ for } \beta = 0;$$

$$\frac{I_Q}{I_{\text{Total}}} = [\sqrt{-\beta(1+\beta)} - \sin^{-1} \sqrt{-\beta} / \beta - \sqrt{-\beta/(1+\beta)}], \text{ for } \beta < 0;$$

where  $I_Q$  refers to the intensity of the Q-branch.

For parallel bands an increase in  $I_Q$  is observed for any decrease in  $\beta$  in the range  $\infty > \beta > 0$ . For negative values of  $\beta$ ,  $I_Q$  increases rapidly and reaches maximum for  $\beta = -0.5$ . In the two limiting cases  $\beta = 0$  (spherical top molecules) and  $\beta = \infty$  (linear molecule), the values of  $I_Q/I_{\text{Total}}$  are zero and  $\frac{1}{3}$  respectively.

For perpendicular bands, the intensity of Q-branch should be comparable to the P- and R branches when  $\beta \sim -0.5$ .  $I_Q$  increases with the increase in  $\beta$  and equals  $\frac{1}{3}$  of the total intensity of the band for  $\beta = 0$  (there is no distinction between parallel and perpendicular bands for  $\beta = 0$ ). The intensity of the Q-branch increases rapidly for positive values of  $\beta$  and all branches become broader with their maxima lower. For very large values of  $\beta$ , the PQR structure of the band disappears and the shape of the band resembles a Gaussian error curve.

The second factor determining the total structure of the band is the PR separation. According to Gerhard and Dennison (14) the PR separation of the parallel bands may be written as

$$\Delta\nu_{\text{PR}} (||) = 5S(\beta) [2\beta T/9]^{\frac{1}{2}} \text{ cm}^{-1} \quad (42)$$

It may be seen from the above formula that for  $\beta = 0$  (the molecule is spherical top) the PR separation is given by

$$\Delta\nu_{\text{PR}} = 10 \left[ \frac{\beta T}{9} \right]^{\frac{1}{2}} \text{ cm}^{-1} \quad (43)$$

The parallel and perpendicular bands would not be distinguishable in this case. For  $\beta = \infty$ , i.e.  $S(\beta) = 1$ , the molecule is linear and the PR spacing is given as

$$\Delta\nu_{PR} = 5 \left[ \frac{2\beta T}{9} \right]^{1/2} \text{ cm}^{-1} \quad (44)$$

In both the spherical top and linear molecules the PR separation of parallel and perpendicular type bands will be equal.

For the PR separation of the perpendicular bands Gerhard and Dennison (14) have proposed the following relation

$$\Delta\nu_{PR} (1) = 10 \bar{x} \left[ \frac{\beta T}{9} \right]^{1/2} \text{ cm}^{-1} \quad (45)$$

where  $\bar{x}$  refers to the distance between those points of the envelope where the absorption coefficient of the P and R branches is maximum.

Seth-Paul and Dijkstra (15) have suggested the formula

$$\Delta\nu_{PR} (1) = (\beta+1)^{1/2} \Delta\nu_{PR} (||) \quad (46)$$

for the range  $-\frac{1}{2} \leq \beta \leq \frac{3}{4}$  and this relation may be used as a substitute for this interpolation technique.

#### 1.45 A Symmetric Top Molecules

Hollas (16) has found that band contours can be considerably influenced by the differences between rotational constants of ground and upper vibrational states, and therefore any program for computing the contours of vibrational bands must take care of this fact. Franks and Innes (17) have demonstrated the use of this method to deduce  $k$  from measured values of  $I_Q/I_{\text{Total}}$  in favourable cases.

The calculations of Gerhard and Dennison were extended to asymmetric top molecules by Badger and Zurnwalt (18). Using a computer program band envelopes were drawn for different combinations of molecular parameters  $\rho = \frac{1}{3}, \frac{1}{2}, \frac{3}{4}$  and  $\frac{5}{6}$  and  $k = -\frac{1}{2}, 0$  and  $+\frac{1}{2}$ . General formulae, neither for the band contours nor for the PR separations, were given. PR separations of A-, B- and C-type contours could be calculated by estimating  $\tilde{X}$  values from the figures (19) and then substituting in the formula (20) for symmetric top molecules. Though this method is quite convenient for a large number of molecules, the main difficulty is experienced when the  $\rho^*$  and  $k$  values lie beyond the range for which the band envelopes are drawn.

In order to overcome these limitations Seth-Paul and Dijkstra (15) worked out a procedure and gave the formula

$$\Delta\nu_{\text{PR}} = 10 \tilde{x} \left[ \frac{\tilde{\theta}^T}{9} \right]^{1/2} \text{ cm}^{-1} \quad (47)$$

where  $\tilde{x}$  is either a number (a constant ratio of rotational constants) or a function of molecular parameters and

$$\tilde{B} = \frac{BC}{B+C} \quad \text{or} \quad \frac{AB}{A+B}$$

and

$$\tilde{\beta} + 1 = \frac{A}{2\tilde{B}} \quad \text{or} \quad \frac{C}{2\tilde{B}}$$

for near prolate or near oblate asymmetric top molecules respectively so that,

$$\tilde{\beta} = \beta \quad \text{and} \quad S(\tilde{\beta}) = S(\beta)$$

As a result, the equation (42) is transformed into

$$\begin{aligned} \Delta v_{PR} (||) &= 10 S(\tilde{\beta}) \left[ \frac{\tilde{B}T}{9} \right]^{1/2} \\ &= S(\tilde{\beta}) \cdot \tilde{\delta} \end{aligned} \quad (48)$$

For B(1) and C(1) bands in the range  $\frac{3}{4} < \rho^* < 3$  (a case of interest in the present study) Seth-Paul and Dijkstra's (15) expressions may be put in the form

$$\Delta v_{PR} B(\underline{1}) = \tilde{\delta} \quad (49)$$

and

$$\Delta v_{PR} C(\underline{1}) = \frac{3}{2} S(\tilde{\beta}) \cdot \tilde{\delta} \quad (50)$$

Expressions are not available for the ratio  $I_Q/I_{\text{Total}}$  for bands of asymmetric top molecules. We, therefore, propose to extend the application of relation (41) to asymmetric top molecules just replacing  $\beta$  by  $\beta$ .

#### 1.46 Hybrid Bands

Seth-Paul and De Meyer (21) found a better agreement between the expected and observed PR separations by using the formula

$$\Delta\nu_{\text{PR}}(\alpha\beta) = [\{\bar{x} \tan(\alpha+1)\} / \tan(\alpha+1)] S_\alpha \quad (51)$$

where  $S_\alpha$  denotes the PR separation for pure  $\alpha$ -type band,  $\alpha$  and  $\beta$  are the angles between the oscillating dipole and the  $a$  and  $b$  axes of the molecule respectively. If  $\Delta\nu(A)$  and  $\Delta\nu(B)$  are the PR separations for pure A-type and pure B-type bands respectively, the formula (51) is equivalent to,

$$\Delta\nu_{\text{PR}}(\alpha\beta) = \frac{\Delta\nu(A) \cos \alpha + \Delta\nu(B) \cos \beta}{\cos \alpha + \cos \beta} \text{ cm}^{-1} \quad (52)$$

However, this is again an empirical formula. The uncertainties in measurements of  $\Delta\nu_{\text{PR}}$  values (particular in hybrid bands) are so large that the relation (52) can at the most be used only to check the hybrid character but not for deducing the direction of the dipole-oscillations within any narrow range. In fact we find that simple rule of three formulae like

$$\Delta\nu_{PR}(\alpha\beta) = \frac{\alpha\Delta\nu(A) + \beta\Delta\nu(B)}{\alpha + \beta} \quad (53)$$

gives as good a fit as formula (52) in almost all cases.

### 1.5 The Normal Coordinate Analysis

The frequency of the normal vibration is determined by the kinetic and the potential energies of the system. K.E. is determined by the masses of the individual atoms and their geometrical arrangement in the molecule. On the other hand, the P.E. arises from interaction between the individual atoms and is described in terms of the force constants.

Since P.E. provides valuable information about the nature of inter-atomic forces, it is highly desirable to obtain the force constants from the observed frequencies. This is usually done by calculating the frequencies assuming a suitable set of force constants. If the agreement between the calculated and observed frequencies is satisfactory, the set of the force constants is adopted as representative of the P.E. for the system. The whole process is known as normal coordinate analysis.

#### 1.51 Aim of the Normal Coordinate Analysis

Work on the force fields of individual molecules may broadly be divided into two categories. Firstly, there are approximate treatments, using, as feasible, a few force constant parameters which are designed to aid the interpretation of

the observed spectra and which act as a guide to the approximate values of any missing frequencies. Secondly, there are more exact treatments which are possible when all the frequencies are known and have been assigned to their symmetry classes. These more elaborate treatments are aimed at finding force fields which are as accurate as possible. These more accurate data can be used for

- (a) a comparison with wave mechanical treatments
- (b) a comparison between molecules and suggesting trial force constants for related molecules.  
and
- (c) determining the form of the normal coordinates which, in turn, are required for interpreting observations of infrared and Raman band intensities in terms of dipole moments, polarizabilities and their derivatives.

## 1.52 Calculation Procedure

To calculate the vibrational frequencies it is necessary first to express both the potential and kinetic energies in terms of some common coordinates. Internal coordinates which are the changes in bond-lengths, bond-angles, out of plane-wags and torsions are more suitable for this purpose than rectangular coordinates, since



- (i) the force constants expressed in terms of internal coordinates have a clear physical meaning than those expressed in terms of rectangular coordinates, and
- (ii) a set of internal coordinates does not involve translational and rotational motion of the molecule as a whole.

The Wilson's G.F. matrix method (22, 23) is mostly used for calculating the normal modes of vibration. The Kinetic (T) and potential (V) energies in terms of internal displacement coordinates are written as,

$$2T = \underline{\dot{R}}^T \underline{G}^{-1} \underline{\dot{R}} \quad (54)$$

and

$$2V = \underline{R}^T \underline{F} \underline{R} \quad (55)$$

respectively. The elements of the F matrix are not independent and a transformation Z is defined (24) such that

$$F_{K1} = \sum_j^J Z_{K1}^J \phi_j \quad (56)$$

where  $\phi_j$  are the independent Urey-Bradley or valence force constants. The G matrix or inverse kinetic energy matrix in terms of the transformation matrix B is written as

$$\underline{G} = \underline{B} \underline{M}^{-1} \underline{B}^+$$

or

$$G_{K1} = \sum_{i=1}^{3N} B_{Ki} B_{1i} / m_i \quad (57)$$

(K=1,2,3,---3N-6)

where  $m_i$  is the mass of the  $i$ -th atom,  $N$  is the number of atoms and  $M^{-1}$  is a diagonal matrix whose  $i$ -th diagonal element  $\mu_i$  is the reciprocal of the mass of the  $i$ -th atom.

In terms of the internal coordinates the vibrational secular equation which is to be solved takes the familiar form (25).

$$\underline{L}^{-1} \underline{G} \underline{F} \underline{L} = \underline{\Lambda} \quad (58)$$

or

$$\underline{G} \underline{F} \underline{L} = \underline{L} \underline{\Lambda} \quad (59)$$

where  $\underline{\Lambda}$  is a diagonal matrix of the frequency parameters  $\lambda_i$  and  $\underline{L}$  is the transformation matrix from normal coordinates  $Q$  to internal coordinates  $R$

$$\underline{R} = \underline{L} \underline{Q} \quad (60)$$

The transformation of Cartesian coordinates  $\underline{X}$  to internal coordinates  $\underline{R}$  is expressed as

$$\underline{R} = \underline{B} \underline{X} \quad (61)$$

The solution of equation (59) yields the eigenvalue,

$$\lambda_i = \sum_{K1}^n L_{Ki} L_{1i} Z_{K1}^J \phi_j \quad (62)$$

related to the vibrational frequency  $\omega$  (in wave numbers) by the relation

$$\lambda_i = \frac{4\pi^2 w_i^2 c^2}{N} \quad (63)$$

and eigen vector  $\underline{L}$  of the dynamical matrix. The terms

$\sum_{Kl} L_{Ki} L_{li} z_{Kl}^j$  may be considered as the elements  $(JZ)_{ij}$  of a matrix  $(JZ)$  of dimension  $nm$  where  $n$  is the number of vibrational frequencies and  $m$  is the number of independent force constants in the assumed potential function. Equation (59) can be written in the matrix form as

$$\underline{\Lambda} = \underline{J} \underline{Z} \underline{\phi} \quad (64)$$

Thus a measure of the nature of the normal vibrations (mixing of various modes), i.e., the fractional potential energy distribution (PED) associated with each internal coordinate defined as an array of terms, each of which represents that fraction of the potential energy in a normal mode of vibration which stems from a particular force constant is given by (25).

$$PED = \underline{\Lambda}^{-1} \underline{J} \underline{Z} \underline{\phi}$$

Thus the fractional potential energy of the  $i$ -th normal mode associated with the  $K$ -th internal coordinate and  $\phi_j$  (UBFC) is given by

$$(PED)_K^i = \sum_{jKl} L_{Ki} L_{li} z_{Kl}^j \phi_j / \lambda_i \quad (65)$$

## 1.6 Electronic Spectra

The electronic spectra arise from **transitions** between electronic states and are accompanied by simultaneous changes in the vibrational and rotational states. Consequently, in the ultraviolet and visible regions, the absorption or emission is associated with the familiar progressions and sequences of bands corresponding to each of the  $3N-6$  (or  $3N-5$  for linear molecules) vibrations (26,27). In addition, the rotational energy levels associated with the vibrations in both the electronic states result in the observed rotational structure in each of the gyrovibronic bands. The individual lines in the rotational structure in case of light molecules could be easily isolated with the high resolution spectrographs available today. In heavier molecules, having large values of principal moments of inertia, only gyrovibronic contours are obtained even under the highest resolution available. This occurs primarily because the separation between two lines becomes smaller than the Doppler band width of lines. However, these band contours provide information about the symmetry, nature, and geometry of the electronic states involved.

### 1.61 Intensity of Electronic Transition

Similar to the intensity expressions of absorption line discussed in section 1.35, the electronic intensity probability between the states  $n$  and  $m$  is given by

$$B_{mn} = \frac{8\pi^3}{3h^2c} |R_{nm}^e|^2 \quad (66)$$

where  $R_{nm}^e$  is the electronic transition moment given by equation (33). The total absorption of the electronic transition is given by

$$A = \int_{\text{band}} kw \, dw = N_m B_{mn} h w_{nm} \\ = \frac{8\pi^3 w_{nm}}{3hc} N_m |R_{nm}^e|^2 \quad (67)$$

The absorption coefficient  $kw$  and its integral over the whole band is the experimentally determined quantity. The oscillator strength  $f_{nm}$  is related with the transition probability by

$$f_{nm} = \frac{\mu h c^2 w_{nm}}{\pi e^2} B_{mn} \quad (68)$$

where  $\mu$  and  $e$  are the mass and charge of the electron. For strong transitions  $f_{nm}$  is of the order of one.

### 1.7 Fermi Resonance

Fermi resonance occurs when two energy levels of a molecule having the same symmetry and approximately the same energy interact with each other; in other words when they are accidentally almost degenerate. The phenomenon results in the

repulsion of two levels and large enhancement in the intensity of weaker transition.

Theoretically, if  $\psi_1^0$  and  $\psi_2^0$  represent the unperturbed wavefunctions of two states involved in Fermi resonance, the perturbed states would be defined by

$$\psi_1' = a_1 \psi_1^0 - a_2 \psi_2^0 \quad (69)$$

$$\psi_2' = a_2 \psi_1^0 + a_1 \psi_2^0 \quad (70)$$

where  $a_1$  and  $a_2$  are such that

$$a_1^2 + a_2^2 = 1 \quad (71)$$

and

$$a_1 = \left| \frac{\Delta + \delta}{2\Delta} \right|^{1/2}$$

$$a_2 = \left| \frac{\Delta - \delta}{2\Delta} \right|^{1/2} \quad (72)$$

when  $\delta = 0$ , we obtain equal mixture of  $\psi_1^0$  and  $\psi_2^0$  and when  $\delta$  is very large  $\psi_1' \rightarrow \psi_1^0$  and  $\psi_2' \rightarrow \psi_2^0$ . Here  $\delta$  is the separation between unperturbed energy levels while  $\Delta$  is that observed between perturbed levels.

The ratio of intensities  $I_1'$  and  $I_2'$  of observed transitions may be computed in terms of intensities  $I_1$  and  $I_2$  of respective

unperturbed transitions from the following equations (28);

$$\frac{I_1'}{I_2'} = \frac{a_1^2 I_1 + a_2^2 I_2 \mp 2a_1 a_2 (I_1 I_2)^{\frac{1}{2}}}{a_2^2 I_1 + a_1^2 I_2 \pm 2a_1 a_2 (I_1 I_2)^{\frac{1}{2}}} \quad (73)$$

The choice of the combination of signs depends on whether the matrix element of perturbation potential  $V_{12} > 0$  or  $< 0$ . The intensity  $I_2$  of unperturbed overtone (or combination) mode can reasonably be regarded as zero. We have therefore

$$\frac{I_1'}{I_2'} = \frac{a_1^2}{a_2^2} = \frac{\Delta + \delta}{\Delta - \delta} \quad (74)$$

For known values of  $I_1'$ ,  $I_2'$  and  $\Delta$ , this equation can provide the value of  $\delta$ .

### 1.8 Thermodynamic Properties

On the basis of data obtained from molecular spectroscopy, one could deduce the thermodynamic functions (ie the Gibbs energy  $G^0$ , the enthalpy  $H^0$ , the specific heat  $C_p^0$  and the entropy  $S^0$ ) with a great precision. Such calculations provide the unique method to obtain these data for some molecules in which no such data could be obtained by direct experiments. In general, however, a comparison of the calculated and observed quantities provides an additional evidence for the validity of the vibrational assignments.

### 1.81 Mathematical Relations

The well known formulae (4,29) are used to obtain the following:

Free energy content function:

$$\frac{G^{\circ} - H_{\circ}^{\circ}}{T} = -R \log \frac{Q}{N} \quad (75)$$

Heat content function

$$\frac{H^{\circ} - H_{\circ}^{\circ}}{T} = RT \left[ \frac{d}{dT} (\log Q) \right] + R \quad (76)$$

Entropy

$$S^{\circ} = \left( \frac{H^{\circ} - H_{\circ}^{\circ}}{T} \right) - \left( \frac{G^{\circ} - H_{\circ}^{\circ}}{T} \right) \quad (77)$$

and Heat capacity,

$$\begin{aligned} C_p^{\circ} &= C_v^{\circ} + R = \frac{\partial}{\partial T} (E^{\circ} - E_{\circ}^{\circ}) + R \\ &= \frac{R}{T^2} \left[ \frac{d^2 \log Q}{d(1/T)^2} \right] + R \end{aligned} \quad (78)$$

where  $R$  is the gas constant,  $H_{\circ}^{\circ}$  is the zero point energy,  $T$  is the absolute temperature of the molecular system,  $E^{\circ} - E_{\circ}^{\circ}$  is the total energy in excess of the zero point energy, and  $Q$  is the total partition function which is given under well known approximation by

$$Q = Q_{\text{tr}} \cdot Q_{\text{rot}} \cdot Q_{\text{vib}}. \quad (79)$$



where tr, rot and vib denote the translational, rotational and vibrational contributions respectively. The expressions for the Q's can be given as:

$$Q_{tr} = V \left( \frac{2 \pi m kT}{h^2} \right) \quad (80)$$

where V is the total volume of the system, m is the molecular weight (in grams) and other symbols have their usual meanings. Likewise:

$$Q_{rot} = \frac{(\pi I_A I_B I_C)^{\frac{1}{2}}}{\sigma} \left( \frac{8 \pi^2 kT}{h^2} \right)^{3/2} \quad (81)$$

Here  $\sigma$  is the symmetry factor and  $I_A$ ,  $I_B$  and  $I_C$  are the three principal moments of inertia. Similarly

$$Q_{vib} = \prod_i [1 - \exp(-hc\omega_i/kT)]^{-d_i} \quad (82)$$

In the above expression  $\omega_i$  stands for  $i$ th vibrational frequency (in  $\text{cm}^{-1}$ ) and  $d_i$  denotes its degeneracy.

For the purpose of actual calculations the thermodynamic functions may be arranged in the following form:

$$\frac{G^0 - H^0}{T} = -R \left[ \log \left[ \left( \frac{4kT}{h^2} \right)^3 \pi^5 m^{3/2} (I_A I_B I_C)^{\frac{1}{2}} \frac{1}{\sigma} \frac{V}{N} \right] \right. \\ \left. + \sum_i d_i \{ \log [1 - \exp(X_i)] \} \right] \quad (83)$$

$$\frac{H^0 - H^0}{T} = R \left[ 4 + \sum_i d_i \frac{X_i}{(e^{X_i} - 1)^2} \right] \quad (84)$$

and

$$C_p^0 = R \left[ 4 + \sum_i \frac{d_i (X_i)^2 \exp X_i}{(\exp X_i - 1)^2} \right] \quad (85)$$

$$\text{where } X_i = \frac{h c W_i}{k T} = \frac{1.4388 W_i}{T} \quad (86)$$

$W_i$  being one of the fundamental frequencies in wave number.

Substituting the values of various constants (30) for an ideal gas at one atmospheric pressure, equation (83) may be simplified as:

$$\frac{G^0 - H^0}{T} = -R \left[ -8.2866 + 4 \log T + 1.5 \log M + 0.5 \log (I_A I_B I_C) - \log - \sum_i d_i \log \{ 1 - \exp (-\frac{1.4388 W_i}{T}) \} \right] \quad (87)$$

where  $M$  is the mass of the molecule in amu and  $I_A$ ,  $I_B$  and  $I_C$  are the principal moments of inertia in  $\text{amu} \cdot \text{\AA}^2$ .

### 1.82 Entropy and Free Energy of Mixing

According to Schottkey and Wagner (31) the entropy and free energy changes due to mixing of non-interacting ideal gases (for a total of 1 mole of the mixture of ideal gas) are given by

$$\Delta S^0 = -R \sum_i N_i \log N_i \quad (88)$$

$$\frac{\Delta G^0}{T} = R \sum_i N_i \log N_i \quad (89)$$

where  $N_i$  is the mole fraction of the  $i$ th species.

### 1.83 Heat, Free Energy and Equilibrium constant of Formation

The calculated thermodynamic functions, the experimental heat of formation  $H_f^{\circ}$  and thermodynamic functions of C (graphite),  $H_2$ (gas),  $O_2$ (gas), and  $Cl_2$ (gas) (30) may be used to compute values of  $\Delta H_f^{\circ}$ ,  $\Delta G_f^{\circ}$  and  $\log_{10} K_P$  at the desired temperatures using the following relations

$$\Delta H_f^{\circ} = \Delta H_f^{\circ}_{298.16} + (H_T^{\circ} - H_{298.16}^{\circ}) \text{ Compound} - \sum (H_T^{\circ} - H_{298.16}^{\circ}) \text{ elements} \quad (90)$$

$$G_f^{\circ} = \Delta H_f^{\circ} - T \Delta S_f^{\circ} \quad (91)$$

where

$$\Delta S_f^{\circ} = S_T^{\circ} (\text{compound}) - \sum S_T^{\circ} (\text{elements})$$

$$\log_{10} K_P = \frac{-\Delta G_f^{\circ}}{0.004575845T} \quad (92)$$

$\Delta H_f^{\circ}$  and  $\Delta G_f^{\circ}$  are heat of formation and Gibbs energy (or Free energy) of formation,  $\log_{10} K_P$  is the equilibrium constant in terms of pressure and  $\Delta S_f^{\circ}$  is the entropy change for the formation of the molecule.

### 1.9 Numbering of Normal Modes

The vibrational modes in the substituted Pyridines are numbered after those of benzene (4,5). As there are more than one convention for denoting the vibrations of benzene itself (4,5,32), we have followed the Wilson's method (32). Wilson has arranged the symmetry species of  $D_{6h}$  benzene in

the order  $A_{1g}$ ,  $A_{2g}$ ,  $B_{1g}$ ,  $B_{2g}$ ,  $E_{2g}$ ,  $E_{1g}$ ,  $A_{1u}$ ,  $A_{2u}$ ,  $B_{1u}$ ,  $B_{2u}$ ,  $E_{2u}$  and  $E_{1u}$ . Subsequently, the frequencies are arranged in the increasing order of their magnitudes in each of the above species. Thus, each of the vibrations has been denoted by a number running from 1 through 20 in benzene. A very significant point to understand Wilson's numbering is the following: Normal coordinates of the vibrational modes are expressed in terms of the generalized coordinates of carbon and hydrogen; and for the modes involving similar expressions for normal coordinates, those involving carbon coordinates are given lower number than those involving hydrogen coordinates in any of the above species.

In Table 1.1 Wilson's numbering (32) has been compared with those given by Herzberg (4) and Whiffen (33). Subscripts "a" and "b" with the Wilson's numbering have been used to denote the two components of the degenerate vibrations of benzene which split in the monosubstituted benzenes or pyridines having  $C_{2v}$  point group. The symmetry classes of the vibrational modes, in the last column of Table 1.1 are denoted after Mulliken (34). The normal modes of vibrations for monosubstituted benzenes are shown in Fig 1.1.

REFERENCES

1. M. Born and R. Oppenheimer, Ann Physik 84, 457 (1927)
2. Harry C. Allen Jr. and P.C. Cross, Molecular Vib-Rotors, John Wiley and sons, INC, New York (1963)
3. W.A. Seth-Paul, J. Mol. Structure, 3, 403 (1969)
4. G. Herzberg, Molecular Spectra and Molecular Structure Vol II Infrared and Raman Spectra of Polyatomic Molecules, D. Van Nostrand Company, INC Princeton (1962)
5. E.B. Wilson Jr., J.C. Decius and P.C. Cross, "Molecular Vibrations" Mc Graw Hill Book Co., INC, New York (1955)
6. S. Bhagvantam and T. Venkatarayudu, Proc. Ind. Acad. Sci. 9A, 224 (1939)
7. R.S. Halford, J. Chem. Phys. 14, 8 (1946)
8. D.F. Hornig, J. Chem. Phys. 16, 1063 (1953)
9. A. Smekal, Naturwissenschaften 11, 873 (1923)
10. C.V. Raman, Ind. J. Phys. 2, 387 (1928)
11. G. Placzek, Handbuch Der Radiologie 2, 205 (1934)
12. P.M.A. Sherwood, Vibrational Spectroscopy of Solids, Cambridge University Press, Cambridge (1972)
13. H. Smith, Phil. Trans. Roy. Soc. London A241, 105 (1948)
14. S.L. Gerhard and D.M. Dennison, Phys. Rev. 43 197 (1933)
15. W.A. Seth-Paul and G. Dijkstra, Spectrochim.Acta, 23A, 2861 (1964)
16. J.M. Hollas, Spectrochim.Acta, 22, 81 (1966)

17. L.A. Franks and K.K. Innes, J. Chem. Phys. 47, 863 (1964)
18. R.M. Badger and R.L. Zumwalt, J. Chem. Phys. 6, 711 (1938)
19. V.N. Sarin, M.M. Rai, H.D. Bist and D.P. Khandewal, Chem. Phys. Letters 6, 473 (1970)
20. M.M. Rai, H.D. Bist and D.P. Khandelwal, Appl. Spectry. 25A 442 (1971)
21. W.A. Seth-Paul and D. Meyer, Spectrochim. Acta 25, 1671 (1967)
22. E.B. Wilson Jr., J. Chem. Phys. 7, 1047 (1939), 9, 76 (1941)
23. E.B. Wilson Jr., J.C. Decius and P.C. Cross, 'Molecular Vibrations' McGraw Hill, New York (1955)
24. J. Overend and J.R. Scherer, J. Chem. Phys. 32, 1289 (1960)
25. J.H. Schachtschneider and R.G. Snyder, Spectrochim. Acta 19, 117 (1963)
26. G. Herzberg, Electronic Spectra and Electronic Structure of Polyatomic Molecules, D. Van Nostrand Co. INC. Princeton, New Jersey, (1966)
27. H.H. Jaffe and M. Orchin, 'Theory and Applications of Ultraviolet Spectroscopy' John Wiley and Sons, INC New York (1962)
28. J.F. Bertran, L. Ballester, L. Dabrihalova, N. Sanchez and R. Arrieta, Spectrochim. Acta 24A, 1765 (1968)
29. George J. Janz, Thermodynamic Properties of Organic Compounds Academic Press (1967)
30. D.R. Stull, I. Carr, J. Chao, T.E. Dergazarian, L.A. du Plessis, R.E. Josted, S. Levine, F.L. Oetting, R.V. Petrele, H. Prophet and G.C. Sinke, JANAF Thermodynamic Tables, Clearing-house for Federal Scientific and Technical Information Spring field, Va.(1960).

31. W. Schottky and C. Wagner, cited by W. Schottky, H. Ulich...  
and C. Wagner, Thermodynamics, Springer-Verlag, Berlin,  
(1929)
32. E.B. Wilson Jr., Phys. Rev. 45, 706 (1934)
33. D.H. Whiffen, J. Chem. Soc. 1350 (1956)
34. R.S. Mulliken, J. Chem. Phys. 23, 1997 (1955)

TABLE 1.1

COMPARISON OF SYSTEM OF NOTATIONS FOR MONOSUBSTITUTED BENZENES

Vibra- tional species of Benzene	Descrip- tion (a)	Wilson's Number	Herzberg's Number	Whiffen's Symbols	Species of C <sub>2v</sub> Symmetry
A <sub>1g</sub>	νCC	1	2	p	A <sub>1</sub>
A <sub>1g</sub>	νCH	2	1	z <sub>1</sub>	A <sub>1</sub>
A <sub>2g</sub>	βCH	3	3	e	B <sub>2</sub>
B <sub>2g</sub>	τCC	4	8	v	B <sub>1</sub>
B <sub>2g</sub>	γCH	5	7	j	B <sub>1</sub>
E <sub>2g</sub>	αCCC	6a 6b	18' 18	t s	A <sub>1</sub> B <sub>2</sub>
E <sub>2g</sub>	νCH	7a 7b	15' 15	q z <sub>5</sub>	A <sub>1</sub> B <sub>2</sub>
E <sub>2g</sub>	νCC	8a 8b	16' 16	k l	A <sub>1</sub> B <sub>2</sub>
E <sub>2g</sub>	βCH	9a 9b	17' 17	a c	A <sub>1</sub> B <sub>2</sub>
E <sub>1g</sub>	γCH	10a 10b	11 11'	g i	A <sub>2</sub> B <sub>1</sub>
A <sub>2u</sub>	γCH	11	4	f	B <sub>1</sub>
B <sub>1u</sub>	αCCC	12	6	r	A <sub>1</sub>
B <sub>1u</sub>	νCH	13	5	z <sub>2</sub>	A <sub>1</sub>
B <sub>2u</sub>	νCC	14	9	o	B <sub>2</sub>
B <sub>2u</sub>	βCH	15	10	d	B <sub>2</sub>
E <sub>2u</sub>	τCC	16a 16b	20 20'	w x	A <sub>2</sub> B <sub>1</sub>

Contd ...



---

$E_{2u}$	$\gamma CH$	17a	19	h	$A_2$
		17b	19'	y	$B_1$
$E_{1u}$	$\beta CH$	18a	14	b	$A_1$
		18b	14'	u	$B_2$
$E_{1u}$	$\nu CC$	19a	13	m	$A_1$
		19b	13'	n	$B_2$
$E_{1u}$	$\nu CH$	20a	12	$z_3$	$A_1$
		20b	12'	$z_4$	$B_2$

---

(a) In these notations,  $\nu$ ,  $\alpha$ ,  $\beta$ ,  $\gamma$  and  $\tau$  denote bond stretching, angle deformation, in plane bending, out-of-plane bending, and torsional deformation or twist of the bonds or angles between the atoms written after each symbol, respectively.



## CHAPTER II

### EXPERIMENTAL DETAILS

#### 2.1 Purification of Samples

The original compounds of Analar grade were obtained from Aldrich Co., E. Merck, British Drug House and Eastman (red label) Co. for present investigation. To ensure the grade purity of the samples they were further purified by using the sublimation apparatus (where necessary) and the vacuum system described below.

##### 2.11 Sublimation Apparatus

The vacuum sublimation apparatus is illustrated Fig 2.1. This apparatus was used for initial purification of Pyridine N-oxide. The jacket 'J' containing the sample was heated to 50°C in a water bath B. The jacket was evacuated and the cold water was circulated into the inside tube T, shown in the figure. The compound evaporated under low pressure in the jacket, was deposited on the cooler surface of the tube T in a pure solid form. The compound thus purified was collected in a pyrex tube for further purification by fractional distillation.

## 2.12 Vacuum System

The vacuum system shown in Fig 2.2 was fabricated for (i) purifying the samples immediately before recording the spectrum (ii) filling the gas cell (iii) obtaining thin solid films of samples at liquid nitrogen temperature (LNT). The glass manifold from J<sub>1</sub> to J<sub>5</sub> shown in Fig 2.2 could easily be detached from the rest of the vacuum system. All the stopcocks, joints and connecting tubes were always thoroughly cleaned before any new compound was introduced in the system. Special care was always taken to leave no trace of impurities inside the manifold. Traps T<sub>1</sub> and T<sub>2</sub> were cooled externally by liquid nitrogen to prevent the contamination of the Duo Seal forepump (model 1402 from Welch Scientific Company) and/or the single stage oil diffusion pump by the vapours of the samples. Three-litre capacity bulb B is a safety storage tank for the oil of the vacuum forepump in case of breakdown of the power-supply. S<sub>10</sub> is a release valve for the forepump and F<sub>1</sub>, F<sub>2</sub> and F<sub>3</sub> are the three flasks used to purify the sample. The system was capable of giving vacuum of the order of  $10^{-5}$  cm of Hg inside the glass manifold.

For purification, the sample was kept in one of the flasks (say F<sub>1</sub>) which was attached to the system through a joint (J<sub>2</sub>). Initially the whole system was evacuated except the flask F<sub>1</sub>. Subsequently the stop cocks S<sub>3</sub> and S<sub>4</sub> were closed and the flask F<sub>1</sub> was opened to the vacuum line for a small period, after it was cooled to liquid nitrogen temperature. Then the inlet S<sub>3</sub> of

another flask (say  $F_2$ ) cooled to LNT was also opened to the vacuum system. After about half an hour the stopcock  $S_5$  was closed and the coolant outside the flask  $F_1$  was removed. The flask  $F_1$  gradually attained the room temperature and the sample evaporated and collected in the flask  $F_2$ . After collecting adequate amount of the first portion of the sample in flask  $F_2$ , the middle portion of the sample (which must be comparatively more pure) was collected in flask  $F_3$  in a similar fashion. This process was repeated several times for all the compounds to obtain the pure samples. We purified our compounds at least three times by the above process before filling them into the gas cell or pyrex break seal tube.

## 2.2 Sample Handling

The infrared, Raman and electronic spectra in the solid, liquid and vapour phases were recorded by using suitable sample handling techniques, depending upon the nature of the sample.

### 2.21 Vapour phase: Filling of the Sample in the Multiple Reflection Gas Cell

The vacuum system including the multiple reflection gas cell was evacuated to the desired pressure and then the stopcock  $S_5$  was closed. Purified sample was evaporated into the gas cell till a required band intensity was obtained. In case of samples with low vapour pressure, the tube connecting the cell and the vacuum system, was heated by wrapping a

I. I. T. KANPUR  
CENTRAL LIBRARY  
Acc. No. A 46651

heating tape on it. The samples having very low vapour pressure, were collected in a small pyrex tube and directly kept inside the cell. The cell was evacuated for a long period to obtain the desired pressure and then heated by heating tape till the required vapour pressure of the sample was obtained.

#### 2.22 Adjustment of Path Length of the Multiple Reflection Gas Cell

The vapour phase spectra of the samples were recorded on the P.E. 521 spectrophotometer using the multiple reflection cell with an adjustable path length from 1 to 10 meters in steps of 1 meter. The optical path of the cell is shown in Fig 2.3.

Before maintaining the hard vacuum in the multiple reflection cell, the desired path length was obtained by adjusting the mirrors  $M_1$ ,  $M_2$  and  $M_3$  and counting the images of the slit in  $M_2$ . We used 4 meter path lengths at low pressures to obtain well resolved band contours. Longer path lengths could not be used because beyond 4 meters the total intensity of the sample beam was less than 25 percent of the reference beam. This was due to medium quality coating of the mirrors.

#### 2.23 Filling Gas Sample for Electronic Studies

For high resolution electronic absorption spectra of pyridine N-oxide, the compound was put in a side tube of 1.25 meter long cell of pyrex with 2 inch diameter quartz windows fixed to its ends with epoxy resin. The cell was

## 2.25 Solid phase Sample in Low Temperature Cell

The spectra of the samples in solid state were recorded using the low temperature cell shown in Figure 2.4. This cell is slightly different from the conventional Wagner-Harning type cell (1). The low temperature cell can directly be inserted in the sample beam of the infrared spectrophotometer without any material change in the optical path. Prior to cooling, cell was evacuated to a pressure of about  $10^{-5}$  cm of Hg. Then the vapour of the sample from vacuum system (cf section 2.12) were evaporated into the low temperature cell in an identical fashion and there they were deposited on the cesium bromide plate on the cold finger after few heating and cooling operations. Extremely deliquescent samples having low vapour pressures were pressed between the two cesium bromide windows and put in the cold finger of the cell. Then the cell was evacuated for some time to get an spectrum of water free sample at room temperature. Now the liquid nitrogen was poured in the dewar and the temperature of the sample was measured by Copper-constantan thermocouple. After some time the copper frame, and the sample in cesium bromide plates in the cold finger attained the temperature of the refrigerant (LNT), and well-resolved infrared spectrum was obtained.

## 2.26 Quartz capillary and Pyrex Tube for Raman spectra

The triply distilled sample was filled under vacuum in a Quartz capillary tube of 1.5 mm diameter and a pyrex

break-seal tube of 1.2 cm diameter. Initially the Raman spectrum of the microcrystalline sample in the quartz capillary was excited with 514.5 nm radiation of the  $\text{Ar}^+$  ion laser and recorded on Cary-82 spectrophotometer. The other Raman spectra were recorded on a spex 1400 double monochromator. Here the sample was excited in a pyrex break-seal tube with an  $\text{Ar}^+$  ion laser (coherent Radiation Model 52) operating at 488.0 nm.

### 2.3 Recording of spectra

Infrared, Raman and high resolution electronic spectra of the compounds under study were recorded on the following instruments.

#### 2.31 Infrared spectrophotometer

The infrared spectra in the solid, liquid, and vapour phases were recorded in the region  $4000\text{--}250\text{ cm}^{-1}$  on the Perkin-Elmer Model 521 spectrophotometer (2) designed on the optical null principle (see figure 2.5 for its ray diagram). Two diffraction gratings with 100 lines/mm and 25 lines/mm, respectively fixed back to back are used in the monochromator. The first grating is used in the first order ( $630\text{--}2000\text{ cm}^{-1}$ ) and also in the second order ( $2000\text{--}4000\text{ cm}^{-1}$ ), and the second grating is used only in the first order in the region  $250\text{--}630\text{ cm}^{-1}$ . Suitable interference filters are used in the instrument to eliminate higher spectral orders. The source of infrared radiation is the Nernst glower. A resolution of about  $0.3\text{ cm}^{-1}$  is



obtained at  $1000\text{ cm}^{-1}$  with slit widths of about 70 microns. The instrument automatically records the infrared transmittance of the sample as a function of frequency of the incident radiation. The abscissa and ordinate of the chart papers are linear in  $\text{cm}^{-1}$  and percent transmittance (0-100), respectively. In the high resolution runs the scale factor of the chart paper was adjusted to give a separation of  $1\text{ cm}^{-1}$  per division on the recording chart (Cf  $10\text{ cm}^{-1}$  per division for normal runs). The accuracy is  $\pm 0.5\text{ cm}^{-1}$  over the entire range with a reproducibility of  $\pm 0.25\text{ cm}^{-1}$ .

The P.E. 521 spectrophotometer has been provided with a wide range of adjustments for scanning the spectrum of a sample. To obtain a well resolved spectrum of a sample, a suitable adjustment of the slitwidth, gain, signal-to-noise ratio and the scanning speed are of vital importance. A choice of proper combination of the above parameters was possible after enough experience with the machine.

The wave number calibration of the spectrophotometer was made by recording the infrared spectra of  $\text{H}_2\text{O}$ ,  $\text{CO}_2$  and  $\text{D}_2\text{O}$  vapour under conditions identical to that of the spectrum to be investigated. The calibration data were taken from standard texts (3-4). In case of liquids, Indene bands were used for calibration (5).

### 2.32 Raman Studies

The Raman spectra were recorded on Cary 82 and spex model 1400 spectrophotometers (6).

In Figure 2.6 the basic requirements for a conventional laser Raman spectrometer are shown schematically. Inside the block LASER the six letters SHRIMP signify the six advantages from laser sources: i.e. (1) Small samples (2) High directivity (3) Required coherence (4) Intensity (5) Monochromaticity and (6) Polarization of the incident light. Other blocks are self-explanatory.

Figure 2.7 illustrates the excitation train in the Cary 82 (also in Cary 83) machine. The laser light from argon ion laser passes through 5 prisms, 3 lens, a slit and a beam splitter before it falls onto the sample kept above the lens  $L_3$ . The reference phototube provides the required compensation for the back ground signal.

The optical ray diagram of the spex model-1400 double monochromator is shown in Fig 2.8. Two square gratings (102 mm x 102 mm) have 1200 Lper mm and are blazed at  $5000 \text{ \AA}$ . The gratings are driven by a sine bar arrangement which yields a spectral output with wavelength as a linear function of drive screw rotation. The scanning speeds may be varied between 0.12 and  $2300 \text{ \AA/min}$ . The bilateral, curved slits may be used upto a height of 50 mm; the resolution is  $0.08 \text{ \AA}$  at  $6328 \text{ \AA}$ . The

wavelength counter mechanism is stated to be accurate to  $1\text{\AA}$  and to be reproducible to  $0.2\text{\AA}$  over a  $6000\text{\AA}$  wavelength interval.

Argon ion laser model 52 (Coherent Radiation Laboratory) tuned at  $4880\text{\AA}$  was used as a source of excitation with the spex-1400 monochromator. Interference filters were used to avoid plasma lines. The spectra were recorded by Dr. H. D. Bist in the laboratories of Prof. H. J. Bernstein at N.R.C. Ottawa, Canada and Prof. J. C. D. Brand at U.W.O., London, Canada.

The calibration of Raman spectra was achieved by using sharp lines of neon discharge in  $4880\text{--}6000\text{\AA}$  region and also by making use of the anti-stokes and Stokes components of observed Raman shifts.

### 2.35 Ultraviolet Spectrograph

Ultraviolet absorption spectra of pyridine N-oxide were photographed on 3.4 meter Jernell Ash Ebert spectrograph (7). The optical ray diagram of the instrument is shown in Fig 2.9. The grating which was used for 15th-18th order has 57000 lines in it, and is driven by a sine bar arrangement which produces a motion that is always proportional to the sine of the angle of incidence at the grating. The optimum sensitivity at low concentrations is achieved because of the excellent line to the spectral background ratio resulting from the high dispersion, definition and complete isolation of the camera from all extraneous scattered radiation. A high

pressure 150 watt air-cooled Xenon arc lamp (isolated by a predisperser) was used as a source for absorption studies. A band of 60 to 120  $\text{\AA}$ <sup>0</sup> is passed through the slit of 3.4 meter spectrograph to avoid overlapping of the different orders from the grating. The spectra were recorded by Dr H D Bist in the laboratory of Professor J C D Brand, Chemistry Department, University of Western Ontario, London, Canada.

The calibration lines in the UV spectra were provided by neon filled Fe-hollow cathode lamp run at 40 milli amp current.

#### 2.4 Comparator Densitometer

The Microdensitometer tracings of some of the  $\underline{B_e}$  - and  $\underline{A_e}$ -type bands were taken on a Grant automatic comparator densitometer equipped with amplifier and recorder arrangement. The procedure for the densitometer tracing can be concluded from the block diagram shown in Fig 2.10. A gear system is attached to the plate holder, and the portion of the spectrum to be traced is exposed by the source light through the slit  $S_1$ . The light enters into the photomultiplier through the slit  $S_2$  and the intensity of different bands against their wavelengths is recorded.

REFERENCES

1. E W Wagner and D F Horning, J Chem Phys 18, 296 (1950)
2. Perkin-Elmer Corporation, Instruction Manual for Model-521 Spectrophotometer, Norwalk, Connecticut, U S A (July 1965)
3. K N Rao, C J Humphreys and D H Rank, "Wavelength Standards in Infrared", Academic Press, New York (1966).
4. "Tables of Wave Numbers for the calibration of Infrared spectrometers", Butterworth, London (1961)
5. R N Jones, N B W Jonathan, M A Mackenzie and A Nadeau, spectrochim Acta 17, 77 (1961)
6. A Anderson, The Raman Effect, Marcel Dekker, New York (1971)
7. Jarrell-Ash Company, Instruction Manual for 3.4 M Ebert Mark IV Model 70-000 Massachusetts (December 1963)

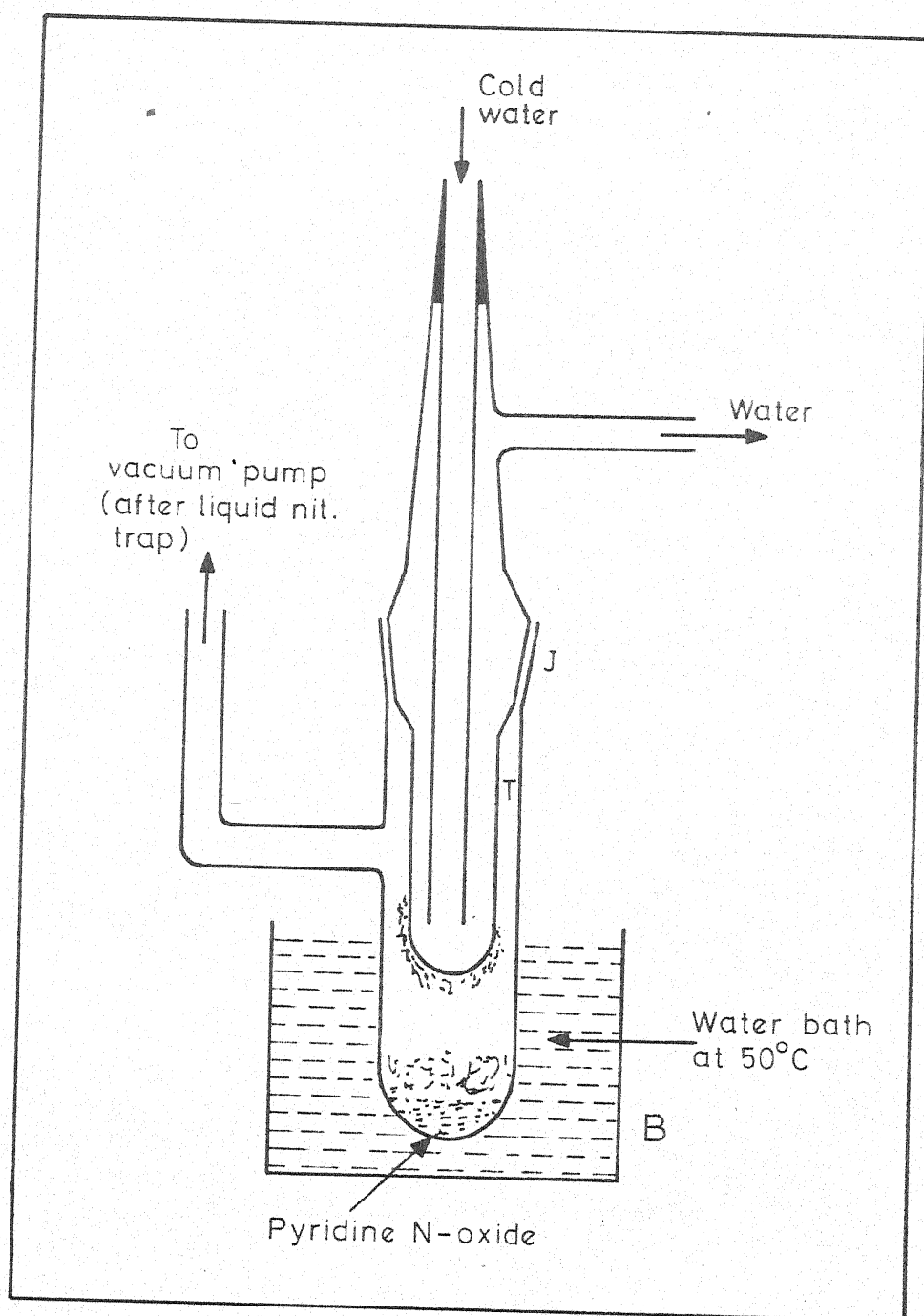


Fig. 2.1 Vacuum sublimation apparatus.

# VACUUM SYSTEM

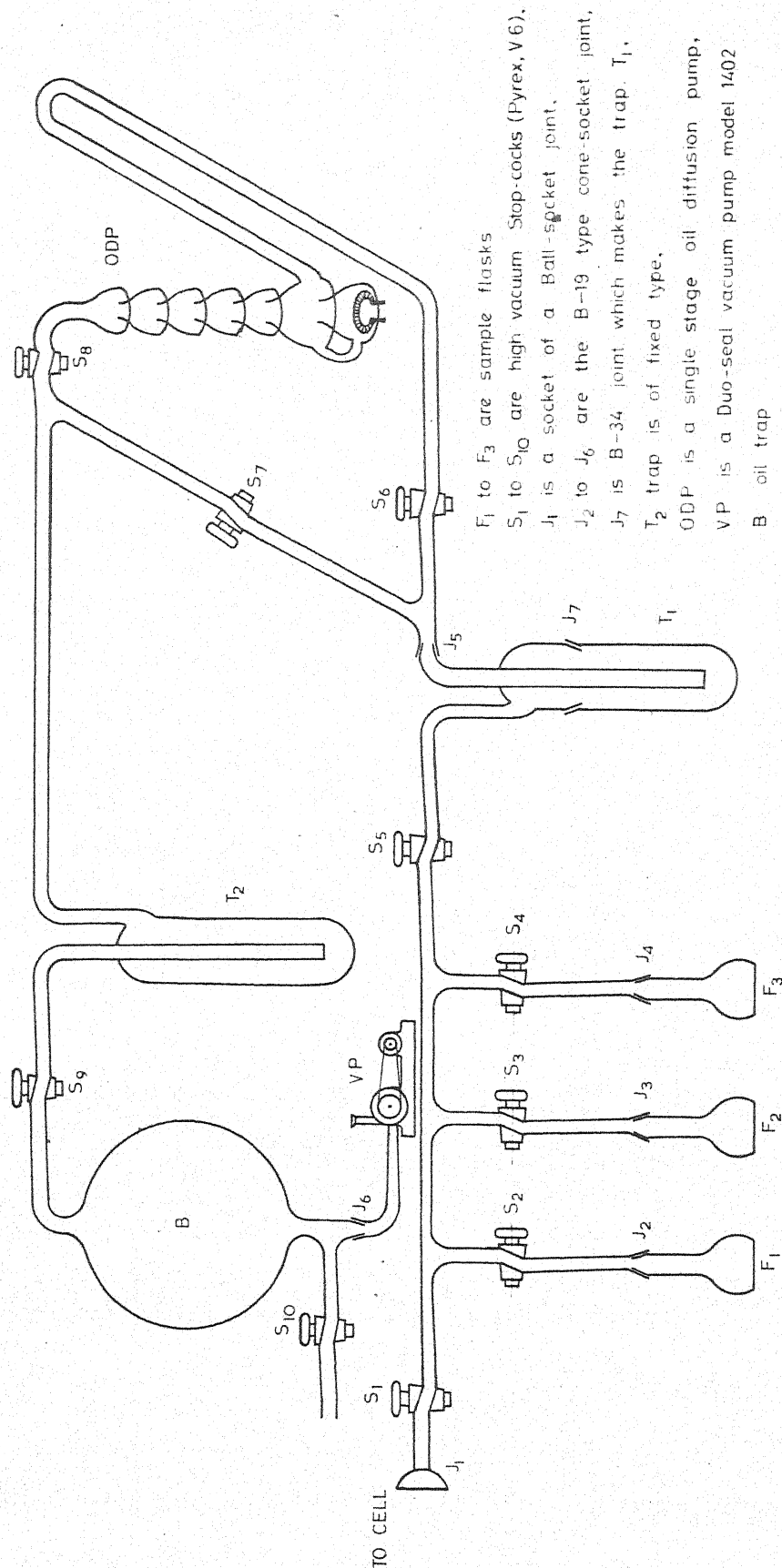
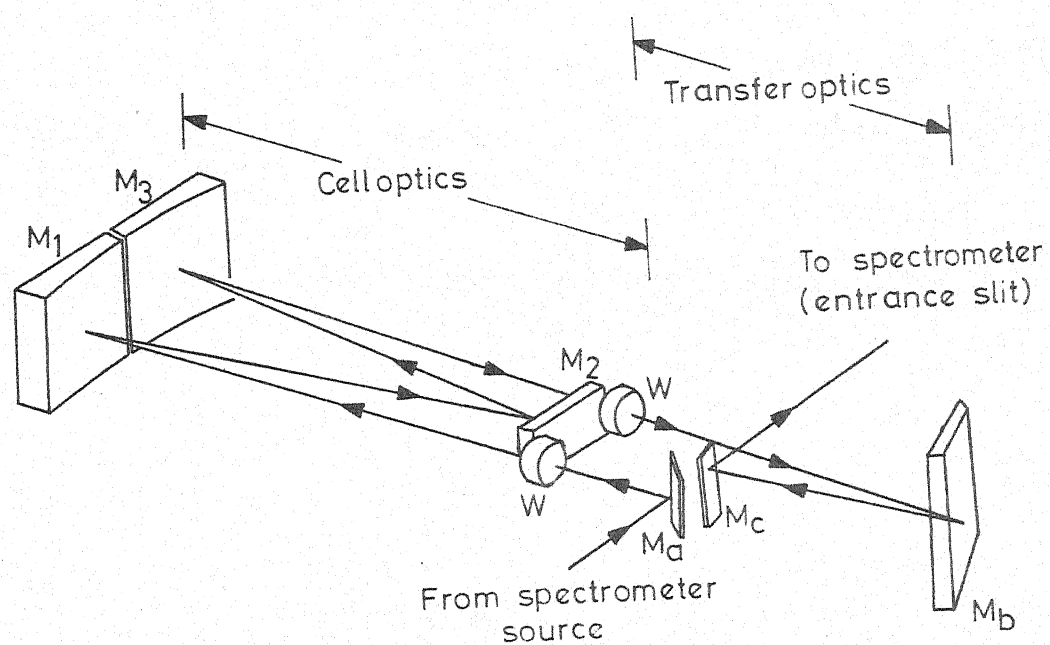


Fig. 2.2



Mirrors:-  $M_1$ ,  $M_2$  and  $M_3$  and two windows  $W$  are inside the cell.

$M_d$ ,  $M_b$  and  $M_c$  are outside the cell.

Fig. 2.3 Optical system of ten-meter multiple reflection cell.



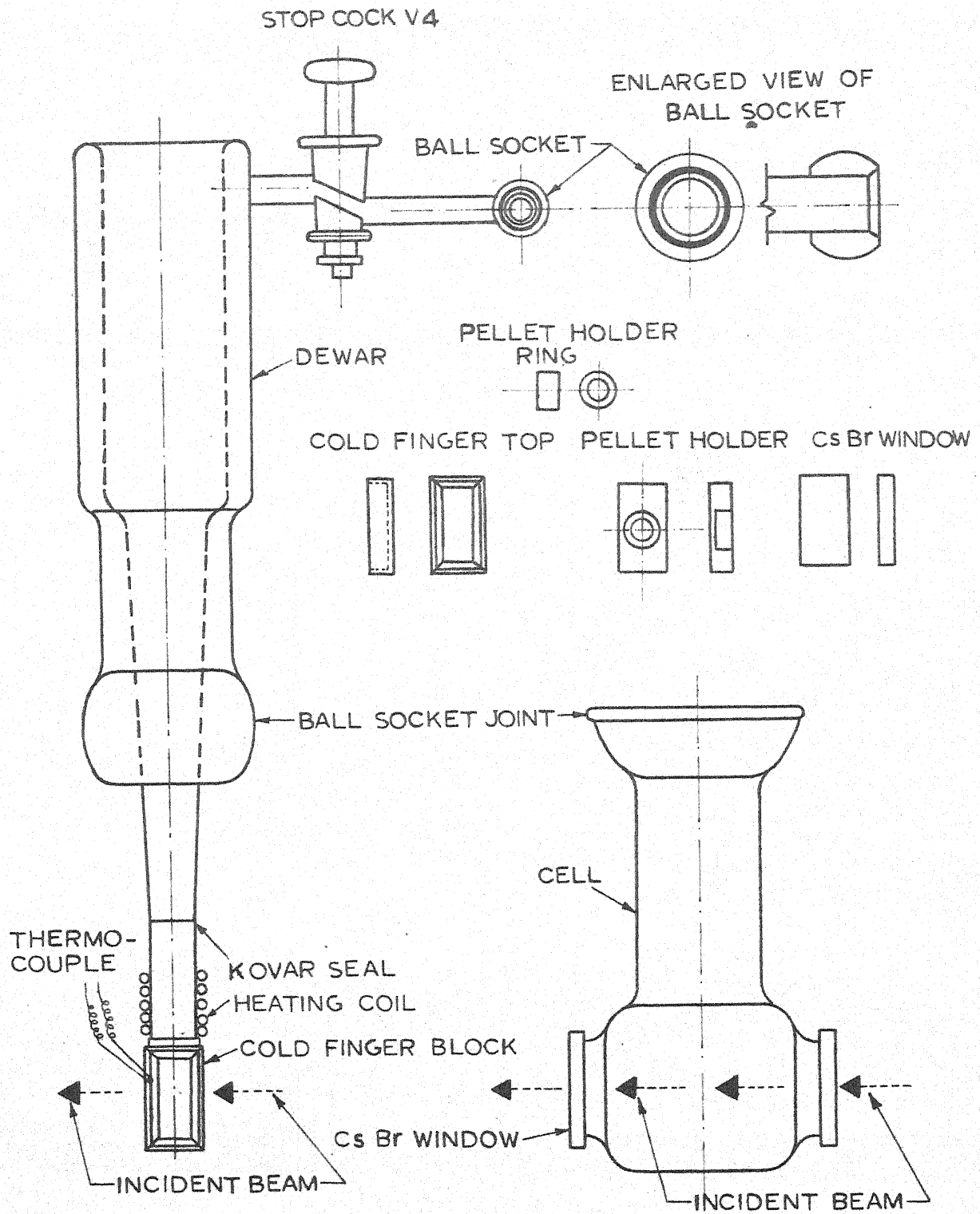
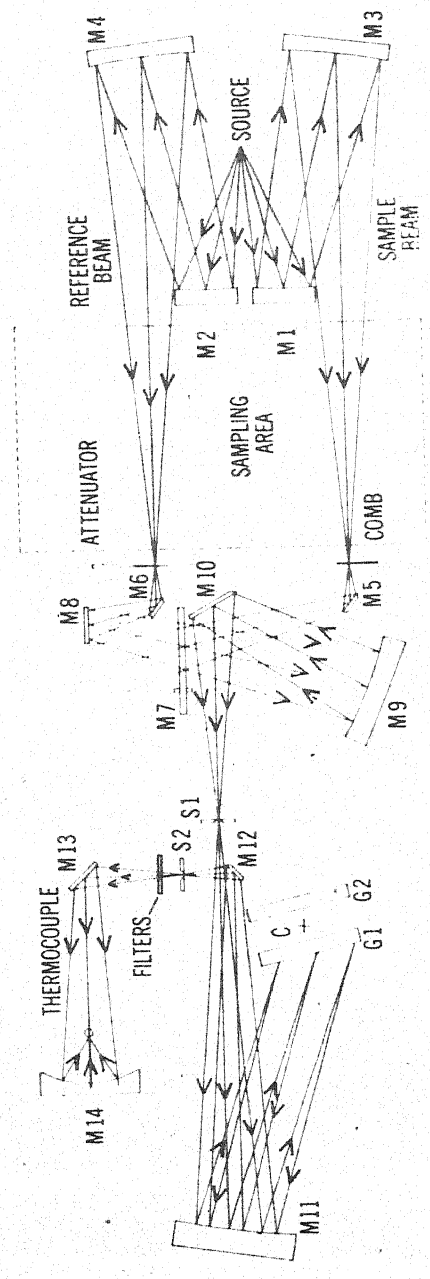


Fig.2.4 Low temperature cell

PERKIN-ELMER - 521 INFRARED SPECTROPHOTOMETER.



Glomer (Source); Mirrors (M<sub>1</sub>, M<sub>2</sub>, M<sub>3</sub>, M<sub>4</sub>, M<sub>5</sub>, M<sub>6</sub>, M<sub>7</sub>, M<sub>8</sub>, M<sub>9</sub>, M<sub>10</sub>, M<sub>11</sub>, M<sub>12</sub>, M<sub>13</sub> and M<sub>14</sub>); Entrance slit (S<sub>1</sub>); Exit slit (S<sub>2</sub>), Grating (G<sub>1</sub> and G<sub>2</sub>).

Fig. 2.5

## BASIC REQUIREMENTS (LASER RAMAN SPECTROMETER)

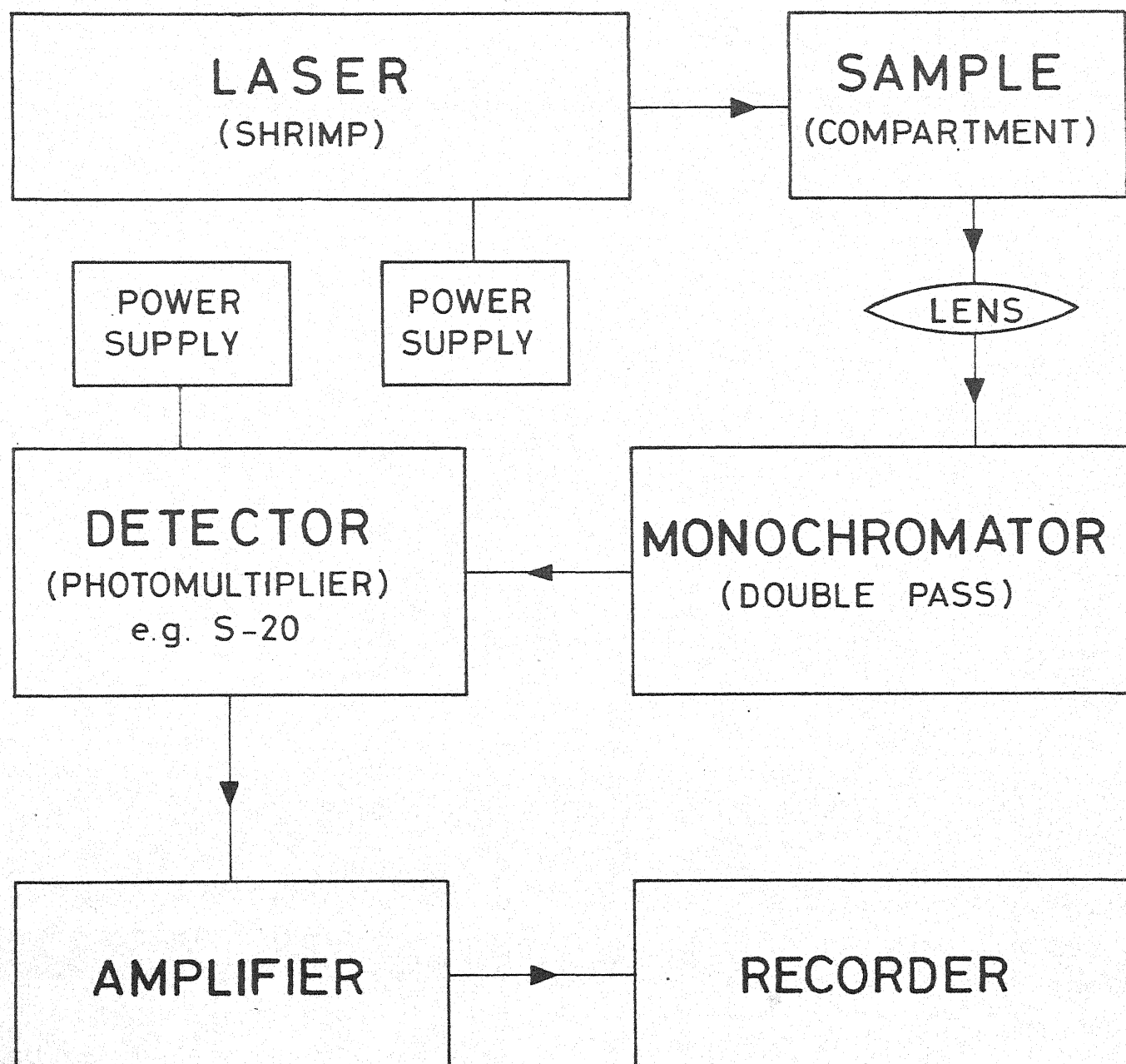
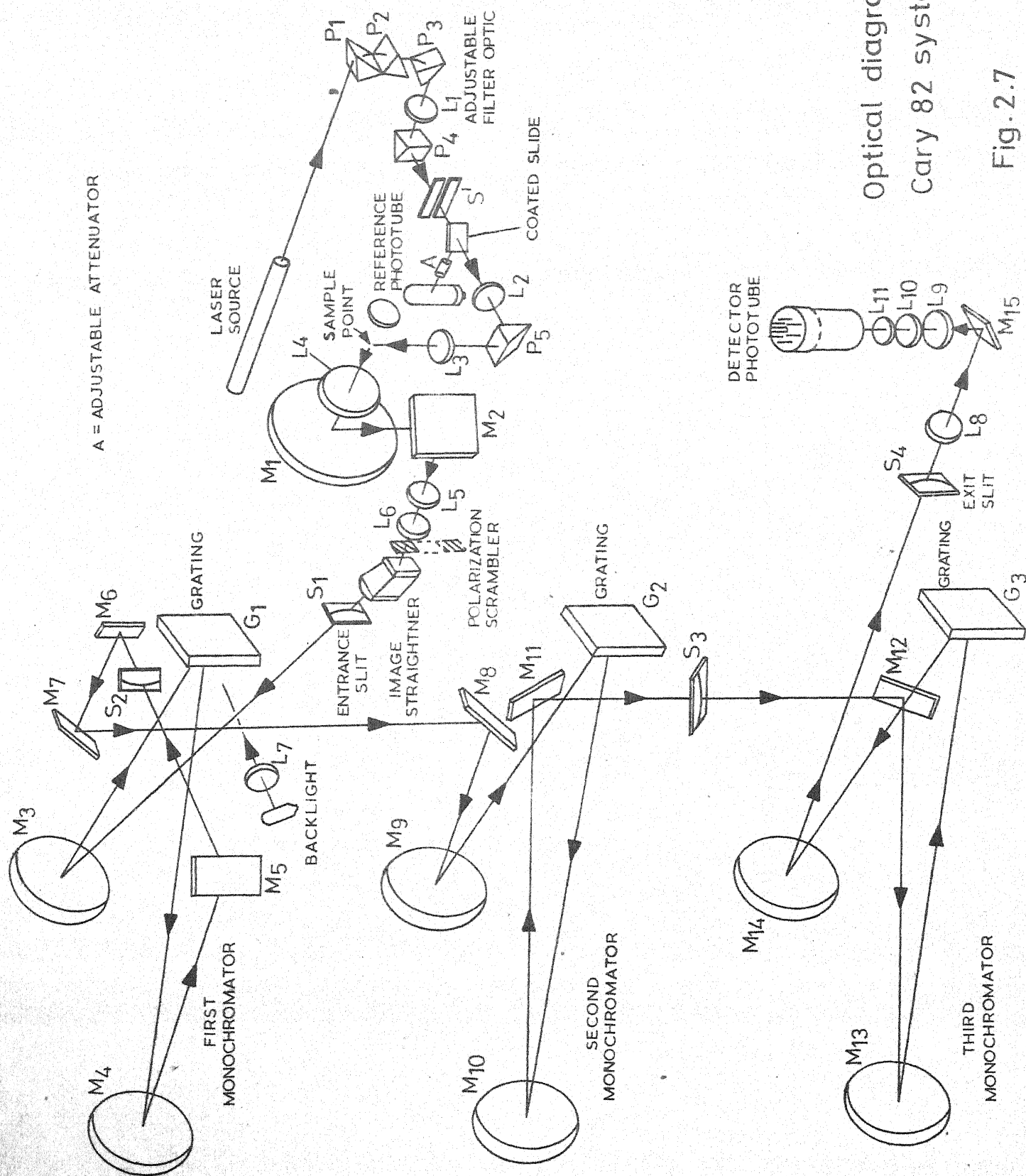


Fig. 2.6 Schematic diagram for Raman studies.



Optical diagram  
Cary 82 system

Fig. 2.7

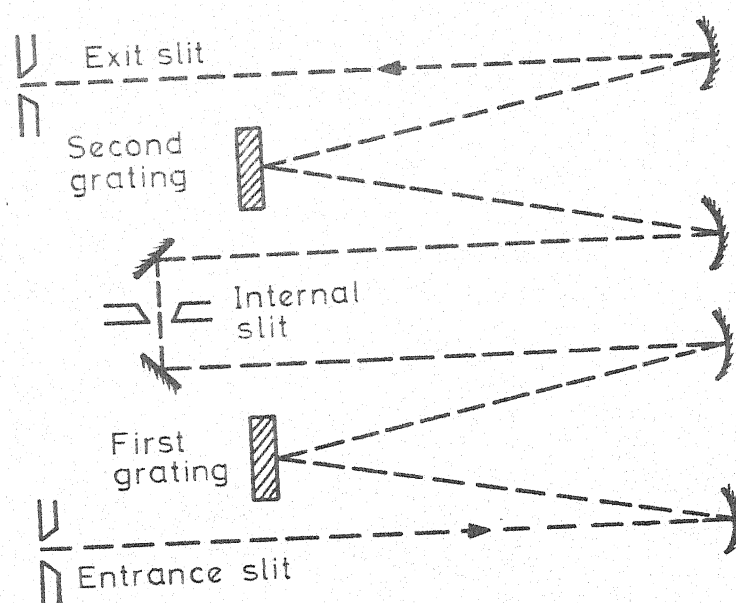


Fig.2.8 Optical diagram of the spex model 1400 double monochromator.

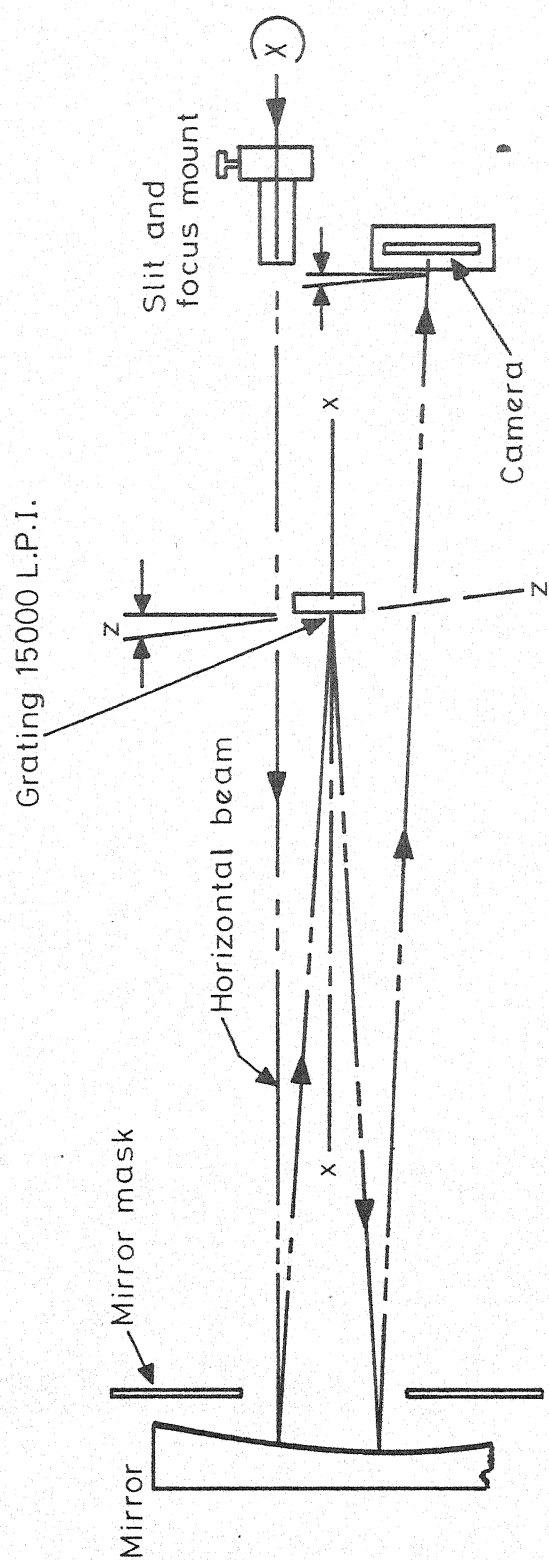


Fig.2.9 Optical diagram of 3.4 meter Jarrell-Ash Ebert spectrograph.

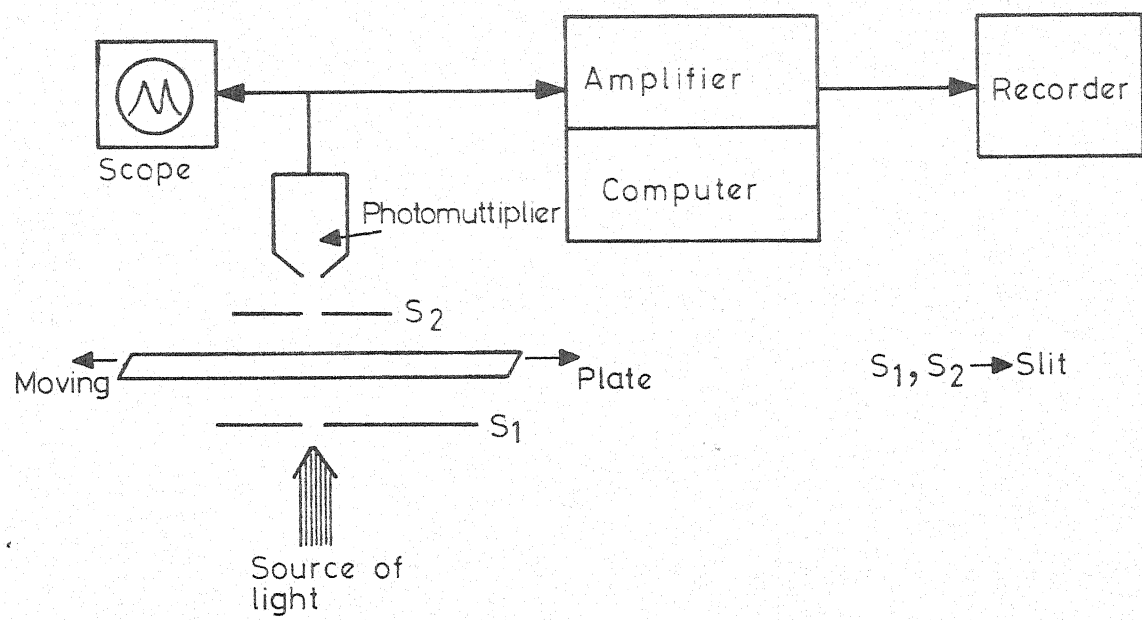


Fig. 2 .10 Block diagram of grant comparator densitometer .

### CHAPTER III

#### THE 341.0 nm BAND SYSTEM OF PYRIDINE N-OXIDE

##### ABSTRACT

The ultraviolet absorption spectrum of pyridine N-oxide has been photographed at high resolution in the range 295.0 - 365.0 nm. The  $\underline{A}_e$ -type contours have been identified in the spectrum for the first time. The observation of both the  $\underline{A}_e$ - and  $\underline{B}_e$ -types of in-plane polarizations in the electronic band contours establishes conclusively that the transition is  $\pi^* \leftarrow \pi ({}^1\underline{B}_2 \leftarrow {}^1\underline{A}_1)$ .

Unambiguous evidence for  $11\underline{a}_1$  and  $10\underline{b}_2$  modes of the compound in  ${}^1\underline{A}_1$  state has been adduced on the basis of a combined study of: (a) its electronic  $\underline{B}_e$ -type of band contours observed for low lying hot bands of the  $\underline{a}_1$  species; (b) its vapour phase  $\underline{A}$ -type band contours observed for all the  $\underline{a}_1$  modes in the infrared spectrum; (c) its far-and ordinary-infrared studies in solid phase and solutions; (d) its laser-excited Raman studies in solid phase; and (e) its analogy with reliable vibrational data on other iso (valence)-electronic molecules. The two types of observed electronic contours have been used to identify the planar  $\underline{a}_1$  and  $\underline{b}_2$  modes in  ${}^1\underline{B}_2$  state also. Equilibrium geometry in the electronically excited state seems to be affected in such a manner as to (a) enhance the over all ring size (b) diminish the N-O bond length and (c) favour a more pronounced quinonoid structure.



The study of 341 nm electronic band system of pyridine N-oxide has been extended to deduce the out-of-plane ( $6b_1+3a_2$ ) modes of the molecule both in its ground ( $^1A_1$ ) and electronically excited first singlet ( $^1B_2$ ) states. The procedure to extract these modes is based primarily on the identification and assignment of the observed 'sequences', 'cross'-sequences and overtones of the fundamentals in the vapour phase electronic absorption spectrum. Additional evidence for  $b_1$  and  $a_2$  modes in  $^1A_1$  state is deduced on the basis of a combined study of (i) the vapour phase c-type band-contours observed for  $b_1$  modes in the infrared spectrum, (2) the far and ordinary infrared studies of the solid compound and its solutions, (3) the laser excited Raman studies in solid phase, and (4) the analogy with reliable vibrational data with other iso (valence)-electronic molecules. The uniqueness of the assignments of the modes has been critically discussed.

### 3.0 INTRODUCTION

Out of the four electronic band systems observed above 180 nm in the electronic spectrum of pyridine N-oxide (abbreviated hereafter to PyO) (1) the lowest energy one is known to exhibit considerable vibrational structure under low resolution (2-3), and has been extensively investigated both experimentally (2-6) and theoretically (7-11). Although, this lowest energy system in electronic spectrum was assigned to  $\pi^* \leftarrow n$  transition originally (2-3), all recent experimental and theoretical findings are indicative of its belonging to a  $\pi^* \leftarrow \pi$  transition (4-11), which following Mulliken convention (12) would correspond to  ${}^1\text{B}_2 \leftarrow {}^1\text{A}_1$  system in analogy with the substituted-benzenes (13-14).

Structural information concerning the ground  ${}^1\text{A}_1$  state of PyO is available on the basis of microwave (15), infrared (16-20), Raman (21-22), normal co-ordinate analysis (23-25), X-ray (26), electron diffraction (27), and other studies (3,5,10) of the compound. However, the vibrational assignments even for  ${}^1\text{A}_1$  state are not coherent. The only vibrational information regarding the excited  ${}^1\text{B}_2$  state could be obtained from the study of electronic spectra (3,5,6). The preliminary vibrational analysis attempted for the lowest observed transition (referred to have as  ${}^1\text{B}_2 \leftarrow {}^1\text{A}_1$ ) on the basis of low resolution studies, without identification of band contours (3), is confined to noting down a few prominent band intervals from the

0,0 (origin) band. Consequently out of the many reported intervals as fundamentals (3), only 4 frequencies each in the  ${}^1\text{B}_2$  and  ${}^1\text{A}_1$  states are totally symmetric  $a_1$  fundamentals. On the basis of high resolution studies of the 0,0 band of 341 nm system of PyO and computer simulation of the band contour, Brand and Tang (5) have assigned this band contour as  $\text{B}_e$ -type with in-plane polarization; perpendicular to the  $\text{C}_2$  axis passing through N-atom. We have now succeeded in identifying the  $\text{A}_e$ -type contours (with polarization along the  $\text{C}_2$  axis passing through the N-atom and in the plane of the molecule) also in this system. Employing the method developed earlier for the gyrovibronic analysis of the corresponding systems of phenol (13) and chlorobenzene (14) we have also been able to obtain accurate vibrational data for most of the fundamental modes in both the  ${}^1\text{A}_1$  and  ${}^1\text{B}_2$  states of the title compound, based primarily on the identification of the  $\text{A}_e$ - and  $\text{B}_e$ -type contours. For establishing the  ${}^1\text{A}_1$  state fundamentals, additional evidence from vibrational spectra of the ground state has also been used. In this chapter planar and non-planar modes of PyO are discussed.

The main effort has been to establish the 30 fundamental modes both for the  ${}^1\text{A}_1$  and  ${}^1\text{B}_2$  states. Reliable vibrational assignments are a key to quantitative normal coordinate analysis which can further be used for testing the transferrability of force-field and coupling of substituent modes with the internal modes of the ring; e.g. in the present case the coupling of NO

modes with other ring modes. The thermodynamic and other observable properties derived from such spectroscopic data could provide a test for the reliability of the vibrational assignments.

Anharmonicities in normal modes of large molecules are found to be small (28) and this is clearly brought out by the present study. Excited state geometry is measurably different from the ground state in PyO and the information obtained both from rotational analysis and vibrational data is correlated qualitatively.

### 3.1 EXPERIMENTAL

Vacuum sublimation apparatus was used for initial purification of the Eastman red label PyO, an extremely deliquescent material. Subsequently, the compound was purified by fractional distillation and stored under vacuum in a pyrex break-seal tube. The compound was put in a side tube of 1.25 meter long cell with 2 inch diameter quartz windows fixed to its ends with epoxy resin. The cell was evacuated to  $10^{-6}$  mm of Hg with the help of a metal diffusion pump assisted with a fore-pump. Absolutely pure and dry compound from the side tube was transferred to the main tube using suitable transferring technique under vacuum. The cell was heated uniformly upto  $90^{\circ}\text{C}$  with heating tapes, heating being boosted by four 250 watt Infrabrooder lamps from Westing House Company; the procedure avoided deposition of the compound onto the windows while recording the spectra. The

spectra were recorded photographically on Spectrum Analysis films in the 15th-18th orders of a 3.4 meter Jarrell Ash Ebert spectrograph fitted with a 57000 - line Harrison grating and assisted with a predisperser arrangement. A high-pressure 150 watt air-cooled xenon-arc lamp was used as a source for absorption studies. Calibration lines were provided by a neon filled Fe-hollow cathode lamp run at 40 milli amp. current. The films were measured with an Abbe comparator from Carl Zeiss Jena and the measurements are good to  $\pm 0.2 \text{ cm}^{-1}$  for unblended lines; the inherent line width and associated rotational structure putting this limit. The microdensitometer tracings were taken on a Grant automatic comparator-densitometer with an amplifier and recorder arrangement.

Vapour phase infrared measurements in  $250 - 4000 \text{ cm}^{-1}$  range were carried out, using a Perkin Elmer-521 spectrophotometer fitted with a variable path 10-m cell in which the compound had to be heated to about  $80^{\circ}\text{C}$  by heating tapes. The infrared spectra of solid PyO and those of its solutions were also recorded on a PE 521 machine. The procedure to record laser excited Raman spectra using Spex 1400 double monochromator and Cary-82 spectrophotometer (cf. Chapter II) and far infrared spectra in the range  $33-525 \text{ cm}^{-1}$  using PE 180 machine have already been discussed (20). All these measurements are good to  $\pm 1 \text{ cm}^{-1}$  for sharp isolated bands.

### 3.2 SELECTION RULES AND NOTATIONS FOR PLANAR MODES OF PyO

Recent microwave (15) and electron diffraction (27) evidence supports a planar  $C_{2v}$  character for the  $^1A_1$  state of PyO. Assuming a planar configuration for  $^1B_2$  state also, the 30 normal modes in each of the  $^1A_1$  and  $^1B_2$  states of the molecule divide into  $11a_1 + 10b_2 + 3a_2 + 6b_1$  species. The activity and polarization characteristics of all the modes in Raman, infrared and electronic spectra for isolated vapour phase molecules are summarised in Table 3.1 for ready reference.

Indexing the assignments in the electronic spectrum becomes easier following the standard notations explained by H.D. Rist et al (29). However, the correlation of modes with the substituted benzenes is somewhat arbitrary because of differential mixing of different internal modes.

#### 3.21 OBSERVED $B_e$ -AND $A_e$ -TYPE CONTOURS

Both the  $B_e$ - and  $A_e$ -type contours observed in the electronic spectrum of vapour phase PyO are red degraded and are given in Fig 3.1. The 0-0 band, all the totally symmetric  $a_1$  fundamentals, as well as all combinations and overtones of the non-totally symmetric modes giving an effective  $a_1$  vibrational symmetry generate  $B_e$ -type profiles (see Fig 3.1(a)) with two intense peaks separated by 3.2 to 4.8  $\text{cm}^{-1}$  with weaker rotational K-structure spread over about 40  $\text{cm}^{-1}$  (5). However, three moderately strong sequences (see appendix 3.1) at -6.0,

-30.2 and -33.3  $\text{cm}^{-1}$  and one stronger one at -16.0  $\text{cm}^{-1}$ , assigned as  $18\text{b}_1^1$ ,  $6\text{a}_1^1$ ,  $1_1^0 18\text{a}_0^1$  and  $11_1^1$ , in that order, interfere very heavily to identify the associated K-structure (5). The sequence structure has now been identified and marked on the top of the band using standard notations explained by Rist et al (29).

Brand and Tang (5) have analysed rotationally - by computer simulation - the 0-0 band profile of this band system. They have established that the vibrationless excited state of the system is  $^1\text{B}_2$  and the inertial constants deduced for this state suggest a fatter ring with significant quinoid structure. Further, it has been suggested that with the same set of inertial constants for both the  $^1\text{A}_1$  and  $^1\text{B}_2$  states, the  $\text{A}_e$ -type selection rules would generate a single main peak in the band profile analogous to that generated in the spectrum of phenol (13) or chlorobenzene (14). The  $\text{A}_e$ -type band contours, now identified in the electronic spectrum (see Fig 3.1 (b)), confirm their predictions. Although, the overall relative intensity of the whole  $\text{A}_e$ -type sub-system is not as low as that of the corresponding sub-system in the spectrum of phenol (14), yet it is significantly smaller than the total contribution from  $\text{B}_e$ -type bands in the system. However, all the inplane non-totally symmetric  $\text{b}_2$  vibrations for the excited  $^1\text{B}_2$  state and several combinations having net  $\text{b}_2$  symmetry have been observed in the spectrum with  $\text{A}_e$ -type profiles. Fig 3.1 (b) shows three typical

$\underline{b}_2$  fundamentals  $3_0^1$ ,  $9\underline{b}_0^1$ , and  $15_0^1$  in  $^1\underline{B}_2$  state and other structure (seq. I and seq. II, representing  $18\underline{b}_1^1$  and  $11_1^1$  sequences, respectively) associated with  $3_0^1$  and  $15_0^1$  bands along with two more identified transitions  $6\underline{a}_0^1$ ,  $6\underline{b}_0^1$  and  $14_0^1$ ,  $16\underline{a}_1^1$ . It is inferred from the analysis that the  $\underline{A}_e$ -type contours are due to 'forbidden' subsystem. The positions of all identified bands involving planar modes along with their qualitative intensities are given in Appendix 3.1.

### 3.22 VIBRONIC ANALYSIS

All the measurements utilized to calculate the vibrational frequencies from electronic spectrum refer to the higher frequency stronger peak of the double headed bands and to the main peak of the single peaked bands.

### 3.23 THE SHIFT OF O-O BAND

The O-O band (designated hereafter as  $T_0$ ) is the most intense  $\underline{B}_e$ -type band with its stronger peak at  $29299.7 \text{ cm}^{-1}$  in the absorption spectrum of PyO vapour at  $90^\circ\text{C}$ . Reliable data are also known for: (i) the gyrovibronic origin,  $T_{00}$ , for the gas phase (5), and (ii) the corresponding positions of the O-O band of the title compound at  $4.2^\circ\text{K}$  in (a) the paradichlorobenzene matrix, and (b) the neat solid (6). These values are summarized in Table 3.2. The significance of the blue shift ( $\Delta T_0$ ) in the matrix spectrum with respect to the gas phase spectrum and/or the analogous shift of  $700.4 \text{ cm}^{-1}$  between the neat solid and the



matrix diluted PyO can not be understood with the meagre vibrational data for the ground and the excited states in the solid phase (6). However, the blue shift of the 0-0 band by  $123 \text{ cm}^{-1}$  at  $4.2^\circ\text{K}$  in PyO with respect to its deuterated analogue (see Table 3.2) is in line with the shift of  $171.5 \text{ cm}^{-1}$  between phenol  $-h_6$  and phenol  $-d_5$  species (13).

### 3.24 THE $a_1$ MODES IN $^1A_1$ STATE

The  $a_1$  modes deduced on the basis of a combined analysis of : (i) the high resolution electronic spectrum, (ii) the infrared band contours and (iii) the laser excited Raman spectrum of PyO are discussed below under separate headings.

#### (i) The High Resolution Electronic Spectrum

The  $a_1$  modes in  $^1A_1$  state for vapour phase are given in column 2 of Table 3.3, the first column giving their approximate description as explained earlier (29). The first figure in column 2 for each of the modes is deduced by calculating the separations of the higher frequency peak of the moderately strong leading B-type 'hot' bands below  $1650 \text{ cm}^{-1}$  from the  $T_0$  band peak at  $29299.7 \text{ cm}^{-1}$ . The leading bands are characterized by an associated sequence structure which is similar to that of the  $T_0$  band. The numbers in parentheses in the second column are the mean values of the modes deduced from the sequence structure by

a method explained earlier (29) and summarized in Table 3.4(a)<sup>1</sup>. The last figure in column 2 is deduced from the vapour phase infrared spectrum (see Section 3.24 (ii), below). Additional evidence for  $a_1$  modes in  $^1A_1$  state adduced from the electronic emission data (6) and Raman and infrared studies of solid samples is summarized in columns 3, 4 and 5, respectively, of the Table. It may be remarked that out of the 10 bands assigned as fundamentals by Hochstrasser et al (6) on the basis of emission data at 4.2°K, four bands belong to the  $a_1$  species involving the N-O bond in some manner or other (See column 3 of Table 3.3); and 4 to the  $b_2$  species (see Column 3 of Table 3.6) while two bands at 1553 (543 + 1013) and 1674 (637 + 1045)  $\text{cm}^{-1}$  may be combination bands.

(ii) The Infrared Band Contours

The replotted infrared band profiles below 1650  $\text{cm}^{-1}$ , except for few C-type bands to be discussed in Section 3.3 are given in Fig 3.2(a). For most of the bands the contour is quite distinct and the positions of P, Q and R peaks (written at the top of each peak) are given in the figure; and thus the observed PR separations,  $\Delta\nu_{PR}$ , can be obtained directly. Few composite bands have been

---

<sup>1</sup> For pyridine N-oxide larger deviations for the combination differences are expected and hence accommodated in the tables. The separations between the two peaks of the  $B_e$ -type bands have been noted experimentally to vary between 4.8 and 3.2  $\text{cm}^{-1}$ . Thus, a variation as large as 1.6  $\text{cm}^{-1}$  between the two peaks suggests a large change in the gyro vibronic origins of different bands due to coriolis and other interactions; naturally leading to the observed combination differences.

resolved and profiles have been isolated by dotted curves. In A - and C-type bands (30-31) the Q branch contributing has also been shown qualitatively by dotted lines. The ratio  $I_Q/I_{\text{Total}}$  (where  $I_Q$  is the intensity of the Q branch and  $I_{\text{Total}}$  the intensity of the complete band profile) has been measured for all A - and C-type bands, by a procedure explained in Refs. (30,31); and the values are given along with each contour in Fig 3.2.

The computed PR separations for A-, B- and C-type bands and the ratio  $I_Q/I_{\text{Total}}$  for A-type bands along with other relevant parameters explained in Ref. (31) are summarized in Table 3.5, for the sake of completeness. These computed values of  $\Delta\nu_{\text{PR}}$  and  $I_Q/I_{\text{Total}}$  are especially helpful in isolating the overlapping contours by graphical resolution technique (31). It is interesting to note that though there is expected discrepancy of about  $\pm 12$  percent between the computed and observed values of  $I_Q/I_{\text{Total}}$  ratio, almost all of the observed  $\Delta\nu_{\text{PR}}$  values agree exactly with the computed  $\Delta\nu_{\text{PR}}$  separations. The A-type IR band contours are the primary source for ascertaining the totally symmetric fundamentals above  $1046 \text{ cm}^{-1}$ ; especially so in the CH stretching region (Cf Fig 3.2b). The Q peak positions of fundamental IR bands summarised in the second column (last figure) of Table 3.3 exhibited an excellent agreement with the frequencies of various a<sub>1</sub> modes deduced from electronic spectrum.

There are four other bands in Fig 3.2a, which are not included in Table 3.3. One of them is the C-type band with Q-peak at  $508.5\text{ cm}^{-1}$  (32) and the other bands at 993.0, 1065.0 and  $1081.5\text{ cm}^{-1}$  can be explained as combinations  $(11)_1(10b)_1$ ,  $(11)_1(10a)_1$  and  $(6a)_2$ , in that order.

(iii) The Laser - Excited Raman Spectrum

The internal mode region of the laser excited Raman spectrum is given in Fig 3.3 from which the peak frequencies are summarised in the fourth column of Table 3.3 for  $a_1$  modes, in the fourth column of Table 3.6 for  $b_2$  modes and in Table 3.7 for the rest of the bands. The ring breathing mode 1 and symmetric CH stretching mode 2 appear as the most intense bands and other totally symmetric bands characterized by low depolarization ratio (33) have moderate intensity. The  $b_2$  modes which also appear with moderate intensity have high value of depolarization ratio. It is interesting to note that  $b_1$  fundamentals do not show up markedly in the Raman spectrum.

There is a good agreement between IR vapour and Raman solid frequencies except for X-sensitive mode  $7a$  which is weak and broad in the Raman spectrum. Most of the isolated Raman bands have Lorentzian shapes; the asymmetry is found only in overlapped bands which could be resolved into Lorentzian components. Raman data have been of special use in ascertaining the CH stretching frequencies where the bands are overlapped in the vapour IR spectrum.

### 3.25 $a_1$ MODES IN $^1B_2$ STATE

All the excited state totally symmetric  $a_1$  fundamental modes produce the typical  $B_e$ -type contours associated with sequence structure similar to that with  $T_0$  band. The frequency of each of these modes is deduced by subtracting the  $T_0$  position from the stronger peak of the identified leading  $B_e$ -type 1-0 band; all the frequencies thus obtained are the first figures in column 6 of Table 3.3. The mean values of different modes deduced from sequence structure and summarized in Table 3.4(b) are also given in parentheses in the 6th columns of Table 3.3. The sequences and cross-sequences connecting  $a_1$  fundamental modes are shown in Fig 3.4 (a). The  $a_1$  modes in the  $^1B_2$  state are corroborated by the overtones and combination bands (given in Appendix 3.1) lying towards the higher frequency side of the  $T_0$  position. Out of the eight bands observed in  $^1B_2$  state in the absorption spectrum of PyO in p-dichlorobenzene matrix at 4.2°K (6) five are definitely attributable to the  $a_1$  modes as summarized in the 7th column of Table 3.3, and two to the  $b_2$  modes (see column 7 of Table 3.6). The band at +1513  $\text{cm}^{-1}$  seems to be a combination transition  $6a_0^1 18a_0^1$  (harmonic value + 1522  $\text{cm}^{-1}$ ), although it could belong to CC stretching mode  $8a$  in the excited state.

### 3.26 $b_2$ MODES IN $^1A_1$ AND $^1B_2$ STATES

The  $b_2$  modes in the  $^1B_2$  state are observed as the  $A_e$ -type profiles, associated with  $A_e$ -type sequence structure. The frequencies for these modes in the  $^1B_2$  state, deduced from the separations of the leading  $A_e$ -type band peaks from the stronger peak of the  $T_0$  band, are summarized in sixth column of Table 3.6; the values in the parentheses being the mean derived from sequence structure explained in Table 3.4(c). The sequences and cross-sequences connecting  $b_2$  fundamental modes are shown in Fig 3.4(b). The observed combinations and overtones of the bands have been given in Appendix 3.1. The  $A_e$ -type hot bands have not been observed and hence the ground state  $b_2$  fundamentals have been deduced with the help of observed sequences and cross-sequences connecting the ground and excited state  $b_2$  fundamentals. The lowest  $b_2$  fundamental mode  $18b$  in  $^1A_1$  state has been fixed from the observed sequence  $18b_1^1$  (at  $-6.0 \text{ cm}^{-1}$ ) leading to the fundamental  $18b_1^0$  at  $469.3 \text{ cm}^{-1}$ , which is in excellent agreement with the Raman depolarized band at  $470 \text{ cm}^{-1}$ . Other ground state  $b_2$  fundamentals of PyO, established on the basis of sequences and cross-sequences explained in Table 3.4(d), are given in parentheses in column 2 of Table 3.6. The assignment of most of the  $b_2$  fundamentals in the  $^1A_1$ -state is supported by the depolarized Raman bands (33) and infrared bands of solid PyO given respectively in columns 4 and 5 of Table 3.6.

### 3.27 DIFFERENCES WITH ANALOGOUS MODES OF PHENOL AND CHLOROBENZENE

In Figs 3.5 (a) and 3.5 (b) we have illustrated the  $\underline{a}_1$  and  $\underline{b}_2$  vibrations, respectively, of PyO and two other iso (valence)-electronic aromatic molecules phenol (29) and chlorobenzene (14), both in their  $^1\underline{A}_1$  and  $^1\underline{B}_2$  states. The best values for the vibrational frequencies are written at the center for each of the molecules and are distributed to scale in the figure, except for suitable breaks in the ordinates, whenever necessary. The gyro-vibronic origin ( $T_{00}$ ) for  $^1\underline{B}_2 \leftarrow ^1\underline{A}_1$  transition is also given in the figures for all the three molecules. The levels depicting analogous modes have been joined by dotted lines for the three compounds, though the analogy between different modes can not be taken too rigorously. The  $\underline{a}_1$  modes in both the ground and the excited states of PyO show a general enhancement in their magnitudes with respect to the corresponding modes of phenol and chlorobenzene in both the  $^1\underline{A}_1$  and  $^1\underline{B}_2$  states, except for the mode 19a which is lower for PyO in both the states. This change may be due to the CN stretching contributions in the mode 19a. In phenol and chlorobenzene, the mode 19a corresponds to the CC stretching in the phenyl ring. Two of the  $\underline{b}_2$  fundamental modes 18b and 6b in PyO are higher for both the ground and the excited states with respect to their counterparts in phenol and chlorobenzene. The modes 15, 9b, and 8b have similar values for all the

three molecules in their  ${}^1\text{A}_1$  states; but in the excited state obviously due to the intermixing of various modes, they do not show a regular pattern. Another  $\text{b}_2$  mode 14 in PyO is lower in the ground state and higher in the excited state as compared to the corresponding mode of phenol or chlorobenzene. The other remaining  $\text{b}_2$  fundamental modes 3, 19b, 7b and 20b of PyO are lower in both the states. These small changes in frequencies of  $\text{b}_2$  modes can be explained as due to the presence of NO bond in PyO.

### 3.28 INTENSITY DISTRIBUTION AND PRINCIPAL PROGRESSIONS

The intensities are given in Appendix 3.1 in a quantitative manner for all the bands observed in electronic absorption spectrum. Amongst the totally symmetric  $\text{a}_1$  fundamentals, the modes 6a and 12 are strongly coupled in both the ground and the excited states. The ring breathing mode 1 is medium strong (obviously due to low Boltzmann factor) in the  ${}^1\text{A}_1$ -state and very strong in  ${}^1\text{B}_2$ -state. The other prominent  $\text{a}_1$  modes are 18a, 7a and 19a in the electronic absorption. The transitions  $15_0^1$ ,  $9\text{b}_0^1$ ,  $3_0^1$  and  $14_0^1$  coupling the  $\text{b}_2$  modes appear with moderate intensity and others are weaker.

The principal progressions in the  ${}^1\text{B}_2$ -state are formed by the modes 6a, 12 and 18a with 2, 4 and 3 members, respectively. In addition each of the modes 9a, 7a, 8a, 6b, 15 and 9b appear with two members. In these progressions the 1-0 band is weaker than 0-0 band and intensity goes on decreasing with higher members of each mode. From the fundamental and first overtones



of these bands, the equilibrium frequency  $\omega_g$  and the anharmonicity  $\omega_e x_e$  have been calculated (28) and summarized in Table 3.8.

From the above analysis we conclude that there is (a) a generalized increase in overall ring size (mode 1) (b) a decrease in NO distance (mode 7<sub>a</sub>) and (c) an increase in ring quinoid structure (mode 8<sub>a</sub>) in the  ${}^1\text{B}_2$  state compared to the  ${}^1\text{A}_1$  state.

### 3.3 SELECTION RULES AND NOTATIONS FOR NON PLANAR MODES

Out of the 30 normal modes of Pyridine N-oxide 11<sub>a<sub>1</sub></sub> and 10<sub>b<sub>2</sub></sub> fundamental modes giving B<sub>e</sub>- and A<sub>e</sub>-type contours respectively in the high resolution electronic spectrum could easily be identified and assigned (34). However, non-planar vibrations are forbidden in the electronic spectrum, and do not appear as 1-0 or 0-1 transitions in the spectrum, since the selection rules for these are given by

$$\Delta v_K = 0, 2, \dots$$

The assignment of non-planar modes is based on the identification of sequence bands, which are mostly strong and fall below  $1200\text{ cm}^{-1}$ . Standard notations have been used for indexing the assignments.

#### 3.31 ELECTRONIC SEQUENCES AND CROSS SEQUENCES

Sequences and cross-sequences connecting b<sub>1</sub> and a<sub>2</sub> fundamental modes are shown in Figures 3.6(a) and 3.6(b). The numbers shown in the middle portion of each figure denote the

approximate intensity of the transitions with respect to arbitrarily chosen intensity of the origin (0-0) band as 100. As 1-0 and 0-1 transitions do not appear in the electronic spectrum for the non-planar  $\underline{b}_1$  and  $\underline{a}_2$  modes, the assignments to these modes have been made from the observed  $\Delta v_k = 0$  and 2 transitions. The combination differences between the pairs of levels having the same symmetry species have been computed from the observed sequences and cross-sequences shown in Tables 3.9 (a) to 3.9 (d).

### 3.32 $\underline{b}_1$ MODES IN ${}^1\underline{A}_1$ AND ${}^1\underline{B}_2$ STATES

For the  $\underline{b}_1$  modes the 1-0 and 0-1 transitions are not observed in the electronic spectrum. Both the ground ( ${}^1\underline{A}_1$ ) and the excited ( ${}^1\underline{B}_2$ ) state  $\underline{b}_1$  fundamentals deduced with the help of connecting sequences and cross-sequences are summarised in columns 2 and 5 (in parentheses) of Table 3.10. The observed combinations and overtones of the bands have been given in Appendix 3.1.

The assignment of the mode  $16\underline{b}$  in  ${}^1\underline{B}_2$  is supported by its overtone 2-0 transition  $16\underline{b}_0^2 = 723.6 \text{ cm}^{-1}$  giving the fundamental  $16\underline{b}_0^1 \sim 361.8 \text{ cm}^{-1}$ . Starting with this level as base value frequencies of each of the fundamentals have been thus calculated by adding or subtracting the combination differences from the base frequency (see Table 3.9(a)).

The ground state  $b_1$  fundamentals are also deduced from the same set of levels by making suitable combination differences as shown in Table 3.9(b). Few identified overtone bands (e.g.  $16b_2^0$  at  $-1019.0 \text{ cm}^{-1}$  giving harmonic  $16b_1^0$ , at  $-509.5$ ) and the observed C-type infrared bands with strong Q branches centered near the frequency deduced from sequence structure are a good testimony for the correct identification of electronic transitions.

(i) C-type Infrared Bands

The replotted prominent C-type bands of vapour phase infrared spectrum of PyO are given in Fig 3.7. Out of three C-type bands, the contour is quite distinct for the two, and the positions of P, Q and R peaks (written at the top of each peak) are directly available in the spectrum. These distinct bands having the characteristic shapes are located with Q-peaks at  $671.0$ , and  $758.5 \text{ cm}^{-1}$ . However, another C-type band with Q-peak at  $508.5 \text{ cm}^{-1}$  has been isolated using the graphical resolution technique (30), shown qualitatively by dotted lines. The relative Q-branch intensity ( $\frac{I_Q}{I_{\text{Total}}}$ ) for C-type bands has been calculated and given at the top of each contour except for the band with Q-peak at  $671.0$ . The intensities were measured by following procedure discussed in Refs.(30,31).

The computed PR separations and the intensity ratio  $I_Q/I_{\text{Total}}$  for A-type bands is given in Table 3.5. There is a satisfactory agreement between the observed and calculated values of PR

been obtained with the help of the observed sequence and overtone bands, following the method discussed in the earlier section for  $\underline{b}_1$  modes. The frequencies thus obtained are summarised in columns 2 and 4 of Table 3.11 for the  ${}^1\text{A}_1$  and  ${}^1\text{B}_2$  states respectively. The observed combinations and overtones of the  $\underline{a}_2$  modes for PyO are given in the Appendix 3.1 along with those for other fundamental modes.

To fix the mode  $16\underline{a}$  in  ${}^1\text{A}_1$  state, use has been made of the observed overtone transition  $16a_2^0 = -830.9$ , giving  $16a_1^0 = 415.4 \text{ cm}^{-1}$ . This assignment is well supported by a solid phase for infrared band at  $415.0 \text{ cm}^{-1}$  shown in Fig 3.8. The 1-0 transition of the mode  $16\underline{a}$  could now be easily deduced by using the sequence transition  $16a_1^1 = -251.2 \text{ cm}^{-1}$  giving  $16a_0^1 = +164.2 \text{ cm}^{-1}$ . This transition is well supported by the overtone transition  $16a_0^2 = +330.2$ . The other  $\underline{a}_2$  fundamentals are deduced in the similar method as shown in Table 3.9 (c) and 3.9 (d). Ito and Mizushima (3) have assigned some of the prominent bands in the  ${}^1\text{A}_1$  state, e.g. the bands at  $-251.2$  and  $-275.0 \text{ cm}^{-1}$  as the 0-1 transitions of the  $\underline{b}_1$  fundamentals which are not consistent with the present study. The intense bands at  $-251.2$  and  $-275.0 \text{ cm}^{-1}$  are undoubtedly the 1-1 transitions of the  $\underline{a}_2$  modes  $16\underline{a}$  and  $17\underline{a}$  respectively, connecting the ground and excited state fundamentals.

### 3.34 DIFFERENCES WITH ANALOGOUS MODES OF PHENOL AND CHLOROBENZENE

Figures 3.9 (a) and 3.9 (b) show the  $\underline{b}_1$  and  $\underline{a}_2$  fundamental modes of PyO and two other iso (valence)-electronic aromatic

molecules phenol (13) and chlorobenzene (35) both in their  $^1\text{A}_1$  and  $^1\text{B}_2$  states. The vibrational frequencies are written at the center for each of the molecules and are distributed to scale in the figure, except for suitable breaks in the ordinates, whenever necessary. The gyrovibronic origin  $T_{00}$  for  $^1\text{B}_2 + ^1\text{A}_1$  transition is also given in the figures for all the three molecules. The levels depicting analogous modes have been joined by dotted lines for the three compounds, though the analogy between different modes can not be taken too rigorously. All the  $\text{b}_1$  and  $\text{a}_2$  fundamental modes of PyO both in  $^1\text{A}_1$  and  $^1\text{B}_2$  states are almost similar with respect to the corresponding modes of phenol, except the  $\text{b}_1$  modes 10b, 17b and 5 which are higher in  $^1\text{B}_2$  state. General enhancement of the modes has been found for all the  $\text{b}_1$  fundamentals for PyO in  $^1\text{B}_2$  state with respect to those for chlorobenzene, whereas a good agreement between the  $\text{a}_2$  fundamental modes of PyO and chlorobenzene has been found both in the ground and the excited states.

As explained in a recently communicated paper (32) for planar modes the changes of some of the  $\text{b}_1$  fundamental modes in  $^1\text{B}_2$  may also be due to the presence of NO bond in PyO. The modes 10b and 17b have the CN torsion and NO out of plane bending contribution respectively and hence enhancement of the frequencies has been observed. The change of the mode 5 (which corresponds to  $\nu_{\text{CH}}$ ) is due to the increase in ring quinonoid structure.

### 3.4 INFRARED SPECTRA OF PYRIDINE N-OXIDE IN SOLUTIONS

The infrared spectrum of PyO and its metal complexes were reported earlier (16, 18, 36) in the range 250-2000  $\text{cm}^{-1}$ . The frequencies above 2000  $\text{cm}^{-1}$  are not available in the literature except few in CH stretching region.

In the present study of the high resolution infrared spectra of PyO in vapour and solid phases, we have been able to resolve the complex structure of the bands in the region 250-1650  $\text{cm}^{-1}$  and is discussed in sections 3.24 & 3.32. To record the weak bands of PyO, 0.05 mm and 0.1 mm thick CsBr liquid cells were used and the infrared spectrum of free ligand of PyO in  $\text{Cs}_2$  and  $\text{CCl}_4$  solutions at different concentrations were recorded. Some of the bands of free PyO (in solutions) are strong but weaker in vapour and solid phases. The frequencies thus obtained have been listed in columns 4 and 5 of Table 3.12 along with those for vapour and solid phases of PyO. The relative intensity of each band has been shown in different columns of the Table. The frequencies of the fundamental modes of PyO observed in vapour, solutions and solid phases (at different temperatures) and their observed combinations have been critically discussed and a suitable assignment is suggested.

### 3.5 INTENSITIES OF INFRARED BANDS

The infrared spectra of PyO in vapour, solid (at room temperature and INT) and in solutions are shown in Figs 3.2, 3.10 and 3.11, respectively. The positions of the bands and

their intensities with approximate description has been given in Table 3.12. The following points have been observed:

The vibrations belonging to  $\underline{a}_1$  class share most of the intensity in the infrared absorption spectra except the mode  $\underline{18a}$  which is weak in solid phase but medium intense in vapour phase and solutions. The ring breathing mode 1 and CC stretching mode  $\underline{19a}$  invariably appear with maximum intensity in all the three phases.

The intensity of the bands belonging to  $\underline{b}_1$  class is similar to that for  $\underline{a}_1$  class. All the modes are strong in the infrared spectra except  $\underline{17b}$  and 5 which are weak in solid and vapour phases but are relatively stronger in solutions. The CH out-of-plane bending mode  $\underline{10b}$  of the compound is very strong in all the phases.

The  $\underline{b}_2$  fundamental modes have not been observed in the vapour phase infrared spectra. But modes progressively gain intensity on going from solid phase to solutions. The mode 14 has not been observed in the infrared spectra. The assignments to this mode was made on the basis of Raman and vapour phase electronic spectra discussed in

Sections 3.34 and 3.26. The mode  $18b$  is strong in the infrared spectra in all the phases. Modes  $6b$ ,  $15$ ,  $19b$  and  $8b$  are weak in solid phase but medium intense in  $ccl_4$  and  $cc_2$  solutions. The CH in-plane bending mode  $3$  is missing in solid phase but in solutions this mode has appeared with medium strong intensity. Most of  $b_2$  modes which have gained intensity are bending ones or those associated with the ring.

The intensity of CH stretching vibrations is maximum in vapour phase and decreases considerably on going to solutions and solid phase except for the mode  $20b$  which is missing in vapour and solid phases, but has appeared with strong intensity in solutions. The  $a_2$  class vibrations were not observed in the vapour phase infrared spectra as they are forbidden by symmetry selection rules. However the lowest  $a_2$  mode  $16a$  has appeared as a weak band in the solid phase for infrared spectrum of PyO.(20).

The fundamental modes of PyO do not show much difference in frequencies in different phases of infrared spectra. The ring breathing mode  $1$  of  $a_1$  species is almost similar in all the phases. The differences in other modes are within experimental limitations except the x-sensitive  $a_1$  fundamental mode  $7a$ . However, the x-sensitive modes show up relatively larger differences on going from vapour to solid phase of PyO and also in solutions. The largest difference in frequencies of mode  $7a$  may



be regarded as arising from the decrease of  $N = O$  double bond character which may be due to  $N-O$  dipole association (36). The mode  $7a$  is very strong in all the phases and has smallest value in solid phase and maximum in vapour. In solutions the observed value of this mode is intermediate.

Knowing the complex structure of bands in the region  $250-1650\text{ cm}^{-1}$ , observed in vapour phase IR spectra we have explained all the binary combinations over the total range  $250-4000\text{ cm}^{-1}$ . It has been found that the out of plane fundamental vibrations of  $b_1$  and  $a_2$  symmetry and totally symmetric  $a_1$  fundamentals form most of the combinations that have been observed. The non totally symmetric  $b_2$  fundamentals have shown a few combination bands. The most intense binary combination has been observed in the infrared spectra of PyO in solutions with the combination of  $b_1$  and  $a_2$  fundamental modes ( $17b + 10a$ ) at  $1716\text{ cm}^{-1}$  ( $\text{CCl}_4$  soln.). The x-sensitive fundamental modes of the compound under discussion form most of the combination bands listed in table 3.12. The intensities of the binary combinations in different phases in general have been found to be below 20% of the strongest band in the spectra. As the intensity of the combination bands is a complex function of mechanical and electrical anharmonicities, it is not possible to give an ab-initio explanation of the observed intensities.

### 3.6 LOW TEMPERATURE STUDIES

No data on low temperature studies of PyO compound are available in literature. This is primarily because the compound PyO is extremely deliquescent, and has very low vapour pressure, which makes difficult of the deposition of its vapour onto the cold finger of low temperature cell. We have been able to make a water free microcrystalline film of the compound on the cesium bromide windows after evacuation of the cell for a long time.

In the infrared spectra of microcrystalline film of PyO at LNT certain new bands have been observed (cf in Fig 3.10b) over tones and have been assigned as the fundamentals overtones combination bands. The vibrational modes of PyO belonging to  $\underline{b}_2$  species could not be observed in the vapour phase IR spectra and some of them (e g mode  $\underline{3}$ ) are missing in solid phase spectra also, at room temperature. But at liquid nitrogen temperature all the  $\underline{b}_2$  modes of PyO have appeared (cf Table 3.12) in the solid phase infrared spectra. The  $\underline{b}_2$  mode 19b is very weak at LNT and has been shown with asterisk. The  $\underline{a}_1$  mode 18a has not been observed at liquid nitrogen temperature several overtones and combination bands of low lying fundamental modes e.g.  $(6a)_1$   $(11)_1$ ,  $(6a)_2$  and  $(6b)_1$   $(18b)_1$  have been observed at liquid nitrogen temperature, but absent in solid phase IR spectra at

room temperature. However, these modes of PyO have appeared in  $\text{CCl}_4$  and  $\text{CS}_2$  solutions.

In PyO molecule the solid phase splittings do occur in a few fundamental vibrational bands as shown in Table 3.12. The possibility of the site group splitting of the infrared bands may be ruled out, because there are no degenerate modes of vibration in PyO. But the factor group splitting may occur due to resonance interaction between inequivalent molecule in the unit cell. It may always be small in magnitude and depends on number of molecules per unit cell. The crystal structure of the compound PyO has recently been investigated (26). It belongs to the space group  $D_2^5$  in the orthorhombic class and has 8 molecules per unit cell. The site symmetry of the molecule is  $C_2$ .

Most of the totally symmetric  $a_1$  modes show shift in their band positions towards high frequency side on going from room temperature to INT. However, the modes 12 and 1 do not show any shift in their band positions. The fundamentals  $9a$  and  $8a$  get splitted in two bands. The  $b_2$  modes 3 and  $8b$  have resulted due to this splitting at INT.

The  $b_2$  modes (of Table 3.12) do not show larger shifts in frequencies. However, the lowest  $b_2$  fundamental mode  $18b$  gets splitted into two at INT. The band positions of these splittings are  $467.2$  and  $470.0 \text{ cm}^{-1}$  which have been assigned

to  $(18b)_1$  and  $(11)_2$  respectively. The  $b_1$  modes have shown, in general, shift in their band positions towards high frequency side. The maximum shift has been observed in the X-sensitive  $b_1$  fundamental mode  $16b$ . The  $b_1$  fundamental mode  $10b$  gets splitted in two bands. The band at  $783\text{ cm}^{-1}$  observed at LNT has been assigned as the combination of  $a_1$  and  $b_1$  fundamental modes ( $6a + 11$ ). The CH stretching frequencies do not show any remarkable shifts at LNT. From the above spectral behavior of the compound PyO at LNT we conclude that the width of the bands and some of the observed frequencies of the fundamental modes are temperature dependent. The temperature dependence of these frequencies of fundamental modes is largely due to Pseudo-harmonicity (37). The general shift of the frequencies is towards higher frequencies on cooling. Because of the superimposition of the fundamentals, overtone or combination bands having approximately the same frequency the bands show larger band width at room temperature. These bands get splitted on cooling.

### 3.7 LATTICE MODES OF PYRIDINE N-OXIDE

The replotted ( $35\text{--}170\text{ cm}^{-1}$ ) and retraced ( $200\text{--}525\text{ cm}^{-1}$ ) portions of the far infrared spectrum is given in Fig 3.8. From the spectrum the frequency  $\nu$  of the band peaks and their qualitative relative intensities are given in Column 1 of Table 3.13(a). The Raman data of solid PyO are given in column 2 of the Table. For the liquid phase the IR and Raman data are from earlier work (17). The vapour phase data have also been given in columns

5 and 6 of Table 3.13(a) for comparison. The three lattice modes deduced from a Lorentzian analysis of the replotted Far infrared contour in the range 35 to 170  $\text{cm}^{-1}$  are also given (cf Table 3.13(a)).

The intense bands at 513, 466, and 415  $\text{cm}^{-1}$  given in far infrared have already been explained (20) in earlier sections, and unambiguous assignments of these frequencies are given in column 7 of Table 3.13 (a). The three observed bands in the lattice mode region are too few and broad to arrive at unambiguous assignments, especially as the solid is known to have eight molecules per unit cell (26), and in all 24 librational and 21 translational optical phonons for the  $D_2^5$  space group would be expected (22). However, on comparison with the laser excited Raman spectra of diazines (38), and PyO (22), in the lattice mode regions, the highest of the three observed modes at 112, 86  $\text{cm}^{-1}$  could be attributed to a librational (L) mode and the lowest at 56  $\text{cm}^{-1}$  to a translational mode (T) mode.

The lattice Raman spectrum reported earlier (22) has been resolved again and shown in Fig 3.12, taking the exciting line to be very intense. The positions of stokes and antistokes Raman bands of solid pyridine N-oxide has been given in Table 3.13(b). The peak positions are the same as reported earlier (22), but the intensities of all the bands is different.

### 3.8 MOLECULAR GEOMETRY

The PyO molecule is planar in its ground ( $^1A_1$ ) state as suggested by (i) its definite A- and C- type vapour phase

infrared band contours (ii) the  $\underline{B}_e$ -type envelopes of the 'hot' bands observed in the electronic spectrum (iii) Raman polarization data (33) and (iv) the smallness of inertial defect observed from the microwave studies (15). Assuming a planar ring with the bond lengths and bond angles described by Chiang (27) we have illustrated in Fig 3.13 the most probable and simplest conceivable geometry of PyO in its ground state as computed on IBM 7044 computer. The computed parameters are corresponding to the best fit of the observed rotational constants (15) shown in Table 3.5. We have also mentioned the coordinates of all the atoms in the centre of mass system for better understanding. In Fig 3.13, Z-axis has been shown as the symmetry axis, which passes through the H, C, N and O atoms. The Y coordinates on this axis have also been shown at the 4th decimal points, which indicate some infinitesimal bend of the symmetry axis, and hence the proposed molecular geometry needs some minor modifications.

### 3.81 THEORETICAL CALCULATION OF FUNDAMENTAL MODES

The fundamental modes of Pyridine N-oxide have been computed by normal coordinate calculations using Wilson's G-F matrix method (39, 40). These calculations have been performed on IBM 7044 using the programme used earlier by Schachtschneider et al (41). The Programme is set up in internal displacement coordinate and is similar to that adopted by Overend and Scherer (42). The programme is designed to determine the cartesian

coordinates and to evaluate G and Z matrices. The assumed geometry and the definition of the internal coordinates of PyO are given in Tables 3.14 and 3.15. The normal modes of vibration, the L-column vectors, the PED among the diagonal elements of F matrix, the mean square amplitude of the individual atoms for each mode and mean amplitude for atoms summed over all normal modes are obtained as output in a tabulated form. A simplified UBFF comprising of force constants transferred from benzene (43) and chlorobenzene (44) is set up. During calculations, minor and systematic alternations in stretching, bending wagging and torsional force constants given in Table 3.16, have been made in order to fit to observed frequencies of Pyridine N-oxide. The observed and computed vibrational frequencies are listed in Table 3.17.

### 3.9 CONCLUSION

#### (i) Nature of Transition

The 341 nm band system has been unambiguously attributed to  $\pi^* \leftarrow \pi$  ( ${}^1B_2 \leftarrow {}^1A_1$ ) transition by identifying the  $\underline{A}_c$ -type band contours and  $\underline{b}_2$  fundamentals in the excited state. This is in conformity with the recent calculations of Leibovici and Streith (11) and predictions of Brand and Tang (5) who suggested that phenol-like single main peak in  $\underline{A}_c$ -type contours would be generated as a result of changes in the inertial constants and thereby simulating the  $\underline{B}_c$ -type band contour identical to the observed 0,0 (origin) band.

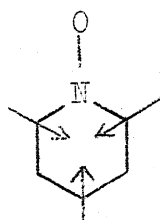
(ii) Geometry Change in the Excited State

The rotational analysis of the O-O band of the system by Brand and Tang (5) and the present vibronic analysis suggest a small but observable geometry change on going from  $^1\text{A}_1$  to  $^1\text{B}_2$  state. Exact geometric parameters cannot be calculated in the excited state by the limited data in hand but qualitatively it is inferred that

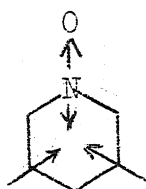
(a) the overall ring size is increased in the excited state (mode 1 goes from  $1013\text{ cm}^{-1}$  in  $^1\text{A}_1$  state to  $978\text{ cm}^{-1}$  in  $^1\text{B}_2$  state).

(b) N=O bond length is decreased in the excited state (mode 7a is increased from  $1303$  to  $1323\text{ cm}^{-1}$ ). One can, therefore, estimate the shortening of N=O bond by applying Badgers rule Clarks rule, etc.

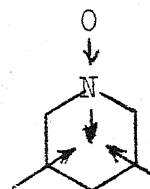
(c) A more pronounced triangular distortion in the ring (mode 12 is decreased from  $842\text{ cm}^{-1}$  in  $^1\text{A}_1$  state to  $818\text{ cm}^{-1}$  in  $^1\text{B}_2$  state) given as follows (cf Fig 1.1).



(1)



(7a)



(12)

(iii) Vapour-Solid Changes

It seems that there is a very large change both in geometry and electronic charge distribution on going from the vapour to the solid phase even at room temperature. The evidence available from electron diffraction (27) and X-ray studies (26)



clearly brings out that N=O bond changes from 1.29 Å to 1.35 Å (1.35 and 1.37 Å in the two inequivalent molecules of PyO in crystalline solid). Comparing corresponding changes in phenol where  $\Delta r_{\text{CO}} = 1.379$  Å and  $r_{\text{CO}}^* = 1.30$  Å and  $\Delta r_{\text{CO}} = 0.08$  Å it is seen that a change of  $r_{\text{NO}}$  in PyO equivalent to 0.06 Å is fairly large. This change in electron structure both in the ground and excited states is also exhibited by the large change in the 0,0 transition on going from vapour to p-dichlorobenzene host crystal and then to pure solid form, as given in Table 5.2, 29295.4 cm<sup>-1</sup> in vapour, 29599.6 cm<sup>-1</sup> in pDCB and 30300.0 cm<sup>-1</sup> in neat solid. Thus considerable redistribution of charge takes place on going from vapour to solid even in  $^1\text{A}_1$  state whereas subsequent change on going from  $^1\text{A}_1$  solid to  $^1\text{B}_2$  solid is smaller.

REFERENCES

1. M. Yamakawa, T. Kubota and M. Akazawa, *Theoret. Chim. Acta* 15, 244 (1969).
2. M. Ito and N. Hata, *Bull. Chem. Soc. Japan* 28, 260 (1955)
3. M. Ito and W. Mizushima, *J. Chem. Phys.* 23, 495 (1956)
4. K. Siebold, G. Wagniere and H. Labhart, *Helv. Chim. Acta* 52, 789 (1969).
5. J.C.D. Brand & K.T. Tang, *J. Mol. Spectrosc.* 39, 171 (1971).
6. R.N. Hochstrasser & D.A. Wiersma, *J. Chem. Phys.* 55, 5339 (1971).
7. J. Sidman, *Chem. Rev.* 58, 689 (1958)
8. E.M. Evleth, *Theoret. Chim. Acta (Berl)* 11, 145 (1968).
9. J.D. Bene and H.H. Jaffe, *J. Chem. Phys.* 49, 1221 (1968)
10. S. Kobinata and S. Nagakura, *Theoret. Chim. Acta (Berl)* 14, 415 (1969).
11. C. Leibovici and J. Streith, *Tetrahedron Lett.* 5, 387 (1971)
12. R.S. Mulliken, *J. Chem. Phys.* 23, 1997 (1955).
13. H.D. Bist, J.C.D. Brand and D.R. Williams, *J. Mol. Spectrosc.* 24, 413 (1967).
14. H.D. Bist, V.N. Sarin, A. Ojha and Y.S. Jain, *Applied Spectrosc.* 24, 292 (1970).
15. R.D. Brown, F.R. Burden and W. Garland, *Chem. Phys. Letters* 7, 461 (1970).
16. Y. Kakiuti, S. Kida and J.V. Quagliano, *Spectrochim. Acta* 19, 201 (1963).
17. P. Mirone, *Atti Acad. Nazl. Lincei, Rend., Classe Sci. Fis., Mat. Nat.* 35(b), 530 (1963).
18. D.H. Brown, D.T. Stewart and D.H. Jones, *Spectrochim. Acta* 29A, 213 (1973).

19. S. Ghersetti, S. Giorgianni, P.L. Capurcci and S. Spunta, *Spectrochim. Acta* 29A, 1207 (1973).
20. H.D. Bist and J.S. Parihar, *Chem. Phys. Letters* 32, 244 (1975).
21. K. Ramaiah and V.R. Srinivasan, *Proc. Ind. Acad. Sci.* A50, 213 (1959).
22. P.R. Pujari and H.D. Bist, *J. Raman Spectrosc.* 1, 255 (1973).
23. G. Costa and V. Galasso, *Atti Acad. Nazl. Lincei, Rend., Classe Sci., Fis., Mat. Nat.* 37(5), 289 (1964).
24. V.I. Berezin, *Opt.Spectrosc.(USSR)*, 18, 119 (1965).
25. Y. Kakiuti, H. Saito and M. Akiyama, *J. Mol. Spectrosc.* 35, 66 (1970).
26. D. Ulku, B.P. Huddle and J.C. Morrow, *Acta Cryst.* B27, 432 (1971).
27. J.F. Chiang, *J. Chem. Phys.* 61, 1280 (1974).
28. H.D. Bist, V.N. Sarin, A. Ojha and Y.S. Jain, *Spectrochim. Acta* 26A, 841 (1970).
29. H.D. Bist, J.C.D. Brand and D.R. Williams, *J. Mol. Spectrosc.* 21, 76 (1966).
30. M.M. Rai, H.D. Bist and D.P. Khandelwal, *Appl. Spectrosc.* 25, 442 (1971).
31. V.N. Sarin, M.M. Rai, H.D. Bist and D.P. Khandelwal, *Chem. Phys. Lett.* 6 473 (1970).
32. H.D. Bist, J.S. Parihar and J.C.D. Brand, *J. Mol. Spectrosc.* (in Press).
33. P. Mirone and B. Fortinato, *Atti Accad. Nazl. Lincei, Rend., Classe Sci. Fis. Mat. Nat.* 34(2), 168 (1963).
34. H.D. Bist et al (communicated)
35. Y.S. Jain and H.D. Bist, *J. Mol. Spectrosc.* 47, 126 (1973).

36. S. Kida et al, Spectrochim Acta 19, 189 (1963)
37. P.M.A. Sherwood, Vibrational Spectroscopy of Solids Cambridge University Press (1972).
38. R.H. Larkin and H.D. Stidham, Spectrochim Acta 29, 781 (1973).
39. E.B. Wilson, Jr., J. Chem. Phys. 7, 1047 (1939).
40. E.B. Wilson, Jr., J.C. Decius and P.C. Cross, Molecular Vibrations, McGraw Hill, New York (1955).
41. J.H. Schachtschneider and R.G. Snyder, Spectrochim. Acta 19, 117 (1963).
42. J. Overend and J.R. Scherer, J. Chem. Phys. 32, 1289 (1960).
43. N. Neto, M. Scrocco and S. Califano, Spectrochim. Acta, 22, 1981 (1966).
44. J.R. Scherer, Spectrochim. Acta, 20, 345 (1964).

Table 3.1

Selection rules for  $C_{2v}$  Pyridine N-Oxide in Raman, Infrared  
and Electronic Spectra

Symmetry Species*	Activity†		
	Raman	Infrared	Electronic
11, $\underline{a}_1$	R, p	IR, type- $\underline{A}$ (observed)	UV, $\underline{B}_{\underline{e}}$ -type (observed)
10, $\underline{b}_2$	R, dp	IR, type- $\underline{B}$	XX, $\underline{A}_{\underline{e}}$ -type (observed)
3, $\underline{a}_2$	R, dp	XX	XX $\underline{C}_{\underline{e}}$ -type (not observed)
6, $\underline{b}_1$	R, dp	IR, type- $\underline{C}$ (observed)	XX

\*Nomenclature of species is after Mulliken (12)

†R, IR, UV denote activity in Raman, infrared, and electronic spectra, XX forbidden, p, polarized; dp, depolarized.  $\underline{A}$ ,  $\underline{B}$ ,  $\underline{C}$ , and  $\underline{A}_{\underline{e}}$ ,  $\underline{B}_{\underline{e}}$ ,  $\underline{C}_{\underline{e}}$  denote the type of band-contours in IR and electronic spectra, respectively.

Table 3.2

Band origins,  $T_{00}$ , ( $\text{cm}^{-1}$ ) for  ${}^1\text{B}_2 \leftarrow {}^1\text{A}_1$  transition of  
Pyridine N-Oxide in gas and solid (matrix  
and neat solid) phases

	Gas Phase near RT <sup>(a)</sup>	Solid at 4.2°K <sup>(b)</sup> in		
		p-C <sub>6</sub> H <sub>4</sub> Cl <sub>2</sub> matrix		Pure form
	C <sub>6</sub> H <sub>5</sub> NO	C <sub>6</sub> H <sub>5</sub> NO	C <sub>6</sub> D <sub>5</sub> NO	C <sub>6</sub> H <sub>5</sub> NO
$T_{00}$	29295.4	29599.6	29722.6	30300.0
$\Delta\nu^{(c)}$		304.2	123.0	577.4
$\Delta T_c^{(c)}$	0	304.2	427.2	1004.6

(a) Value of gyrovibronic origin from reference (5) for gas phase

(b) From reference (6)

(c)  $\Delta\nu$  represents the shifts between consecutive columns, and  
 $\Delta T_c$  depicts the shift towards higher frequency from the gas  
phase  $T_{00}$  in C<sub>6</sub>H<sub>5</sub>NO

Table 3.3

a<sub>1</sub> Fundamental Modes (in  $\text{cm}^{-1}$ ) in Vapour and Solid Pyridine  
N-Oxide in  $^1\text{A}_1$  and  $^1\text{B}_2$  States

	$^1\text{A}_1$ State				$^1\text{B}_2$ State	
	Vapour	Solid			Electronic Absorption	
	Absorption ( $360^\circ\text{K}$ )	Electronic Emission ( $4.2^\circ\text{K}$ )	Raman <sup>a</sup> ( $296^\circ\text{K}$ )	IR <sup>a</sup> ( $303^\circ\text{K}$ )	Vapour ( $360^\circ\text{K}$ )	Solid ( $4.2^\circ\text{K}$ )
6 <sub>a</sub>	540.3, (540.3) 540.2	543	544 m	546 s	510.1 (510.1)	527.0
12	842.8, (843.4) 843.5	820	843 s	838.5 s	818.4 (817.4)	766.0
1	1013.0, (1013.8) 1013.3	-	1018 vs	1012.5 vs	978.3 (917.6)	946.0
18 <sub>a</sub>	1044.9, (1045.4) 1046.0	-	1045 ms	1043 m	961.8 (962.7)	995.0
9 <sub>a</sub>	1164.8, (1164.1) 1165.0	-	1170 m	1168 s	1117.1 (1117.1)	-
7 <sub>a</sub>	1303.0, (1302.3) 1302.4	1232	1255 m	1257.5 vs	1323.0 (1322.5)	-
19 <sub>a</sub>	1460.4, (1461.3) 1461.0	1464	1470 w	1463 vs	1480.0 (1479.3)	1417.0
8 <sub>a</sub>	1609.3, (1610.6) 1608.5	-	1604 s	1603 s	1639.2 (1640.1)	1513 ?
13	- 3045.0	-	3040 w	3043 m	3112.3	-
2	- 3076.0	-	3083 vs	3085 s ( $\text{CCl}_4$ soln)	3127.5	-
20 <sub>a</sub>	- 3099.0	-	3110 ms	3100 s	3203.6	-

$$T_0 = 29299.7 \text{ cm}^{-1}$$

a The notations vs, s, ms, m, w denote the intensities of the bands and represent very strong, strong, medium strong, medium, and weak respectively.

Table 3.4(a)

$a_1$  levels; Combination Differences and Fundamental frequencies (in  $\text{cm}^{-1}$ ) for Pyridine N-Oxide for  ${}^1A_1$  State

Attached to Difference	$6a_0$	$12_0$	$18a_0$	$1_0$	$7a_0$	$19a_0$	$8a_0$	Mean	Fundamental Frequency*
$8a_1-6a_1$	-	-	-	-	-	-	1070.3	1070.3	1610.6
$19a_1-6a_1$	-	-	921.7	-	-	920.1	921.2	921.0	1461.3
$7a_1-6a_1$	761.0	762.8	-	760.9	763.4	-	-	762.0	1302.3
$9a_1-6a_1$	-	623.8	-	-	-	-	-	623.8	1164.1
$18a_1-6a_1$	504.5	505.5	-	-	505.5	-	-	505.1	1045.4
$1_1-6a_1$	-	473.1	474.1	-	-	-	473.3	473.5	1013.8
$12_1-6a_1$	302.5	-	-	302.7	304.1	303.5	-	303.1	843.4
$6a_1$									540.3

\*Base value,  $6a_1^0 = 540.3 \text{ cm}^{-1}$  is from observed  $B_{ee}$ -type band at  $T_0 = 540.3 \text{ cm}^{-1}$



Table 3.4 (b)

$a_1$  levels; Combination Differences and Fundamental Frequencies (in  $\text{cm}^{-1}$ ) for Pyridine N-Oxide for  ${}^1\text{B}_2$  State

Attached to Difference	$6a_1^0$	$12_1^0$	$18a_1^0$	$7a_1^0$	Mean	Fundamental Frequency
$8a_0^1 - 6a_0^1$	1129.1	1131.0	-	-	1130.0	1640.1
$19a_0^1 - 6a_0^1$	-	-	969.2	-	969.2	1479.3
$7a_0^1 - 6a_0^1$	813.7	811.9	812.7	811.3	812.4	1322.5
$9a_0^1 - 6a_0^1$	-	607.2	-	606.9	607.0	1117.1
$1_0^1 - 6a_0^1$	467.6	467.2	-	467.7	467.5	977.6
$18a_0^1 - 6a_0^1$	-	-	-	452.6	452.6	962.7
$12_0^1 - 6a_0^1$	308.4	-	307.2	306.4	307.3	817.4
$6a_0^1$						510.1

Table 3.4(C)

$\underline{b}_2$  levels: Combination Differences and Fundamental Frequencies (in  $\text{cm}^{-1}$ ) for Pyridine N-Oxide for  ${}^1\underline{B}_2$  State

Attached to Difference	$18b_1^0$	$6b_1^0$	$15_1^0$	$3_1^0$	$19b_1^0$	$8b_1^0$	Mean	Fundamental Frequency*
$8b_0^1-18b_0^1$	1156.3	-	-	-	1155.4	1154.6	1155.4	1618.7
$19b_0^1-18b_0^1$	978.1	976.3		978.0	978.4	-	977.9	1441.2
$14_0^1-18b_0^1$	831.3	832.4	831.2	-	830.3	-	831.3	1294.6
$3_0^1-18b_0^1$	-	-	-	618.0	621.1	619.0	619.3	1082.6
$9b_0^1-18b_0^1$	596.0	-	-	-	-	596.4	596.2	1059.5
$15_0^1-18b_0^1$	-	-	575.2	576.3	-	-	575.7	1039.0
$6b_0^1-18b_0^1$	101.5	-	101.8	-	-	100.8	101.3	564.7
$18b_0^1$								463.3

\*Base value,  $18b_0^1 = 463.3 \text{ cm}^{-1}$  is from the observed electronic  $\underline{A}_e$ -type band at  $T_0 + 463.3 \text{ cm}^{-1}$ .



Table 3.5

Calculated rotational parameters and PR separations  
at 300°K for IR band contours of Pyridine N-Oxide

Rotational Constants <sup>a</sup> MC/sec	Computed parameters <sup>b</sup>	Calculated $\Delta\nu_{PR}$ and ( $I_Q/I_{Total}$ )
A = 5899.74	$S(\bar{\beta}) = 1.275$	$\Delta\nu_{PR}^A(   ) = 14.5 \text{ cm}^{-1}$
B = 2794.61	$\bar{\beta} = 1.515$	$PR^B(\perp) = 11.5 \text{ cm}^{-1}$
C = 1896.26	$\bar{B} = 2345.435$ MC/sec	$PR^C(\perp) = 21.8 \text{ cm}^{-1}$
		$(\frac{I_Q}{I_{Total}})^A(   ) = 0.22$

- The rotational constants are from microwave study (15)
- The parameters  $S(\bar{\beta})$ ,  $\bar{\beta}$  and  $\bar{B}$  for the near asymmetric top molecules are defined in Refs. (30, 31) along with quantities  $\Delta\nu_{PR}$  and  $(I_Q/I_{Total})$  for A-type bands. Neat B-type bands do not show Q branch under symmetric top approximation and C-type bands have pronounced Q peak (see text).

Table 3.6

117

$\underline{b}_2$  Fundamental Modes (in  $\text{cm}^{-1}$ ) in Vapour and Solid Pyridine  
N-Oxide in  ${}^1\text{A}_1$  and  ${}^1\text{B}_2$  States

Mode	${}^1\text{A}_1$ State				${}^1\text{B}_2$ State	
	Vapour	Solid			Electronic absorption	
	Absorption (360°K)	Electronic emission (4.2°K)	Ramana (296°K)	IR <sup>a</sup> (303°K)	Vapour (360°K)	Solid (4.2°K)
18 $\underline{b}$	-, (469.3)	453	470 m	466 s	463.3 (463.3)	439
6 $\underline{b}$	-, (637.6)	608	637 s	635 w	563.9 (564.7)	556
15	-, (1068.5)	-	1069 vw	1068 m	1040.2 (1039.0)	-
9 $\underline{b}$	-, (1148.9)	-	1148 s	1145 w	1059.1 (1059.5)	-
3	-, (1184.5)	-	1175 m	1184 s (CCl <sub>4</sub> soln)	1084.3 (1082.6)	-
14	-, (1244.1)	1213	1232 m	1244 vs	1293.7 (1294.6)	-
19 $\underline{b}$	-, (1327.3)	-	1325 vw	1325 w	1440.7 (1441.2)	-
8 $\underline{b}$	-, (1595.3)	1542	1597 ms	1587 w	1618.1 (1618.7)	-
7 $\underline{b}$	-, -	-	-	3003 s	3069.7	-
20 $\underline{b}$	-, -	-	3059 s	-	3108.8	-

$$T_0 = 29299.7 \text{ cm}^{-1}$$

a = The notations vs, s, ms, m, w denote the intensities of the bands and represent very strong, strong, medium strong, medium, and weak respectively.

Table 3.7

Raman bands ( $\text{cm}^{-1}$ ) of pyridine-N-Oxide  
(not included in Tables III and VI)

Raman frequency	Assignment	Harmonic value*
465 (m)	$(11)_2$	462
683 (w)	$(11)_3$	693
830 (s)	$(16a)_2$	831
960 (w)	5	=
982 (w)	17a	-
1003 (w)	$(6a)_1(11)_2$	1002.3
1013 (m)	$(6a)_1(18b)_1$	1009.6
1260 (mw)	$(10b)_1(16b)_1$ ?	1270.2
1461 (vw)	$(16a)_2(6b)_1$	1468.6
1589 (w)	$(6a)_1(18a)_1$	1585.2
1615 (w)	$(9b)_1(18b)_1$	1618.2
3098 (w)	$(8a)_1(19a)_1$ ?	3070

\*For calculating harmonic values the data for fundamental frequencies have been taken from high resolution electronic spectra.

Table 3.8

Anharmonicities in Typical  $a_1$  and  $b_2$  Modes (in  $\text{cm}^{-1}$ ) of  
Pyridine N-Oxide in  $^1\text{A}_1$  and  $^1\text{B}_2$  States

Transition	Observed (UV Data)		Calculated		
	Fundamental	Overtone	Harmonic Value of Overtone	$2\omega_e x_e$	$\omega_e$
$6a_1^0$	-540.2	-1080.9	-1080.4	0.5	-539.7
$6a_0^1$	510.1	1020.1	1020.2	0.1	510.2
$12_0^{1*}$	818.4	1635.7	1636.8	1.1	819.5
$1_0^1$	978.3	1954.9	1956.6	1.7	980.0
$9a_0^1$	1117.1	2233.0	2234.2	1.2	1118.3
$7a_0^1$	1323.0	2644.6	2646.0	1.4	1324.4
$8a_0^1$	1639.2	3279.2	3278.4	-0.8	1638.4
$6b_0^1$	563.9	1129.1	1127.8	1.3	562.6
$15_0^1$	1040.2	2085.3	2080.4	-4.9	1035.3
$9b_0^1$	1059.0	2120.8	2118.0	-2.8	1056.2

\* 3rd and 4th members of the transition have also been observed.

Table 3.9(a) :  $b_{-1}$  levels; Combination Differences and Fundamental Frequencies  
(in  $\text{cm}^{-1}$ ) for Pyridine N-oxide for  ${}^1B_{-2}$  state

Attached to : Difference	$11_1^0$	$16b_1^0$	$4_1^0$	$10b_1^0$	$17b_1^0$	$5_1^0$	Mean	Fundamental Frequency*
$5_0^1 - 11_0^1$	578.1	578.8	581.0	-	-	579.3	579.3	794.3
$17b_0^1 - 11_0^1$	510.5	511.1	-	512.7	-	511.1	511.4	726.4
$10b_0^1 - 11_0^1$	422.8	-	-	422.4	421.8	423.0	422.5	637.5
$4_0^1 - 11_0^1$	203.1	205.2	203.8	202.0	-	201.2	203.0	418.0
$16b_0^1 - 11_0^1$	146.2	148.6	-	145.2	-	146.4	146.6	361.6 (361.8)*
$11_0^1$								215.0

\*Base value  $16b_0^2 = 723.6 \text{ cm}^{-1}$



Table 3.9(b) :  $b_{-1}$  levels; Combination Differences and Fundamental Frequencies  
(in  $\text{cm}^{-1}$ ) for Pyridine N-oxide for  ${}^1A_{-1}$  state

Attached to : Difference	$11_1^1$	$16b_1^1$	$4_1^1$	$10b_1^1$	$17b_1^1$	$5_1^1$	Mean	Fundamental Frequency
$5_1^0 - 11_1^0$	742.9	742.8	-	742.7	742.3	741.7	742.5	973.0
$17b_1^0 - 11_1^0$	-	652.2	652.4	649.3	651.2	651.1	651.2	881.7
$10b_1^0 - 11_1^0$	530.0	531.0	531.1	530.4	527.8	-	530.1	760.6
$4_1^0 - 11_1^0$	-	-	444.1	440.1	438.8	442.0	441.2	671.7
$16b_1^0 - 11_1^0$	281.5	279.1	279.4	-	280.8	280.8	280.3	510.8
$11_1^0$								230.5

Table 3.9(c) :  $a_2$  levels; Combination Differences and Fundamental Frequencies  
(in  $\text{cm}^{-1}$ ) for Pyridine N-oxide for  ${}^1A_1$  state

Attached to Difference	$16a_0^1$	$10a_0^1$	$17a_0^1$	Mean	Fundamental Frequency*
$17a_1^0 - 16a_1^0$	573.3	575.1	574.0	574.1	989.6
$10a_1^0 - 16a_1^0$	418.8	420.9	418.6	419.4	834.9
$16a_1^0$					415.5

\* Base value  $16a_2^0 = 830.9 \text{ cm}^{-1}$ .

Table 3.9(d) :  $a_2$  levels; Combination Differences and Fundamental Frequencies  
(in  $\text{cm}^{-1}$ ) for Pyridine N-oxide for  ${}^1B_{-2}$  state

Attached to : Difference	$16a_1^0$	$10a_1^0$	$17a_1^0$	Mean	Fundamental Frequency
$17a_0^1 - 16a_0^1$	550.3	550.5	549.5	550.1	715.1
$10a_0^1 - 16a_0^1$	477.1	475.0	475.2	475.7	640.7
$16a_0^1$					165.0

TABLE 3.10  
 $b_{-1}$  Fundamental Models (in  $\text{cm}^{-1}$ ) in Vapour and Solid  
 Pyridine N-oxide.

Mode	${}^1A_1$ state		${}^1B_2$ state
	Vapour Absorption	Solid IR	Vapour Electronic absorption
11	- (230.5)	233.0	- (215.0)
16b	508.5m (510.8)	514.5m	- (361.6)
4	671.0s (671.7)	671.0s	- (418.0)
10b	758.5s (760.6)	761.5s	- (637.5)
17b	881.0w (881.7)	886.0s ( $\text{ccl}_4$ solution)	- (726.4)
5	971.0w (973.0)	976.0w	- (794.3)

Table 3.11  
 $a_2$  Fundamental Modes (in  $\text{cm}^{-1}$ ) in Vapour and Solid  
 Pyridine N-oxide.

Mode	${}^1A_1$ state		${}^1B_2$ state
	Vapour	Solid	Vapour
16a	- (415.5)	415.0 (FIR)	- (165.0)
10a	- (834.9)	830.0 R	- (640.7)
17a	- (989.6)	-	- (715.1)

TABLE 3.12

INFRARED BAND POSITIONS (IN  $\text{cm}^{-1}$ ) OF PYRIDINE N-OXIDE

Vapour	Solid		Solution		Assignment
	at RT	at INT	in $\text{CCl}_4$	in $\text{CS}_2$	
469.3	466.0 s	467.0 s 470.0 s	471.0 s	467.0 s	18b (11) <sub>2</sub>
508.5 m	514.5 m	524.5 m	513.5 ms	508.5 s	16b
540.2 m	546.0 s	550 s	544 s	544 s	6a
637.6	635 vw	633 vw	634 w	634 w	6b
670.5 s	671	684 s	670 vs	669 vs	4
758.5 vs	761.5	776.5 s 783.5 s	-	758.5vs 781.5 m	10b (6a)(11)
843.5 s	835.5 s	836	843.5 s	839.5vs	12
881.0 w	-	-	889 ms	886 s	17b
-	907 wb	912.0 w	-	-	(4)(11)
970.0 w	976 vw	980.0vw	976 w	-	5
1013.3 s	1012.5 s	1013.5	1014.0 vs	1012 vs	1
1046.0 w	1043.0 w	-	1043 m	1042 m	18a
1068.5	1068.0	1075 mw 1092 w	1068 ms 1090 w	1067 ms 1089 w	15 (6a) <sub>2</sub>
-	-	1105 vw	1104.5 vw	1104.5 w	(6b)(18b)
1148.9	1145.0 w	1152 vw	1145 m	1144 m	9b
1165.0 s	1168.0 s	1176 s	1173 vs	1164 vs	9a
1184.5	-	1182 s	1184 s	1183 s	3

contd

Vapour	Solid		Solution		Assignment
	at RT	at INT	in CCl <sub>4</sub>	in Cs <sub>2</sub>	
1244.2	-	1243	-	1256 vs	14
-	-	-	-	1265 vs	(6b) <sub>2</sub>
1302.5 s	1246 ms	1252 ms	1276 vs	1272 vs	7a
1327.3	1330 w	1330 vw	1332 vw	1332 m	19b
-	1370 vw	1364 vw	1358 m	1364 w	(12)(16b)
-	-	-	1385 mw	1383 vw	(5)(16a)
-	-	-	1405 m	1395 vw	(17b)(16b)
1461.0 s	1460 vs	1467 vs 1471 vs	1463 vs 1471 vs	-	19a (6b)(12)
-	1480 m	1480 m	1487 s	-	(5)(16b)
-	1514.5	1515 vw	1518 w	-	(10b) <sub>2</sub>
-	1553 vw	1554 vw	1550 ms	-	(17b)(4)
-	1567 vw	1564 vw	1567	-	(9b)(16a)
-	1588	1590	1589	-	(12)(10b)
(1595.3)	-	1604 m	-	-	8b
1608.5 s	-	1610 m	1605 vs	-	8a
			1614 m	1615 w	(9b)(18b)
			1631 w	1630 w	(17b)(10b)
			-	1696 m	(9b)(6a)
			-	1701 m	(14)(18b)
			1716 s	1705 m	(17b)(10a)
			1771 w	1770 w	(17b) <sub>2</sub>
			1840 mw	1835 m	(8a)(11)
			1857 mw	1855 m	(5)(17b)

Vapour	Solid		Solution		Assignment
	at RT	at INT	in CCl <sub>4</sub>	in Cs <sub>2</sub>	
			1918 mw	1915 m	(9a)(10b)
			1941 mw	1935 m	(5) <sub>2</sub>
			2006 vw	2006 vw	(9a)(12)
			2095 mw	2095 w	(18a) <sub>2</sub>
			2298 mw	-	(9b) <sub>2</sub>
			2392 w	-	(15)(19b)
			2447 mw	2443 mw	(8a)(12)
			2519 m	2443 mw	(9b)(19b)
			2633 w	2625 w	(8a)(1)
			2724 w	2722 w	(19a)(7a)
			2774 mw	2771 mw	(8b)(3)
2938.5			2927 m	-	(19a) <sub>2</sub>
2986.0 w					(12) <sub>2</sub> (7a)
3011.0 mw	3003 ms	3003 ms	3006 ms	3004 ms	7b
3045.5	-	3043 m	3043 ms	3038 m	13
-	-	-	3067 s	3064.5 s	20b
3076.0 m	-	3077 m	3085 s	3081 s	2
3099.0 mw	3110 s	3100 s	3110 s 3061 w	3110 s 3157 w	20a (19a)(8b)

TABLE 3.13 (a)

THE LOW FREQUENCY VIBRATION (in  $\text{cm}^{-1}$ ) OF PYRIDINE N-OXIDE

Solid <sup>(a)</sup>		Liquid <sup>(b)</sup>		Vapour <sup>(c)</sup>		Assignment <sup>(d)</sup>
Infrared	Raman	Infrared	Raman	Infrared	Electronic	
513 s	-	514	511	508	508	$\tau_{\text{CC}}$ , 16b
466 vs	470 s	468	469	-	470	$\beta_{\text{NO}}$ , 18b
-	465 m	452	-	-	-	(11) <sub>2</sub>
415 w	-	-	415	-	415	$\tau_{\text{CC}}$ , 16a
233 s	-	-	226	-	231	$\gamma_{\text{NO}}$ , 11
112 w	108*vs	-	-	-	-	L
86 w	80*m	-	-	-	-	L or T
-	71*m	-	-	-	-	L or T
56 w	49*s	-	-	-	-	T
-	36*m	-	-	-	-	T
-	20*m	-	-	-	-	T

(a) The notations vs, s, m and w denote the intensities of the bands and weak respectively. The data marked with an asterisk are given in reference (11).

(b) The liquid values are from Mirone (4).

(c) Vapour phase data are from recent high resolution studies [10].

(d) The notations have been explained earlier (11-12).



TABLE 3.14ASSUMED GEOMETRY FOR PYRIDINE N-OXIDE IN  
THE GROUND STATE (SEE TEXT 3.8)

$R(C_1H_1)$	=	$1.070 \text{ \AA}$
$R(C_1C_2)$	=	1.381
$R(C_2C_3)$	=	1.393
$R(N C_1)$	=	1.384
$R(N O)$	=	1.29
$\angle C_1C_2C_3$	=	$124.6^\circ$
$\angle H_1C_1C_2$	=	121.0
$\angle H_2C_2C_3$	=	117.7
$\angle C_2C_3C_4$	=	114.1
$\angle H_3C_3C_4$	=	122.95
$\angle C_5N C_1$	=	120.9

The suffixes with the atoms represent their positions  
(cf Fig 3.13)

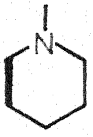
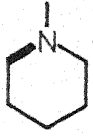
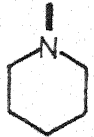
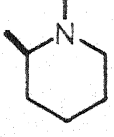
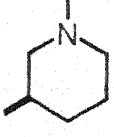
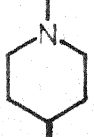

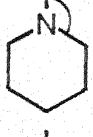
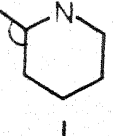
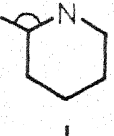
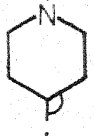


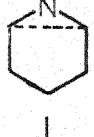
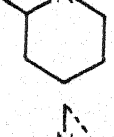

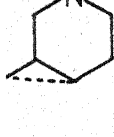
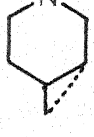

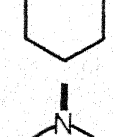
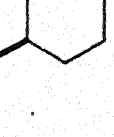
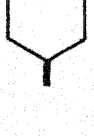
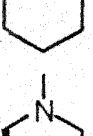



TABLE 3.15

DEFINITIONS OF THE INTERNAL COORDINATES  
FOR PYRIDINE N-OXIDE

Planar Modes				Non-planar Modes	
Internal Coordinate	Definition	Internal Coordinate	Definition	Internal Coordinate	Definition
S <sub>1</sub>	$\nu(\text{C}_1\text{C}_2)$	S <sub>16</sub>	$\alpha(\text{C}_1\text{C}_2\text{C}_3)$	S <sub>31</sub>	$\gamma(\text{C}_1\text{H}_1)$
S <sub>2</sub>	$\nu(\text{C}_2\text{C}_3)$	S <sub>17</sub>	$\beta(\text{C}_1\text{C}_2\text{H}_2)$	S <sub>32</sub>	$\gamma(\text{C}_2\text{H}_2)$
S <sub>3</sub>	$\nu(\text{C}_3\text{C}_4)$	S <sub>18</sub>	$\beta(\text{H}_2\text{C}_2\text{C}_3)$	S <sub>33</sub>	$\gamma(\text{C}_3\text{H}_3)$
S <sub>4</sub>	$\nu(\text{C}_4\text{C}_5)$	S <sub>19</sub>	$\alpha(\text{C}_2\text{C}_3\text{C}_4)$	S <sub>34</sub>	$\gamma(\text{C}_4\text{H}_4)$
S <sub>5</sub>	$\nu(\text{C}_5\text{N})$	S <sub>20</sub>	$\beta(\text{C}_2\text{C}_3\text{H}_3)$	S <sub>35</sub>	$\gamma(\text{C}_5\text{H}_5)$
S <sub>6</sub>	$\nu(\text{NC}_5)$	S <sub>21</sub>	$\beta(\text{H}_3\text{C}_3\text{C}_4)$	S <sub>36</sub>	$\gamma(\text{NO})$
S <sub>7</sub>	$\nu(\text{C}_1\text{H}_1)$	S <sub>22</sub>	$\alpha(\text{C}_3\text{C}_4\text{C}_5)$	S <sub>37</sub>	$\tau(\text{C}_1\text{C}_2)$
S <sub>8</sub>	$\nu(\text{C}_2\text{H}_2)$	S <sub>23</sub>	$\beta(\text{C}_3\text{C}_4\text{H}_4)$	S <sub>38</sub>	$\tau(\text{C}_2\text{C}_3)$
S <sub>9</sub>	$\nu(\text{C}_3\text{H}_3)$	S <sub>24</sub>	$\beta(\text{H}_4\text{C}_4\text{C}_5)$	S <sub>39</sub>	$\tau(\text{C}_3\text{C}_4)$
S <sub>10</sub>	$\nu(\text{C}_4\text{H}_4)$	S <sub>25</sub>	$\alpha(\text{C}_4\text{C}_5\text{N})$	S <sub>40</sub>	$\tau(\text{C}_4\text{C}_5)$
S <sub>11</sub>	$\nu(\text{C}_5\text{H}_5)$	S <sub>26</sub>	$\beta(\text{C}_4\text{C}_5\text{H}_5)$	S <sub>41</sub>	$\tau(\text{C}_5\text{N})$
S <sub>12</sub>	$\nu(\text{NO})$	S <sub>27</sub>	$\beta(\text{H}_5\text{C}_5\text{N})$	S <sub>42</sub>	$\tau(\text{NC}_1)$
S <sub>13</sub>	$\alpha(\text{NC}_1\text{C}_2)$	S <sub>28</sub>	$\alpha(\text{C}_5\text{NC}_1)$		
S <sub>14</sub>	$\beta(\text{NC}_1\text{H}_1)$	S <sub>29</sub>	$\beta(\text{C}_5\text{NO})$		
S <sub>15</sub>	$\beta(\text{H}_1\text{C}_1\text{C}_2)$	S <sub>30</sub>	$\beta(\text{ONC}_1)$		

The running suffixes with the internal coordinates (S) show their identifying number while the suffixes with atoms represent their positions (cf Fig 3.13).

REFINED UBFF FOR PLANAR AND NON-PLANAR VIBRATIONS  
OF PYRIDINE-N-OXIDE. (Table 3.16)

$K_{CC},$ $K_{CN}, K_{NO}$	 ,  , 	5.145 , 4.10 , 4.50
$K_{CH}$	 ,  , 	4.752 , 4.865 , 4.745
$H_{CC}, H_{NO}$	 , 	0.66 , 0.455
$H_{CH}$	 ,  , 	0.335 , 0.233 , 0.45
$F_{NC},$ $F_{CC}, F_{CN}$	 ,  , 	0.75 , 0.52 , 0.803
$F_{CH}$	 ,  ,  , 	0.4395 , 0.3395 0.260 , 0.260
$F_{NO}$		0.9226
$\gamma_{CH}$	 ,  , 	0.15 , 0.192 , 0.225
$\gamma_{NO}$		0.645
$\tau_{CC},$ $\tau_{CC}, \tau_{NC}$	 ,  , 	0.045 , 0.083 , 0.095

Units: K in m dynes/Å  
H, F,  $\gamma$  and  $\tau$  in  $10^{-11}$  erg/rad<sup>2</sup>

TABLE 3.17

OBSERVED AND CALCULATED VALUES OF FUNDAMENTAL  
MODES (IN cm<sup>-1</sup>) OF PYRIDINE N-OXIDE

Symmetry	Designation	Description	Fundamental Frequency	
			Observed(a)	Calculated
<u>a<sub>1</sub></u>	<u>6a</u>	X-sensitive	540.3	541
	12	X-sensitive	842.8	825
	1	Ring	1013.0	969
	18a	β CH	1044.9	1007
	9a	β CH	1164.8	1122
	7a	X-sensitive	1303.0	1363
	19a	ν CC , CN	1460.4	1479
	8a	ν CC	1609.3	1575
	13	ν CH	3045 <sup>I</sup>	3088
	2	ν CH	3076 <sup>I</sup>	3091
	20a	ν CH	3099 <sup>I</sup>	3098
	18b	X-sensitive	469.3	461
	6b	Ring deformation	637.6	626
<u>b<sub>2</sub></u>	15	β CH	1068.5	1039
	9b	β CH	1148.9	1122
	3	β CH	1184.5	1224
	14	ν CC	1244.1	1268
	19b	ν CC, CN	1327.3	1392
	8b	ν CC	1595.3	1543
	7b	ν CH	3003 <sup>I</sup>	3046
	20b	ν CH	3059 <sup>R</sup>	3085

cont'd ...

Table 3.17 contd

$b_1$	11	X-sensitive	230.5	285
	16b	X-sensitive	510.5	463
	4	$\tau$ CC	671.7	644
	10b	$\gamma$ CH	758.5 <sup>I</sup>	757
	17b	$\gamma$ CH	881.7	870
	5	$\gamma$ CH	973.0	960
$a_2$	16a	$\tau$ CC	415.0*	448
	10a	$\gamma$ CH	834.9	851
	17a	$\gamma$ CH	989.6	995

a : High Resolution electronic spectra (vapour phase)

I : IR Vapour

R : Raman Solid

\* : Far infrared solid

APPENDIX 3.1

BAND POSITIONS AND RELATIVE INTENSITIES. The intensities (I) are relative to origin band (0,0) = 100 in the electronic spectrum.

Assignment <sup>+</sup>	Frequency cm <sup>-1</sup>	$\Delta\nu(\text{cm}^{-1})$		I
		Observed	Calculated*	
$12_1^0 15_1^0$	27385.194	-1914.6*	-1911.3	.01
$6b_1^0 14_1^0$	27422.520	-1877.2	-1877.7	.02
$6b_1^0 17a_1^0$	27672.953	-1626.8	-1627.2	.02
$18b_1^0 9b_1^0$	27682.059	-1617.7	-1621.2	.05
$8a_1^0$	27690.453	-1609.3	A.O.	0.05
$6a_1^0 18a_1^0$	27721.453	-1578.3	-1582.2	0.05
$6a_1^0 1_1^0$	27744.833	-1554.9	-1553.3	0.05
$7a_1^0 16a_1^1$	27747.112	-1552.6	-1554.3	0.1
$4_1^0 17b_1^0$	27747.112	-1552.6	-1553.4	0.1
$18b_1^0 15_1^0$	27761.510	-1538.2	-1537.8	0.02
$6a_1^0 5_1^0$	27791.253	-1508.5	-1512.3	0.09
$19a_1^0 1_1^1$	27801.713	-1498.0	-1493.7	0.1
$19a_1^0 6a_1^1$	27809.533	-1490.2	-1490.6	0.1
$19a_1^0 11_1^1$	27821.565	-1478.2	-1476.4	0.08
$19a_1^0 18b_1^1$	27831.327	-1468.4	-1466.4	0.08
$19a_1^0$	27839.377	-1460.4	A.O.	0.02

Assignment <sup>+</sup>	Frequency cm <sup>-1</sup>	$\Delta\nu(\text{cm}^{-1})$		I
		Observed	Calculated*	
$9a_1^0 17a_1^1$	27862.469	-1437.3	-1439.8	0.01
$4_1^0 10b_1^0$	27865.964	-1433.8	-1432.3	0.01
$16a_1^0 17a_1^0$	27898.427	-1401.3	-1405.1	0.01
$16b_1^0 17b_1^0$	27913.247	-1386.5	-1392.5	0.3
$6a_1^0 12_1^0$	27916.729	-1383.0	-1383.1	0.25
$4_2^0$	27958.339	-1341.4	-1343.4	0.3
$7a_1^0 1_1^1$	27962.654	-1337.1	-1336.3	0.3
$7a_1^0 18b_1^1$	27989.030	-1310.7	-1309.0	0.01
$7a_1^0$	27996.726	-1303.0	A.O.	0.08
$18a_1^0 16a_1^1$	28000.227	-1299.5	-1296.2	0.03
$1_1^0 17a_1^1$	28011.446	-1288.3	-1288.0	0.04
$16b_1^0 10b_1^0$	28032.476	-1267.3	-1271.4	0.1
$1_1^0 16a_1^1$	28035.732	-1264.0	-1264.3	0.09
$17a_1^0 11_1^0$	28079.294	-1220.5	-1220.1	0.06
$9a_1^0 11_1^1$	28121.483	-1178.3	-1180.8	0.2
$16b_1^0 4_1^0$	28121.483	-1178.3	-1182.5	0.2
$9a_1^0 18b_1^1$	28129.339	-1170.4	-1170.8	0.02
$9a_1^0$	28134.938	-1164.8	A.O.	0.03

Assignment <sup>+</sup>	Frequency cm <sup>-1</sup>	$\Delta\nu(\text{cm}^{-1})$		I
		Observed	Calculated*	
$1_1^0 16b_1^1$	28138.786	-1161.0	-1161.9	0.02
$8b_1^0 18b_0^1$	28168.644	-1131.1	-1132.0	0.03
$18a_1^0 6b_1^1$	28178.763	-1121.0	-1117.0	0.03
$11_1^0 17b_1^0$	28191.506	-1108.2	-1112.2	0.01
$12_1^0 16a_1^1$	28202.876	-1096.9	-1094.1	0.5
$6a_2^0$	28218.811	-1080.9	-1080.6	0.3
$18a_1^0 11_1^1$	28239.327	-1060.4	-1060.9	0.01
$18a_1^0$	28254.871	-1044.9	A.O.	0.01
$8b_1^0 6b_0^1$	28269.429	-1030.3	-1031.4	0.2
$1_1^0 11_1^1$	28269.429	-1030.3	-1029.0	0.2
$1_1^0 18b_1^1$	28280.699	-1019.1	-1019.0	0.03
$16b_2^0$	28280.699	-1019.1	-1021.6	0.03
$1_1^0$	28286.718	-1013.0	A.O.	0.3
$11_1^0 10b_1^0$	28307.441	- 992.3	- 991.1	0.05
$12_1^0 16b_1^1$	28307.441	- 992.3	- 991.7	0.05
$16b_1^0 16a_1^0$	28371.180	- 928.6	- 926.3	0.05
$12_1^0 1_1^1$	28421.340	- 878.4	- 876.1	0.2
$12_1^0 6a_1^1$	28426.905	- 872.8	- 873.0	0.1



Assignment <sup>+</sup>	Frequency cm <sup>-1</sup>	$\Delta\nu$ (cm <sup>-1</sup> )		I
		Observed	Calculated*	
$19b_1^0 18b_0^1$	28436.199	- 863.6	- 863.6	0.3
$12_1^0 11_1^1$	28439.617	- 860.1	- 858.8	0.3
$12_1^0 18b_1^1$	28451.366	- 848.4	- 848.8	0.1
$12_1^0$	28456.941	- 842.8	A.O.	1
$16a_2^0$	28468.824	- 830.9	- 831.0	0.03
$17a_1^0 16a_0^1$	28475.202	- 824.5	- 824.6	0.1
$6a_1^0 17a_1^1$	28483.608	- 816.1	- 815.3	0.2
$7a_1^0 6a_0^1$	28508.522	- 791.2	- 792.9	0.8
$6a_1^0 16a_1^1$	28508.522	- 791.2	- 791.6	0.8
$12_1^0 4_1^0 17b_0^1$	28514.019	- 785.7	- 787.1	0.05
$5_1^0 11_0^1$	28540.830	- 758.9	- 758.0	0.03
$12_1^0 18b_1^0 6b_0^1$	28554.836	- 744.9	- 747.3	0.05
$3_1^0 18b_0^1$	28577.934	- 721.8	- 721.2	0.6
$6a_1^0 16b_1^1$	28611.774	- 688.0	- 689.2	0.4
$10a_1^0 16a_0^1$	28629.651	- 670.1	- 669.9	0.02
$17b_1^0 11_0^1$	28635.501	- 664.3	- 666.7	0.04
$8a_1^0 1_0^1$	28669.361	- 630.4	- 631.0	0.2
$6a_1^0 6b_1^1$	28687.186	- 612.6	- 612.4	0.5

Assignment <sup>+</sup>	Frequency (cm <sup>-1</sup> )	$\Delta\nu$ (cm <sup>-1</sup> )		I
		Observed	Calculated*	
$5_1^0 16b_0^1$	28687.186	- 612.6	- 611.4	0.5
$15_1^0 18b_0^1$	28694.395	- 605.4	- 605.2	0.3
$9b_1^0 6b_0^1$	28715.285	- 584.5	- 585.0	1
$6a_1^0 6a_1^1$	28728.633	- 571.1	- 570.5	1
$5_1^0 4_0^1$	28742.087	- 557.7	- 555.0	1.5
$6a_1^0 11_1^1$	28742.087	- 557.7	- 556.6	1.5
$8b_1^0 15_0^1$	28742.087	- 557.7	- 555.1	1.5
$6a_1^0 18b_1^1$	28753.763	- 546.0	- 546.3	0.5
$10b_1^0 11_0^1$	28753.763	- 546.0	- 545.6	0.5
$6a_1^0$	28759.485	- 540.3	A.O.	5
$8b_1^0 9b_0^1$	28765.031	- 534.7	- 536.1	0.3
$18a_1^0 6a_0^1$	28765.031	- 534.7	- 534.8	0.3
$17b_1^0 16b_0^1$	28777.829	- 521.9	- 520.1	1
$8b_1^0 3_0^1$	28787.611	- 512.1	- 511.0	0.3
$15_1^0 6b_0^1$	28796.121	- 503.6	- 504.6	0.2
$19a_1^0 18a_0^1$	28801.739	- 498.0	- 498.6	0.1
$8a_1^0 9a_0^1$	28809.409	- 490.3	- 492.2	2
$7a_1^0 12_0^1$	28814.927	- 484.8	- 484.6	0.01

Assignment <sup>+</sup>	Frequency (cm <sup>-1</sup> )	$\Delta\nu(\text{cm}^{-1})$		I
		Observed	Calculated*	
$19a_1^{0,1}1_0$	28817.028	- 482.7	- 482.1	0.02
$6b_1^0 ?$	28829.337	- 470.4	A.O. ?	0.3
$17b_1^{0,4}1_0$	28834.510	- 465.3	- 463.7	0.03
$11_2^0$	28838.986	- 460.8	- 461.0	0.1
$4_1^{0,1}11_0$	28838.986	- 460.8	- 456.7	0.1
$10b_1^{0,16}b_0^1$	28898.941	- 400.8	- 399.0	0.05
$17a_1^{0,10}a_0^1$	28950.562	- 349.3	- 348.9	0.2
$9a_1^{0,12}1_0$	28953.993	- 345.8	- 346.4	0.2
$19a_1^{0,9}a_0^1$	28955.779	- 344.0	- 343.3	0.3
$10b_1^{0,4}1_0$	28955.779	- 344.0	- 342.6	0.3
$7a_1^{0,18}a_0^1$	28961.194	- 338.6	- 341.2	0.4
$5_1^{0,10}b_0^1$	28963.800	- 335.9	- 335.5	1
$12_1^{0,6}a_0^1$	28967.245	- 332.5	- 332.7	1
$7a_1^{0,1}1_0$	28976.251	- 323.5	- 324.7	0.5
$16b_1^{0,11}1_0$	29002.255	- 297.5	- 295.8	1

Assignment <sup>+</sup>	Frequency (cm <sup>-1</sup> )	$\Delta\nu(\text{cm}^{-1})$		I
		Observed	Calculated*	
17a <sub>1</sub> <sup>1</sup> 18b <sub>1</sub> <sup>1</sup>	29019.014	- 280.7	- 280.5	0.05
17a <sub>1</sub> <sup>1</sup>	29024.724	- 275.0	- 274.6	5
16a <sub>1</sub> <sup>1</sup> 18b <sub>1</sub> <sup>1</sup>	29042.711	- 257.0	- 256.5	1
4 <sub>1</sub> <sup>1</sup>	29042.711	- 257.0	- 253.7	1
16a <sub>1</sub> <sup>1</sup>	29048.498	- 251.3	- 250.5	15
5 <sub>1</sub> <sup>0</sup> 17b <sub>0</sub> <sup>1</sup>	29051.930	- 247.8	- 246.6	0.01
17b <sub>1</sub> <sup>0</sup> 10b <sub>0</sub> <sup>1</sup>	29057.216	- 242.5	- 244.2	0.01
19b <sub>1</sub> <sup>0</sup> 3 <sub>0</sub> <sup>1</sup>	29057.216	- 242.5	- 243.0	0.01
19b <sub>1</sub> <sup>0</sup> 3 <sub>0</sub> <sup>1</sup>	29060.739	- 239.0	- 243.0	0.01
18a <sub>1</sub> <sup>0</sup> 12 <sub>0</sub> <sup>1</sup>	29072.238	- 227.5	- 226.5	0.01
14 <sub>1</sub> <sup>0</sup> 15 <sub>0</sub> <sup>1</sup>	29092.761	- 207.0	- 203.9	0.5
1 <sub>1</sub> <sup>0</sup> 12 <sub>0</sub> <sup>1</sup>	29104.652	- 195.1	- 194.6	0.3
10a <sub>1</sub> <sup>1</sup>	29104.652	- 195.1	- 194.2	0.3
9a <sub>1</sub> <sup>0</sup> 1 <sub>0</sub> <sup>1</sup>	29115.449	- 184.3	- 186.5	0.05
7a <sub>1</sub> <sup>0</sup> 9a <sub>0</sub> <sup>1</sup>	29115.449	- 184.3	- 185.9	0.05
5 <sub>1</sub> <sup>1</sup>	29120.137	- 179.6	- 178.7	0.01
6b <sub>1</sub> <sup>0</sup> 18b <sub>0</sub> <sup>1</sup>	29124.503	- 175.2	- 174.3	0.01

Assignment <sup>+</sup>	Frequency (cm <sup>-1</sup> )	$\Delta\nu$ (cm <sup>-1</sup> )		I
		Observed	Calculated*	
$14_{10}^{01}$	29143.094	- 156.7	- 159.8	0.01
$17b_1^1$	29143.094	- 156.7	- 155.3	0.01
$8b_{10}^{01}19b_0^1$	29143.094	- 156.7	- 154.6	0.01
$16b_1^1$	29150.857	- 148.9	- 148.4	1
$3_{10}^{01}15_0^1$	29154.281	- 145.5	- 144.3	0.01
$8a_{10}^{01}19a_0^1$	29171.186	- 128.6	- 129.3	0.05
$3_{10}^{01}9b_0^1$	29171.186	- 128.6	- 126.0	0.05
$10b_1^1$	29176.120	- 123.6	- 123.1	0.05
$10a_{10}^{01}17a_0^1$	29180.122	- 119.6	- 119.8	0.05
$9b_{10}^{01}15_0^1$	29193.743	- 106.0	- 108.7	0.3
$3_1^1$	29195.910	- 103.8	- 100.2	0.3
$16b_{10}^{01}4_0^1$	29207.474	- 92.3	- 92.8	0.5
$9b_1^1$	29210.781	- 89.0	- 89.9	1
$17b_{10}^{01}5_0^1$	29210.781	- 89.0	- 87.4	1
$18a_1^1$	29213.736	- 86.0	- 83.6	1
$6b_1^1$	29227.621	- 72.1	- 74.1	5
$18a_{10}^{01}1_0^1$	29233.940	- 65.8	- 66.6	0.05

Assignment <sup>+</sup>	Frequency (cm <sup>-1</sup> )	$\Delta\nu(\text{cm}^{-1})$		I
		Observed	Calculated*	
$1_1^0 18a_0^1$	29249.305	- 50.4	- 51.2	0.5
$9a_1^1$	29252.280	- 47.5	- 47.7	0.5
$1_1^1$	29266.478	- 33.3	- 34.7	2
$10b_1^0 17b_0^1$	29266.478	- 33.3	- 34.2	2
$4_1^0 10b_0^1$	29266.478	- 33.3	- 34.2	2
$19b_1^0 14_0^1$	29266.478	- 33.3	- 33.2	2
$6a_1^1$	29269.552	- 30.2	- 30.1	2
$15_1^1$	29269.552	- 30.2	- 28.3	2
$11_1^1$	29283.798	- 16.0	- 16.0	24
$18b_1^1$	29293.703	- 6.0	- 6.0	8
0,0 (origin)	29299.751	0,0	-	100
$7a_1^1$	29319.875	20.1	20.0	0.4
$19a_1^1$	29319.875	20.1	19.6	0.4
$8b_1^1$	29323.215	23.5	22.8	0.6
$10b_1^0 15_0^1$	29328.330	28.6	33.7	1
$8a_1^1$	29328.330	28.6	29.9	1
$4_1^0 17b_0^1$	29355.446	55.7	54.7	1

Assignment <sup>+</sup>	Frequency (cm <sup>-1</sup> )	$\Delta\nu(\text{cm}^{-1})$		I
		Observed	Calculated*	
$18b_1^0 6b_0^1$	29395.226	95.5	94.6	4
$19b_1^1$	29414.572	114.8	113.8	0.08
$4_1^0 5_0^1$	29419.953	120.2	122.6	0.09
$16b_1^0 10b_0^1$	29429.926	130.2	126.7	0.5
$11_1^0 16b_0^1$	29429.926	130.2	131.1	0.5
$12_1^0 1_0^1$	29434.442	134.7	135.5	0.5
$19a_1^0 8a_0^1$	29477.467	177.7	178.8	0.8
$11_1^0 4_0^1$	29486.875	187.1	187.5	0.8
$16b_1^0 17b_0^1$	29513.438	213.7	215.6	0.01
$16a_1^0 10a_0^1$	29525.583	225.8	225.2	0.9
$15_1^0 14_0^1$	29525.583	225.8	225.5	0.9
$6a_1^0 12_1^0 8b_0^1$	29535.893	236.1	235.0	0.8
$3_1^0 19b_0^1$	29555.968	256.2	256.2	5
$12_1^0 9a_0^1$	29574.409	274.7	274.3	3
$6a_1^0 12_0^1$	29577.793	278.0	278.1	4
$18a_1^0 7a_0^1$	29577.793	278.0	278.1	4
$16b_1^0 5_0^1$	29581.042	281.3	283.5	0.5

Assignment <sup>+</sup>	Frequency (cm <sup>-1</sup> )	$\Delta\nu(\text{cm}^{-1})$		I
		Observed	Calculated*	
$19b_1^0 8b_0^1$	29591.593	291.8	291.2	0.4
$9b_1^0 19b_0^1$	29591.593	291.8	291.7	0.4
$16a_1^0 17a_0^1$	29598.740	293.0	299.6	5
$9a_1^0 19a_0^1$	29615.292	315.5	315.2	1
$16a_0^2$	29630.026	330.3	330.0	7
$7a_1^0 8a_0^1$	29630.026	330.3	336.2	7
$6a_0^1 16b_1^1$	29659.832	360.1	361.2	0.8
$14_1^0 8b_0^1$	29677.261	377.5	373.9	0.2
$11_1^0 10b_0^1$	29706.5	406.8	407.0	0.3
$6b_1^0 9b_0^1$	29723.465	423.7	421.1	0.4
$11_0^2$	29734.205	434.5	430.0	1
$6a_1^0 1_0^1$	29737.183	437.4	438.0	1
$6a_0^1 6b_1^1$	29737.183	437.4	438.0	1
$18b_0^1 11_1^1$	29747.094	447.3	447.3	1.5
$18b_0^1$	29763.026	463.3	A.O.	4
$6a_0^1 6a_1^1$	29779.164	479.4	479.9	5
$12_1^0 17a_0^1$	29779.164	479.4	480.2	5



Assignment <sup>+</sup>	Frequency (cm <sup>-1</sup> )	$\Delta v$ (cm <sup>-1</sup> )		I
		Observed	Calculated*	
$6a_0^1 11_1^1$	29794.239	494.5	494.1	8
$11_1^0 17b_0^1$	29794.239	494.5	495.9	8
$6a_0^1 18b_1^1$	29803.951	504.2	504.1	3
$6a_0^1$	29809.869	510.1	A.O.	30
$18b_0^1 4_1^0 17b_0^1$	29818.202	518.5	518.9	3
$6b_1^0 6a_1^1$	29830.465	530.7	530.6	4
$15_1^0 8b_0^1$	29847.237	547.5	549.6	3
$6a_0^1 4_1^0 17b_0^1$	29859.759	560.0	565.8	0.9
$11_1^0 5_0^1$	29861.853	562.1	563.8	1
$6b_0^1$	29863.647	563.9	A.O.	10
$18b_1^0 15_0^1$	29868.387	568.6	570.9	11
$11_0^1 16b_0^1$	29868.387	568.6	576.6	11
$18b_1^0 9b_0^1$	29889.776	590.0	589.8	0.1
$6a_0^1 18b_1^0 6b_0^1$	29900.848	601.1	605.6	0.3
$1_1^0 8a_0^1$	29925.339	625.6	626.2	0.5
$11_1^0 4_0^1$	29929.438	629.7	633.0	0.5
$12_1^0 19a_0^1$	29940.420	640.7	637.2	0.3

Assignment <sup>+</sup>	Frequency (cm <sup>-1</sup> )	$\Delta\nu(\text{cm}^{-1})$		I
		Observed	Calculated*	
$1_0^{11}2_1^06a_0^1$	29948.110	648.4	645.6	0.8
$6b_1^014_0^1$	29956.922	657.2	656.1	0.3
$12_0^{11}16b_1^1$	29967.931	668.2	669.5	3
$1_0^{11}17a_1^1$	30001.946	702.2	703.3	6
$16b_0^2$	30023.319	723.6	723.2	2
$1_0^{11}16a_1^1$	30026.695	726.9	727.0	10
$12_0^{11}19b_1^1$	30026.695	726.9	729.4	10
$12_0^{11}16b_1^1$	30045.097	745.3	746.3	7
$16b_0^{11}4_0^1$	30083.254	783.5	779.6	5
$6a_1^017a_0^1$	30083.254	783.5	782.7	5
$12_1^08a_0^1$	30098.244	798.5	796.4	12
$12_0^{11}11_1^1$	30100.863	801.1	802.4	13
$6b_1^019b_0^1$	30100.863	801.1	802.7	13
$16a_0^{11}10a_0^1$	30109.163	809.4	805.7	6
$12_0^1$	30118.165	818.4	A.O.	50
$18b_1^014_0^1$	30125.052	825.3	824.4	0.4
$4_0^2$	30139.935	840.2	836.0	4
$9a_0^{11}16a_1^1$	30165.950	866.2	865.8	2

Assignment <sup>+</sup>	Frequency (cm <sup>-1</sup> )	$\Delta\nu(\text{cm}^{-1})$		I
		Observed	Calculated*	
$16a_0^1 17a_0^1$	30180.083	880.3	880.1	2
$16a_0^1 17b_0^1$	30190.592	890.8	891.4	3
$1_0^1 6b_1^1$	30204.986	905.2	906.2	7
$12_0^1 6b_0^1 18b_1^0$	30212.371	912.6	913.9	3
$12_0^1 6b_0^1 18b_1^0$	30216.798	917.0	919.0	4
$6a_1^0 19a_0^1$	30243.960	944.2	939.7	8
$17b_0^1 11_0^1$	30243.960	944.2	941.4	8
$18a_0^1 11_1^1$	30243.960	944.2	945.8	8
$18a_0^1$	30261.517	961.8	A.O.	40
$1_0^1 18b_1^1$	30271.860	972.1	972.3	7
$1_0^1$	30278.008	978.3	A.O.	60
$16b_0^1 10b_0^1$	30295.512	995.8	999.1	0.5
$16b_0^1 10a_0^1$	30303.878	1004.1	1002.1	1
$6a_0^2$	30319.805	1020.1	1020.2	3
$15_0^1 11_1^1$	30324.771	1025.0	1024.2	5
$15_0^1 18b_1^1$	30333.061	1033.3	1034.2	3
$15_0^1$	30339.990	1040.2	A.O.	25
$14_0^1 16a_1^1$	30348.346	1048.6	1041.4	7

Assignment <sup>+</sup>	Frequency (cm <sup>-1</sup> )	$\Delta\nu$ (cm <sup>-1</sup> )		I
		Observed	Calculated*	
9b <sub>0</sub> <sup>1</sup>	30358.813	1059.1	A.O.	15
4 <sub>0</sub> <sup>1</sup> 10a <sub>0</sub> <sup>1</sup>	30358.813	1059.1	1058.7	15
3 <sub>0</sub> <sup>1</sup> 11 <sub>1</sub> <sup>1</sup>	30366.359	1066.6	1068.3	8
6a <sub>0</sub> <sup>1</sup> 6b <sub>0</sub> <sup>1</sup>	30373.234	1073.5	1074.0	3
16b <sub>0</sub> <sup>1</sup> 17a <sub>0</sub> <sup>1</sup>	30378.084	1078.3	1076.7	4
3 <sub>0</sub> <sup>1</sup> 18b <sub>1</sub> <sup>1</sup>	30378.084	1078.3	1078.3	4
3 <sub>0</sub> <sup>1</sup>	30384.047	1084.3	A.O.	15
6a <sub>1</sub> <sup>0</sup> 8a <sub>0</sub> <sup>1</sup>	30398.680	1098.9	1098.9	2
9a <sub>0</sub> <sup>1</sup> 11 <sub>1</sub> <sup>1</sup>	30402.240	1102.5	1101.1	3
9a <sub>0</sub> <sup>1</sup> 18b <sub>1</sub> <sup>1</sup>	30410.014	1110.3	1111.1	1
9a <sub>0</sub> <sup>1</sup>	30416.847	1117.1	A.O.	8
6b <sub>0</sub> <sup>2</sup>	30428.845	1129.1	1127.8	11
4 <sub>0</sub> <sup>1</sup> 17a <sub>0</sub> <sup>1</sup>	30429.749	1130.0	1133.1	11
4 <sub>0</sub> <sup>1</sup> 17b <sub>0</sub> <sup>1</sup>	30446.820	1146.3	1144.4	8
18b <sub>1</sub> <sup>0</sup> 8b <sub>0</sub> <sup>1</sup>	30450.089	1150.3	1154.8	9
16b <sub>0</sub> <sup>1</sup> 5 <sub>0</sub> <sup>1</sup>	30460.503	1160.8	1155.9	1
4 <sub>0</sub> <sup>1</sup> 5 <sub>0</sub> <sup>1</sup>	30514.684	1214.9	1212.3	1
9a <sub>0</sub> <sup>1</sup> 6b <sub>0</sub> <sup>1</sup> 18b <sub>1</sub> <sup>0</sup>	30514.684	1214.9	1212.7	1

Assignment <sup>+</sup>	Frequency (cm <sup>-1</sup> )	$\Delta\nu$ (cm <sup>-1</sup> )		I
		Observed	Calculated*	
$14_0^1 6b_1^1$	30521.224	1221.5	1221.6	5
$19a_0^1 16a_1^1$	30527.960	1228.2	1228.7	6
$14_0^1 9a_1^1$	30541.145	1241.4	1243.3	4
$14_0^1 6a_1^1$	30560.259	1260.5	1260.5	7
$14_0^1 11_1^1$	30576.916	1277.2	1277.7	11
$10a_0^1 10b_0^1$	30576.916	1277.2	1278.2	11
$14_0^1 18b_1^1$	30587.939	1288.2	1287.7	4
$14_0^1$	30593.478	1293.7	A.O.	45
$7a_0^1 11_1^1$	30608.795	1309.0	1307.0	5
$7a_0^1$	30622.727	1323.0	A.O.	18
$6a_0^1 12_0^1$	30627.684	1327.9	1328.5	15
$10b_0^1 17a_0^1$	30652.144	1352.4	1352.6	0.5
$12_0^1 6b_0^1$	30683.084	1383.3	1382.3	2
$8a_0^1 16a_1^1$	30686.438	1386.7	1387.9	3
$1_0^2 6a_1^0$	30717.449	1417.7	1416.3	10
$19b_0^1 11_1^1$	30725.824	1426.1	1424.7	1
$18a_0^1 18b_0^1$	30725.824	1426.1	1425.0	1
$19b_0^1$	30740.459	1440.7	A.O.	4

Assignment <sup>+</sup>	Frequency (cm <sup>-1</sup> )	$\Delta\nu(\text{cm}^{-1})$		I
		Observed	Calculated*	
$10a_0^{15}1_0^1$	30740.459	1440.7	1435.0	4
$17b_0^{11}17a_0^1$	30740.459	1440.7	1441.5	4
$1_0^{11}18b_0^1$	30740.459	1440.7	1441.6	4
$19a_0^{16}a_1^1$	30749.251	1449.5	1449.8	2
$17b_0^2$	30749.251	1449.5	1452.8	2
$19a_0^{11}11_1^1$	30763.050	1463.3	1464.0	13
$19a_0^1$	30779.781	1480.0	A.0	50
$17b_0^{15}1_0^1$	30817.759	1518.0	1520.7	1
$18b_0^{19}b_0^1$	30824.186	1524.4	1522.4	1
$18a_0^{16}b_0^1$	30824.186	1524.4	1525.6	1
$12_0^{29}b_1^1$	30845.109	1545.4	1547.8	3
$18b_0^{13}1_0^1$	30845.109	1545.4	1547.6	3
$6a_0^{11}15_0^1$	30849.114	1549.4	1550.3	4
$8a_0^{19}b_1^1$	30849.114	1549.4	1550.2	4
$12_0^{26}b_1^1$	30862.358	1562.6	1564.7	3
$8b_0^{11}1_1^018a_0^1$	30868.132	1568.4	1568.7	2
$6a_0^{19}b_0^1$	30868.132	1568.4	1569.2	2
$5_0^2$	30892.659	1592.9	1588.6	3

Assignment <sup>+</sup>	Frequency (cm <sup>-1</sup> )	$\Delta\nu$ (cm <sup>-1</sup> )		I
		Observed	Calculated*	
$3_0^1 6a_0^1$	30892.659	1592.9	1594.4	3
$8a_0^1 6a_1^1$	30908.332	1608.6	1609.0	0.5
$8b_0^1$	30917.897	1618.1	A.O.	2
$12_0^2 11_1^1$	30917.897	1618.1	1620.8	2
$6a_0^1 9a_0^1$	30926.682	1626.9	1627.2	1
$12_0^2$	30935.428	1635.7	1636.8	5
$8a_0^1$	30938.996	1639.2	A.O.	4
$1_0^2 16a_1^1$	31002.956	1703.2	1705.3	0.5
$18b_0^1 14_0^1$	31058.918	1759.2	1757.0	0.8
$12_0^1 18a_0^1$	31081.571	1781.8	1780.2	3
$7a_0^1 18b_0^1$	31085.924	1786.2	1786.3	2
$12_0^1 1_0^1$	31094.816	1795.1	1796.7	14
$1_0^2 16b_1^1$	31102.620	1802.2	1807.7	2
$6a_0^1 7a_0^1$	31133.358	1833.6	1833.1	5
$6b_0^1 14_0^1$	31156.403	1856.7	1857.6	7
$12_0^1 9b_0^1$	31175.135	1875.4	1877.5	5
$1_0^2 6b_1^1$	31182.930	1883.2	1884.5	1
$7a_0^1 6b_0^1$	31187.887	1888.1	1886.9	2

Assignment <sup>+</sup>	Frequency (cm <sup>-1</sup> )	$\Delta\nu$ (cm <sup>-1</sup> )		I
		Observed	Calculated*	
$12_0^1 3_0^1$	31200.015	1900.3	1902.7	10
$18b_0^1 19b_0^1$	31207.364	1907.6	1904.0	2
$12_0^1 9a_0^1$	31237.457	1937.7	1935.5	4
$1_0^1 18a_0^1$	31237.457	1937.7	1940.1	4
$1_0^2 11_1^1$	31237.457	1937.7	1940.6	4
$19a_0^1 18b_0^1$	31245.990	1946.2	1943.3	5
$1_0^2$	31254.649	1954.9	1956.6	6
$6a_0^1 19a_0^1$	31286.771	1987.0	1990.1	5
$1_0^1 15_0^1$	31316.465	2016.7	2018.5	5
$18a_0^1 9b_0^1$	31322.432	2022.7	2020.9	3
$9a_0^2$	31332.745	2233.0	2234.2	2
$19a_0^1 6b_0^1$	31341.753	2042.0	2043.9	4
$18a_0^1 3_0^1$	31350.665	2050.9	2046.1	4
$6a_0^2 15_0^1$	31358.974	2059.2	2060.4	2
$18a_0^1 8a_0^1$	31375.283	2075.5	2078.9	2
$18b_0^1 8b_0^1$	31385.052	2085.3	2081.4	3
$1_0^1 9a_0^1$	31392.929	2093.2	2095.4	4
$12_0^1 14_0^1$	31411.037	2111.3	2112.1	8



Assignment <sup>+</sup>	Frequency (cm <sup>-1</sup> )	$\Delta v$ (cm <sup>-1</sup> )		I
		Observed	Calculated*	
$9b_0^2$	31420.620	2120.9	2118.2	3
$6a_0^1 8b_0^1$	31427.407	2127.7	2128.2	0.5
$7a_0^1 12_0^1$	31437.375	2137.6	2141.4	0.9
$9b_0^1 3_0^1$	31441.924	2142.2	2143.2	7
$1_0^2 4_1^0 17b_0^1$	31516.093	2216.3	2212.3	1
$9a_0^2$	31532.764	2233.0	2234.0	1
$18a_0^1 14_0^1$	31552.780	2253.0	2255.5	2
$12_0^1 19b_0^1$	31561.514	2261.8	2259.1	1
$1_0^1 14_0^1$	31569.506	2269.8	2272.0	10
$1_0^1 7a_0^1 1_0^1 7a_0^1$	31598.995	2299.2	2301.3	12
$7a_0^1 15_0^1$	31664.628	2364.9	2363.2	2
$3_0^1 14_0^1$	31674.408	2374.7	2377.9	2
$7a_0^1 3_0^1$	31707.273	2407.5	2407.3	0.5
$9a_0^1 14_0^1$	31708.924	2409.2	2410.8	1
$12_0^3$	31753.005	2453.3	2455.2	6
$19a_0^1 15_0^1$	31818.281	2518.5	2520.2	4
$19a_0^1 3_0^1$	31859.871	2560.1	2564.3	2
$18a_0^1 8a_0^1$	31901.958	2602.2	2601.0	2

Assignment <sup>+</sup>	Frequency (cm <sup>-1</sup> )	$\Delta v$ (cm <sup>-1</sup> )		I
		Observed	Calculated*	
$12_{00}^{21}$	31912.383	2612.6	2615.1	3
$7a_{00}^{1141}$	31920.351	2620.6	2616.7	4
$7a_{00}^2$	31944.378	2644.6	2646.0	4
$9b_{00}^{18b1}$	31972.985	2673.2	2677.2	3
$8a_{00}^{1151}$	31972.985	2673.2	2679.4	3
$9a_{00}^{18a1}$	32054.382	2754.6	2756.3	4
$19a_{00}^{1141}$	32071.951	2772.2	2773.7	9
$19b_{00}^2$	32177.985	2878.2	2881.4	6
$8a_{00}^{1141}$	32227.560	2927.8	2932.9	1
$1_{00}^3$	32235.864	2936.1	2934.9	1
$7a_{00}^{18a1}$	32258.053	2958.3	2962.2	0.5
$19a_{00}^2$	32263.243	2963.5	2960	0.5
$1_{00}^{29b1}$	32312.075	3012.3	3015.7	0.8
$19b_{00}^{18b1}$	32356.167	3056.4	3058.8	5
$7b_{00}^1$	32369.498	3069.7	A.O.	2
$19a_{00}^{18b1}$	32399.786	3100.0	3098.1	1
$20b_{00}^1$	32409.536	3109.8	A.O.	2

Assignment <sup>+</sup>	Frequency (cm <sup>-1</sup> )	$\Delta\nu$ (cm <sup>-1</sup> )		I
		Observed	Calculated*	
13 <sub>0</sub> <sup>1</sup>	32412.089	3112.3	A.O.	3
2 <sub>0</sub> <sup>1</sup>	32427.271	3127.5	A.O.	4
20a <sub>C</sub> <sup>1</sup>	32503.399	3203.6	A.O.	1
7a <sub>0</sub> <sup>2</sup> 6b <sub>0</sub> <sup>1</sup>	32509.293	3209.5	3209.9	1
12 <sub>0</sub> <sup>4</sup>	32572.557	3272.8	3273.6	1
9a <sub>0</sub> <sup>2</sup> 15 <sub>0</sub> <sup>1</sup>	32577.994	3278.2	3274.4	2
8a <sub>0</sub> <sup>2</sup>	32577.994	3278.2	3278.4	2
9a <sub>0</sub> <sup>2</sup> 9b <sub>0</sub> <sup>1</sup>	32597.793	3298.0	3293.3	1
9a <sub>0</sub> <sup>2</sup> 3 <sub>0</sub> <sup>1</sup>	32620.063	3320.3	3318.5	1
18a <sub>0</sub> <sup>3</sup> 18b <sub>0</sub> <sup>1</sup>	32643.293	3343.5	3348.7	2
18a <sub>C</sub> <sup>2</sup> 3 <sub>0</sub> <sup>1</sup>	32665.793	3366.7	3364.3	1
18a <sub>0</sub> <sup>3</sup> 6a <sub>0</sub> <sup>1</sup>	32692.096	3392.3	3395.5	1
7a <sub>0</sub> <sup>2</sup> 12 <sub>0</sub> <sup>1</sup>	32760.063	3460.3	3464.4	2
9a <sub>0</sub> <sup>2</sup> 14 <sub>0</sub> <sup>1</sup>	32827.183	3527.4	3527.4	3

+ All the measured bands involving planar modes are given in this table. The four main sequences involving out of planar modes (11, 16a, 16b and 17a) have also been given as the sequence structure has been one of the diagnostic features to identify the leading fundamental modes.

\* Frequencies have been calculated from the observed fundamentals in the electronic spectra.

A.O. As observed.

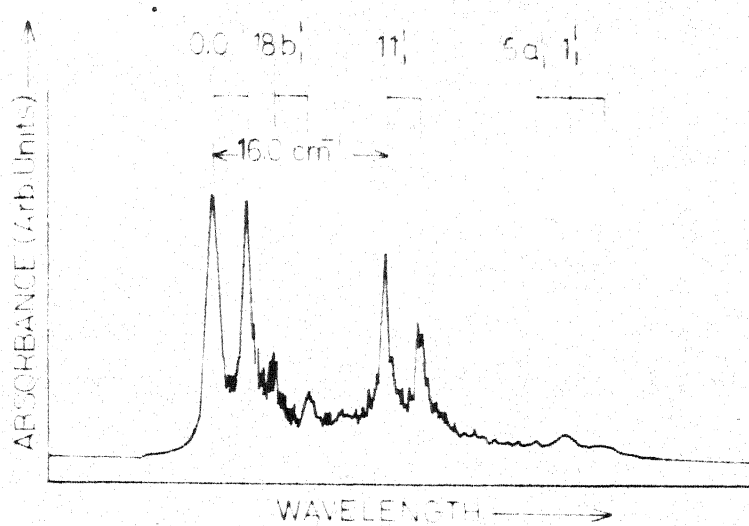


Fig.1(a) Microphotometer traces of high resolution electronic spectrum of Pyridine N-oxide (Typical Be-type contours in a small region near 0-0 (origin)).

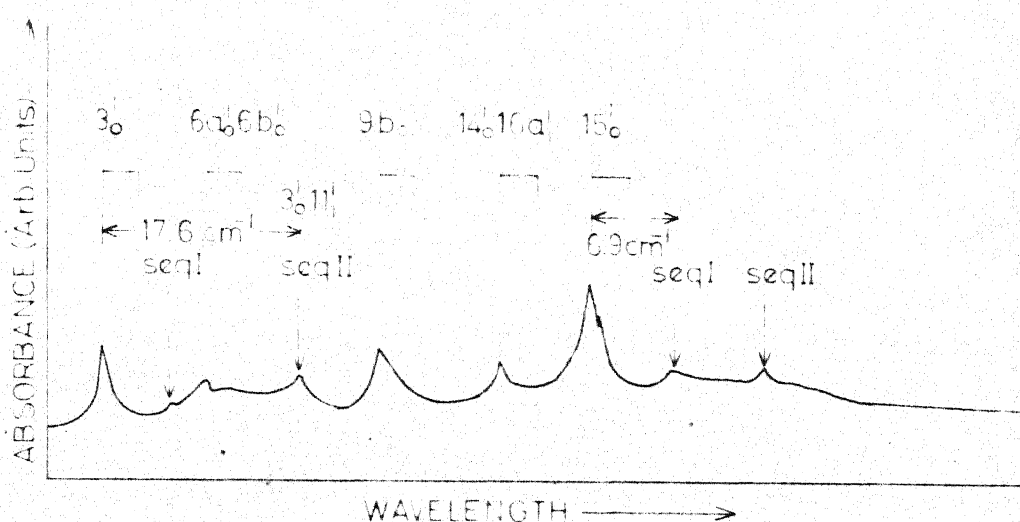


Fig.1(b) Microphotometer traces of high resolution electronic spectrum of Pyridine N-oxide (Typical Ae<sup>-</sup> type contours on longer wavelength side of  $3_0$  band)

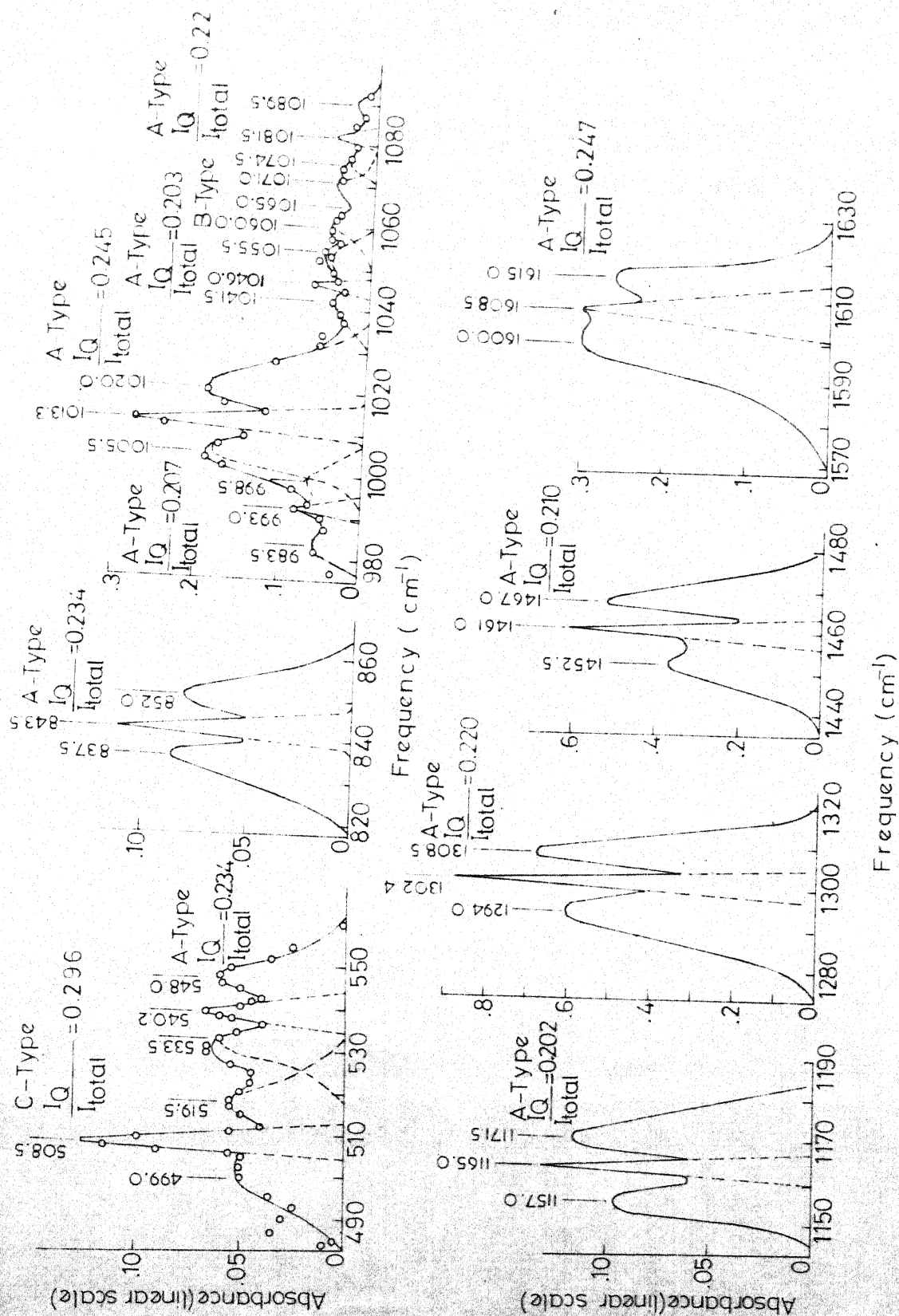
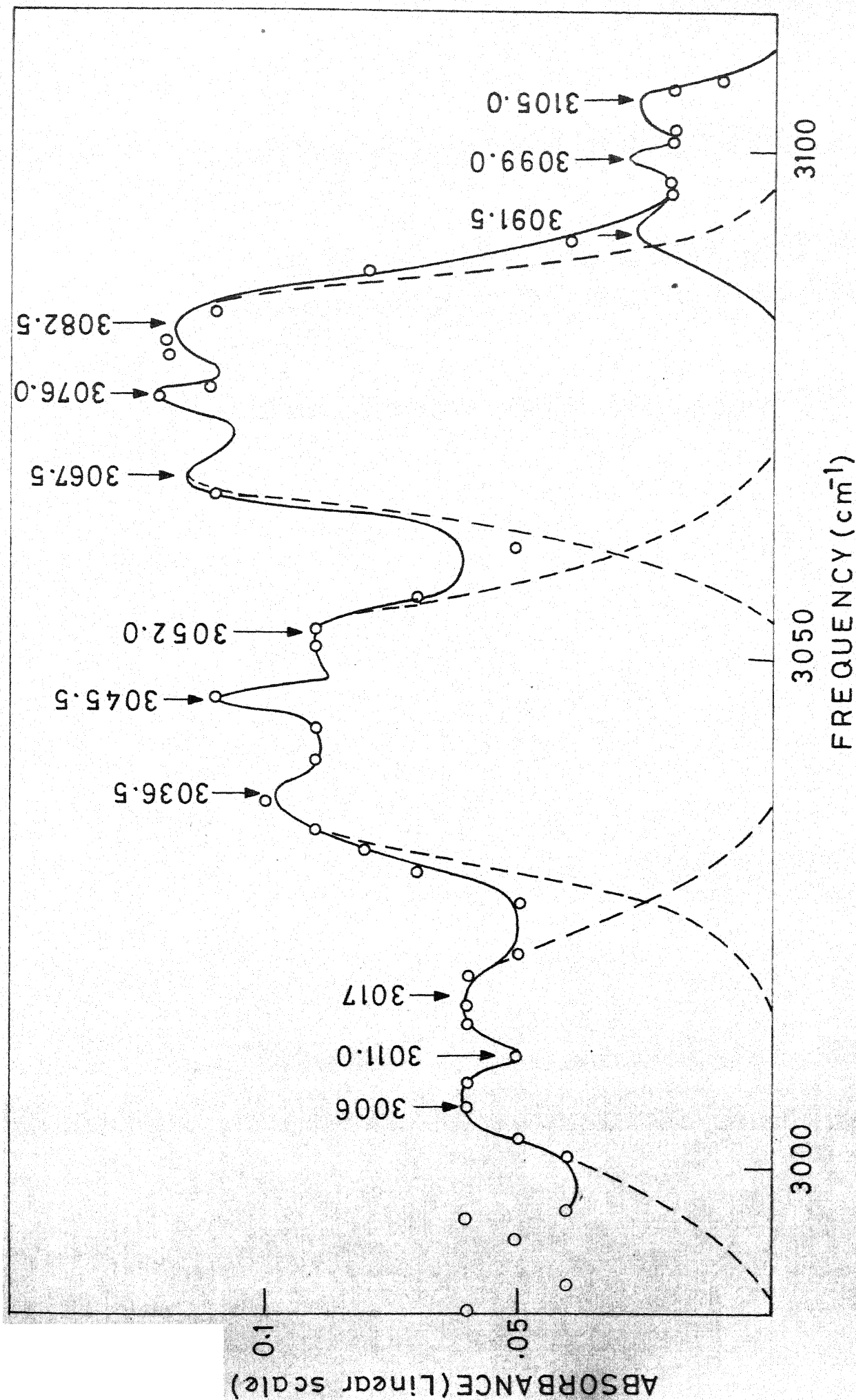


Fig.3.2(a) Vapour phase infrared band profiles of Pyridine N-oxide. The positions(in  $\text{cm}^{-1}$ ) of P Q and R branch peaks and the intensity ratio  $\frac{I_Q}{I_{total}}$  are given in the figure ( see text )



Fib. 3.2(b) Vapour phase infrared spectrum of Pyridine N-oxide in the C-H stretching region.

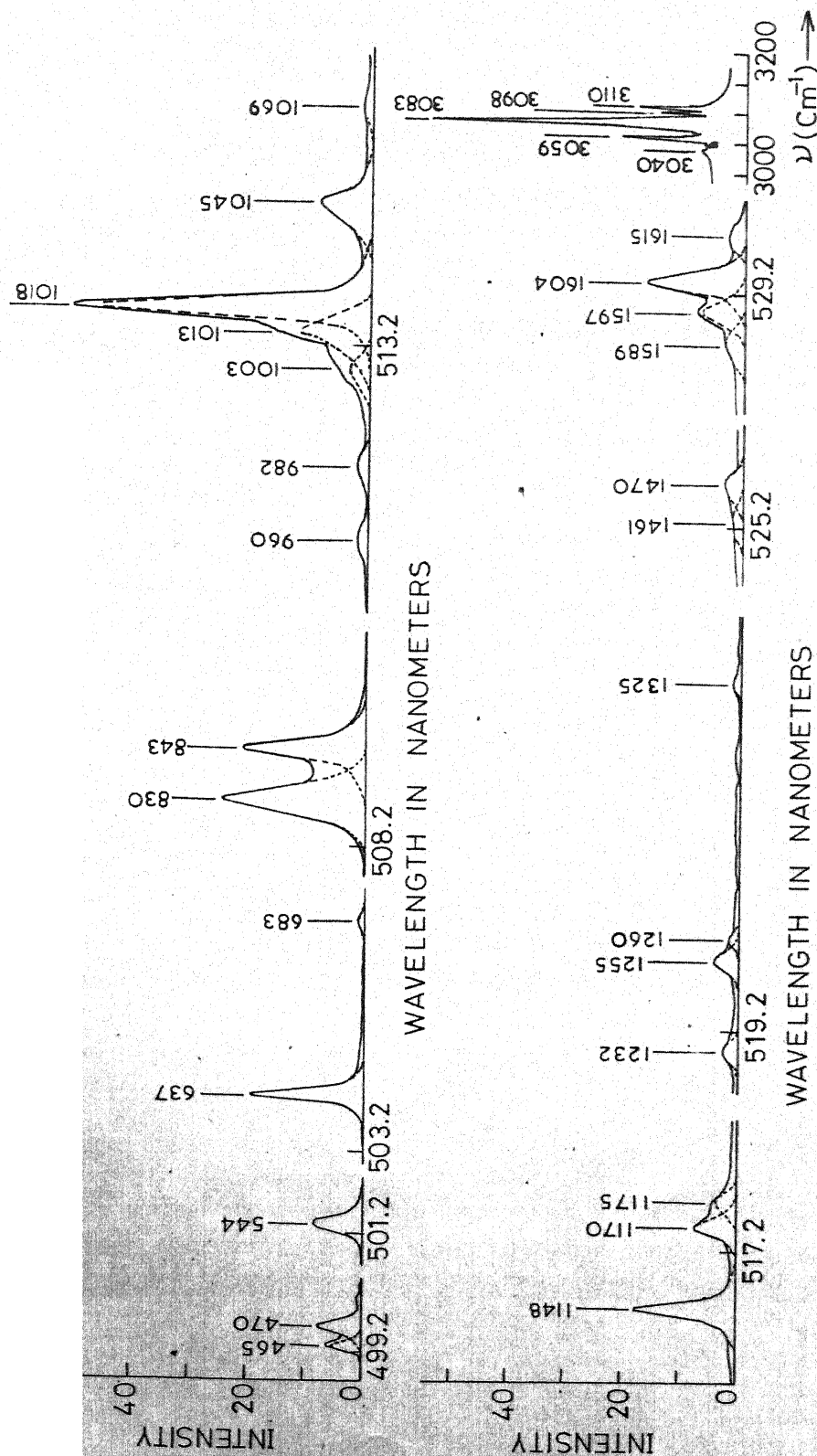


Fig. 3.3(a) The argon-ion laser excited Raman spectrum of Pyridine N-oxide in its internal mode region using a spex-1400 double monochromator (22) and cary-82 spectrophotometer for CH-stretching region.

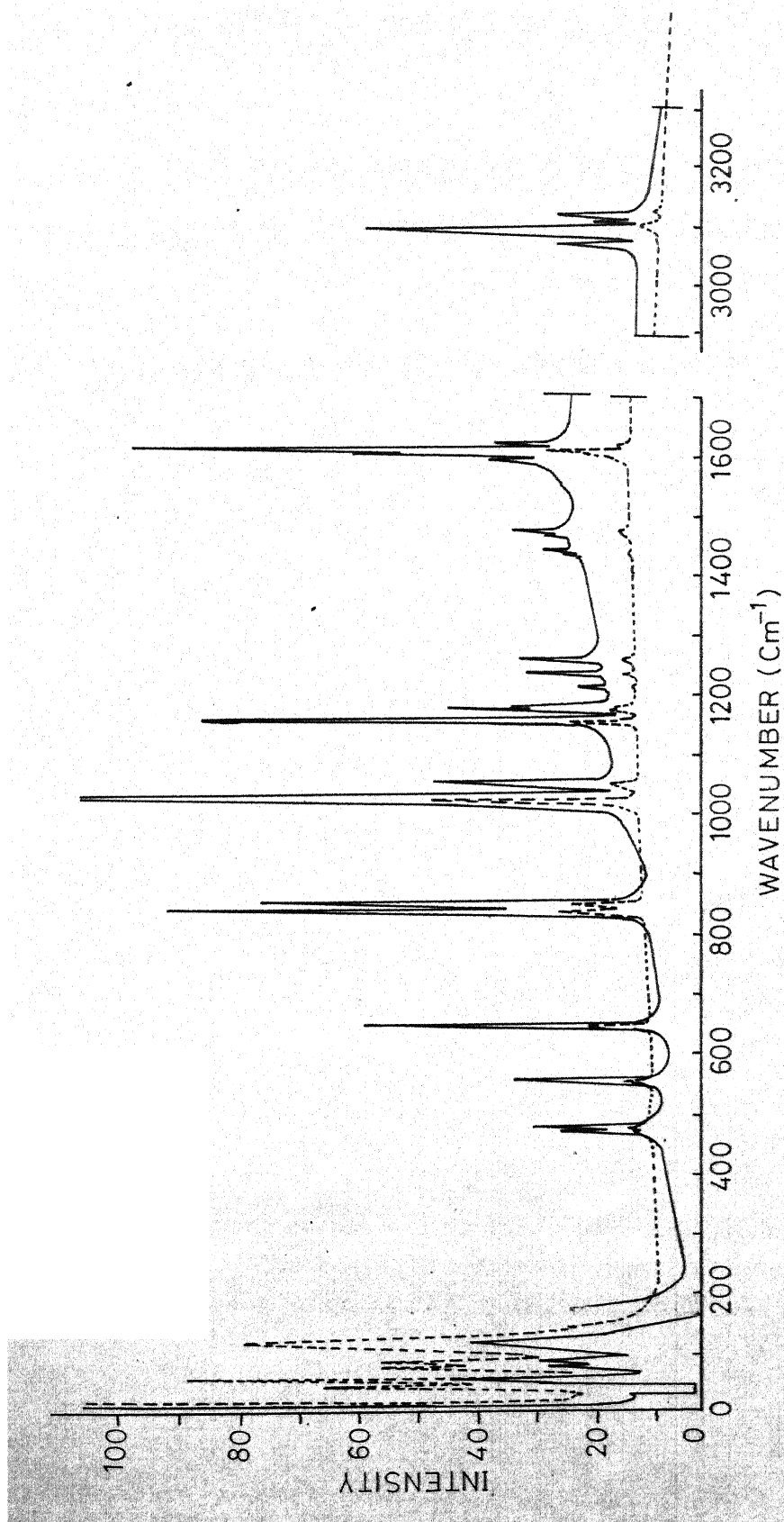
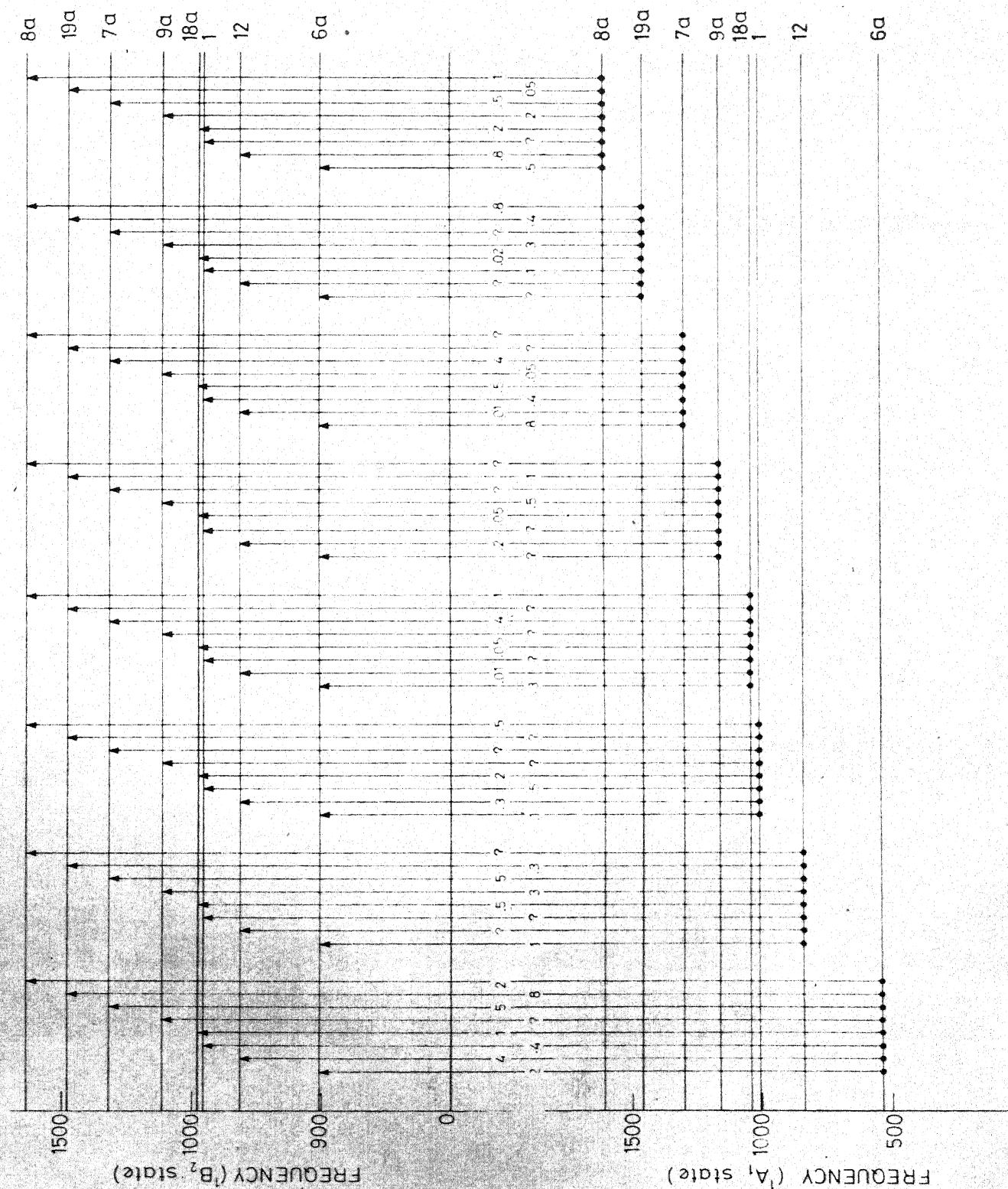


Fig. 3.3(b) The argon ion laser-excited Raman spectrum of Pyridine N-oxide using Cary-82 spectro photometer.



# Sequences and Cross-sequences Connecting $a_1$ Fundamentals of Pyridine N-oxide.



Sequences and Cross-sequences Connecting  $b_2$  Fundamentals of Pyridine N-oxide

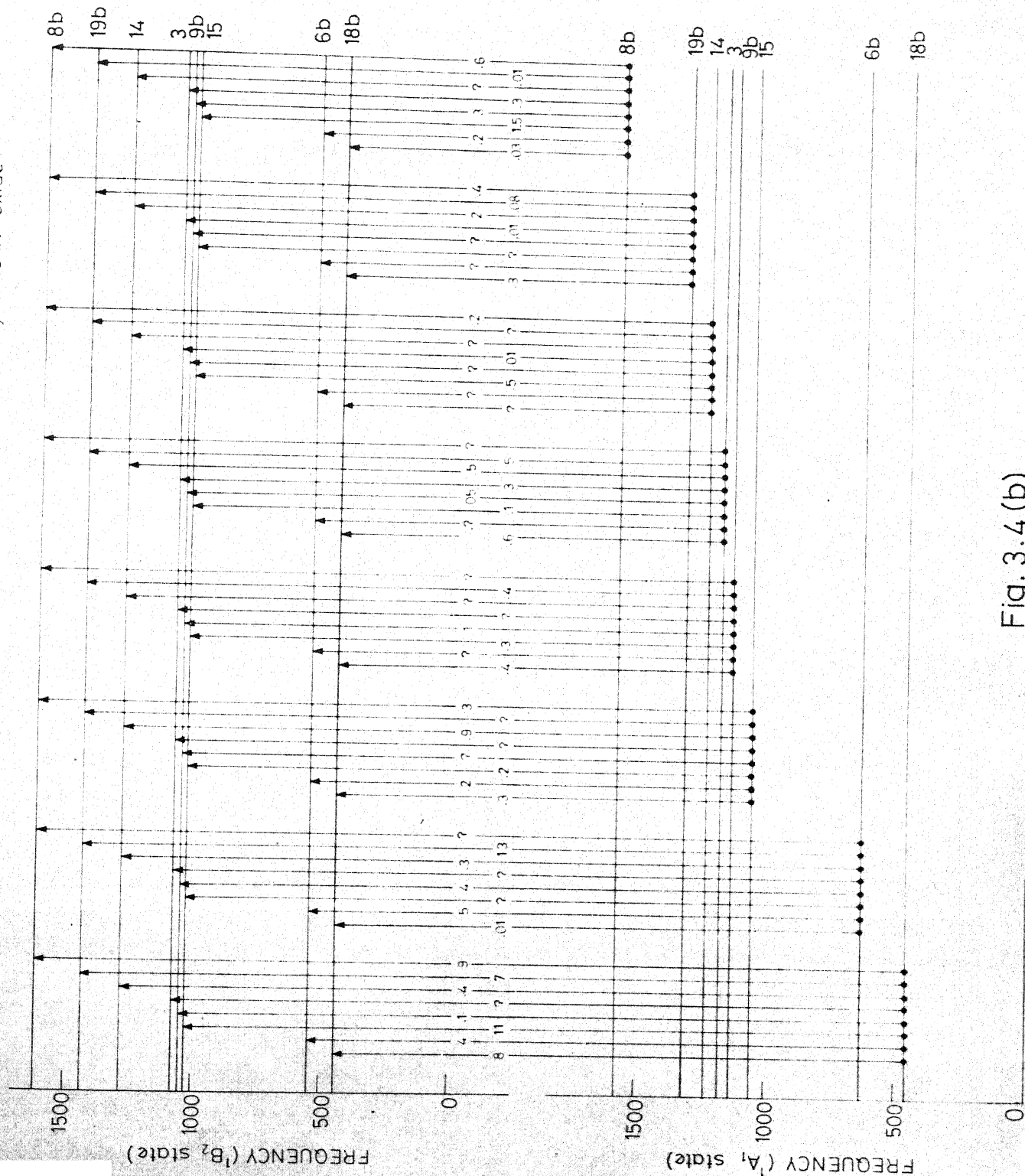


Fig. 3.4 (b)

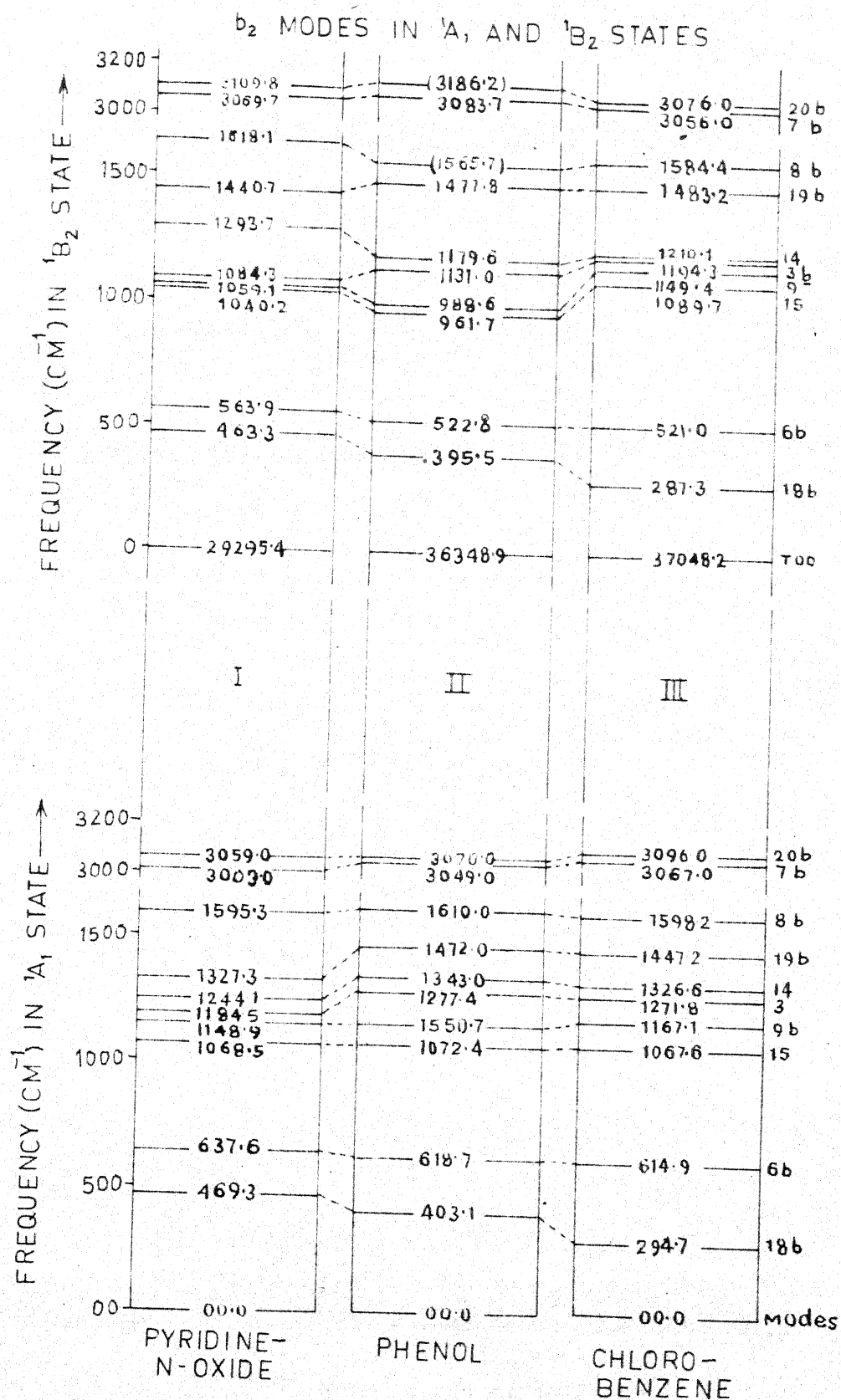


FIG.3.5(b). Comparison of levels in  $^1A_1$  and  $^1B_2$  states of Pyridine N oxide with iso(valence)-electronic molecules phenol and chlorobenzene ( $b_2$  modes)

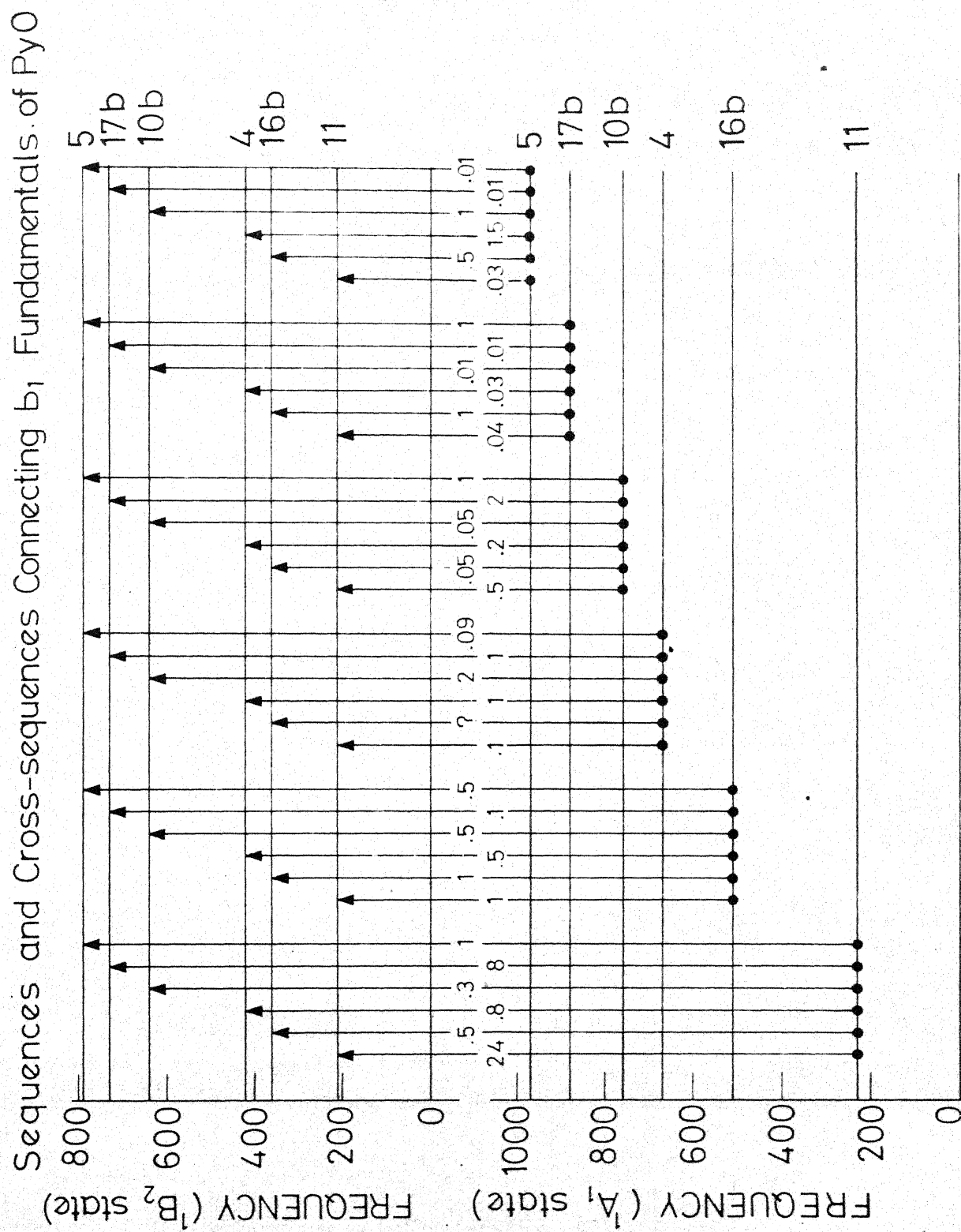


Fig. 3.6(a)

# Sequences and Cross-sequences Connecting $a_2$ Fundamentals of Pyridine N-oxide.

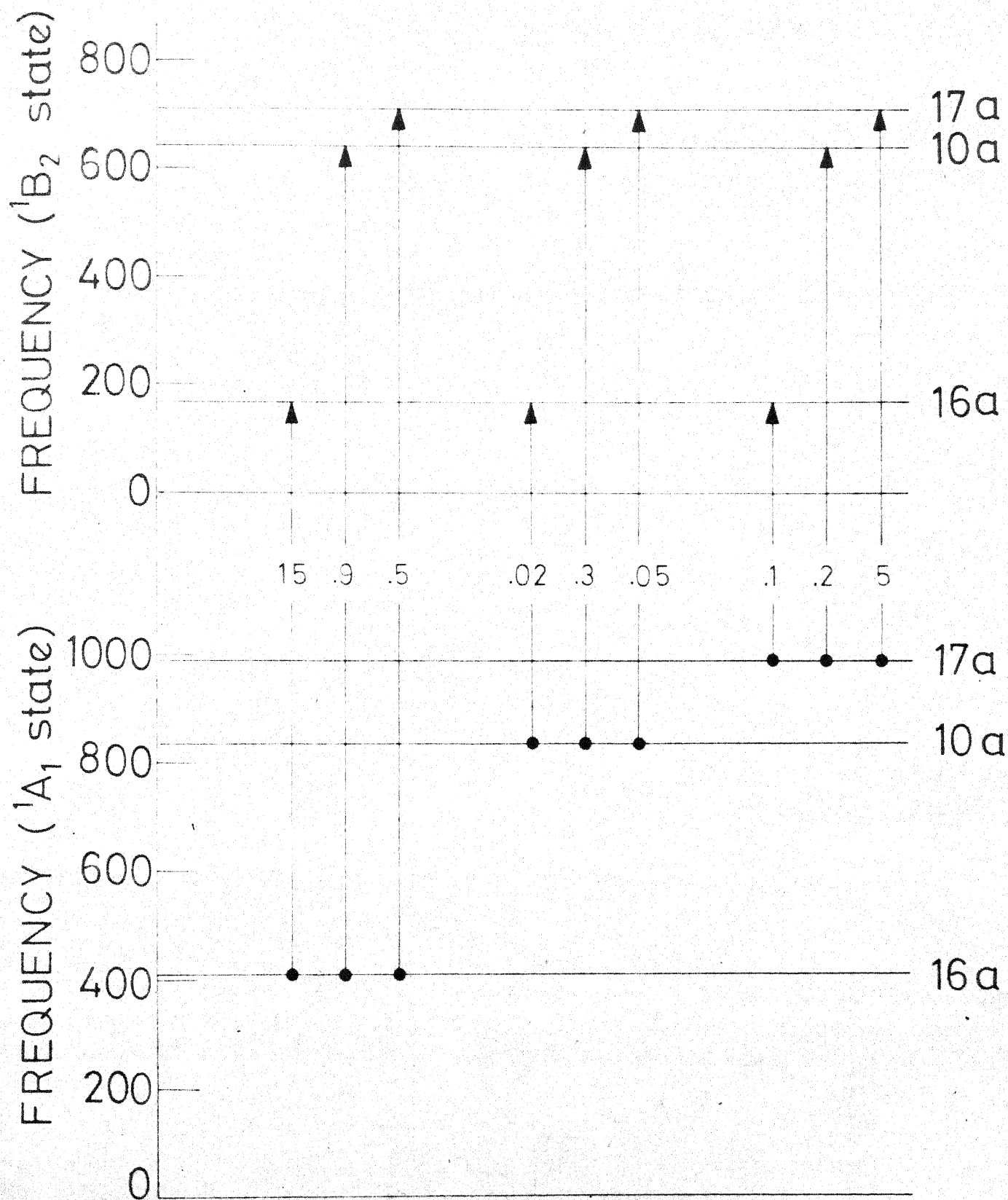


Fig. 3.6 (b)

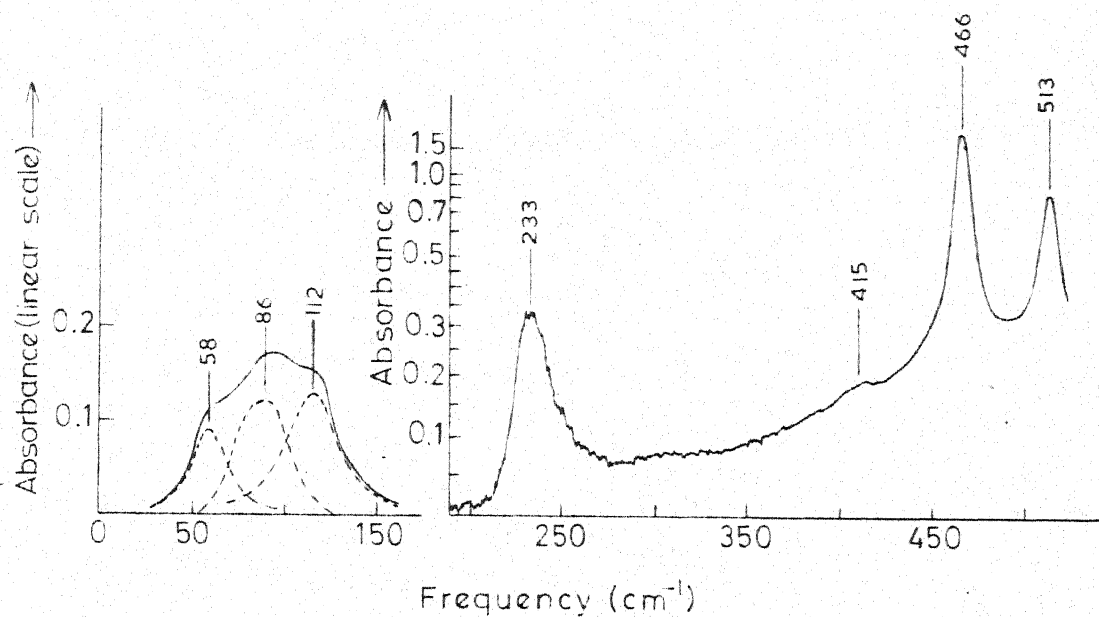


Fig.3.8 Far-infrared spectrum of Pyridine N-oxide in a polythene pellet in the range 33–525  $\text{cm}^{-1}$ . (The portion between 33–180  $\text{cm}^{-1}$  is replotted in a linear absorbance scale).

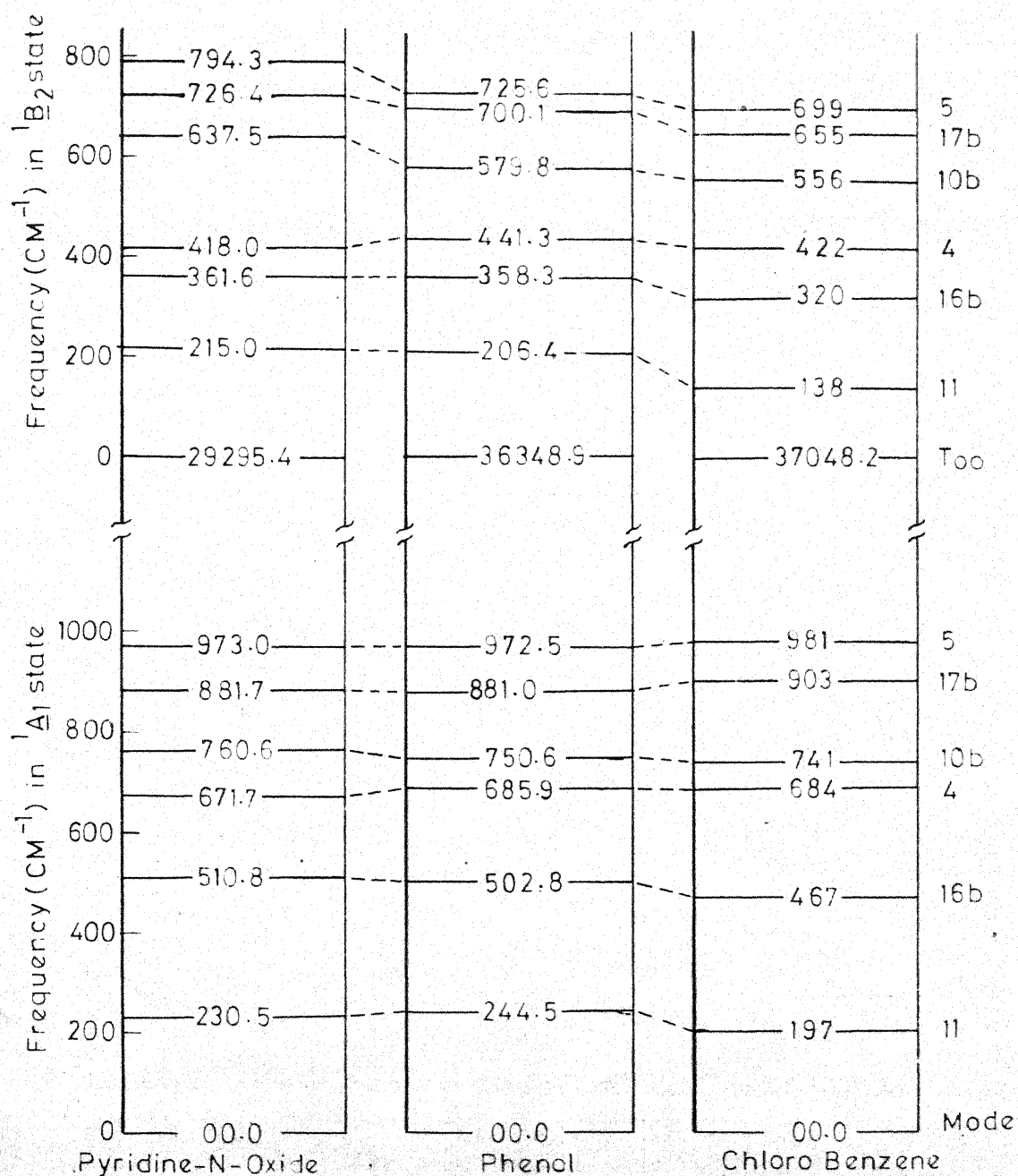
$b_1$  Modes in  $^1A_1$  and  $^1B_2$  states


FIG.3.9(a) COMPARISON OF THE LEVELS IN  $^1A_1$  AND  $^1B_2$  STATES OF PYRIDINE N-OXIDE WITH ISO (VALENCE) ELECTRONIC MOLECULES; PHENOL AND CHLOROBENZENE; FOR  $b_1$  MODES

$a_2$  Modes in  ${}^1A_1$  and  ${}^1B_2$  states

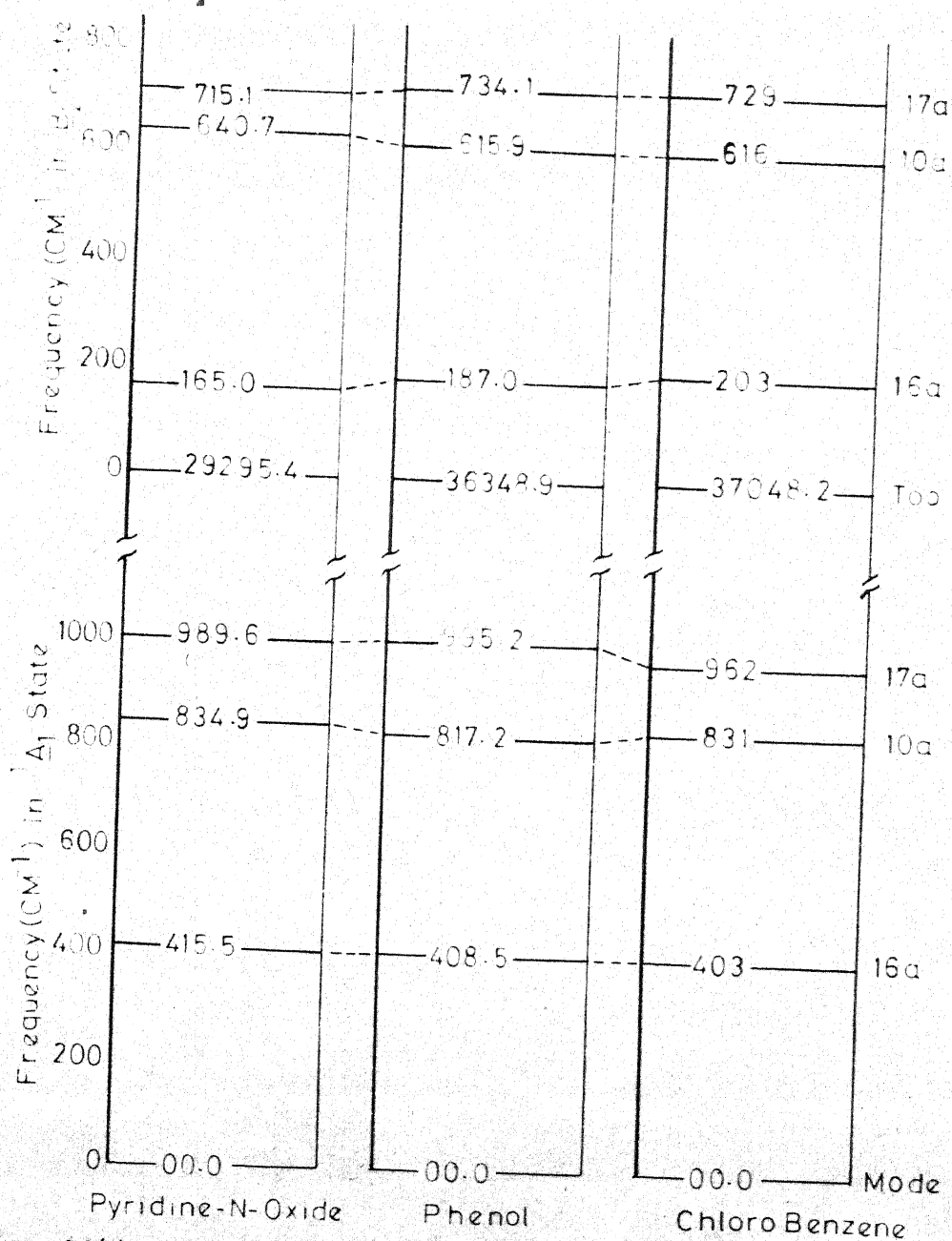


FIG.39(b) COMPARISON OF THE LEVELS IN  ${}^1A_1$  AND  ${}^1B_2$  STATES OF PYRIDINE N-OXIDE WITH ISO (VALENCE) ELECTRONIC MOLECULES, PHENOL AND CHLOROBENZENE; FOR  $a_2$  Mode





FIG. 3.10 THE INFRARED SPECTRA OF PYRIDINE N-OXIDE (A) SOLID PHASE SPECTRUM AT LIQUID NITROGEN, TEMPERATURE (B) SOLID PHASE SPECTRUM AT ROOM TEMPERATURE.

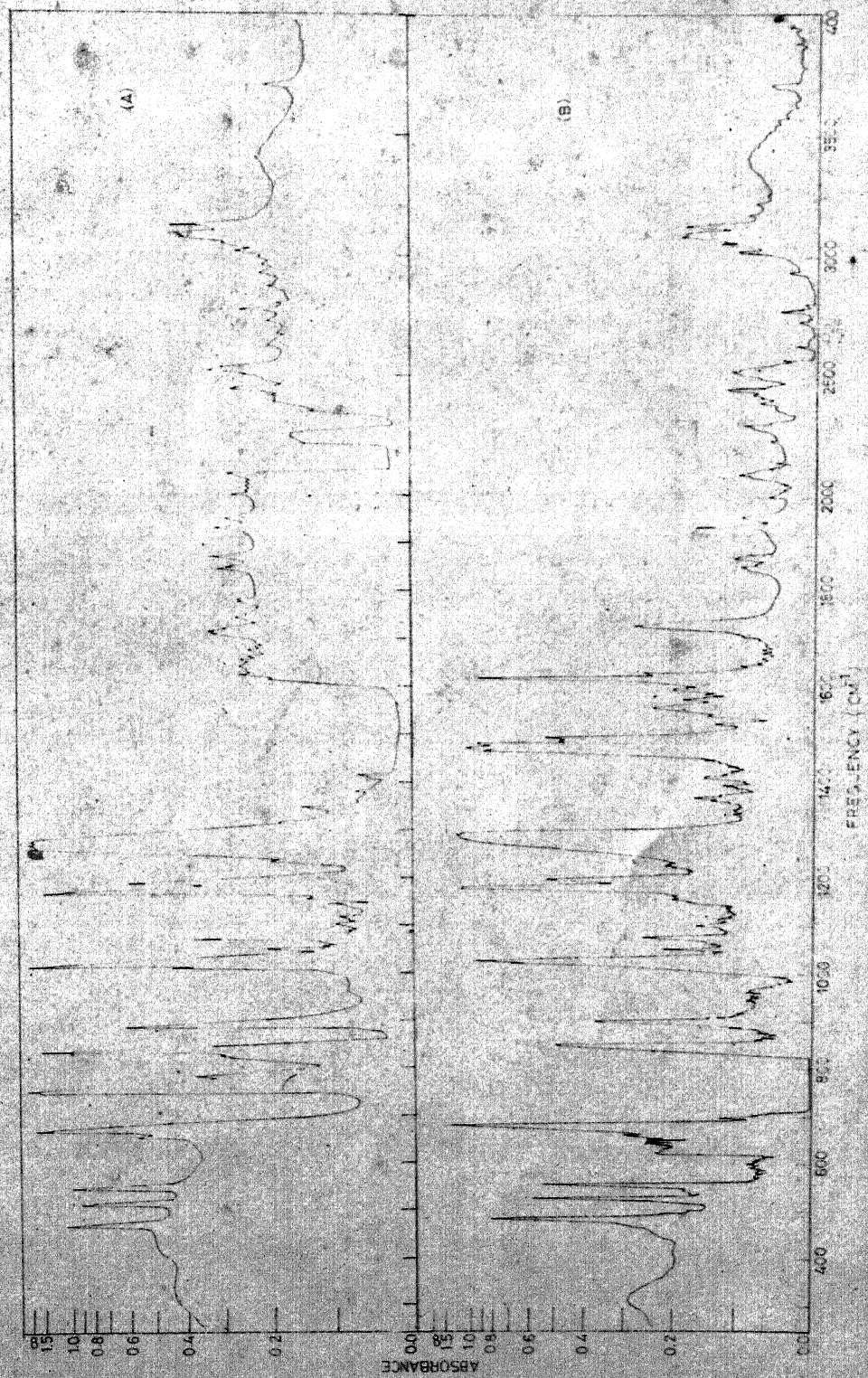


FIG. 11 THE INFRARED SPECTRA OF PYRIDINE N-OXIDE (A) IN CS<sub>2</sub> SOLUTION (B) IN CCl<sub>4</sub> SOLUTION, USING 0.5 MM. CELL.



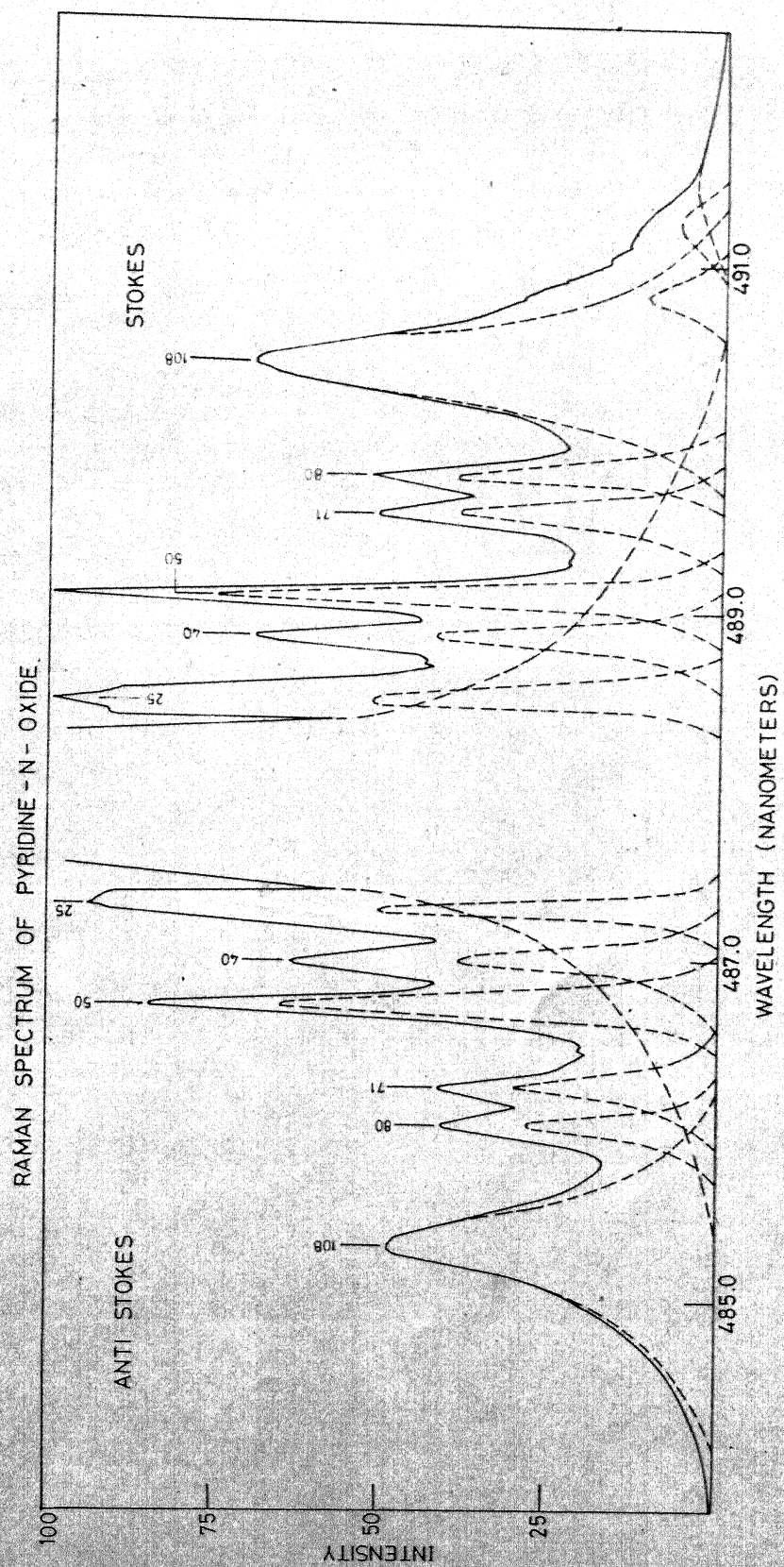


FIG. 3.12 LATTICE RAMAN SPECTRUM OF PYRIDINE N-OXIDE.

## Pyridine N-oxide

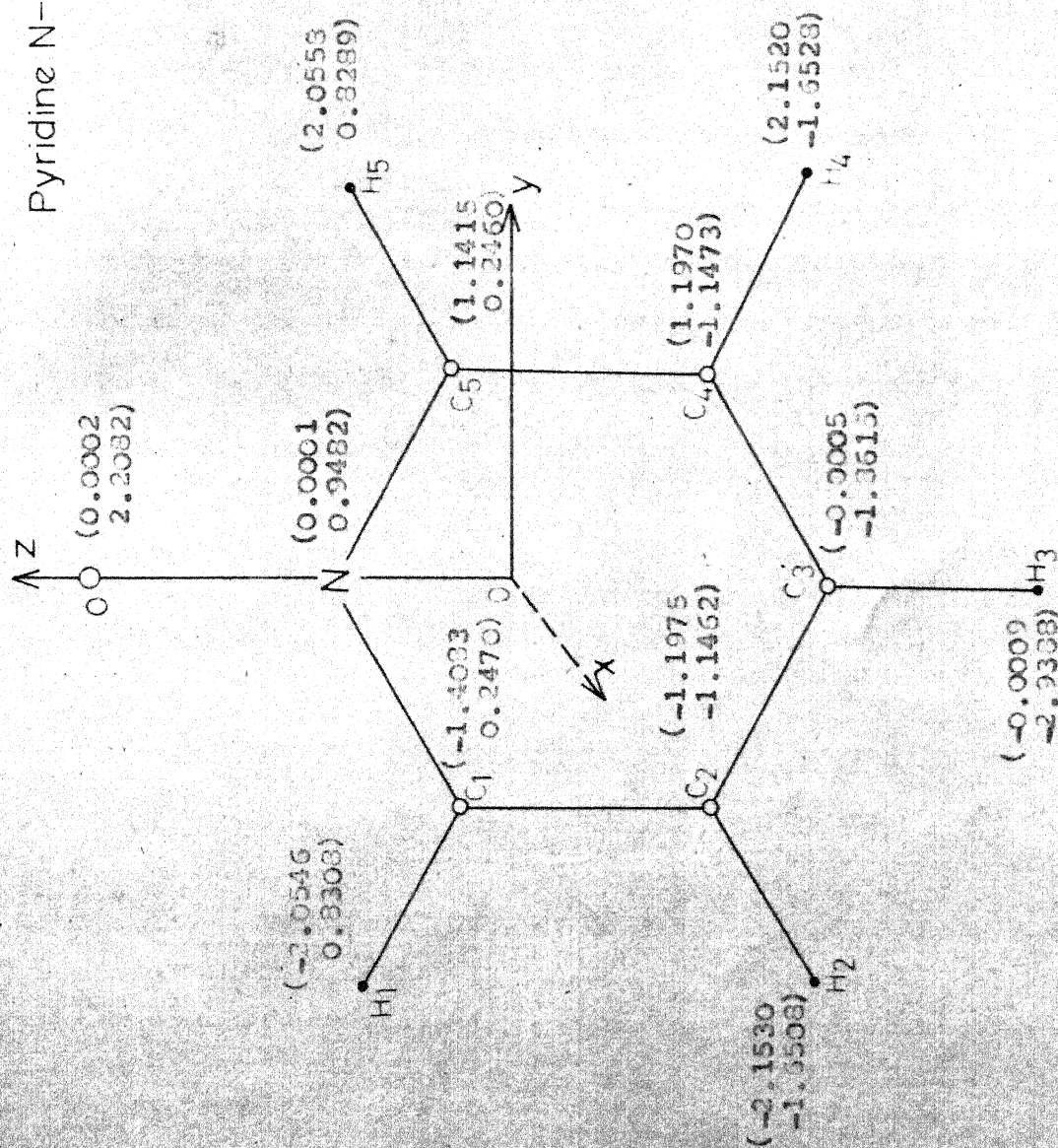


Fig. 3.13 Vapour phase geometry of pyridine N-oxide in ground state. The number in parentheses denote z, y coordinates (in Å units) of the atoms with respect to origin (0,0) the centre of mass of the molecule.

CHAPTER IVVIBRATIONAL SPECTRA OF  $\alpha$ -,  $\beta$ -, AND  $\gamma$ -PICOLINESABSTRACT

Accurate vibrational frequencies for gas phase  $\alpha$ -,  $\beta$ -, and  $\gamma$ -picolines have been deduced on the basis of infrared band-contour analysis. Supplementary information from gas phase electronic spectra, Raman data (liquid) and infrared spectra of liquid and solid (INT) phases, have also been used. Preliminary normal coordinate analysis results are given. The vapour phase frequencies have latter been used (Chapter VI) to deduce the thermodynamic constants for the compounds.

#### 4.0 INTRODUCTION

The study of the vibrational spectra of methyl substituted pyridines have attracted considerable interest in the past on account of their intrinsic interest as important biological compounds.

Structural informations concerning the ground state of  $\alpha$ -,  $\beta$ -, and  $\gamma$ -picolines are available on the basis of infrared (1-18) Raman (19-22), low resolution electronic spectra (23-25) and other studies (26-29) of the compounds. The vapour phase Raman spectra for the compounds under present investigation and microwave data for  $\alpha$ -, and  $\beta$ -picolines are not available in the literature. However, the microwave data are available for  $\gamma$ -picoline (29). The vibrational assignments for the compounds are not coherent (7, 10) and most of the assignments, below  $700\text{ cm}^{-1}$ , have been proposed on the basis of liquid phase spectra. Thus the assignment of the bands are not very reliable.

Therefore the aim of the present investigation is many fold: to report infrared spectra in vapour liquid and solid phases (INT) of  $\alpha$ -,  $\beta$ -, and  $\gamma$ -picolines, and also to make the detailed interpretation of the vibrational frequencies using their well resolved band contours. This is helpful in confirming or modifying the earlier assignments. Further we wish to examine the transferability of the force constants

in various situations, and to calculate the vibrational frequencies of the molecules utilizing the Urey-Bradley force constants (30). These constants have been known to be moderately transferable between chemically different molecules (31,32) especially if the substituents surrounding the appropriate coordinate are exactly identical (33), and were used to estimate the frequencies..

#### 4.1 EXPERIMENTAL

The samples for  $\alpha$ -,  $\beta$ -, and  $\gamma$ -Picolines were obtained from Messrs E. Merck and British Drug house. All the samples were dehydrated by refluxing over potassium hydroxide pellets, and then purified carefully by triple distillation under vacuum. In each subsequent distillation the middle fraction of the earlier distillate was used. The infrared spectra of vapour, liquid and solid states were recorded using P.E. 521 double beam infrared spectrophotometer. The spectra of vapours at various pressures and path lengths were measured over the frequency range  $250-4000\text{ cm}^{-1}$  at ambient temperature using a 10 meter variable path multiple reflection cell. To observe the distinct features in the spectra the scale factor was adjusted to give  $1\text{ cm}^{-1}$  equal to one division on the recording chart paper. Continuous dry air was flushed into the spectrophotometer to eliminate the water bands. The liquid phase spectra of  $\alpha$ -,  $\beta$ -, and

$\gamma$ -picolines were recorded using fixed cells of thickness .025 mm and 0.5 mm with CsBr and NaCl windows. The solid phase spectra of the compounds were recorded using the low temperature cell. Care was taken to deposit a uniform, thin crystalline film of the sample (from the vacuum system) onto the CsBr plate in the cold-finger to obtain a good spectrum. This was achieved by repeating the process of deposition several times.

The frequency accuracy for the vapour phase spectrum for the sharp bands may be taken to be better than  $\pm 0.5 \text{ cm}^{-1}$  and for liquid and solid phases about  $\pm 2 \text{ cm}^{-1}$ .

#### 4.2 SELECTION RULES AND NOTATIONS

Regarding the  $\text{CH}_3$  group as a single substituent 'X', the compounds  $\alpha$ -,  $\beta$ -, and  $\gamma$ -picolines have the same symmetries as the ortho, meta and para-di-substituted benzenes, respectively (6). The ring CH vibrations of these samples are the same as those for disubstituted benzenes. The  $\alpha$ -, and  $\beta$ -, picolines will still have strictly Cs symmetry. However, a non-rigid  $\gamma$ -picoline may be regarded as having  $\text{C}_{2v}$  symmetry and this greatly aids the correlation with pyridine N-oxide discussed in Chapter III. The modes of the benzene ring vibrations are essentially the same in a substituted benzene or pyridine as in benzene itself, so the universally accepted system of numbering the benzene vibrations (34) can be used without modification. This numbering scheme has been



followed for  $\alpha$ -,  $\beta$ -, and  $\gamma$ -picolines. The description of the substituent vibrations ( $\text{CH}_3$  group) has been given as such and are not allocated any vibrational number.

The fundamental frequencies of  $\gamma$ -Picoline can be divided into three parts: If we remove the  $\text{CH}_3$  group from  $\gamma$ -position of pyridine ring, the 24 fundamental modes of  $\gamma$ -pyridyl can be classified as  $9a_1 + 8b_2 + 5a_2 + 4b_1$ . As a result of substitution of  $\text{CH}_3$  group in the  $\gamma$ -position, 12 new modes will appear. Three of these may be considered as belonging to rigid methyl group having the mass 15, substituted for the  $\gamma$ -hydrogen of pyridine, and classified as  $1a_1 + 1b_1 + 1b_2$ . The other nine modes will appear from the internal motions of the methyl group and are classified as  $2a_1 + 3b_2 + 1a_2 + 3b_1$ . Thus the 36 fundamental modes of  $\gamma$ -Picoline are classified as  $12a_1 + 12b_2 + 8b_1 + 4a_2$  (8).

The classification of vibrations for  $\alpha$ -,  $\beta$ -picolines can be made only under  $C_s$  point group, even if a non-rigid  $\text{CH}_3$  group is assumed. Therefore the  $12a + 12b_2$  modes will belong to  $24a'$  species and likewise  $8b_1 + 4a_2$  modes classified in the second para above will belong to  $12a''$  species. However, to preserve the uniformity of description and assuming that pyridyl radical and  $\text{CH}_3$  group would largely retain their identities in different compounds we have used the notations described in the first paragraph in section 4.2.

The selection rules for all the ring modes in the infrared spectra for isolated vapour phase  $C_{2v}$  molecules are summarised and discussed in Chapter III (cf. Table 3.1). For the molecules belonging to  $C_s$  point group, the  $a_2$  modes can also appear in the infrared vapour phase spectra as C-type band contours.

#### 4.3 VIBRONIC ANALYSIS

The infrared absorption spectra of  $\alpha$ -,  $\beta$ -, and  $\gamma$ -picolines in vapour, liquid and solid (INT) phases in the range  $250\text{--}4000\text{ cm}^{-1}$  are shown in Figures 4.1 to 4.9. Typical A-, B-, and C-type vapour phase infrared band contours for the compounds have been replotted and shown in Figures 4.3, 4.6 and 4.9; where knowledge of isolated bands has been used to resolve the overlapping bands. All the observed infrared bands of these compounds in the three phases vapour, liquid and solid (at INT) along with the available liquid phase Raman bands (19,20) have been listed in columns 2, 4, 5 and 6 respectively, of tables 4.1 to 4.3. The interpretation of the observed frequencies along with the probable assignments to different modes has been given in column 7 of the tables. Numbering of the fundamental modes has been done according to the scheme described by E.B. Wilson (34) and has been given in column 2 along with their approximate description given in column 3 of Table 4.4 for  $\alpha$ -,  $\beta$ -, and  $\gamma$ -picolines. The internal modes of the

substituted  $\text{CH}_3$  group have also been given in Table 4.4 with their symmetry species (under the approximation discussed in section 4.2).

#### 4.31 THE INFRARED BAND CONTOURS

Vapour phase ir absorption spectra of  $\alpha$ -,  $\beta$ -, and  $\gamma$ -picolines in the range  $250\text{--}3150\text{ cm}^{-1}$  are shown in Figures 4.1, 4.4 and 4.7. The region beyond  $3150\text{ cm}^{-1}$  has been omitted because it does not contain prominent bands. In some of the bands the contour is quite distinct and the positions of P, Q and R branches (written at the top of each replotted band) are directly readable in the spectrum. However, when two or more bands overlap, the experimental intensity contour has been analysed graphically. Representative cases of such graphical analysis are indicated by dotted lines in the above figures. In most cases the characteristic vapour phase ir band envelopes and group theoretical considerations and comparison with electronic spectrum (23) have sufficed in making assignments and also in decomposing the overlapping bands into A-, B-, or C-types. In some cases this method of decomposition was not effective because of inherent complex nature of the bands and also due to excessive overlapping of different bands. The A-, B-, and C-type vapour phase infrared band contours are the primary sources for ascertaining the  $\underline{a}_1$ ,  $\underline{b}_2$  and  $\underline{b}_1$  modes in  $\alpha$ -,  $\beta$ -, and  $\gamma$ -picolines some of the  $\underline{a}_2$  modes listed in tables

4.1 to 4.4 also show C-type band contours especially in  $\alpha$ -, and  $\beta$ -picolines; evidently due to relaxation of  $C_{2v}$  selection rules (the actual symmetry being Cs).

The observed P, Q, and R positions of infrared vapour phase bands of the picolines are given in Tables 4.1 to 4.3. For A- and C-type bands, P, Q, and R represent the peaks positions of the corresponding vibration-rotation branches. For B-type bands the dip between the P and R branches is given in parentheses and represents the position of Q-head. The other symbols have their usual meanings. The observed separation between peak position of P and R branches,  $\Delta\nu_{PR}$  values, are shown in column 3 of tables 4.1 to 4.3. The observed band positions in infrared spectra in liquid states are given in column 4 of the tables. Most of frequencies used in column 7 of the above tables for the interpretation of the observed bands are taken from the vapour phase infrared data of the present work. In some cases, where contour is not distinct in vapour phase, liquid phase data have been used for the interpretation.

The relative Q-branch intensity ( $I_Q/I_{Total}$ ) of all the A-, and C-type bands has been estimated using semi empirical relation (35,36) and given at the top of each contour along with the peak positions. There is satisfactory agreement between the observed and computed values of  $\Delta\nu_{PR}$  and  $I_Q/I_{Total}$  within the experimental limitations. The computed rotational

parameters along with the calculated  $\nu_{PR}$  values are given in Table 4.5.

#### 4.4 FUNDAMENTAL VIBRATIONS

The assignments of the fundamental vibrations of  $\alpha$ -,  $\beta$ -, and  $\gamma$ -picolines have been made on the basis of infrared data obtained in the present study and compared with the earlier results. As picolines have higher molecular weight, and complex structure than those for pyridine N-oxide (PyO, discussed in Chapter III), the correlation between molecular structure and principle absorption is not very simple. The spectra of  $\alpha$ -,  $\beta$ -, and  $\gamma$ -picolines exhibit a multiplicity of bands in comparison with the spectra of simpler molecules like PyO (37-39), phenol (40-42) and chlorobenzene (43,44). The distinct bands have carefully been isolated and assigned to the respective modes. The striking features in the infrared spectra, the vibrational frequencies whose assignments have been changed and the assignments of the infrared vapour phase inactive vibrations have been discussed in the following pages.

##### 4.41 THE $a_1$ FUNDAMENTAL MODES

The observed totally symmetric  $a_1$  modes for the vapour phase  $\alpha$ -,  $\beta$ -, and  $\gamma$ -picoline molecules are given in column 4, 6 and 8 respectively of Table 4.4. The computed values of the frequencies for different modes, based on normal coordinate

analysis are listed in columns 5, 7 and 9 for respective molecules. It may be noted from the spectra given in Figures 4.1, 4.3, 4.4, 4.6 and 4.7, 4.9, that most of the vibrations belonging to  $a_1$  mode appear as A-type bands for picolines. In some cases graphical intensity resolution method was used to isolate the bands. The assignments of  $a_1$  fundamental modes below  $1600\text{ cm}^{-1}$  are well supported by liquid phase Raman bands given in Tables 4.1 to 4.3. The assignments of the vibrational frequencies for  $\gamma$ -picoline are also confirmed by the reported Raman depolarization ratio (4). The mode  $18a$  of  $\alpha$ -picoline is weak in vapour phase, but strong in liquid and solid phase IR spectra. The CH stretching modes are not well resolved in the vapour phase infrared spectra and, the bands were isolated graphically. Such bands are located at  $2940.0$ ,  $3024$ , and  $3076.0$  for  $\alpha$ -picoline and at  $2971$ ,  $3006.0$ ,  $3069.0$  and  $2941.0$ ,  $3022.0$ ,  $3100\text{ cm}^{-1}$  for  $\beta$ -, and  $\gamma$ -picolines, respectively. The assignments of the bands and their approximate descriptions are given in columns 2 and 3 of Table 4.4.

The CN and CC stretching modes  $19a$  and  $8a$  are strongest in all the three picolines. The shift in frequency for ring breathing mode 1 in  $\alpha$ -,  $\beta$ -, and  $\gamma$ -picolines is due to substitution of  $\text{CH}_3$  group at different positions in pyridine ring with respect to the nitrogen atom. The A-type infrared bands below  $700\text{ cm}^{-1}$  have not been observed earlier (4,7,10)

and the x-sensitive mode  $6a$  has been left unassigned (10) for  $\alpha$ -, and  $\gamma$ -picolines. (See also under section 4.43 for low lying  $a_1$  and  $b_2$  ( $a'$ ) fundamentals from electronic spectral studies.) Liquid phase infrared frequencies were used for the assignments of other  $a_1$  modes. However, the mode  $6a$  is strong with characteristic A-type shape for  $\alpha$ -, and  $\gamma$ -picolines, observed at 545.5, and 513.0  $\text{cm}^{-1}$  and this mode is at 534.0  $\text{cm}^{-1}$  for  $\beta$ -picoline with weak intensity. Another x-sensitive mode  $7a$  at 1297  $\text{cm}^{-1}$  representing C-X stretching frequency (where X represents the  $\text{CH}_3$  group) was reported earlier (10) as  $b_2$  fundamental for  $\alpha$ -picoline. However, strong A-type infrared vapour phase band has appeared at 1297.0  $\text{cm}^{-1}$  and has been assigned to the mode  $7a$ . The internal modes of substituted  $\text{CH}_3$  group having characteristic shapes denoting  $\nu\text{HCH}$  and  $\nu\text{CH}$  frequencies for picolines have also been given in Table 4.4. The computed values of  $\Delta\nu_{\text{PR}}$  for A(||)-type band using the relation discussed earlier (35,36), are 14.8, 14.2 and 13.7  $\text{cm}^{-1}$  for respective  $\alpha$ -,  $\beta$ -, and  $\gamma$ -picolines given in Table 4.5. These are in good agreement with the observed values.

#### 4.42 THE $b_2$ FUNDAMENTAL MODES:

The typical shapes of B(1)-band contours of  $\alpha$ -,  $\beta$ -, and  $\gamma$ -picolines are shown in Figures 4.1, 4.3, 4.4, 4.6 and 4.7, 4.9; respectively. The observed frequencies of  $b_2$  modes have been given in columns 4, 6 and 8 of Table 4.4

for respective picolines. In almost all the B(1) bands (except for some hybrid character as in  $632.5\text{ cm}^{-1}$  band of  $\beta$ -picoline) there is no Q-branch and the dip between P and R branches is quite characteristic. The ring deformation mode 6b has appeared with characteristic shape at  $633.0$ ,  $632.2$  and  $678.0\text{ cm}^{-1}$  for  $\alpha$ -,  $\beta$ -, and  $\gamma$ -picolines respectively and has been observed for the first time. Information about this mode may be more reliable from electronic spectral studies (23) (see section 4.43). The mode 6b is medium strong in vapour phase infrared spectra for  $\alpha$ -, and  $\beta$ -picolines, but very weak for  $\gamma$ -picoline. However, this mode is strong in liquid and solid phases for all the three picolines. The other b<sub>2</sub> fundamental modes given in Table 4.4 have shown recognizable contours except the CH stretching modes, which have been resolved graphically. The X-sensitive mode 18b in  $\beta$ -, and  $\gamma$ -picolines is overlapped by water bands and could not be isolated in vapour phase infrared spectra. The liquid phase infrared frequencies have been used for the assignment of mode 18b for  $\beta$ -, and  $\gamma$ -picolines (However see section 4.43). The modes 15 and 8b of  $\gamma$ -picoline have appeared in solid phase as a result of splittings of liquid phase bands given in Table 4.3. The internal modes of  $\text{CH}_3$  substituent having the characteristic B-type bands and denoting the  $\nu\text{HCH}$  and  $\nu\text{CH}$  stretching frequencies for the picolines have also been given in Table 4.4. The computed



values of  $\Delta\nu_{PR}$  for B(1)-type bands are 11.6, 11.1 and 10.9  $\text{cm}^{-1}$  for the respective  $\alpha$ -,  $\beta$ -, and  $\gamma$ -picolines. There is a satisfactory agreement between the observed and computed  $\Delta\nu_{PR}$  values within the experimental limitations.

#### 4.43 The $a_1$ and $b_2$ Modes from Electronic Spectral Studies.

The vapour phase electronic spectra provide accurate analysis of low-lying ground state frequencies from the observed hot bands; and sequence and cross-sequence structure observed in such transitions (38-44). Although no such detailed analysis is available for picolines, from the reported data of Rush and Sponer (23), additional excellent corroborative evidence is obtained for three low lying frequencies in  $\alpha$ - and  $\beta$ -picolines and 4 bands in case of  $\gamma$ -picolines. These frequencies obtained from an analysis of 287.7 nm band system of  $\alpha$ -picoline, 288.2 nm band system of  $\beta$ -picoline and 284.3 nm band system of  $\gamma$ -picoline may provide a comparison with the detailed analysis of Pyridine-N-oxide discussed in Chapter III. The  $2b_2$  modes given in table 4.4 for  $\gamma$  picoline have larger uncertainty than expected and may point error in locating the exact band origin from IR studies for these bands.  $376 \text{ cm}^{-1}$  in Table 4.4 from liquid phase ir and  $678 \text{ cm}^{-1}$  is from very weak vapour phase infrared spectra. Hence for these low

lying frequencies electronic data should be more accurate and reliable, except for band origin differences as no gyrovibronic analysis is available at present.

#### 4.44 The $b_1$ Fundamental Modes

Out of 8 vibrations of  $b_1$  class, there are 3 recognized vapour phase C-type band contours for  $\alpha$ -picoline and 4 for each  $\beta$ -, and  $\gamma$ -picolines in the vapour phase infrared spectra given in Figs. 4.1, 4.3, 4.5, 4.7 and 4.9. Liquid phase Raman frequencies (19,20) have been used to assign the lowest  $b_1$  fundamental mode 11. The band at  $796.0\text{ cm}^{-1}$  and a overlapped A-type band at  $801\text{ cm}^{-1}$  in vapour phase IR spectra of  $\gamma$ -picoline was assigned earlier (8) as  $a_1$  and  $b_1$  modes, however, a clearcut C-type band at  $801.0\text{ cm}^{-1}$  has been observed in vapour phase infrared spectra and hence there is no ambiguity in their assignments as the modes 10b and 12 respectively. In all the C-type bands, which have been assigned as  $b_1$  modes, the Q-branch is prominent and their P and R wings are characteristically broad. All the  $b_1$  fundamental modes, including the internal mode of  $\text{CH}_3$  group have been listed in Table 4.4. Out of plane CH stretching frequencies at  $2968.0$ ,  $2971.0$ , and  $2938.0\text{ cm}^{-1}$  have been assigned as  $b_1$  modes for  $\alpha$ -,  $\beta$ -, and  $\gamma$ -picolines

respectively. The other internal modes of  $\text{CH}_3$  group of  $b_1$  class correspond to the wagging mode of  $\text{CH}_3$  group and asymmetric HCH angle deformation for the picolines have been given in Table 4.4. The calculated value of  $\Delta\nu_{\text{PR}}$  for  $\alpha$ -,  $\beta$ -, and  $\gamma$ -picolines are 22.2, 21.4, and 20.5  $\text{cm}^{-1}$  respectively. In all the distinct C-type bands the observed values of  $\Delta\nu_{\text{PR}}$  are within  $\pm 1.0 \text{ cm}^{-1}$ .

#### 4.45 THE $a_2$ FUNDAMENTAL MODES

The vibrational frequencies belonging to  $a_2$  class are listed in Table 4.4. As the picolines have strictly Cs symmetry, some of the C-type bands have also been assigned to the  $a_2$  modes. The modes 16a and 17a have been assigned on the basis of vapour phase C-type band contours at 401.0 and 930.0  $\text{cm}^{-1}$  for  $\alpha$ -picoline. Liquid and solid (INT) phase infrared bands given in Table 4.4 have been used for the assignment of other  $a_2$  modes of  $\alpha$ -,  $\beta$ -, and  $\gamma$ -picolines.  $\text{CH}_3$  group torsion frequency lies at  $< 125 \text{ cm}^{-1}$  (12) for the picolines.

#### 4.5 SOLID PHASE INFRARED SPECTRA

The solid phase infrared spectral data for  $\alpha$ -,  $\beta$ -, and  $\gamma$ -picolines have also been given in Tables 4.1 to 4.3 for comparison with those for liquid and vapour phase data. The sharpening of the bands has been observed for solid picolines

with respect to liquid and vapour phases (cf Figs 4.2, 4.5 and 4.8). Changes in peak positions in some of the bands have been observed, and few new bands appeared in the spectra of pure solid state which were helpful in assignment of some ambiguous bands. In  $\gamma$ -picoline, a band at  $1603\text{ cm}^{-1}$  in liquid phase was splitted at INT in  $1607.0$  and  $15780\text{ cm}^{-1}$  and these have been assigned as the modes  $8a$  and  $8b$ . Similarly, the liquid phase band at  $1068.0$  of  $\gamma$ -picoline was splitted and shifted to  $1094.0$  and  $1078.0\text{ cm}^{-1}$  at INT. A new weak band at  $1115\text{ cm}^{-1}$  in  $\alpha$ -picoline and medium strong band  $1171.0$  in  $\beta$ -picoline were also observed at INT. The most strong band at  $800\text{ cm}^{-1}$  in liquid phase of  $\gamma$ -picoline was splitted in  $816.0$  and  $802.0\text{ cm}^{-1}$  with strong intensity. A tentative interpretation of the new bands and splitted liquid phase bands for picolines have been given in Tables 4.1 to 4.3. These new bands may be due to distortion of rings in the crystals, and low frequency lines are probably due to small group of molecules present in the crystals (19).

#### 4.6 MOLECULAR GEOMETRY

The rotational constants of  $\gamma$ -picoline are known from microwave spectral analysis (29). However, no microwave data were available in literature for  $\alpha$ -, and  $\beta$ -picolines, and the rotational constants for these molecules have been theoretically calculated. For  $\gamma$ -picoline it was suggested earlier (29)

that the methyl group has  $C_{3v}$  symmetry, whereas the molecule as a whole has  $C_{2v}$  symmetry. Assuming a planar ring with the bond lengths and bond angles of pyridine molecule (45) and considering  $CH_3$  group as having  $C_{3v}$  symmetry, the most probable and simplest geometry has been proposed and the rotational constants for  $\alpha$ -,  $\beta$ -, and  $\gamma$ -picolines are calculated and given in Table 4.6 and 4.7. The coordinates of all atoms of picolines with respect to the origin (0,0,0) at atom  $C_1$  are illustrated in Figs. 4.10, and 4.11 as computed on IBM 7044 computer. The computed parameters given in Table 4.5 are corresponding to the best fit of the observed rotational constants (29) and rotational parameters.

#### 4.7 THEORETICAL CALCULATION OF FUNDAMENTAL MODES

The normal coordinate calculation was carried out using Wilson's G-F matrix method (46,47). These calculations have been performed on IBM 7044 using the program used earlier by Schachtschneider et al (48). The program is set up in internal displacement coordinates and is similar to that adopted by Overend and Scherer (49). The program is designed to determine the Cartesian coordinates and to evaluate the numerical values of the G and Z matrices. The normal modes of vibration, the L-column vectors, the PED among the diagonal elements of F matrix, the cartesian displacements of individual atoms for each mode, the mean square amplitude of individual atoms for

each mode and mean amplitude for atoms summed over all normal modes are obtained in tabulated form. Table 4.7 gives the definition of internal coordinates. The computed frequencies are given in Table 4.4 for  $\alpha$ -,  $\beta$ -, and  $\gamma$ -picolines. A simplified UBFF comprising of force constants transferred from benzene (48) and chlorobenzene (49) is set up. During calculations, minor and systematic alternations in stretching, bending, wagging, and torsional force constants have been made in order to fit the observed frequencies of picolines. A set of force constants which yields the best frequency fit for the vibrations of the molecules under study is given in Table 4.8.

# REFERENCES

1. C.G. Cannon and G.B.B.H. Sutherland, *Spectrochim. Acta* 4, 373 (1951)
2. E.A. Coulson, J.L. Hales and E.F.G. Herington, *J. Chem. Soc.* 2127(1951)
3. H. Shindo and H. Ikekawa, *Pharm. Bull. (Japan)* 4, 192(1956)
4. D.L. Long, F.S. Murfin, J. Hales and W. Kynaston, *Trans. Faraday Soc.* 53, 1171 (1957).
5. A.R. Katritzky and A.R. Hands, *J. Chem. Soc.* 2202(1958)
6. L.J. Bellamy, *Infrared Spectra of Complex molecules*, John Wiley and Sons Inc, New York), 1959
7. J.H.S. Green, W. Kynaston and H.M. Paisley, *Spectrochim. Acta* 19, 549 (1963).
8. D.A. Long and W.O. George, *Spectrochim. Acta* 19, 1977(1963)
9. R. Issac, F.F. Bentley, H. Sternglaz, W.C. Coburn Jr. C.V. Stephenson and W.S. Wilcox, *Appl. Spectrosc* 17, 90(1963)
10. E. Spinner, *J. Chem. Soc.* 3860 (1963)
11. A. Roders and H. Perkampus, *Z. Naturforsch* 18b, 600 (1963)
12. V. Lorenzelli and G. Randi, *Atti Acad. Nazl. Lincei, Rend. Classe Sci. Fis., Mat. Nat.* 34 527 (1963)
13. G. Varsanyi, T. Farago and S. Holly, *Acta Chim. Acad. Sci. Hung.* 43, 205 (1965)
14. D.B. Cunliffe-Jones, *Spectrochim Acta* 21, 747 (1965)
15. M. Katocha and T. Urbansk, *Bull. Acad. Pol. Sci. Ser. Sci. Chem.* 15, 413 (1967)
16. A.R. Katritzky, C.R. Palmer, F.J. Swinbourne, T.T. Tidwell and R.D. Topson, *J. Amer. Chem. Soc.* 91, 636 (1969)
17. B.R. Pandey and R.S. Tripathi, *Ind. J. Pure and Appl. Phys.* 9 346 (1971)

18. S.S. Singh, *Labdev* 10 (1), 14 (1972)
19. G.S. Kastha, *Ind. J. Phys.* 31, 395 (1957)
20. K. Ranaiah and V.R. Srinivasan, *Proc. Ind. Acad. Sci.* A55, 221 (1962)
21. S.A. Timoshenko, A.V. Sechkarev and N.I. Dvorenko *Izv. Vyssh. Ucheb. Zaved., Fiz.* 11(8) 87 (1968).
22. R.I. Berezhine and N.K. Sidorov, *Opt. Spektrosk* 32(2) 279 (1972).
23. J.H. Rush and H. Sponer, *J. Chem. Phys.* 20, 1847 (1952)
24. A. Mangini and F. Montanari, *Proc. Intern. Meeting Mol. Spectrosc.* 4th Bologna 1, 458 (1962).
25. J. Kracmar, J. Kramerove, & J. Zyke, *Pharmazie* 30, 567 (1968)
26. M. Goodgame and P.J. Hayward, *J. Chem. Soc. A., Inorg. Phys. Theoret.* 632 (1966).
27. D.H. Brown, D.H. Stewart and D.E.H. Jones, *Spectrochim. Acta* 29A, 213 (1973)
28. Y. Kakiuti, H. Saito and M. Akiyama, *J. Mol. Spectrosc.* 35, 66 (1970)
29. H.D. Rudolph, H. Dreizler and H. Seiler, *Z. Naturforsch.* A22(11), 1738 (1967)
30. T. Shimanouchi, *J. Chem. Phys.* 17, 245 (1949)
31. J. Overend and J.R. Scherer, *J. Chem. Phys* 32, 1681 (1960)
32. J.R. Scherer and J. Overend, *Spectrochim. Acta*, 17, 719 (1961)
33. J.H. Schachtschneider and R.G. Snyder, *Spectrochim. Acta*, 19, 117 (1963)
34. E.B. Wilson, *Phy. Rev.* 45 706 (1934)
35. M.M. Rai, H.D. Bist and D.P. Khandelwal, *Appl. Spectrosc.* 25, 442 (1971).
36. V.N. Sarin, M.M. Rai, H.D. Bist and D.P. Khandelwal, *Chem. Phys. Lett.* 6, 473 (1970)



37. H.D. Bist and J.S. Parihar, Chem. Phys. Lett. 32, 244 (1975)
38. H.D. Bist, J.S. Parihar and J.C.D. Brand, J. Mol. Spectrosc. (in Press)
39. J.S. Parihar and H.D. Bist (communicated)
40. H.D. Bist, J.C.D. Brand and D.R. Williams, J. Mol. Spectrosc. 21, 76 (1966)
41. H.D. Bist, J.C.D. Brand and D.R. Williams, J. Mol. Spectrosc. 24, 402 (1967)
42. H.D. Bist, J.C.D. Brand and D.R. Williams, J. Mol. Spectrosc. 24, 413 (1967)
43. H.D. Bist, V.N. Sarin, A Ojha and Y.S. Jain, Spectrochim Acta 26A, 841 (1970)
44. Y.S. Jain and H.D. Bist, J. Mol. Spectrosc. 47, 126 (1973)
45. B. Bak, L.H. Nygard and J.R. Andersen, J. Mol. Spectrosc. 2, 361 (1958)
46. Bailey, Gordon, Hale, Herzfeld, Ingold and Pole, J. Chem. Phys. 44, 2724 (1966)
47. E.B. Wilson, Jr. J. Chem. Phys. 7, 1047 (1939)
48. N. Neto, M. Scrocco and S. Califano, Spectrochim. Acta, 22, 1981 (1966)
49. J.R. Scherer, Spectrochim. Acta, 20, 345 (1964)

TABLE 4.1

OBSERVED BAND POSITIONS, PR SEPARATIONS AND INTERPRETATIONS IN INFRARED  
BAND CONTOURS OF  $\alpha$ -PICOLINE

Sl. no.	<u>Infrared Band Positions</u>				<u>Raman</u> (19)	<u>Interpreta- tion</u>	<u>Anharmo- nicity</u>
	<u>Vapour phase</u> (RT)	$\Delta\nu$ PR	<u>Liquid Phase</u> (RT)	<u>Solid Phase</u> (INT)	<u>Liquid</u> (RT)		
1	2	3	4	5	6	7	8
1	-	-	-	-	213	11	
2	-	-	322 W				
3	-	-	332 W			(11)( $\tau_{CH_3}$ )=338	6
4	352 P (358) (B) 363 R	11	359 ms	361 366		18b	
5	387 P 401 Q (G) 410 R	21	403 S	402		16a	
6			416 W	406		(11) <sub>2</sub> =426	10
7	459.5 P 468.5 Q (G) 478.0 R	19.5	466 S	468		16b	
8	538.0 P 545.5 Q (A) 553.0 R	15	545 m	547	542	6a	
9	625 P (633) (B) 638 R	12	626 S	626	630	6b	
10	692 P (697) (B) 702 R	11	-	-		(11)(16b)=681	
11	725 P 735 Q (A) 739 R	14	725 S	730		12	

1	2	3	4	5	6	7	8
12	740.5 P 751.5 Q (G) 761.0 R	20.5	751 vs	759 771		$(11)_2^4(18b) = 787$	
13	-	-	797 W	801 ms	810	$10b, (16a)_2 = 802$	5
14	-	-	884 W	893		17b, 10a	
15	924.0 P (930.0) (B) ? 935.0 R	11	-	-		17a	
16	969.0 P 976.0 Q (A) 984.0 R	14	974 mw	979		1	
17	993.0 P (999) (B) 1005.0 R	12	999 ms	1004	998	$(18b)(6b) = 991$	8
18	1026.0 P 1032.0 Q (A) 1039.0 R	13	1037 sh	1037 s		18a	
19	1045.0 P (1050.5) (B) 1056.0 R	11	1047 sh	1042	1051	15	
20	1096.0 P (1103.0) (B) 1108.0 R	12	1095 mw	1100		$\alpha HCH(CH_3 \text{ group})$ $(18b)(12) = 1093$	
21	-		-	1115		$(6a)_2 ?, \gamma CH_3$	
22	1140.0 P 1147.5 Q (A) 1154.5 R	14.5	1145 s	1149		9a	
23	1187.0 P (1193.0) (B) 1199.0 R	12	-	-		$(16a) (10b) = 1198$	5

1	2	3	4	5	6	7	8
24	1231.0 P 1238.0 Q (B) 1243.0 R	12	-	-	1239	3	
25	1238.0 P 1245.0 Q (A) 1252.0 R	14	1234 m	1242		(11) (18a) =1245	0
26	1289.0 P 1297.0 Q (A) 1303.5 R	14.5	1291	1295	1298	7a, (16a) (10a) = 1285	12
27	1349.0 P 1354.0 Q (B) 1362.0 R	13	-	-	-	14.	
28	1374.0 P 1382.0 Q (A) 1388.0 R	14	1378_ms	1378	1380	$\alpha\text{HCH}(\text{CH}_3 \text{ group})$ (a <sub>1</sub> )	
29	1430.0 P (1435.0) (B) 1442.0 R	12	1431 ms	1425		19b	
30	-	-	1453 ms	1455		(18b)( $\alpha\text{HCH}$ )=1461 $\alpha\text{HCH}(\text{CH}_3 \text{ group})$	3
31	1471.0 P 1477.0 Q (A) 1486.0 R	15	1481	1484		19a, (12) <sub>2</sub> = 1470	-7
32	-	-	1541 w	1543		(4) (10b) = 1548.5	7.5
33	-	-	1570 s	1570	1571	8b, (6a) (18a) = 1577.5	7.5
34	1585 P (1594) Q (A) 1600 R	15	1587 s	1587	1595	8a	
35	1598.0 P (1603.0) (B) 1610.0 R	12	1597 s	1598		(6a) (15) =1596	-7
36	-	-	1680 ms*	1677		(4) (17a) =1681 (10a) (17a)=1714	1 -1

1	2	3	4	5	6	7	8
						(10a)(17a)=1714	-1
37	-	-	1715 m*	1702		(12)(1) = 1711	-4
						(18b)(14) = 1712	-3
38	-	-	1775 ms*	1783		(12)(18a)=1767	-8
						(10a) <sub>2</sub> = 1768	-7
39	-	-	1798 w*	1801		(18b)(19b)=1793	-5
40	-	-	1847 m*	-		( $\alpha$ HCH)(12) = 1838	-9
41	-	-	1874 ms*	-		(12)(9a) = 1882	-8
						(6b)(3) = 1871	-3
42	-	-	1922 ms*	1924		(18b)(8b) = 1928	6
43	-	-	1949 ms*	-		(1) <sub>2</sub> = 1952	3
44	-	-	2032 m*	-		(12)(7a) = 2032	0
						(6a)(19a) = 2022	-10
45	-	-	2097 w*	-		(7a)(10b) = 2094	-3
46	-	-	2152 mw*			(15)( $\alpha$ HCH)=2153	1
47	-	-	2173 w*			(18a)(9a) = 2179.5	6.5
48	-	-	2198 w*			( $\alpha$ HCH) <sub>2</sub> = 2206	-8
						(6b)(8b) = 2203	5
49	-	-	2247 w*			(9a)(4b) = 2250.5	3.5
50	-	-	2297 ms*			(9a) <sub>2</sub> = 2295	-2
51	-	-	2342 w*	2328		( $\alpha$ HCH)(3) = 2341	-1
52	-	-	2399 m*	2407 vw		(15)(14) = 2404.5	5.5
53	-	-	2448 m*			(1)(19a) = 2453	5
54	-	-	2479 m*	2467		(3) <sub>2</sub> = 2476	-3
						(15)(19b) = 2485.5	6.5
55	-	-	2531 m*			( $\alpha$ HCH)(19b) = 2538	7
56	-	-	2601 s*			(7a) <sub>2</sub> = 2594	-7

1	2	3	4	5	6	7	8
57	-	-	2626 ms*	2622 2634		(15)(8b) = 2620.5 (9a)(19a) = 2624.5 (18a)(8a) = 2626	-5.5 -1.5 0
58	2873 P 2881 Q (A) 2888 R	15	2865 w	2864		(19b) <sub>2</sub> = 2870	5
59	2933 P 2940 Q (A) 2947 R	15	2928 m	2927	2928	$\nu$ CH (Subs (a <sub>1</sub> )) (14)(8b) = 2924	-4
60	-	-	2968 vw	2963		$\nu$ CH(subs)CH <sub>3</sub> group a <sub>1</sub>	
61	-	-	2998 w	2992		$\nu$ CH(b <sub>2</sub> , b <sub>1</sub> )(CH <sub>3</sub> group)	
62	-	-	3001 w	-			
63	-	-	3008 ms	3008		(8b)(19b) = 3005	-3
64	3019 P (3024) (B) 3030.5 R	11.5	3016 s	3018		2 7b	
65	-	-	-	3052	3054		
66	3069 P 3076 Q (A) 3083 R	14	3075 m	3077	3066	20a, (8a) (19a) <sub>1</sub> = 3071	-5
67	3088 P (3094) (B) 3099 R	11	3092 m	3092 w		20b	
68	-	-	3635 w	-		(20b)(6a) = 3639.5	4.5
69	-	-	3655 w	-		(2)(6b) = 3657	2
70	-	-	3700 w	-		(20a)(6b) = 3709	9

\* Liquid phase IR bands, using thick film of the compound (0.5 mm) in CsBr Cells.

TABLE 4.2

OBSERVED BAND POSITIONS, PR SEPARATIONS AND INTERPRETATIONS  
IN INFRARED BAND CONTOURS OF  $\beta$ -PICOLINE

Sl. no.	IR BAND POSITIONS				Raman(20) Liquid	Interpreta- tion	Anharmonic- ity
	Vapour (RT)	$\Delta\nu_{PR}$	Liquid Phase RT	Solid Phase (INT)	(RT)		
1	2	3	4	5	6	7	8
1	-	-	327 w		218 254	11 ( $\tau\text{CH}_3$ ) <sub>2</sub>	
2	-	-	340	336	334	18b (11)( $\tau\text{CH}_3$ )=343	3
3	387.0 P 400.0 Q (C) 407.5 R	20.5	398 s	398	407	16b	
4	-	-	418 w	418 w		16a	
5	-	-	453 w	456 w			
6	-	-	470 w	475 w	476	(18b)( $\tau\text{CH}_3$ )=465	-5
7	-	-	504 vw	-			
8	525.0 P 534.0 (A) 539.0 R	14	535 vs	535	535	6a	
9	-	-	558 w	-			
10	627 P (632.5)Q (B) 639 R	12	628 s	634 658 mw	605 628 651	6b (6a)( $\tau\text{CH}_3$ )=659	1
11	702.0 P 713.5 Q (C) 723.0 R	21	711 vs	707 vs		4	
12	743.0 P 751.0 Q (A) 758.5 R	15.5	-	-		12	

1	2	3	4	5	6	7	8
13	772.0 P 785.5 Q (C) 793.0 R	21	787 vs	789 804	795	10b, (16b) <sub>2</sub> = 800	-4
14	913.0 P 922.5 Q (C) 934.0 R	21	919 w	924	888 931	17b	
15	-	-	-	944 w	971	10a	
16	978.0 P 986.0 Q (A) 992.0 R	14	987 w	989	989	1	
17	-	-	-	1002 ms		17a	
18	1024.5 P (1030.5) (B) 1036.0 R	11.5	1027 vs	1032	1028	15	
19	1040.0 P 1049.0 Q (A) 1054.0 R	14	1040 ms	1041	1043	18a	
20	-	-	-	1066	1069	$\gamma\text{CH}_3$	
21	1096.0 P (1102.5) (B) 1107.0 R	12	1101 s	1106	1092	$\alpha\text{HCH}(\text{CH}_3\text{ group})$	
22	1118.0 P (1124.0) (B) 1130.0 R	12	1125 s	1125	1146	(16a)(4)=1131	
23	1153.0 P 1162.0 Q (A) 1168.0 R	15	-	1171	-	(6b)(6a)=1166.5	
24	1184.5 P 1192.0 Q (A) 1199.0 R	14.5	1188 s	1189	1206	9a	
25	1221.0 P 1230.0 Q (A) 1236.0 R	15	1225 ms	1226	1228	7a	
26	1236.0 P (1243.0) (B) 1249.0 R	13	1248 w	1256		(6a)(4) = 1247.5	



1	2	3	4	5	6	7	8
27	1279.0 F 1297.0 Q (A) 1304.0 R	15	-	-	1287	(6a)(12) = 1285	
28	1334.0 F 1340.0 Q (A) 1349.0 R	15	1333 w	1333		1+	
29	1380.0 F 1387.0 Q (A) 1394.5 R	14.5	1383 ms	1383	1380	$\alpha$ HCH (CH <sub>3</sub> group)	
30	1418.0 F (1423.0) (B) 1429.0 R	11	1413 s	1413		19b	
31	1472.5 F 1481.0 Q (A) 1488.0 R	15.5	1479 vs	1479	1460 1480	$\alpha$ HCH (CH <sub>3</sub> group) 19a	
32	1576.5 F (1583.0) (B) 1588.0 R	11.5	1576	1579	1577	8b	
33	1594.0 F 1601.5 Q (A) 1608.0 R	14	1593	1601 1609	1598	8a (1)(6b) = 1618.5	
34	-	-	1655 w	1657		(10a)(4)=1657.5	9.5
35	-	-	1709 s*	-		(10b)(17b)=1708.5	-0.5
36	-	-	1722 s*	-		(5a)(9a) = 1726	4
37	-	-	1835 m*	-		(6a)(1 HCH)=1836.5	1.5
38	-	-	1874 m*	-		(6b)(3) = 1875.5	1.5
39	-	-	1918 s*	-		(18b)(8b) = 1923	5
40	-	-	1968 m*	-		(1) <sub>2</sub> = 1972	4
41	-	-	2056 vw*	-		(6b)(19b)=2055.5	-0.5
42	-	-	2074 mw*	-		(15)(18a) = 2079.5	5.5
43	-	-	2145 vw*	-		(9b)(18a) = 2151.5	6.5

1	2	3	4	5	6	7	8
44	-	-	2173 w*	-		(1)(9a) = 2178	5
45	-	-	2210 w*	-		(1)(7a) = 2216	6
46	-	-	2225 m*	-		(12)(19a) = 2232	7
47	-	-	2255 m*	-		(15)(7a) = 2260.5	5.5
48	-	-	2312 w*	-		(8a)(+) = 2315	
49	-	-	2372 ms*	-	-	(15)(14) = 2370.5	-1.5
50	-	-	2417 w*			(9a)(7a) = 2422	5
51	-	-	2460 s*		2453	(1)(19a) = 2467	7
52	-	-	2518 w*		2494	(8b)(17b) = 2524	6
53	-	-	2571 m*			(14)(7a) = 2570	-1
54	-	-	2608 s*			(15)(8b) = 2613.5 (19b)(9a) = 2615	5.5 7
55	-	-	2633 w*			(8b)(18a) = 2632	-1
56	-	-	2667 m			(3)(19b) = 2666	-1
57	-	-	2729 s			(3)(19a) = 2724	-5
58	2816.0 P (2821.0) (B) 2827.0 R	11	-	-	2819	(14)(19a) = 2821	0
59	2878.0 P 2883.0 Q (A) 2893.0 R	15	2869	2896	2870	(7a) <sub>2</sub> (6a) = 2878	5
60	-	-	2928	-	2918	(14)(8b) = 2923	-5
61	2934.0 P 2941.0 Q (A) 2947.0 R	13	2958	2960	2954	(19a) <sub>2</sub> = 2962 vCH X-sensi (b <sub>1</sub> , b <sub>2</sub> )	
62	2964.0 P 2971.0 Q (A) 2978.0 R	14	2985	2995	2991	vCH (CH <sub>3</sub> -group)	

TABLE 4.3

OBSERVED BAND POSITIONS, PR SEPARATIONS AND INTERPRETATIONS  
IN INFRARED BAND CONTOURS OF  $\pi$ -PICOLINE

Sl. no.	IR BAND POSITIONS				Raman (19) Liquid Phase	Interpre- tation	Anhar- monici- ty
	Vapour Phase	Liquid Phase	Solid Phase				
	$\text{cm}^{-1}$	$\Delta\nu_{\text{PR}} \text{ cm}^{-1}$	$\text{cm}^{-1}$	$\text{cm}^{-1}$	$\text{cm}^{-1}$		
1	2	3	4	5	6	7	8
1	-	-	376 w	-	219 352	11 .18b	
2	-	-	388 w	-		.16a	
3	475.0 P 484.5 Q (C) 495.5 R	20.5	486 vs	492 s		.16b	
4	506.0 P 513.0 Q (A) 521.0 R	15	515 s	511 s	518	6a.	
5	-		612 w	608 w		(16b)( $\tau \text{CH}_3$ ) = 609.5	-2.5
6	672.0 P (678.0) (B) 684.0 R	12	666 s	666 w	672	.6b.	
7	705.0 P 713.5 Q (C) 722.0 R	17	710 w				
8	725.0 P 731.5 Q (C) 741.5 R	16	726 s	731 s		4	
9	785.0 P 796.0 Q (C) 801.0 Q 806.5 R	21.5	800 vs	802 816		(6b)( $\tau \text{CH}_3$ ) = 803 10b 12	1
10	-	-	871 w	899		.17b .10a.	
11	928.0 P (935.0) (B) 940.0 R	12	-	-			

1	3	3	4	5	6	7	8
12	960.0 P 967.0 Q (A) 975.0 R	15	970 m	979		(16b) <sub>2</sub> = 969	
13	989.0 P 996.5 Q (A) 1004.0 R	15	995 s	988 996	995	17a 1	
14	1035.0 P 1044.5 Q (C) 1047.5 Q 1055.0 R	20	1039 ms	1043		$\gamma\text{CH}_3$	
15	1066.0 P 1073.5 Q (A) 1080.5 R	14.5	1068 m	1078 1094	1060	18a 15, (11) (17b)=1090	-4
16	1102.0 P (1108.0) (B) 1113.0 R	11	1110 w			$\alpha\text{HCH}$	
17	1155.0 P (1160.0) (B) 1167.0 R	12		1155		(6b)(16b)=1162.5	7.5
18	1185.0 P 1192.0 Q (A) 1199.0 R	14	-	1195 w		9a	
19	1198.0 P 1209.0 Q (A) 1213.0 R	15	1208 m	1214		(16b) (4) = 1198.0	-11
20	1216.0 P 1223.5 Q (A) 1230.5 R	14.5	1222 s	1224	1224	7c	
21	1269.5 P 1276.5 Q (B) 1284.0 R	14.5	1286 ms	1257 1300		(11) ( $\gamma\text{CH}_3$ )= 1263.5	6.5
22	1341.0 P (1348.0) (B) 1354.0 R	13	1333 m	-		14	
23	-	-	1363 w	-		(1)(18b)=1372.5	
24	-	-	1381 ms	1381	1383	$\alpha\text{HCH}(\text{CH}_3 \text{ group})$	
25	1413.0 P (1420.0) (B) 1435.0 R	13	1413	1425		19b	

1	2	3	4	5	6	7	8
26	1452.0 F 1458.0 Q (A) 1465.0 R	13	1444 ms	-	-	OHCH (CH <sub>3</sub> group)	
27	1490.0 F 1498.0 Q (A) 1504.0 R	14	1498 1511 ms 1559 s	1505		(19a) (9a) (1) = 1503.5 (9a) (18b) = 1568	
28	1601.0 F 1608.0 Q (A) 1616.5 R	15.5	1603 vs	1578 1607	1570 1608	8b, 8a, (18b) (7a) = 1599.5	8.5
29	1648.0 F (1654.0) (B) 1661.0 R	13	1662 w	-		(18b)(3) = 1652	-2
30	1735.0 F (1741.0) (B) 1748.0 R	13	1752. s*	-		(6b)(18a) = 1751	10
31	-	-	1799 m*	-		(4)(18a) = 1805	6
32	1833.0 F (1841.0) (B) 845.0 R	12	1848 s*	1878		(10b)(γ CH <sub>3</sub> ) = 1841	0
33	1920.0 F (1927.0) (B) 1932.0 R	12	1934 s*	-		(6a)(19b) = 1933	6
34	-	-	2082 ms*	-		(4)(14) = 2079.5	-2.5
35	-	-	2130 m*	2133		(6a)(8a) = 2121	-9
36	-	-	2158 ms*	-		(4)(19b) = 2151.5	-6.5
37	-	-	2180 s*	2176		(1)(9a) = 2188	8
38	-	-	2213 s*	2213 s*		(1)(7a) = 2220	7
39	-	-	2294 s*	2272		(18a)(7a) = 2297	3
40	-	-	2307 w*			(OHCH)(9a) = 2300	-7
41	-	-	2362 w*	-		(19a) (17b) = 2369	7
42	-	-	2402 w*	-		(10b) (8a) = 2404.5	2.5

1	2	3	4	5	6	7	8
43	-	-	2420 w*	-		(9a)(7a)=2415.5	-4.5
44	-	-	2451 s*	2456		(7a) <sub>2</sub> = 2447	-4
45	-	-	2551 w*	-		(3) <sub>2</sub> = 2552	1
46	-	-	2602 s*			(1)(8a) = 2604.5	2.5
47	-	-	2630 m*	2632		(3)(14) = 2624	6
48	-	-	2673 s*	2675		(18a)(8a) = 2681	8
49	2742 P 2749 Q (A) 2756 R	14	2730 s	2736		(7a)(19a)=2721.5	-8.5
50	2821 P 2824 (B) 2833 R	12	-	-		(7a)(8a)=2831.5	7
51	2874 P 2883 (A) 2889 R	15	2868 w	2862		(8a)(3) = 2884	1
52	2931 2938 (A) 2946	15	2928 ms	2926	2928	$\nu$ CH (CH <sub>3</sub> group)	
53	2961 P (2967) (B) 2972 R	11	2968 w			$\nu$ CH (CH <sub>3</sub> group) (b <sub>2</sub> , b <sub>1</sub> ) <sup>3</sup>	
54	2996 P (3002) (B) 3009 R	13	2996 s	2997		2	
55	3032 P (3039) (B) 3044 R	12	3034 s	3035	3038	7b	
56	3064 P (3072) (B) 3077 R	13	3076	3076	3052	20b	
57	3070 P 3076 Q (A) 3084 R	14	-	-	-	20a	

\* Liquid phase IR bands using thick film of the compound (0.5 mm) in Cs Br Cell.

TABLE 4.4

211

OBSERVED AND CALCULATED VALUES OF FUNDAMENTAL  
MODES (IN  $\text{cm}^{-1}$ ) OF  $\alpha$ -,  $\beta$ -, AND  $\gamma$ -PICOLINES

Symmetry	Designation	Description	Fundamental Frequency $\text{cm}^{-1}$					
			$\alpha$ -Picoline		$\beta$ -Picoline		$\gamma$ -Picoline	
			Obs.*	Cal.	Obs.*	Cal.	Obs.*	Cal.
1	2	3	4	5	6	7	8	9
$\underline{a}_1$	6a	X-sens.	545.5 546**	526	534.0 535**	503	513.0 513**	504
	12	X-sens.	735.0	664	751.0	802	801.0 800**	808
	1	Ring	976.0	983	986.0	913	996.5	964
	18a	$\beta$ CH	1032.0	1040	1049.0	1012	1073.5	1012
	9a	$\beta$ CH	1147.5	1193	1192.0	1126	1192.0	1181
	7a	X-sens.	1297.0	1253	1230.0	1271	1223.5	1187
	19a	$\nu$ CN, CC	1477.0	1491	1481.0	1491	1498.0	1466
	8a	$\nu$ CC	1594.0	1610	1601.5	1599	1608.0	1658
	2	$\nu$ CH	3024.0	3044	3006	3043	3002.0	3087
	20a	$\nu$ CH	3076.0	3048	3069.0	3072	3076.0	3114
		CH <sub>3</sub> group vibration						
		$\alpha$ HCH	1382.0	1395	1387.0	1363	1381.0 <sup>a</sup>	-
		$\nu$ CH	2940.0	2997	2971.0	2899	2938.0	2952
$\underline{b}_2$	18b	X-sens.	358.0 358**	304.7	340.0 338**	356	376 <sup>a</sup> 359**	324
	6b	Ring def.	633.0 628**	630	632.5 624**	590	678.0 666**	631
	15	$\beta$ CH	1050.5	1042	1030.5	917*	1094.0	1032
	3	$\beta$ CH	1238.0	1209	1243.0	1160	1276.0	1252
	14	$\nu$ CN, CC	1354.0	1352	1340.0	1311	1348.0	1335

contd ---

Table 4.4 contd

212

1	2	3	4	5	6	7	8	9
	19b	$\nu$ CN, CC	1435.0	1516	1423.0	1596	1420.0	1439
	8b	$\nu$ CC	1570.0 <sup>a</sup>	1600	1583.0	1564	1578.0 <sup>c</sup>	1568
	7b	$\nu$ CH	(3024)	3034	3022.0	3065	3039.0	3098
	20b	$\nu$ CH	3094	3148	3100	3111	3072.0	3104
		$\alpha$ HCH	1103	1100	1102.5	1058	1108	1090
		$\alpha$ HCH	1453.0 <sup>a</sup>	1594 <sup>*</sup>	1460.0 <sup>b</sup>	1523	1458.0	1485
		$\nu$ CH	2968.0 <sup>a</sup>	2914	2941.0	2820	2967.0	2856
$\underline{b}_1$	11	X-sens.	213.0 <sup>b</sup>	246	218.0 <sup>b</sup>	216	219.0 <sup>b</sup>	228
	16b	X-sens.	468.5	490	400.0	331	484.5	403
	4	$\tau$ CC	751.5	645 <sup>*</sup>	713.5	662	731.5	667
	10b	$\gamma$ CH	797.0 <sup>a</sup>	759	785.5	700	796.5	725
	17b	$\gamma$ CH	930.0	940	922.5	840	871.0 <sup>a</sup>	912
		CH <sub>3</sub> group vibrations						
		$\gamma$ CH <sub>3</sub>	1115.0 <sup>c</sup>	1105	1066.0 <sup>c</sup>	1055	1044.5	983
		$\alpha$ HCH	(1453.0)	1549	(1460.0) <sup>b</sup>	-	1420	1377
		$\nu$ CH	(2968.0) <sup>a</sup>	2867	(2941.0)	2763	(2967)	2809
$\underline{a}_2$	16a	$\tau$ CC	401.0	432	418.0 <sup>a</sup>	451	388 <sup>a</sup>	391
	10a	$\gamma$ CH	884.0 <sup>a</sup>	833	944.0 <sup>c</sup>	1012	(871) <sup>a</sup>	829
	17a	$\gamma$ CH	(930.0)	849	1002.0 <sup>c</sup>	1058	988 <sup>c</sup>	942
		CH <sub>3</sub> group vibrations						
		(12) $\tau$ CH <sub>3</sub>	<125		<125		<125	

( ) assigned more than once

\* IR vapour

\*\* data from Rush and Sponer 23

(a) IR liquid, (b) Raman liquid (cf Tables 4.1, 4.2 and 4.3)

(c) IR solid (INT)



TABLE 4.5

CALCULATED ROTATIONAL PARAMETERS AND PR SEPARATIONS (a) AT 300°K  
FOR INFRARED BAND CONTOURS OF  $\alpha$ -,  $\beta$ -, and  $\gamma$ -PICOLINES

Molecules	A MC/Sec	B MC/Sec	C MC/Sec	B MC/Sec	$\bar{\beta}$	$\bar{S}(\bar{\beta})$	PR Separation (in cm <sup>-1</sup> )			I <sub>Q</sub> I <sub>Total</sub>
							A(I)	B(I)	C(I)	
$\alpha$ - Picoline	5979.4	2331.5	1965.7	2423.6	1.4671	1.2756	14.8	11.6	22.2	0.222
$\beta$ - Picoline	5593.0	2632.2	1831.0	2251.6	1.4840	1.2770	14.2	11.1	21.4	0.224
$\gamma$ - Picoline*	6082.1	2524.8	1783.9	2154.4	1.8231	1.2542	13.7	10.9	20.5	0.206

(a) The rotational constants and parameters  $\bar{B}$ ,  $\bar{\beta}$ ,  $S(\bar{\beta})$  along with the quantities  $\Delta\nu_{PR}$  and  $I_Q/I_{Total}$  for the IR band contours are defined in refs. (35, 36).

\* The rotational constants are from microwave study (29).

TABLE 4.6

ASSUMED GEOMETRY FOR  $\alpha$ -,  $\beta$ -, AND  $\gamma$ -PICOLINE IN THE GROUND STATE

(See Text Section 4.6)

$R(C_1-H_1)$	=	1.0843 <sup>9</sup> <sub>1</sub>
$R(C_2-H_2)$	=	1.0305
$R(C_3-H_3)$	=	1.0773
$R(N-C_1)$	=	1.3402
$R(C_1-C_2)$	=	1.3945
$R(C_2-C_3)$	=	1.3944
$R(C^*-Cs)$	=	1.525
$R(Cs Hs)$	=	1.0750
$\angle C_1C_2C_3$	=	118.53°
$\angle C_5NC_1$	=	116.83°
$\angle H_1C_1C_2$	=	120.24
$\angle H_2C_2C_3$	=	121.30
$\angle C_2C_3C_4$	=	118.33
$\angle C_2C_3H_3$	=	120.84
$\angle CsCC$	=	120.24
$\angle HsCsHs$	=	120.0
$\angle HsCsC$	=	110.0

Suffix s with C and H denotes the atom of the substituent CH<sub>3</sub> group.

\*C is C<sub>5</sub> for  $\alpha$ -picoline, C<sub>4</sub> for  $\beta$ -picoline and C<sub>3</sub> for  $\gamma$ -picoline.

TABLE 4.7

THE DEFINITION OF THE INTERNAL COORDINATES FOR  $\alpha$ -,  $\beta$ -, AND  $\gamma$ -PICOLINE

Internal Coordinate	Definition		Internal Coordinate	Definition	
	$\alpha$ -picoline	$\gamma$ -picoline		$\alpha$ -picoline	$\gamma$ -picoline
S1	$\nu(C_1C_2)$	$\nu(C_1C_2)$	S17	$\beta(NC_1H_1)$	$\beta(NC_1H_1)$
S2	$\nu(C_2C_3)$	$\nu(C_2C_3)$	S18	$\beta(H_1C_1C_2)$	$\beta(H_1C_1C_2)$
S3	$\nu(C_3C_4)$	$\nu(C_3C_4)$	S19	$\alpha(C_1C_2C_3)$	$\alpha(C_1C_2C_3)$
S4	$\nu(C_4C_5)$	$\nu(C_4C_6)$	S20	$\beta(C_1C_2H_2)$	$\beta(C_1C_2H_2)$
S5	$\nu(C_5N)$	$\nu(C_6N)$	S21	$\beta(H_2C_2C_3)$	$\beta(H_2C_2C_3)$
S6	$\nu(NC_1)$	$\nu(NC_1)$	S22	$\alpha(C_2C_3C_4)$	$\alpha(C_2C_3C_5)$
S7	$\nu(C_1H_1)$	$\nu(C_1H_1)$	S23	$\beta(C_2C_3H_3)$	$\beta(C_2C_3C_4)$
S8	$\nu(C_2H_2)$	$\nu(C_2H_2)$	S24	$\beta(H_3C_3C_4)$	$\beta(C_4C_3C_5)$
S9	$\nu(C_3H_3)$	$\nu(C_3H_3)$	S25	$\alpha(C_3C_4C_5)$	$\beta(H_3C_4C_3)$
S10	$\nu(C_4H_4)$	$\nu(C_4C_5)$	S26	$\beta(C_3C_4H_4)$	$\beta(H_3C_4H_4)$
S11	$\nu(C_5C_6)$	$\nu(C_5H_4)$	S27	$\beta(H_4C_4C_5)$	$\beta(H_4C_4H_5)$
S12	$\nu(C_6H_5)$	$\nu(C_5H_5)$	S28	$\alpha(C_4C_5N)$	$\beta(H_5C_4C_3)$
S13	$\nu(C_6H_6)$	$\nu(C_5H_6)$	S29	$\beta(C_4C_5C_6)$	$\alpha(C_3C_5C_6)$
S14	$\nu(C_6H_7)$	$\nu(C_6H_7)$	S30	$\beta(C_6C_5N)$	$\beta(C_3C_5H_6)$
S15	$\alpha(C_5NC_1)$	$\alpha(C_6NC_1)$	S31	$\beta(H_5C_6C_5)$	$\beta(H_6C_5C_6)$
S16	$\alpha(NC_1C_2)$	$\alpha(NC_1C_2)$	S32	$\beta(H_6C_6H_5)$	$\alpha(C_4C_6N)$

contd

contd

S33	$\rho(\text{H}_7\text{C}_6\text{H}_6)$	$\rho(\text{C}_4\text{C}_6\text{H}_7)$	$\rho(\text{C}_5\text{C}_6\text{H}_7)$	S41	$\nu(\text{C}_6\text{H}_6)$	$\nu(\text{C}_5\text{H}_6)$	$\nu(\text{C}_5\text{H}_6)$
S34	$\rho(\text{H}_7\text{C}_6\text{C}_5)$	$\rho(\text{H}_7\text{C}_6\text{N})$	$\rho(\text{H}_7\text{C}_6\text{N})$	S42	$\nu(\text{C}_6\text{H}_7)$	$\nu(\text{C}_6\text{H}_7)$	$\nu(\text{C}_6\text{H}_7)$
S35	$\nu(\text{C}_1\text{H}_1)$	$\nu(\text{C}_1\text{H}_1)$	$\nu(\text{C}_1\text{H}_1)$	S43	$\nu(\text{C}_5\text{N})$	$\nu(\text{C}_6\text{N})$	$\nu(\text{C}_6\text{N})$
S36	$\nu(\text{C}_2\text{H}_2)$	$\nu(\text{C}_2\text{H}_2)$	$\nu(\text{C}_2\text{H}_2)$	S44	$\nu(\text{NC}_1)$	$\nu(\text{NC}_1)$	$\nu(\text{NC}_1)$
S37	$\nu(\text{C}_3\text{H}_3)$	$\nu(\text{C}_3\text{H}_3)$	$\nu(\text{C}_3\text{C}_4)$	S45	$\nu(\text{C}_1\text{C}_2)$	$\nu(\text{C}_1\text{C}_2)$	$\nu(\text{C}_1\text{C}_2)$
S38	$\nu(\text{C}_4\text{H}_4)$	$\nu(\text{C}_4\text{C}_5)$	$\nu(\text{C}_4\text{H}_3)$	S46	$\nu(\text{C}_2\text{C}_3)$	$\nu(\text{C}_2\text{C}_3)$	$\nu(\text{C}_2\text{C}_3)$
S39	$\nu(\text{C}_5\text{C}_6)$	$\nu(\text{C}_5\text{H}_4)$	$\nu(\text{C}_4\text{H}_4)$	S47	$\nu(\text{C}_3\text{C}_4)$	$\nu(\text{C}_3\text{C}_4)$	$\nu(\text{C}_3\text{C}_5)$
S40	$\nu(\text{C}_6\text{H}_5)$	$\nu(\text{C}_5\text{H}_5)$	$\nu(\text{C}_4\text{H}_5)$	S48	$\nu(\text{C}_4\text{C}_5)$	$\nu(\text{C}_4\text{C}_6)$	$\nu(\text{C}_5\text{C}_6)$

The running suffixes with the internal coordinates (S) show their identifying number while the suffixes with atoms represent their positions (Cf. Fig. 4.10 and 4.11.)

TABLE 4.8

REFINED UREY-BRADLEY FORCE-CONSTANTS FOR PLANAR AND  
NON-PLANAR VIBRATIONS OF  $\alpha$ -,  $\beta$ -, and  $\gamma$ -PICOLINES

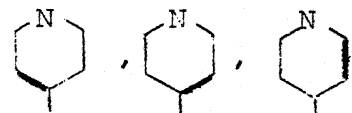
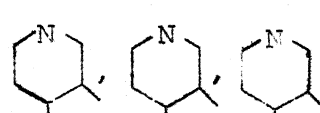
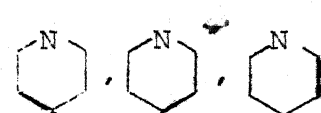
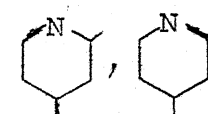
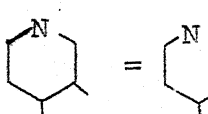
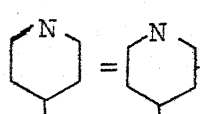
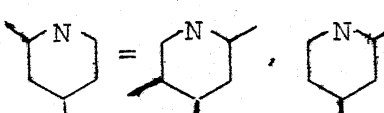
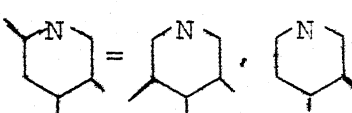
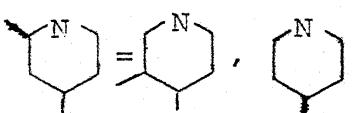
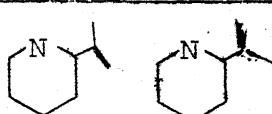
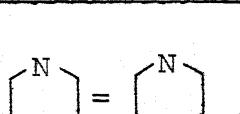
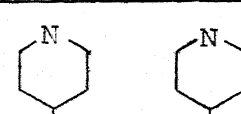
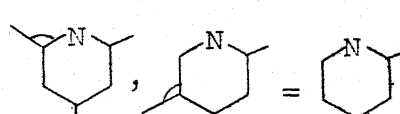
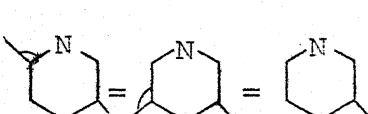
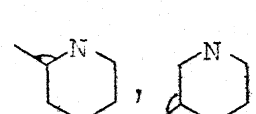
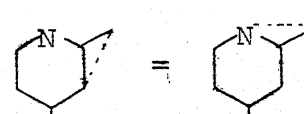
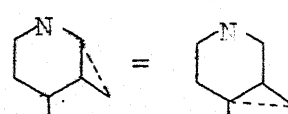
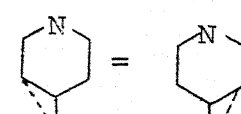
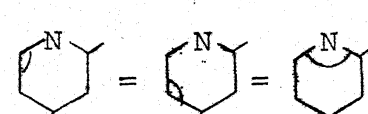
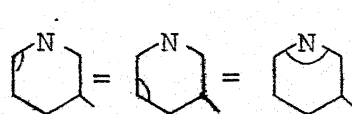
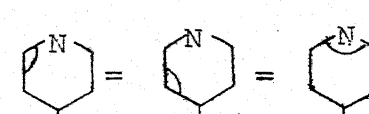
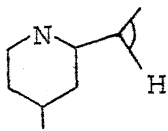
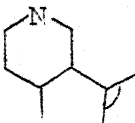

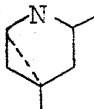
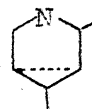
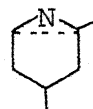
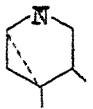


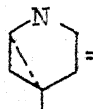
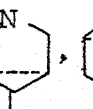

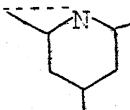
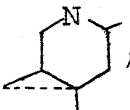
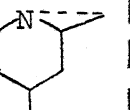
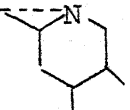
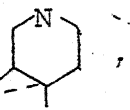
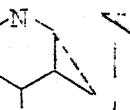
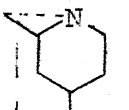
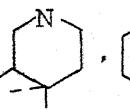
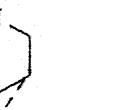
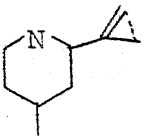
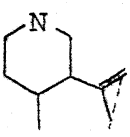

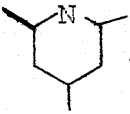
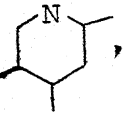
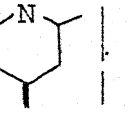
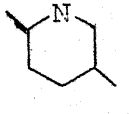
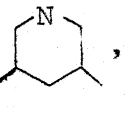
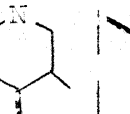
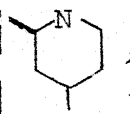
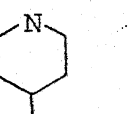
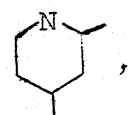
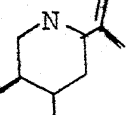
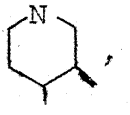
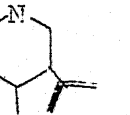
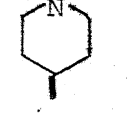
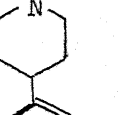
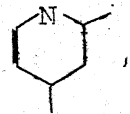
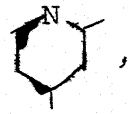
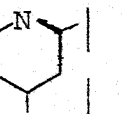
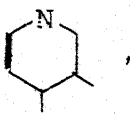
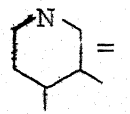
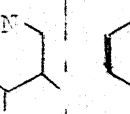
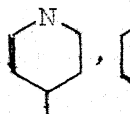
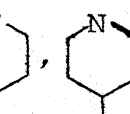

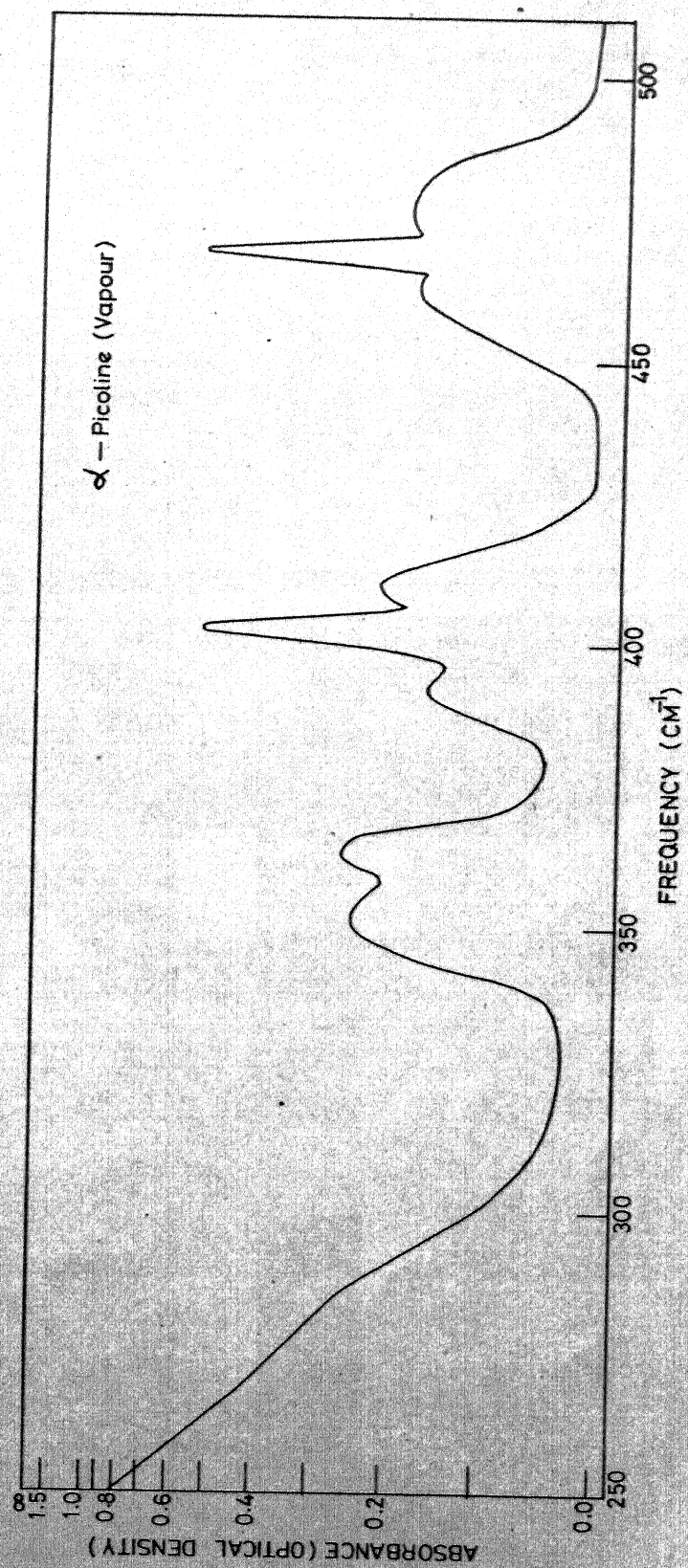
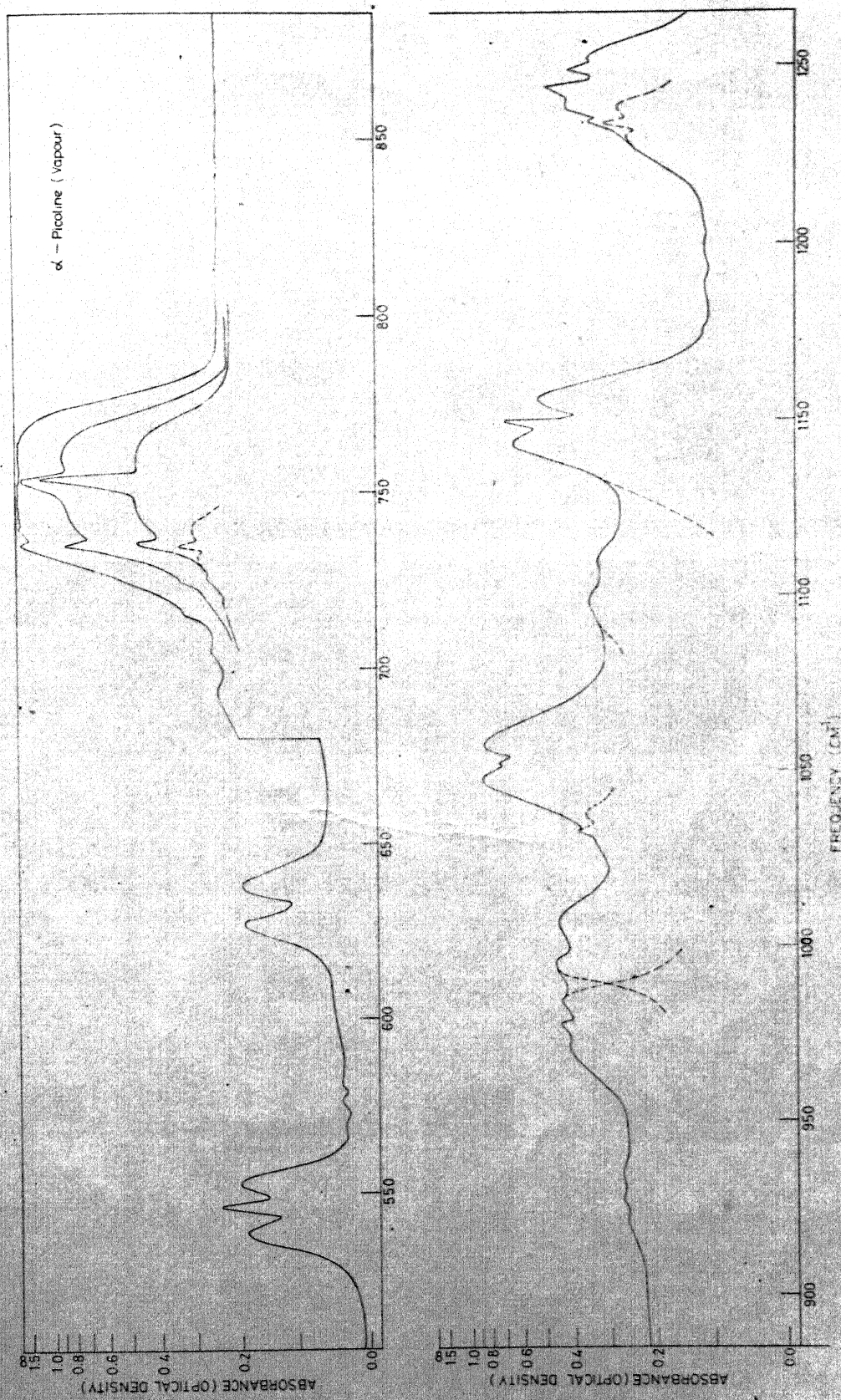
	$\alpha$ -Picoline	$\beta$ -Picoline	$\gamma$ -Picoline
$K_{CC}$	 5.135, 5.130, 5.110	 5.149, 5.149, 5.145	 5.140, 5.140, 5.149
$K_{NC}$	 4.100, 4.05	 = 4.100	 = 4.25
$K_{CH}$ , $K_{CCS}$	 4.745, 4.05	 4.745, 4.100	 4.745, 4.20
$K_{CSH}$	 4.25, 4.15	 4.05	 4.35, 4.25
$H_{CH}$	 0.365, 0.36	 0.40	 0.32, 0.35
$H_{CCS}$	 0.33	 0.39	 0.33
$H_{CC}$ , $H_{CN}$	 0.68	 0.65	 0.65

Table 4.8 (contd.)

	$\alpha$ -Picoline	$\beta$ -Picoline	$\gamma$ -Picoline
$H_{HCH}$	 0.25	 0.26	 0.22
$F_{CC},$ $F_{NC}$	 =  ,  0.7057 0.52	 =  ,  0.7057 0.52	 =  ,  0.7057 0.52
$F_{CH},$ $F_{CCS}$	 ,  ,  0.4395, 0.26, 0.9226	 ,  ,  0.4395, 0.26, 0.803	 ,  ,  0.4395, 0.33, 0.803
$F_{HCH}$	 0.26	 0.22	 0.20
$\gamma_{CH}$	 ,  ,  0.215, 0.22, 0.225	 ,  ,  0.165, 0.205, 0.21	 ,  0.165, 0.205
$\gamma_{CCS},$ $\gamma_{CSH}$	 ,  0.725 0.165	 ,  0.725 0.165	 ,  0.725 0.165
$\tau_{CC},$ $\tau_{CN}$	 ,  ,  0.114 0.105 0.134	 ,  =  0.095 0.015	 ,  ,  0.09, 0.1135, 0.152

Units: K in m dynes/Å, H, F,  $\gamma$ , and  $\tau$  in  $10^{-11}$  erg/rad.<sup>2</sup>







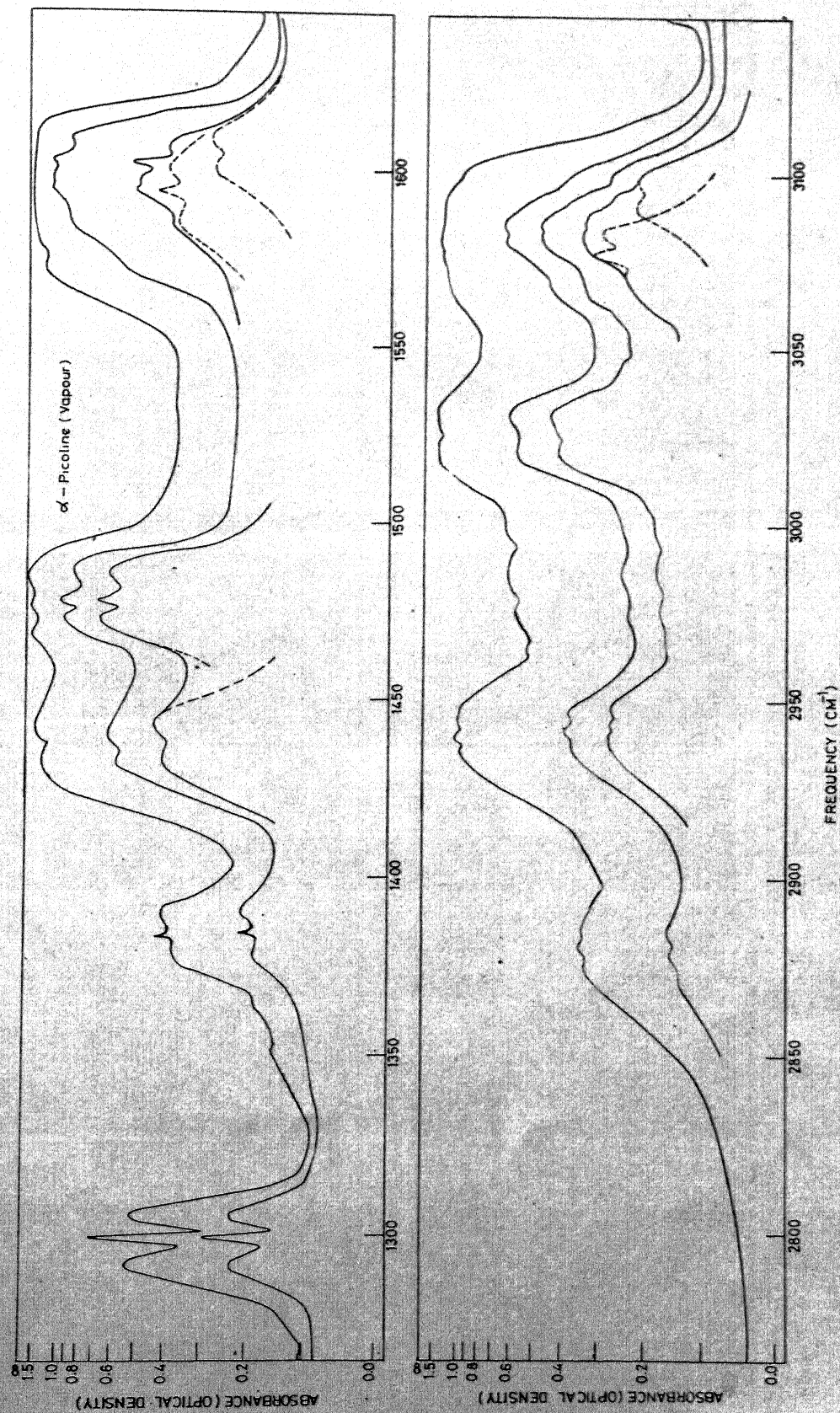


FIG.4.1 THE INFRARED SPECTRA OF  $\alpha$ -PICOLINE IN VAPOUR PHASE AT LOW PRESSURE AND FOUR METER PATH LENGTH ABSORPTION DUE TO ATMOSPHERIC  $H_2O$  AND  $CO_2$  HAVE CAREFULLY BEEN ELIMINATED BY COMPARISON WITH PURE ATMOSPHERIC ABSORPTION UNDER IDENTICAL CONDITIONS.

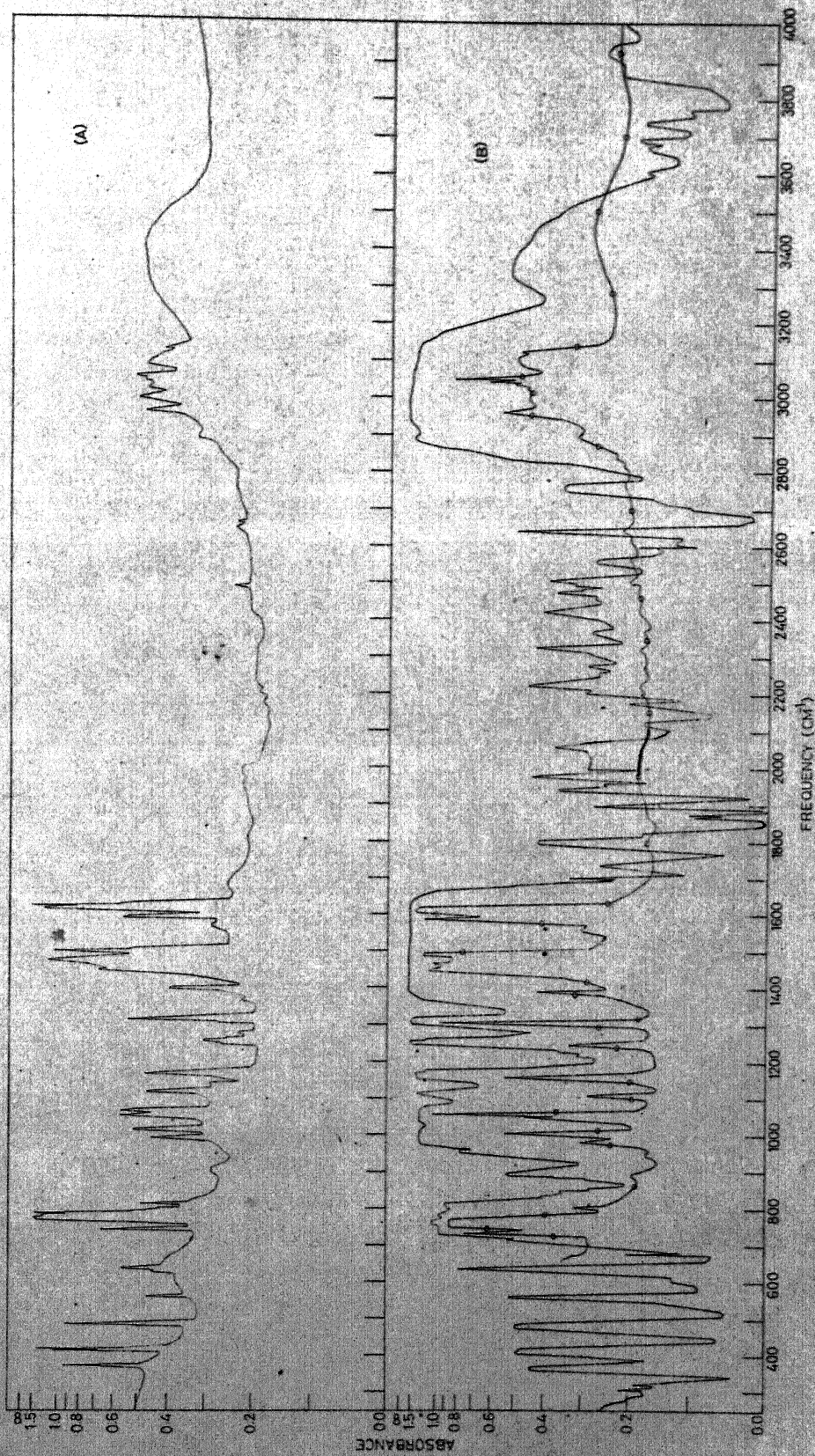
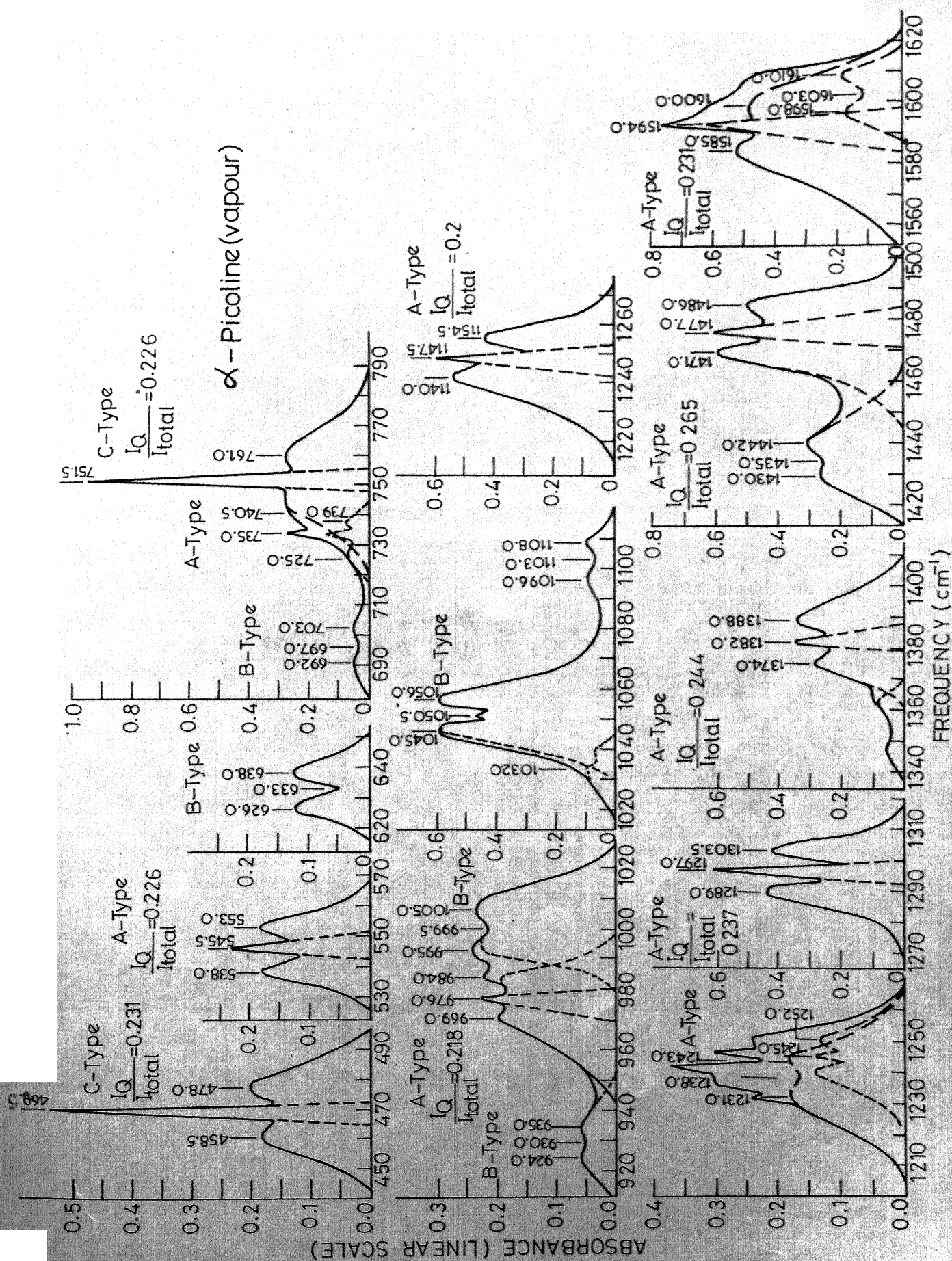
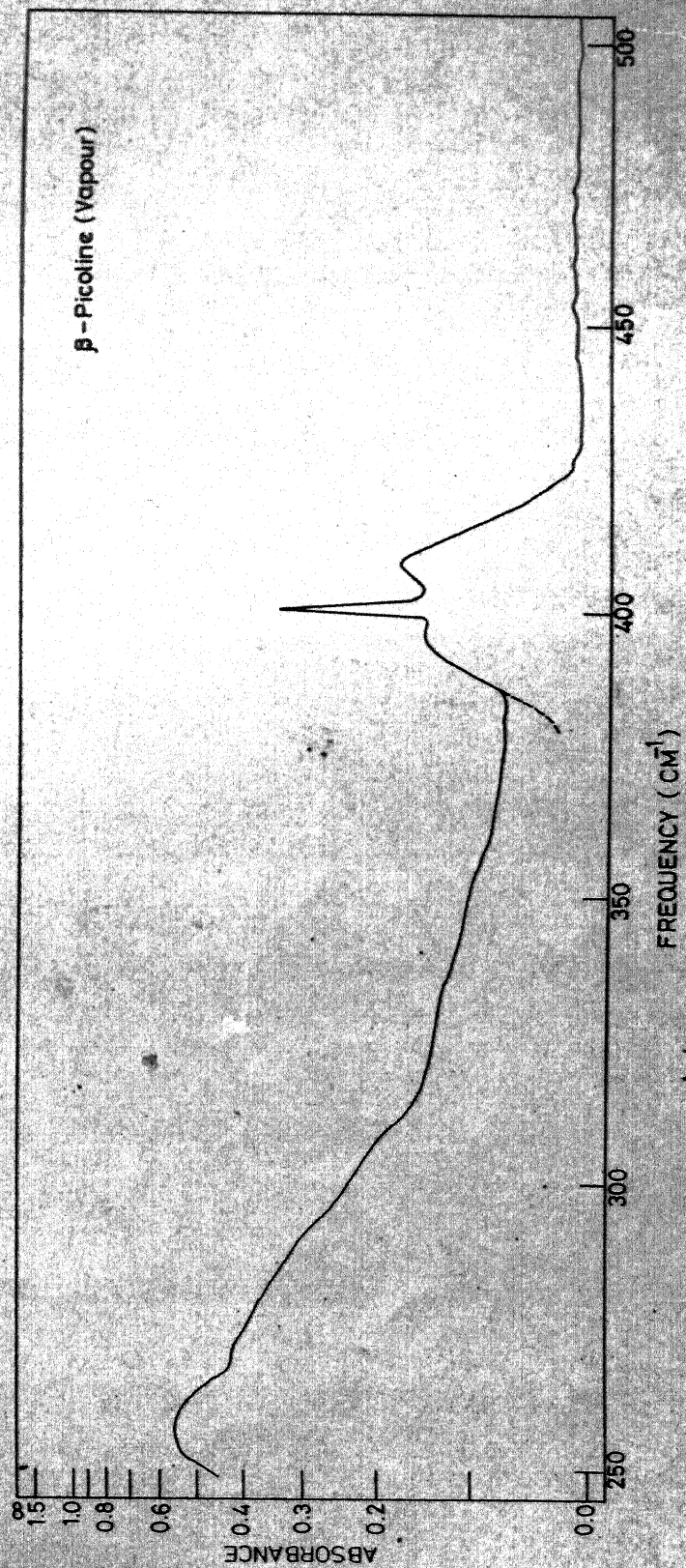


FIG. 4.2 THE INFRARED SPECTRA OF  $\alpha$ -PICOLINE. (A) SOLID PHASE SPECTRUM AT LIQUID NITROGEN TEMPERATURE (B) LIQUID PHASE SPECTRUM USING 0.5 mm CELL DENOTED BY — AND OF 0.025 mm CELL (NaCl) BY  $\circ$

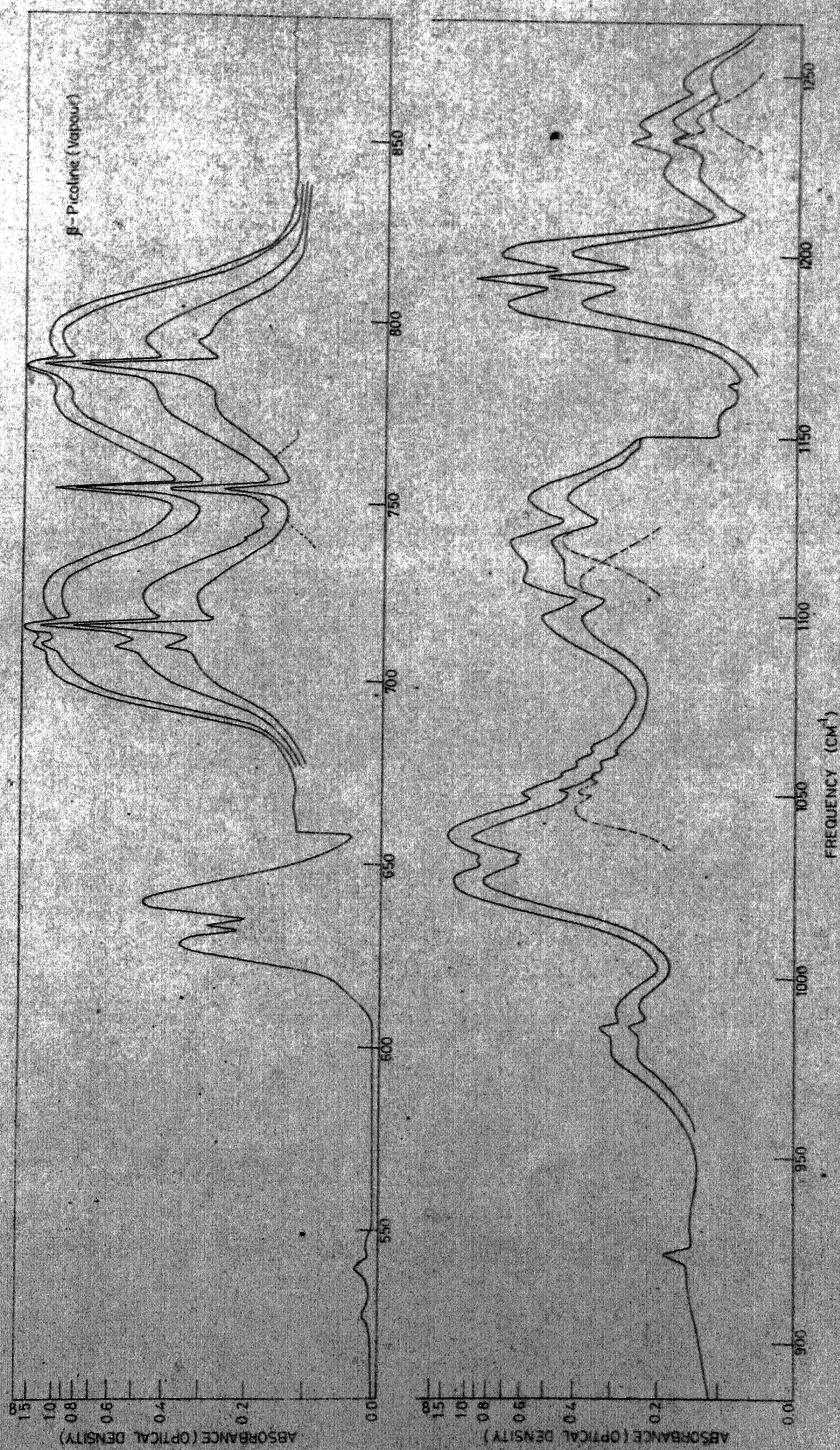


FIG.4.3 CHARACTERISTIC A-B AND C-TYPE VAPOUR PHASE INFRARED BAND CONTOURS OF  $\alpha$ -PICOLINE (VAPOUR)

$\beta$ -Picoline (Vapour)







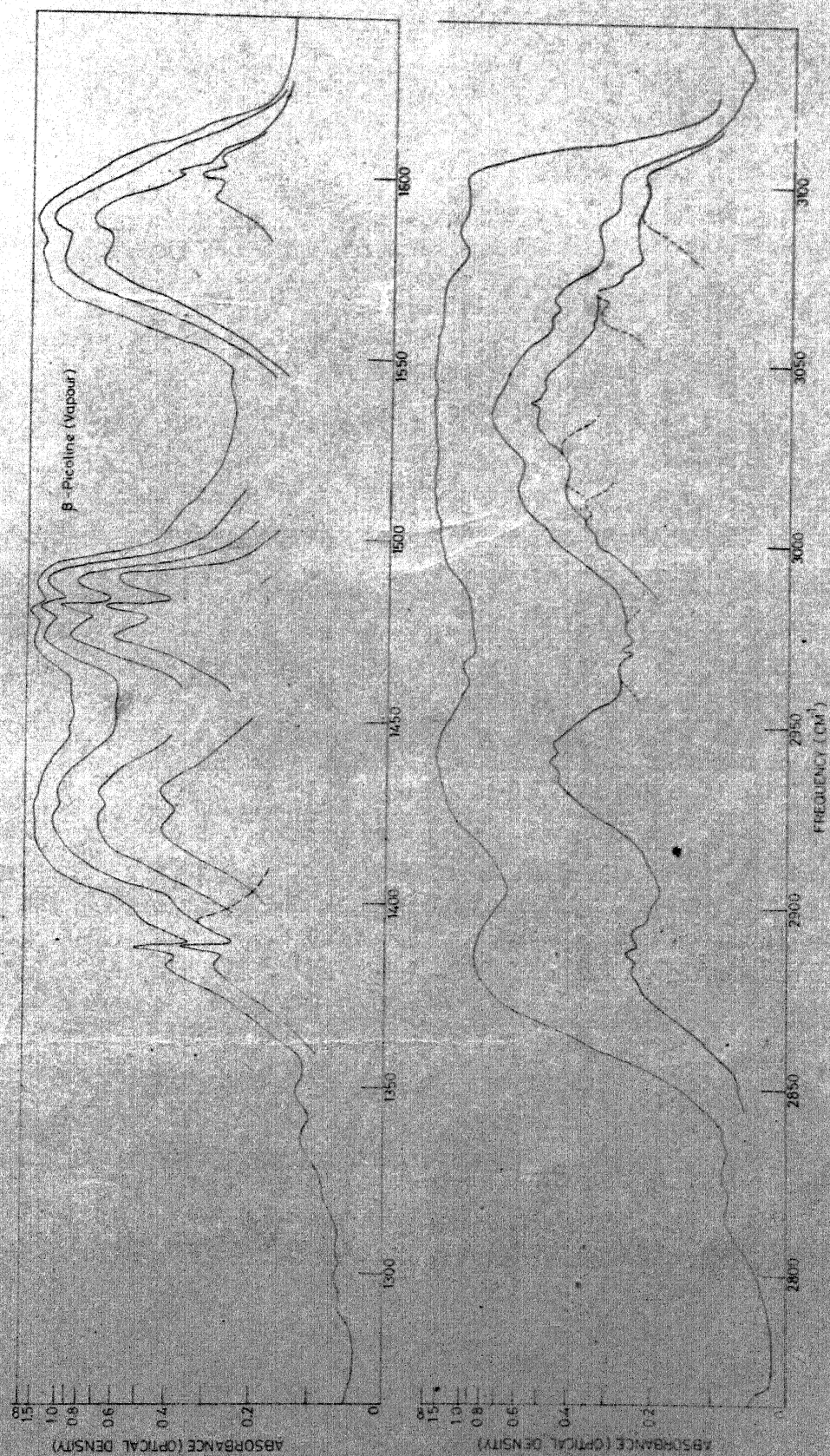


FIG 4.4 THE INFRARED SPECTRUM OF  $\beta$ -PICOLINE IN VAPOUR PHASE AT LOW PRESSURE AND 4 METER PATH LENGTH. ABSORPTION DUE TO ATMOSPHERIC  $\text{H}_2\text{O}$  AND  $\text{CO}_2$  HAVE CAREFULLY BEEN ELIMINATED BY COMPARISON WITH PURE ATMOSPHERIC ABSORPTION UNDER IDENTICAL CONDITIONS



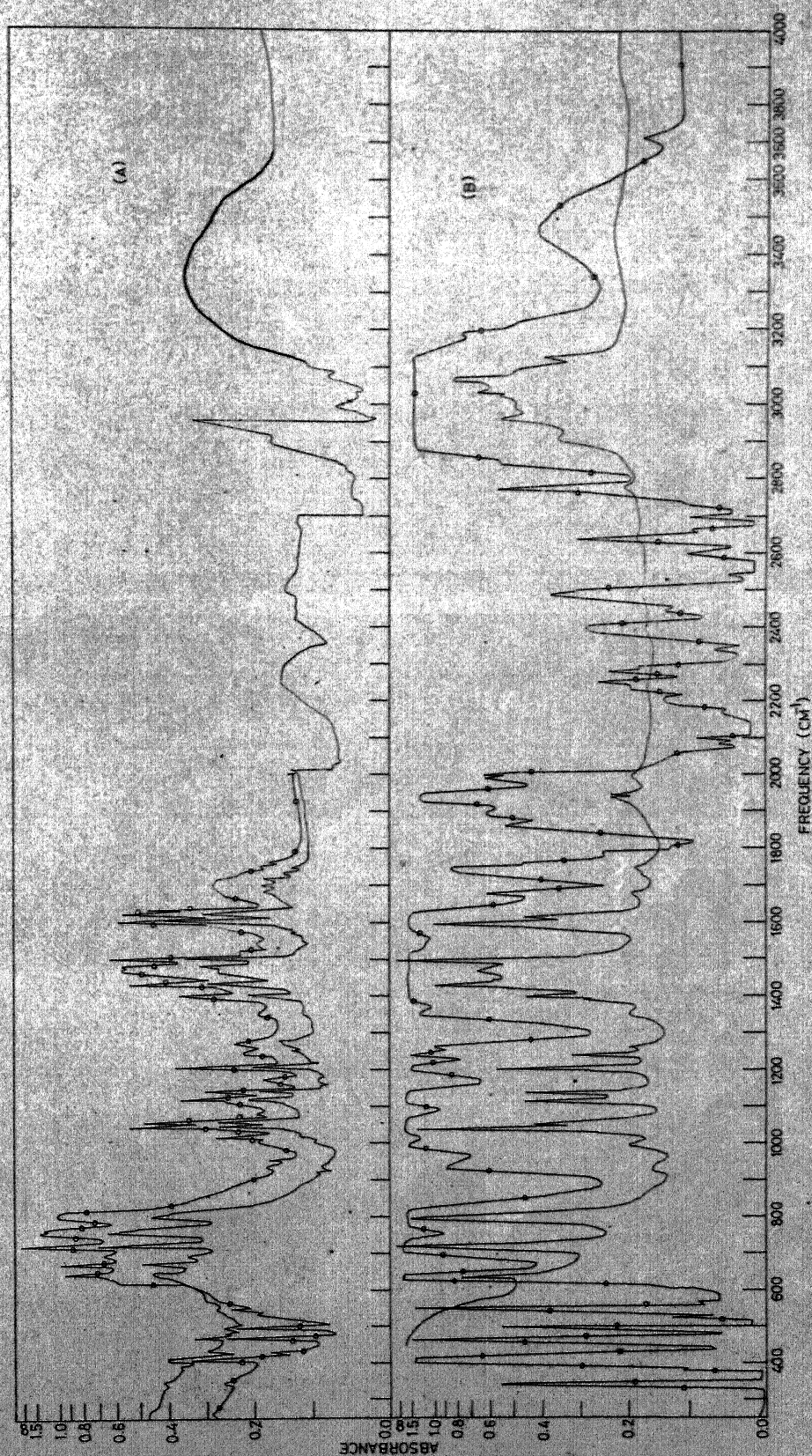


FIG. 4.5 THE INFRARED SPECTRA OF  $\beta$ -PICOLINE (A) SOLID PHASE SPECTRUM AT LIQUID NITROGEN TEMPERATURE THICK DEPOSIT DENOTED BY — AND OF THIN DEPOSIT BY —•— (B) LIQUID PHASE SPECTRUM USING 0.5mm CELL DENOTED BY — AND OF 0.025mm CELL (NaCl) BY —•—

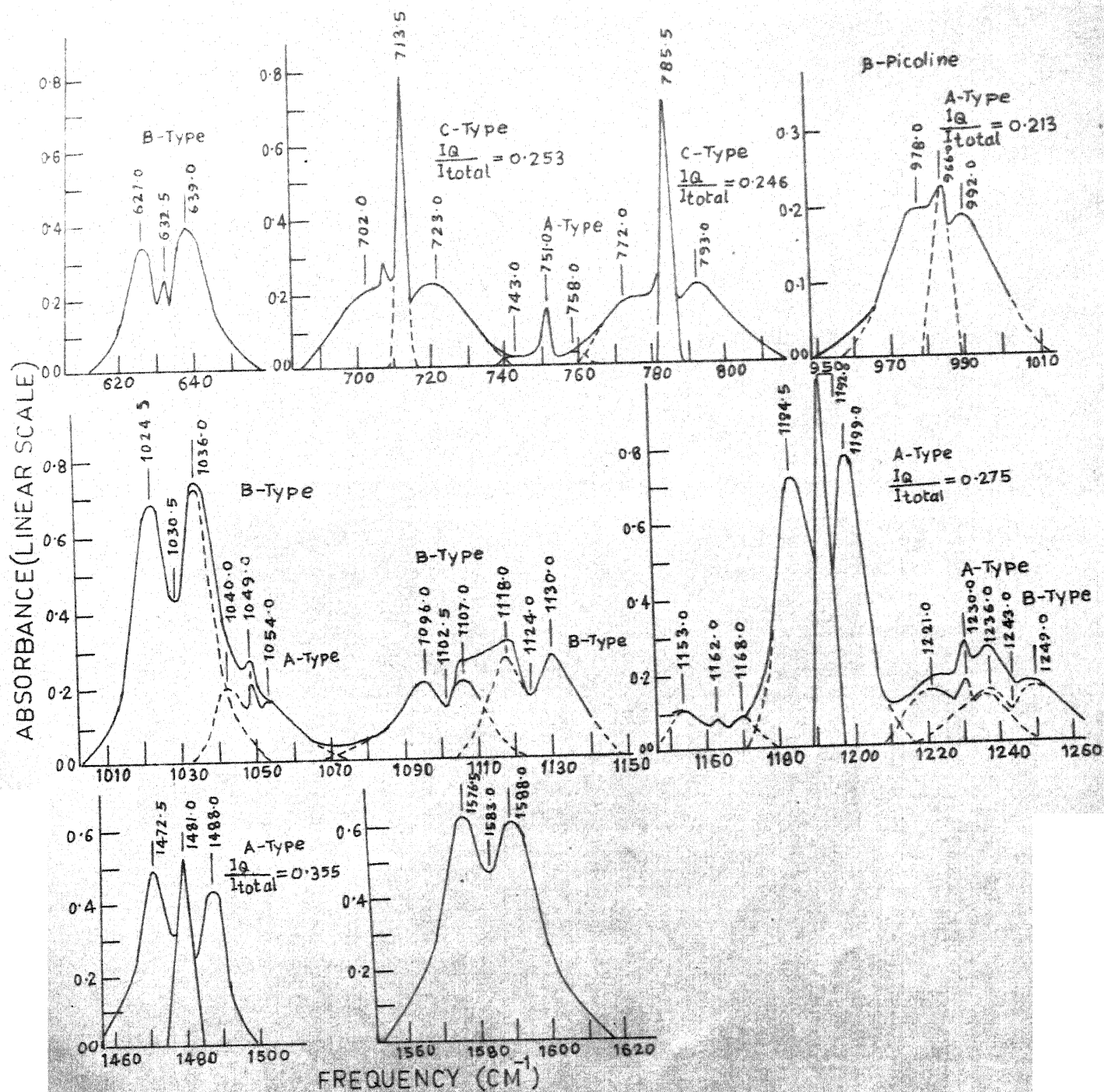
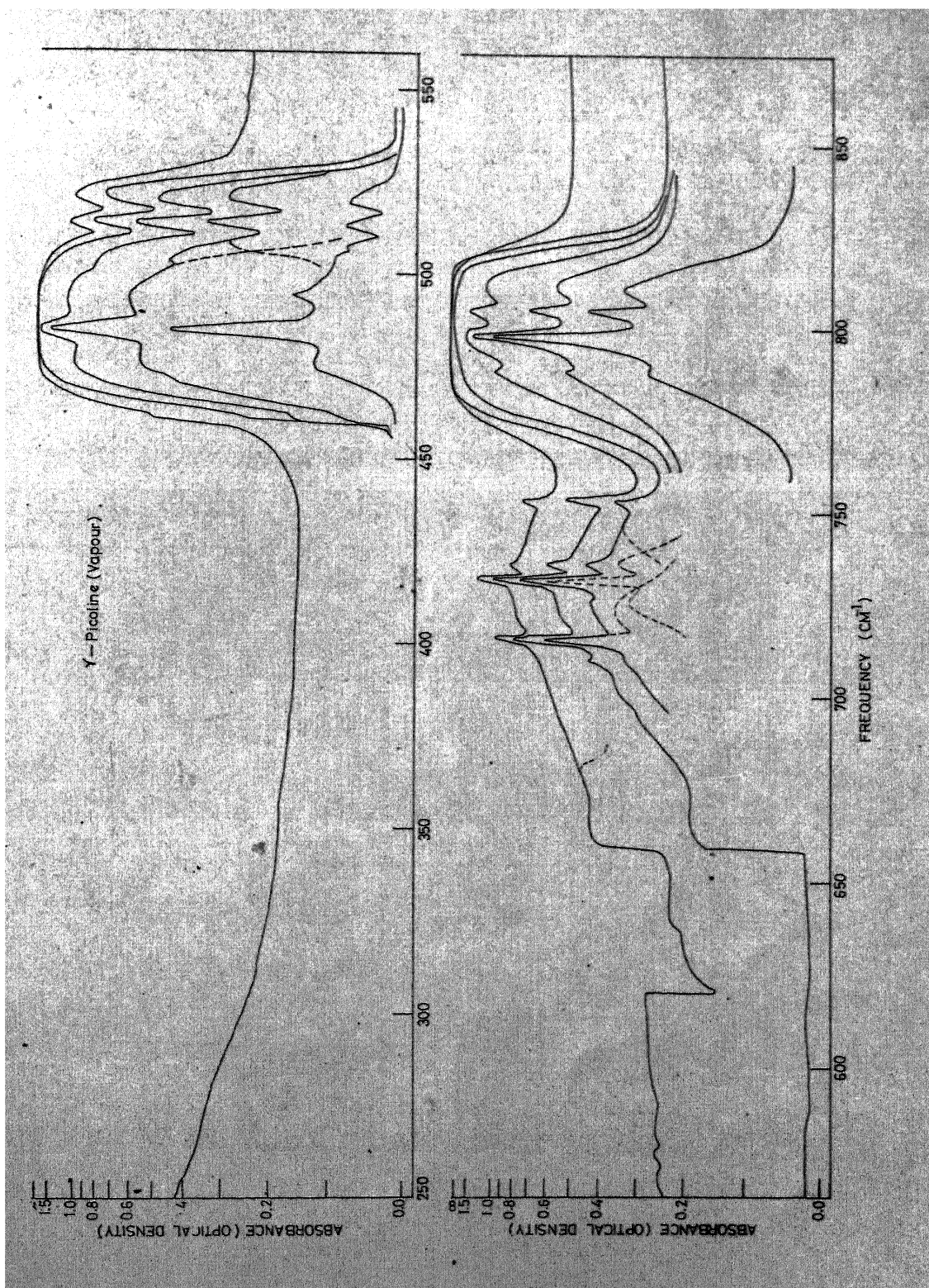
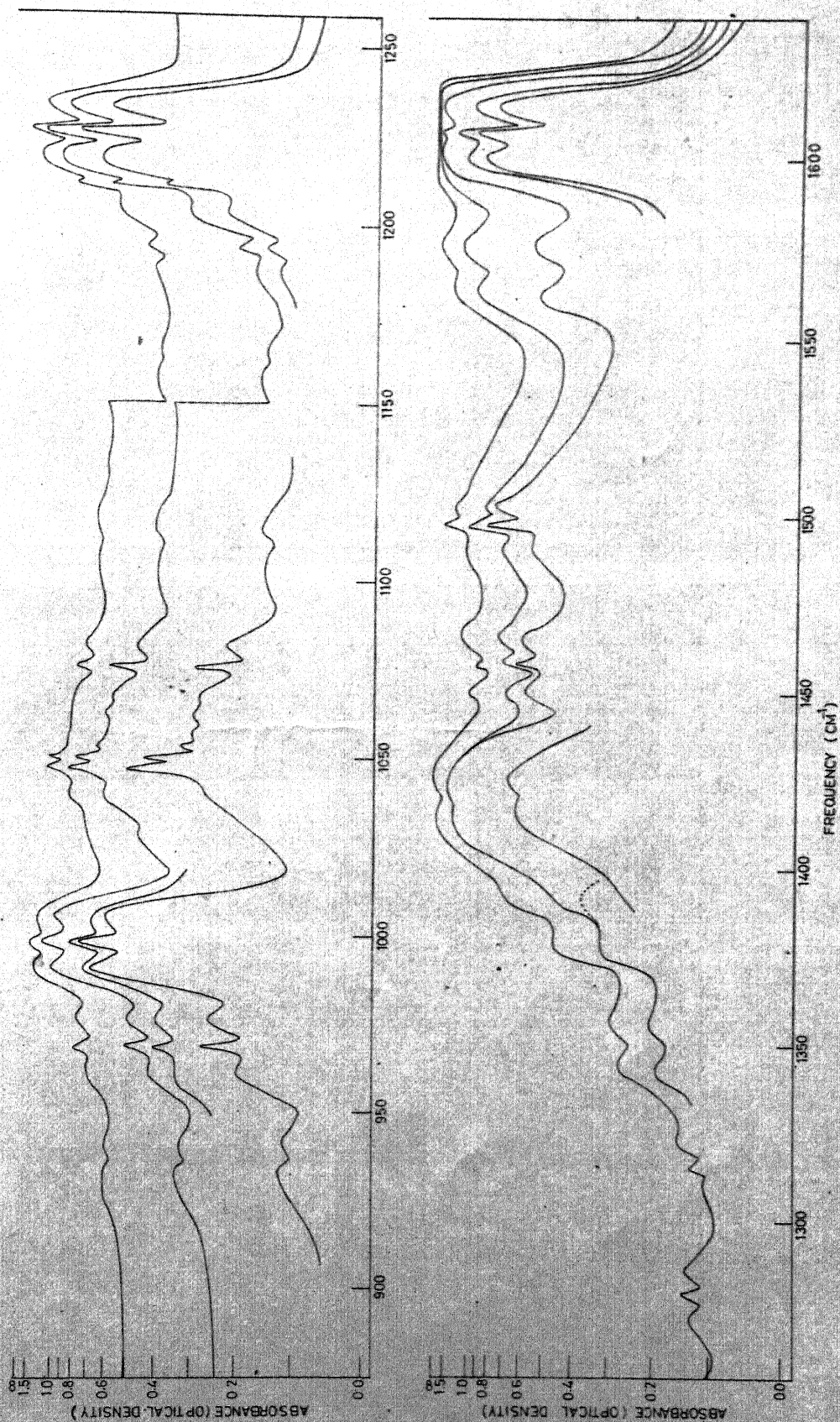


FIG.4-6 CHARACTERISTIC A,B,AND C-TYPE VAPOUR PHASE INFRARED BAND CONTOURS OF  $\beta$ -PICOLINE





$\gamma$ -Picoline

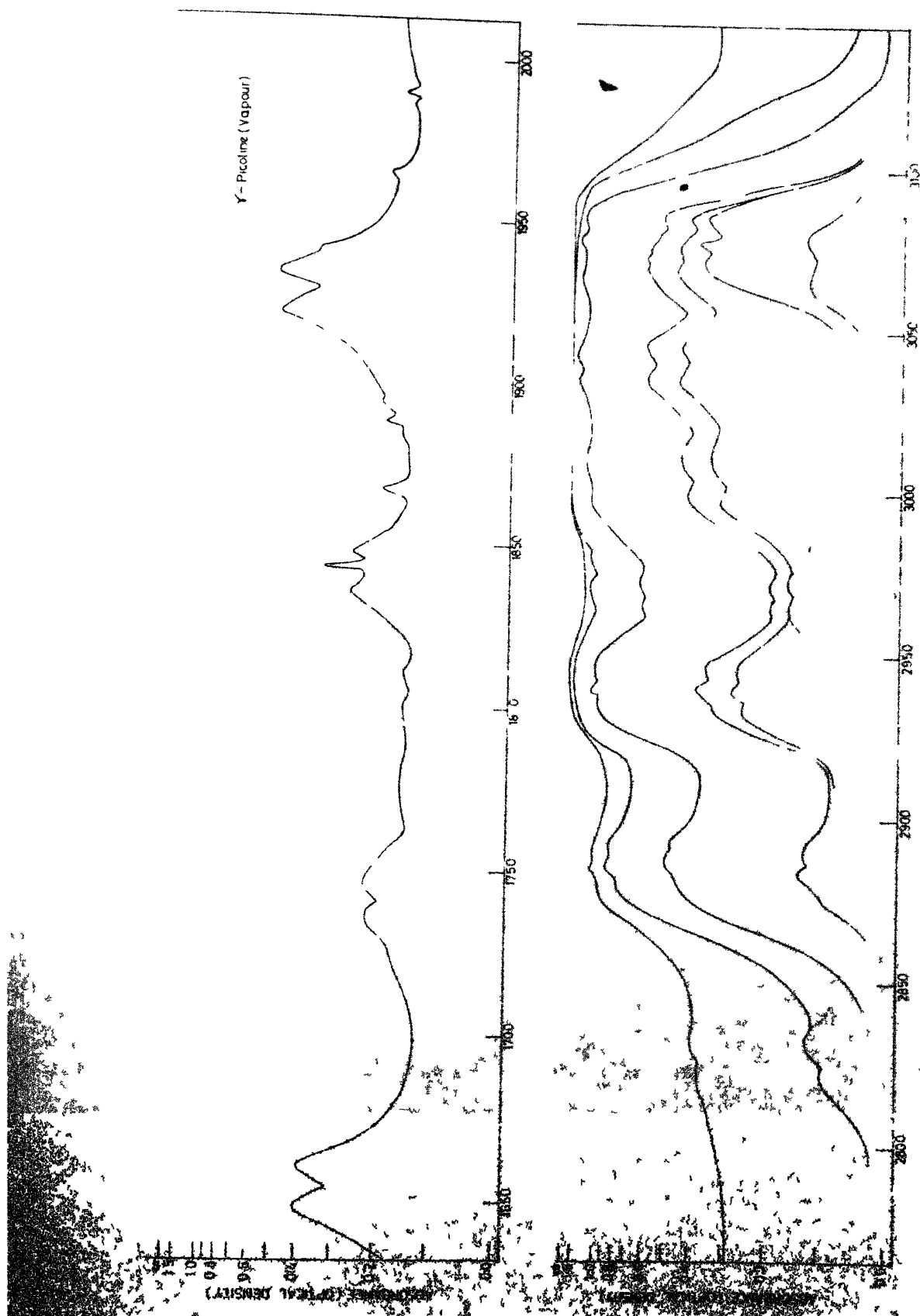
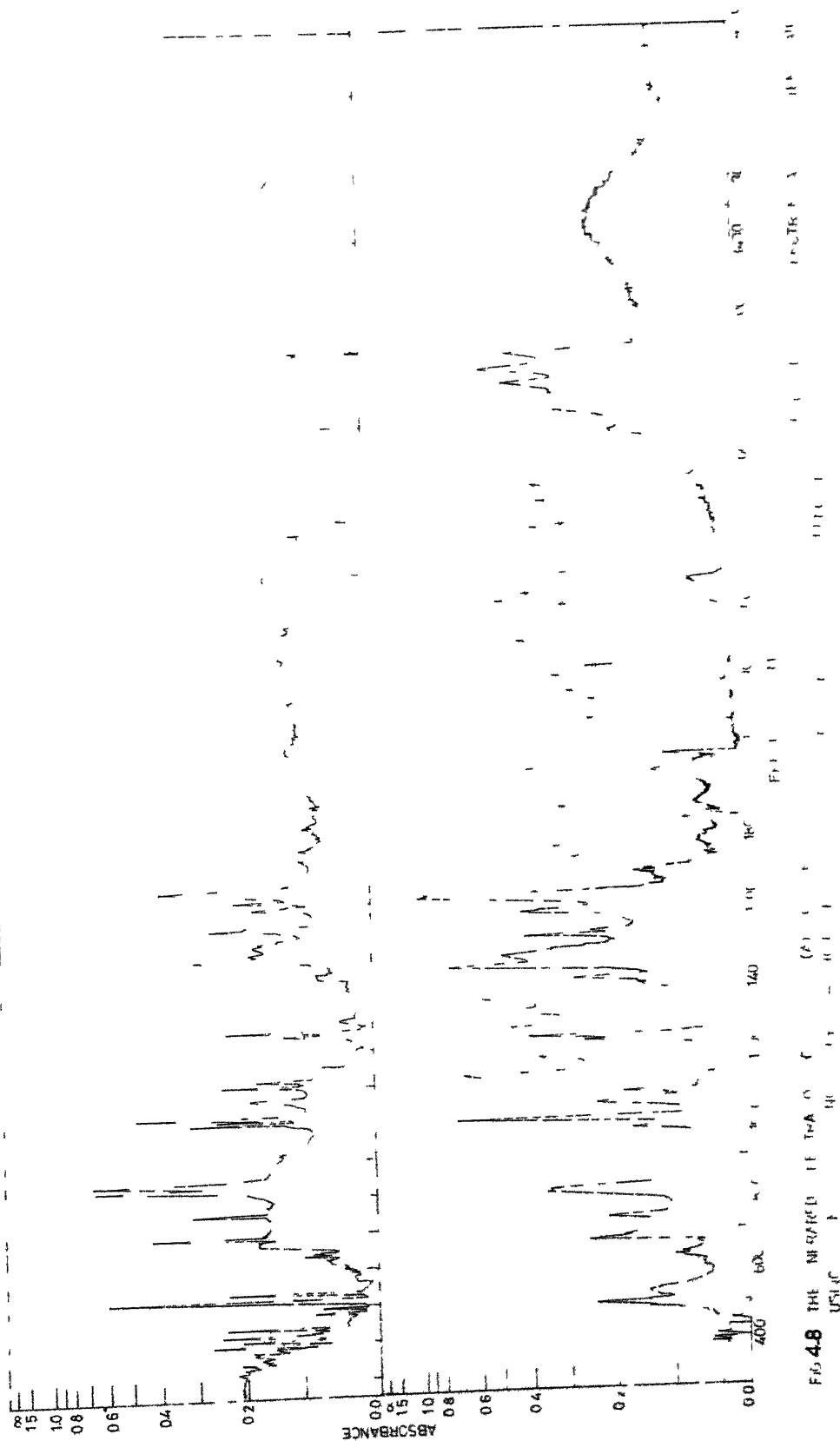


FIG-4.7 THE IR SPECTRA OF Y-PICOLINE IN VAPOUR PHASE AT LOW PRESSURE AND 4METER PATH LENGTH ABSORPTION DUE TO ATMOSPHERIC H<sub>2</sub>O AND CO<sub>2</sub> HAVE BEEN ELIMINATED BY COMPARISON WITH PURE ATMOSPHERIC ABSORPTION UNDER IDENTICAL CONDITION



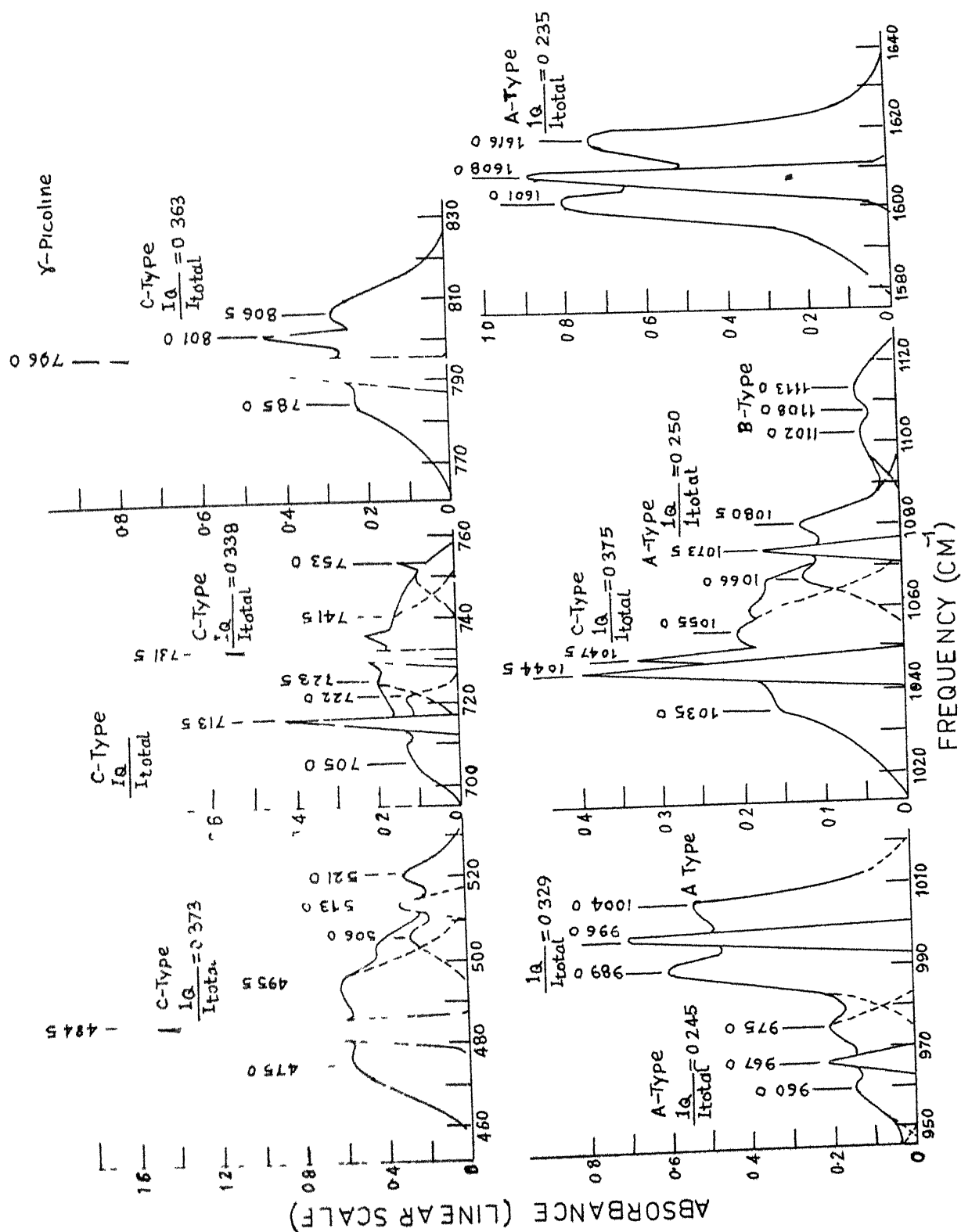


FIG 4.9 CHARACTERISTIC A, B, AND C-TYPE VAPOUR PHASE INFRARED BAND CONTOURS OF γ-PICOLINE

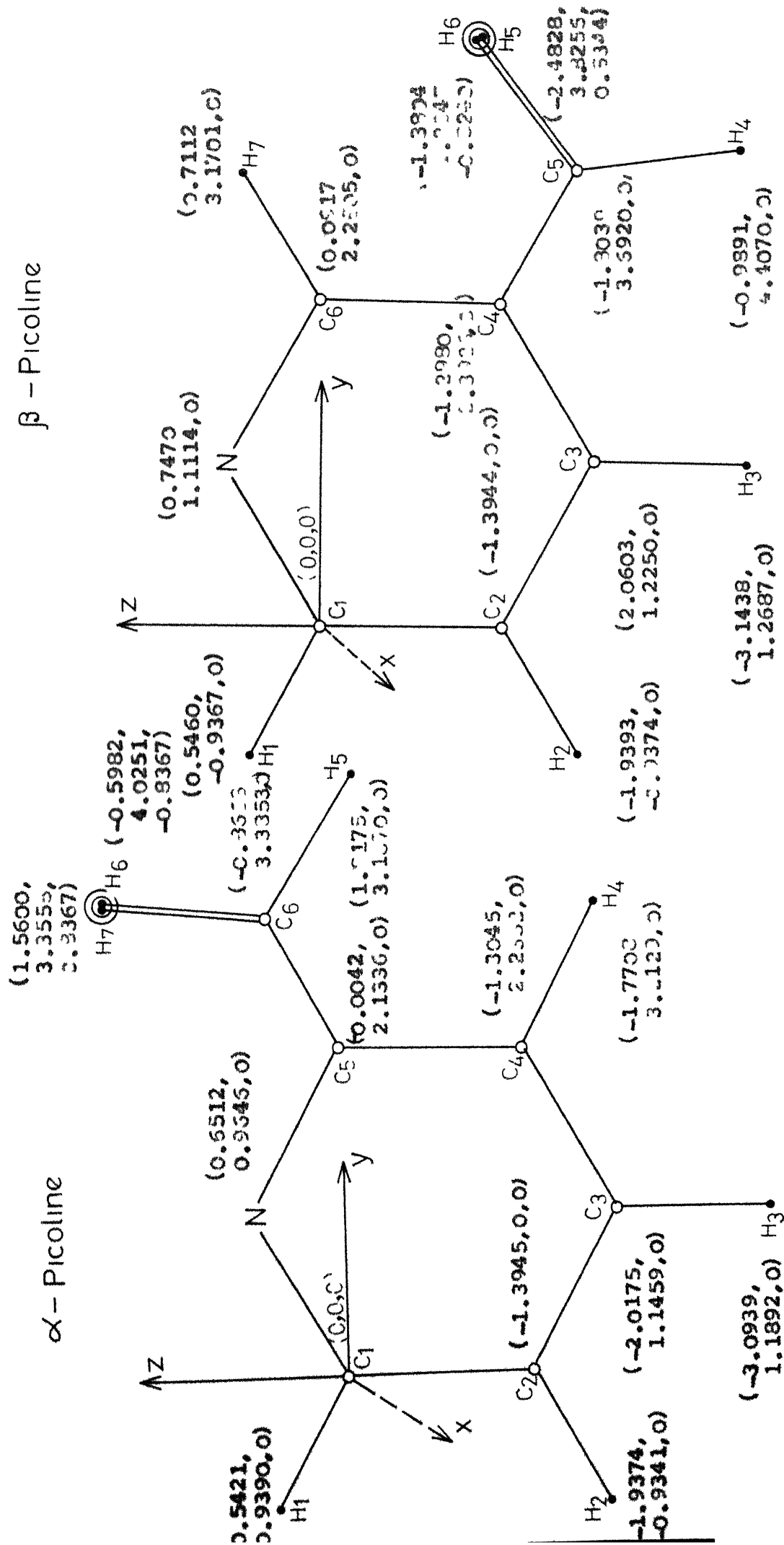


Fig 4 10 Vapour phase geometry of  $\alpha$ - and  $\beta$  - Picolines in ground state The number in parentheses denote z, y coordinates (in Å units) of the atoms with respect to origin (0,0,0)



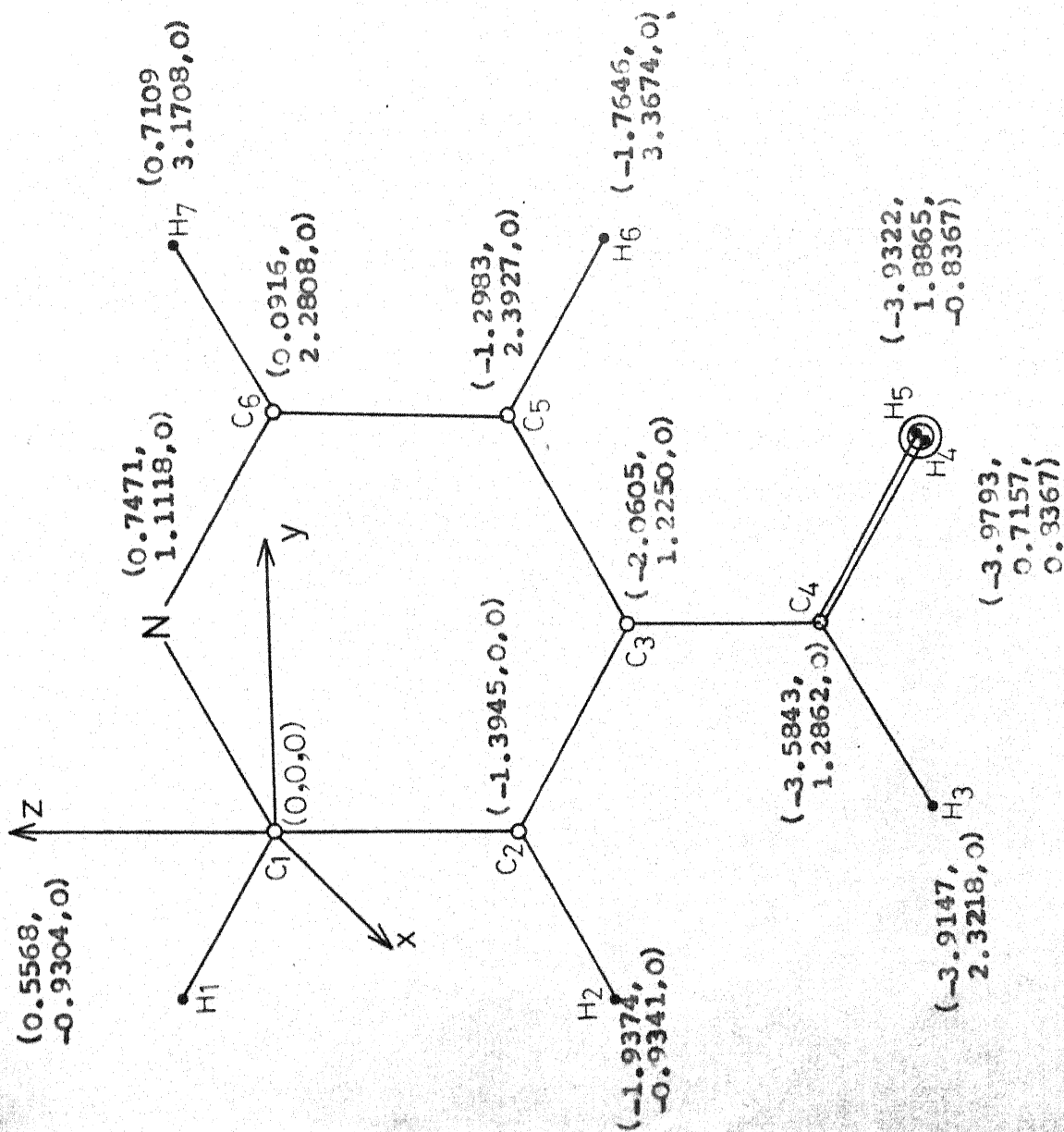
$\gamma$ -Picoline

Fig.4.11 Vapour phase geometry of  $\gamma$ -picoline in ground state. The numbers in the parentheses denote the z,x coordinates (in Å units) of the atoms with respect to the origin (0,0,0).

CHAPTER VVIBRATIONAL SPECTRA OF PARAFINOPHENOL  
AND PARAFLUORO BENZALDEHYDEABSTRACT

The vapour phase vibrational frequencies for gas phase para fluorophenol and para fluorobenzaldehyde have been obtained on the basis of a combined study of gaseous, liquid and solid (INT) phases. Preliminary results for normal coordinate analysis are given. The vibrational frequencies have been used (in Chapter VI) to deduce the thermodynamic quantities for the compounds.



## 5.0 INTRODUCTION

Recently, the fluorinated aromatics have attained considerable importance. The systems are interesting due to highly electronegative character of the fluorine atom which is responsible for intense infrared absorption and large changes in force constants. Vibrational spectra for para fluorophenol (1-9) and parafluorobenzaldehyde (10-19) based on low resolution electronic, liquid phase infrared, and Raman spectra have been presented earlier. The far-infrared spectrum ( $90-426\text{ cm}^{-1}$ ) for vapour phase para fluorobenzaldehyde has been reported by Miller et al (15). However, Raman data for Parafluorobenzaldehyde and the vapour phase infrared spectra for parafluorophenol are not available in literature. The rotational band contours have been studied in the electronic spectrum of parafluorophenol by Hollas et al (20). The microwave data for the compounds are not available. The earlier vibrational assignments for these compounds are incomplete, and based on low resolution electronic, and infrared spectra.

In the present investigations, the infrared spectra of Parafluorophenol, and Parafluorobenzaldehyde in the vapour, liquid, solid and solid (at liquid nitrogen temperature) phases and in solutions in the region  $250-4000\text{ cm}^{-1}$ , have been recorded. The vibrational assignments have been made on the basis of well resolved infrared band contours for all the fundamentals. A large

number of overtones including those due to the lowest torsional mode have been observed and assigned. The internal modes corresponding to CHO group of para fluorobenzaldehyde are contained in the species of Cs point group, and have been observed in vapour phase infrared spectra. The fundamental modes which are not observable or forbidden in the vapour phase infrared spectrum are observed in the solid (at LNT) phase. Some bands are found to show splittings at low temperature in the solid phase. Further the vibrational frequencies of the compounds under present study have been theoretically calculated using the Urey-Bradley force constants (21). These constants are known to be moderately transferable between chemically similar molecules (cf Chapter IV); especially if the substituents surrounding the particular coordinate are exactly identical, the force constants may be transferred to estimate the frequencies. These force constants may subsequently be modified slightly to suit the molecule under investigation.

## 5.1 EXPERIMENTAL

The analytical grade, Para-fluorophenol and para-fluorobenzaldehyde were obtained from Aldrich chemical Co. Both the samples were triple distilled under vacuum just before the experiment. The middle portion of the sample was always used for the experiment. The infrared spectra of vapour, liquid and solid states of the compounds were recorded using P.E. 521 double beam infrared spectro-photometer. For vapour phase spectra,

10 meter variable path multiple reflection gas cell was used. The vapour for each of the compounds was collected in the gas cell from the vacuum system (cf Chapter II) containing the sample. The vapour was kept at low pressure in the cell and longer path lengths ranging from 1.25 meter to 10 meter were used. Path lengths and the pressure of the vapour were varied to get a well resolved spectrum. The other experimental details are the same as given in Chapter II.

## 5.2 SELECTION RULES AND NOTATIONS

Both Para fluorophenol, Para fluorobenzaldehyde molecules belong to  $C_{2v}$  point group to a first approximation. 33 fundamental modes of Para fluorophenol are divided as

$$13a_1 + 10b_2 + 3a_2 + 7b_1$$

whereas 36 vibrations of Para fluorobenzaldehyde are divided as

$$13a_1 + 12b_2 + 4a_2 + 7b_1$$

The universally accepted Wilson's notations (22) have been used to designate the fundamental modes of the compounds except those due to substituent groups OH and CHO. All the fundamentals of parafluorophenol and para fluorobenzaldehyde are allowed in Raman spectrum and all but those belonging to  $a_2$  species in infrared spectrum (cf Table 3.1 Chapter III) are allowed.

### 5.3 VIBRATIONAL SPECTRA

The infrared absorption spectra of Para fluorophenol and para fluorobenzaldehyde in vapour, liquid and solid (RT and LNT) phases and in solutions in the range  $250-4000\text{ cm}^{-1}$  are shown in Figs 5.1 to 5.5. All the observed infrared bands of the compounds under study have been listed in columns 2,4,5,6 and 7 of Table 5.1 in vapour, solid (RT), solid (LNT) and in  $\text{CCl}_4$  and  $\text{CS}_2$  solutions for Para fluorophenol and in columns 2, 4 and 5 of Table 5.2 in vapour, liquid, and solid (at LNT) phases for para fluorobenzaldehyde. The probable assignment of the observed frequencies and anharmonicity of the combination bands have been given in last two columns of Tables 5.1 and 5.2 respectively. Observed and calculated values of vibrational frequencies are listed in Table 5.3.

#### 5.31 THE INFRARED BAND CONTOURS

Vapour phase infrared absorption spectra of para-fluorophenol and para fluorobenzaldehyde are shown in Figures 5.1 and 5.4, respectively. The band contours for some of the bands of the compounds are quite distinct and positions of P, Q and R branches are quite distinct in the spectrum. However, in the overlapped region where two or more bands overlap, the contour has been isolated graphically. The A-, B-, and C-type infrared band contours are the primary sources for ascertaining the  $a_1$ ,  $b_2$  and  $b_1$  modes in the vapour phase of para-fluorophenol and para fluorobenzaldehyde.

The observed P, Q, and R positions of infrared vapour phase bands of para fluorophenol and para fluorobenzaldehyde are given in Tables 5.1 and 5.2. For A-, and C-type bands, P, Q, and R represent the peak positions of the corresponding vibration-rotation branches. For B-type bands the dip between the P and R branches is given in parentheses and represents the position of Q-head. The observed  $\Delta\nu_{PR}$  values are shown in column 3 of Tables 5.1 and 5.2. Most of the frequencies used for interpretation of the observed bands are taken from the vapour phase infrared data of the present work. In some cases where contour is not distinct in vapour phase, liquid phase data have been used for the interpretation. The  $\Delta\nu_{PR}$  values for A-, B-, and C-type bands have been estimated using semi-empirical relations discussed earlier (cf Chapters III & IV). There is satisfactory agreement between the observed and computed  $\Delta\nu_{PR}$  values within the experimental limitations. The computed rotational parameters and  $\Delta\nu_{PR}$  values are given in Table 5.4.

#### 5.4 FUNDAMENTAL VIBRATIONS

The assignment of the fundamental vibrations of Para-fluorophenol and para fluorobenzaldehyde have been made on the basis of infrared data obtained in the present study and compared with the earlier results for phenol (23-25) and benzaldehyde (26), respectively. The important features in the infrared spectra, and the assignments of the infrared vapour phase inactive vibrations have been discussed in the following sections.

#### 5.41 THE $a_1$ FUNDAMENTAL MODES

The observed and theoretically calculated totally symmetry  $a_1$  fundamental modes for parafluorophenol are given in columns 4 and 5 and those for para fluorobenzaldehyde in columns 6 and 7 of Table 5.3. The observed bands are shown in Figures 5.1 and 5.4 and have been observed for the first time. There exists an excellent agreement between the vibrations belonging to  $a_1$  modes of parafluorophenol and phenol (23-25) and Para fluorobenzaldehyde and benzaldehyde (26) except the X-sensitive mode  $6a$ . The CF stretching mode is designated by the notation 13, and has been observed at 1318 and 1228.5  $\text{cm}^{-1}$  for para fluorophenol and para fluorobenzaldehyde, respectively. The X-sensitive mode  $6a$  is same for para fluorophenol and para fluorobenzaldehyde, and has been observed as a weak A-type band in the vapour phase infrared spectra. The shift in frequency for the ring breathing mode 1 in para fluorophenol and parafluorobenzaldehyde is due to the substitution of different groups OH, and CHO in benzene ring. The vapour phase, A type infrared band contours for the compounds have been observed for the first time except few bands below 426  $\text{cm}^{-1}$  for para fluorobenzaldehyde (15). The X-sensitive mode 7a representing CO stretching frequency for para fluorophenol and C-C stretching frequency for para fluorobenzaldehyde has been observed at 1263.0 and 1241.0  $\text{cm}^{-1}$  respectively. The OH stretching of parafluorophenol has appeared at 3656.0  $\text{cm}^{-1}$  as a strong A-type band in the vapour phase infrared

spectrum. The internal modes of CHO group of para fluorobenzaldehyde have been given separately in Table 5.3. The bands at 1720.0 and 2829  $\text{cm}^{-1}$  have been observed as A-type bands in the vapour phase infrared spectra of para fluorobenzaldehyde and are described as  $\nu_{\text{CO}}$  and  $\nu_{\text{CH}}$  of CHO group. The  $\Delta\nu_{\text{PR}}$  values for A(11)-type bands have been computed using the relation discussed earlier (27). They are 10.0 and 8.1  $\text{cm}^{-1}$  for para fluorophenol and para fluorobenzaldehyde respectively and are given in Table 5.4. These are in good agreement with the observed values.

#### 5.42 THE $b_2$ FUNDAMENTAL MODES

The typical shapes of B(1)-band contours of para-fluorophenol and para fluorobenzaldehyde are shown in Figures 5.1 and 5.4. The observed and theoretically calculated frequencies of  $b_2$  fundamentals have been given in columns 4 and 5 for para fluorophenol and in 6 and 7 for para fluorobenzaldehyde, respectively. In almost all the B(1)-bands there is no Q-branch and dip between P and R branches is quite characteristic. The X-sensitive mode 18b for para fluorophenol is overlapped by water bands and could not be isolated in the vapour phase infrared spectra. The liquid phase infrared band at 395.0  $\text{cm}^{-1}$  has been assigned to this mode. However, a strong band at 329  $\text{cm}^{-1}$  has been observed in the vapour phase far-infrared spectra for para fluorobenzaldehyde (15) and assigned as the mode 18b. CF bending frequency ( $\nu_{\text{CF}}$ ) has been observed at 385.0 and 418.0  $\text{cm}^{-1}$  for

6 vibrations listed in column 6 of Table 5.3 for para fluorobenzaldehyde have shown characteristic C-type band in the vapour phase infrared spectrum except the lowest fundamental 11 which has appeared in the vapour phase far infrared spectrum (15). Solutions and liquid phase infrared frequencies have been used for the assignments of the other fundamentals of para fluorophenol. In all the c-type bands which have been assigned as b<sub>1</sub> modes, the Q-branch is prominent and their P and R wings are characteristically broad. The internal mode of CHO group representing CHO wagg may be a strong band in the vapour phase infrared spectrum for para fluorobenzaldehyde at  $592\text{ cm}^{-1}$ . The computed  $\Delta\nu_{PR}$  values for C-type bands are  $15.1$  and  $12.1\text{ cm}^{-1}$  given in Table 5.4 for para fluorophenol and para fluorobenzaldehyde, respectively. There is a satisfactory agreement between the observed and computed  $\Delta\nu_{PR}$  values within the experimental limitations.

#### 5.45 THE a<sub>2</sub> FUNDAMENTAL MODES

The vibrational frequencies belonging to a<sub>2</sub> class for para fluorophenol and para fluorobenzaldehyde are listed in Table 5.3. The a<sub>2</sub> modes have not been observed in the vapour phase infrared spectrum as they are forbidden by symmetry selection rules (cf Table 3.1 Chapter III). However, all the three a<sub>2</sub> modes have appeared as weak bands in the infrared spectrum at liquid nitrogen temperature (INT). There is satisfactory agreement between the vibrations of parafluorophenol, para-



fluorobenzaldehyde and pyridine N-oxide (28). CHO group torsion frequency for para fluorobenzaldehyde has been observed at  $93.5\text{ cm}^{-1}$  in the vapour phase far-infrared spectrum (15).

#### 5.5 INFRARED SPECTRA OF PARA FLUOROPHENOL IN SOLUTIONS

The infrared absorption spectra of para fluorophenol in  $\text{CCl}_4$  and  $\text{CS}_2$  solutions have been given in Figure 5.3 and the observed bands are shown in columns 6 and 7 of Table 5.1. Almost all the fundamentals modes of  $a_1$ ,  $b_2$  and  $b_1$  species given in Table 5.3 have appeared in the infrared spectra of parafluorophenol in  $\text{CCl}_4$  and  $\text{CS}_2$  solutions except the mode  $6a$ . The OH stretching frequency of para fluorophenol which is at  $3656.0\text{ cm}^{-1}$  in vapour phase infrared spectra is decreased in solutions and has been observed at  $3636.0\text{ cm}^{-1}$  in  $\text{CCl}_4$  and  $\text{CS}_2$  solutions with strong intensity. Some of fundamental modes of para fluorophenol, are strong in solutions but weak in solid state spectra at RT and INT. The overtone and combination bands have appeared with medium intensity for para fluorophenol.

#### 5.6 LOW TEMPERATURE STUDIES

The infrared spectra of parafluorophenol and para fluorobenzaldehyde at RT & INT are shown in Figures 5.2 and 5.5. The observed frequencies at INT are given in column 5 of Tables 5.1 and 5.2. Low temperature studies of the compounds have been made for the first time. General sharpening of the bands has been observed for the compounds with respect to the room temperature

infrared spectra. Changes in peak positions in some of the bands have been observed, and few new bands appeared in these spectra, which are helpful in the assignments of some of the fundamentals specially the forbidden bands. A tentative interpretation of the new and splitted room temperature bands for para fluorophenol, and para fluorobenzaldehyde have been given in the last column of Tables 5.1 and 5.2.

### 5.7 MOLECULAR GEOMETRY

The para fluorophenol and para fluorobenzaldehyde molecules are planar as suggested by its definite A-, B-, and C-type vapour phase infrared band contours shown in Figures 5.1 and 5.4. The microwave data for the molecules are not available in literature. Assuming the planar regular hexagonal phenyl ring with all the equivalent CH bond lengths of  $1.084 \text{ \AA}$  (29), CF bond length as  $1.381 \text{ \AA}$  and neglecting the centrifugal distortion effects; we have illustrated in Fig 5.6 the most probable and the simplest conceivable geometry of para fluorophenol and parafluorobenzaldehyde as computed on IBM 7044 computer. The coordinates of all the atoms in the center of mass system have also been mentioned in the Figure. The computed rotational parameters, for the molecules are given in Tables 5.4. A comparison between the observed and calculated rotational parameters ( $\Delta v_{PR}$  values) shows that the proposed geometry for the molecules is correct (Cf. Table 5.5).

## 5.8 THEORETICAL CALCULATION OF FUNDAMENTAL MODES

The observed and computed frequencies for para-fluorophenol and parafluorobenzaldehyde are given in Table 5.3. Details of the normal coordinate calculations have been discussed in Chapter I. A simplified UBFF made up of force constants transferred from benzene (30), chlorobenzene (31), Pyridine N-oxide, and  $\alpha$ -,  $\beta$ -,  $\gamma$ -Picolines (cf Chapters III and IV) are set up. All other nondiagonal force constants except 1-3 interactions and 1-4 interactions among the ring carbon atoms are put equal to zero. The definitions of the internal coordinates for parafluorophenol and parafluorobenzaldehyde are given in Table 5.6. During the calculations minor and systematic alterations in stretching, bending, wagging and torsional force constants have been made in order to obtain a good fit observed frequencies for the molecules. The set of force constants which yields the best frequency fit for almost all the vibrational frequencies for para-fluorophenol and parafluorobenzaldehyde is given in Table 5.7.

REFERENCES

1. R.J. Jakcohsen and E.J. Brewer, Appl. Spectrosc. 16, 32 (1962)
2. D. Sharma and L.N. Tripathi, Indian J. Pure Appl. 1(6), 229 (1963)
3. S.K. Tiwari, Nature, 200, 1202 (1963)
4. D.A. Ibbitson and J.P.B. Sandall, J. Chem. Soc. 4547 (1964)
5. A. Hall and J.L. Wood, Spectrochim. Acta, 23A, 2657 (1967)
6. A. Hall and J.L. Wood, Spectrochim. Acta, 23A, 1257 (1967)
7. S.L. Srivastava and L.N. Tripathi, Indian J. Pure Appl. Phys. 6(3), 151 (1968).
8. S.N. Thakur and S.K. Tiwari, Indian J. Pure Appl. Phys. 7(8), 570 (1969).
9. J.V. Shukla, K.N. Upadhyaya and S.K. Tiwari, Indian J. Phys. 44(2), 128 (1970).
10. M.R. Padhye and V.G. Viladkar, Indian J. pure Appl. Phys. 1, 51 (1963).
11. D. Sharma, Indian J. Phys. 37(8), 405 (1963).
12. G.E. Lewis, Australian J. Chem. 17, 814 (1964)
13. Kailash Chandra, Indian J. pure Appl. Phys. 4(5), 214 (1966)
14. I.A. Rao, J. Sci Industr. Res. 20B, 523 (1961)
15. F.A. Miller, W.G. Fateley and R.E. Witkowski, Spectrochim. Acta 23A, 891 (1967).
16. M.P. Srivastava and I.S. Singh, J. Sci. Res. B.H.U. 17(1), 252 (1967).
17. K. Chandra and D. Sharma, Proc. Int. Conf. Spectrosc. 1st Bombay 1, 260 (1967).

18. V.B. Singh and I.S. Singh, Curr. Sci. 36(14), 365 (1967)
19. M.P. Srivastava and I.S. Singh, Curr. Sci. 36(15), 399 (1967)
20. J. Christoffersen, J.M. Hollas and G.H. Kirby, Mol. Phys. 18(4), 451 (1970).
21. T. Shimancuchi, J. Chem. Phys. 17, 245 (1949).
22. E. B. Wilson Phy. Rev. 45, 706 (1934).
23. H.D. Bist, J.C.D. Brand and D.R. Williams, J. Mol. Spectrosc. 21, 76 (1966).
24. H.D. Bist, J.C.D. Brand and D.R. Williams, J. Mol. Spectrosc. 24, 402 (1967).
25. H.D. Bist, J.C.D. Brand and D.R. Williams, J. Mol. Spectrosc. 24, 413 (1967).
26. V.N. Sarin, PhD Thesis, Indian Institute of Technology Kanpur (India) (1970).
27. V.N. Sarin, M.M. Rai, H.D. Bist and D.P. Khandelwal, Chem. Phys. Lett 6, 473 (1970).
28. J.S. Parihar and H.D. Bist (communicated)
29. B.P. Sticheff, Can. J. Phys. 32, 339 (1954)
30. N. Neto, M. Sctocco and S. Califano, Spectrochim. Acta, 22, 1981 (1966).
31. J.R. Scherer, Spectrochim. Acta, 20, 345 (1964).

TABLE 5.1

OBSERVED BAND POSITIONS, PR SEPARATIONS AND INTERPRETATIONS IN  
INFRARED BAND CONTOURS OF PARAFLUOROPHENOL

Sl. no.	Vapour Phase RT	PR $\Delta$	Solid at RT	Solid at INT	Solutions in CCl <sub>4</sub>	Solutions in CS <sub>2</sub>	Inter- pretation	Anharmonic- ity
1	2	3	4	5	6	7	8	9
1	-	-	-	-	280 w	280 w	11	
2	-	-	-	-	-	300 w		
3	-	-	325 w	330 w	-	-		
4	-	-	350 w	350 w	342 ms	340 ms	*CO	
5	-	-	372 w	360 w	370 w	-		
6	-	-	385 w	375 w	-	-	15	
7	-	-	395 w	400 w	395 w	405 w	18 <sub>b</sub>	
8	-	-	413 w	425 w	415 w	415 w		
9	-	-	-	435 m	440 m	440 m	16 <sub>a</sub>	
10	-	-	458 ms	460 w	455 m	455 ms		
11	493.0 P 503.0 Q (C) 510.0 R	17	513 s	505 s 520 m	508 vs	510 vs	16 <sub>b</sub>	
12	519.0 P 523.0 Q (A) 530.0 R	11	-	520 m	-	-	6 <sub>a</sub>	
13	567.0 P 572.0 Q (A) 577.0 R	10	-	-	-	-	(11) <sub>2</sub> =560	12
14	635.0 P (640.0) (B) 645.0 R	9	-	640 m	640 w	640 w	6 <sub>b</sub>	
15	-	-	-	-	685 w	685 w		

Table 5.1 contd

1	2	3	4	5	6	7	8	9
16			695 w	700 m	695 w	695 w	$(\tau_{CO})_2 = 700$	5
17	743.5 P 748.5 Q (A) 754.0 R	10.5	744 s	730 w	740 w	745 vs	12	
18			754 vs	748 s	765 w	770 m	10 <sub>b</sub>	
19	822.0 P 829.0 Q (C) 838.0 R	16	829 vs	810 ms 830 s	830 m	825 vs	10 <sub>a</sub> 17 <sub>b</sub>	
20	87.0 P (875.0) (B) 880.5 R	8.5	884 w	875 w	880 w	870 m	$(6a)(\tau_{CO}) = 873$	2
21	915.0 P 923.0 Q (C) 929.0 R	12	921 m	920 m	910 w	915 m	5	
22	944.0 P 948.0 Q (A) 955.0 R	11	949 w	950 ms	-	-	1	
23	-	-	-	-	-	1004 m	$(16b)_2 = 1006$	2
24	-	-	1012 ms	1015 m	1010 w	1010 w	17 <sub>a</sub>	
25	-	-	-	-	1020 w		$(6a)(16b) = 1026$	6
26	1080.5 P (1086.0) (B) 1091.0 R	10.5	1089 s	1070 ms 1090 s	1085 vs	1085 vs	9 <sub>b</sub>	
27	-	-	-	1105 w	1113 w	1115 m	$(10b)(\tau_{CO}) =$ 1104	-1
28	-	-	1146 ms	-	1145 m	1145 s	$(12)(15) =$ 1133.5	-12.
29	1163.0 P 1169.0 Q (A) 1173.0 R	10	-	1165 ms	1173 s	1165 s	18a	
30	1195.0 P 1200.0 Q (A) 1205.0 R	10	1192 s	1184 s	1187 s	1185 s	9 <sub>a</sub>	
31	1225.5 P 1231.0 Q (A) 1236.0 R	10.5	1222	1230	1225	1215 s	$p_{OH}$	

Contd ---

1	2	3	4	5	6	7	8	9
32	1257.0 P 1263.0 Q (A) 1268.0 R	10	-	-	1260 m	1260 s	7a	
33	1287 P (1292) (B) 1297 R	10	-	-	-	-	3	
34	1312.5 P 1318.0 Q (A) 1328.5 R	11.0	-	-	1321 s	1325 s	✓CF	
35	-	-	-	-	1338 s	1333 s	14	
36	-	-	1355 ms	1363 ms	-	-	-	-
37	-	-	1393 ms	1403 1415	-	-	(4) <sub>2</sub> =1390	-3
38	1430.5 P 1436.0 Q (A) 1441.5 R	11.0	-	1435 ms	1433 s	-	19b	
39	-	-	-	-	1453 s	-	(12)(4)=1443.5	-9.5
40	-	-	1455 ms	1465 ms	1463 s	-	(1)(6a)=1471	-8
41	-	-	-	1490 s	1495	-	(11)(9a)=1480	-10
42	-	-	1500 s	1500 s	-	-	(12) <sub>2</sub> =1497.0	-3
43	1505.5 P 1511.0 Q (A) 1514.0 Q 1518.0 R	12.5	1510 s	1510 s	1510 s	-	19a	
44	-	-	1530 m	-	-	-	(18a)( $\tau$ CO)= 1519	-11
45	-	-	1535 m	-	-	-	(18a)(15)=1554	
46	1589.0 P (1592.0) (B) 1598.0 R	9	1602 s	1590 ms	1600 m	-	8b	
47	1604.5 P 1610.0 Q (A) 1616.0 R	11.5	1617 ms	-	1617 m	-	8a	

Contd ---



Table 5.1 contd

1	2	3	4	5	6	7	8	9
48			1632 ms	-	-	-	( $\rho_{OH}$ )(18b)=1626	-6
49			1669 vw	1669	-		(18b)(7a)=1658	-1
50			1689 w	1692	-	1697 w	(18a)(6a)=1692	3
51			1736 m	1750	1725 m	1725 m	( $\rho_{OH}$ )(16b)= 1734	-2
52			-	-	1745 w	-	( $\rho_{OH}$ )(6a)=1754	9
53			-	-	-	1827 w	-	
54			-	1865 w	1865 ms	1850 s	( $\rho_{OH}$ )(6b)=1871	-6
55			1884 ms	-	-	1895 w	(19a)(15)=1899	4
56			1901 w	-	-	-	(19a)(18b)=1909	8
57			-	-	-	1925 w	(12)( $\rho_{OH}$ )=1919	-6
58			-	-	-	2050 w	-	
59			2064 w	2074 w	2065 w	2060 w	-	
60			-	-	2115 w	-	(5)(9a)=2123	8
61			2159 w	2170 w	-	-	( $\rho_{OH}$ )(5)=2154	-5
62			2242 w	2242 w	2230	2252 w	(6b)(8b)=2232	-10
63			2277 w	2276 w	-	-	(12)(19a)=2262.5	
64			2297 w	2287 w	-	-	(9a)(9b)=2286	-11
65			2342 m	2340 w	2340 w	2335 w	(12)(8b)= 2340.5	-1.
66			2362 w	2370 w	-	2365 w	(12)(8a)= 2358.5	-4
67			-	-	-	2385 w	(9a) <sub>2</sub> =2400	
68			2424 w	2430 w	2425 w	-	(9a)( $\rho_{OH}$ )=2431	-7
69			2452 m	2450 w	-	-	( $\rho_{OH}$ ) <sub>2</sub> =2462	10
70			2475 w	2480 w	-	-	-	

contd

Table 5.1 contd

255

1	2	3	4	5	6	7	8	9
71			2545 w	2544 w	-		(14)(4a)=2538	-7
72			2590 w	2595 w	-	2580 w	-	
73			-	-	-	2600 w	(14)(7a)=2601	1
74			-	2660 w	-	2655 w	-	
75			2675 w	2685 w	-	2685 w	(18a)(19a)=2683	8
76			2729 w	2744 w	-	-	-	
77			2790 w	2780 w	-	2770 w	(8a)(9a)=2792	2
78			2902 w	2900 w	-	2892	(19b) <sub>2</sub> =2910	8
79	2977 2985 2987	P Q (A) R	12	2983 w	2983 w	-	2992 w	(19a) <sub>2</sub> =3028
80	3012 (3007) 3011	P (B) R	9	-	3003	-	-	7b
81	3033 3038 3043	P Q (A) R	10	3046	3058 w	3035 m	3037 ms	2
82	3064 (3070) 3073	P (B) R	9	3082 w	3082 w	-	-	20b
83	3085 3092 3097	P Q (A) R	12	3109 w	3107 w	-	-	20a
84	3651 3656 3663	P Q (A) R	12	-	-	3636 s	3620 s	v <sub>OH</sub>

TABLE 5.2

OBSERVED BAND POSITIONS, PR SEPARATIONS AND INTERPRETATIONS  
IN INFRARED BAND CONTOURES OF PARA FLUOROBENZALDEHYDE

Sl. no.	Vapour Phase RT	PR	Liquid Phase	Solid Phase	Interpretation	Anharmonicity
1	2	3	4	5	6	7
1	93.5* (s)	-	113*	-	$\tau_{CHO}$	
2	200.0* (s)	-	200.0*	-	18b	
3	270.0* (w)	-	-	-		
4	329* (m)	-	326 ms	331 s	11	
5	387 w	-	381 ms	370 ms 383 ms		
6	414.5 P (418.0) (B) 422.0 R	7.5	418 ms	416 s	$(18b)_2=400$	
7	-	-	424 w	-		
8	495.0 P 499.0 Q (C) 504.0 Q 509.0 R	14	508 ms	500 s	16b	
9	518.0 P 523.0 Q (A) 526.0 R	8	-	508 s	6a	
10	585.0 P 592.0 Q (C) 600.0 R	15	600 s	553 mw 598 vs	$\gamma_{CHO}$	
11	612.0 P 615.0 Q (A) 620.0 R	8	-	-	$(15)(18b)=618$	2
12	631.5 P 635.0 Q (A) 640.0 R	8.5	633 ms	633 s	6b	
13	687.0 P (691.0) (B) 694.0 R	7	685 w	681 m	CHO rock	

Contd ---

Table 5.2 contd

257

1	2	3	4	5	6	7
14	720.0 Q (C)		700 w	705 w	4	-
15	741.5 P (745.0) (B) 749.0 R	7.5	-	745 w	(6a)(16b)=723	-
16	749.5 P 754.0 Q (C) 758.0 R	8.5	-	-	10 <sub>b</sub>	-
17	770.0 P (773.0) (B) 778.0 R	8	773 s	771 ms	(16a) <sub>2</sub> =762	-11
18	802.0 P (806.0) (B) 810.0 R	8	-	-	-	-
19	813.0 P 817.0 Q (A) 821.5 R	8.5	-	814 m	(4) ( $\tau_{\text{CHO}}$ )=813	-4
20	826.0 P 834.0 Q (C) 838.0 R	12	834 s	829 m	17 <sub>b</sub>	-
21	850.0 P 855.0 Q (A) 858.5 R	8.5	861 s	851 s 864	$\frac{12}{10_a}$	-
22	922.0 P 926.5 Q (A) 930.0 R	8	-	-	(18b) <sub>2</sub> (6a)=923	-3.5
23	939.0 Q (C)	-	949 w	944 w	(6a)(15)=941	2
24	980.0 P 985.0 Q (C) 990.0 R	10	-	-		
25	1002.0 Q (A)		-	-	1	
26	1007.0 P 1011.5 Q (A) 1015.0 R	8	1011 ms	1010 ms	18a	-
27	-	-	1056 w	1046 w	(6a) <sub>2</sub> =1046	-10

Contd ---

Table 5.2 contd

1	2	3	4	5	6	7
28	1086.0 P (1092.0) (B) 1094.0 R	8	1096 ms	1094 ms		
29	-	-	1113 m	1105 ms		
30	1143.0 P 1147.5 Q (A) 1152.0 R	9	1159 s	1146 s 1157 s	(6a)(6b)=1158 9a	12
31	1175.0 P (1178.0) (E) 1183.0 R	8	-	-		
32	1195.0 P (1200.0) (B) 1203.0 R	8	1212 ms	1207 vw	9b	
33	1225.0 P 1228.5 Q (A) 1233.0 R	8	1232 vs	1219 vs	13	
34	1238.0 P 1241.0 Q (A) 1246.0 R	8	-	1258.0 w	7a	
35	1285.5 P (1289.0) (B) 1293.0 R	7.5	1295 ms	1290 ms	3	
36	-	-	1308 m	1303 s	(16a)(5)=1320	13
37	1316.5 P (1321.0) (B) 1324.0 R	7.5	1328 w 1338 w	1328 m	14	
38	-	-	1365 m	1368 m	(6a)(12)=1378	13
39	1377.5 P (1383.0) (B) 1385.0 R	7.5	1391 ms	1392 s	$\alpha$ HCO	
40	1416.0 P 1420.0 Q (A) 1424.0 R	8	1423 m	1423 ms 1433 ms	<sup>19a</sup> (18a)(15)=1429.5	6.5
41	-	-	1461 w	1458 w 1468 w	(4)(10b)=1474	6

Contd ---

Table 5.2 contd

1	2	3	4	5	6	7
42	1499.5 F (1503.0) (B) 1507.0 R	7.5	1505 ms	1500 ms	9b	
43	-	-	-	1570 m	(12)(4)=1575	5
44	1597.5 P (1602.0) (B) 1605.0 R	7.5	1599 vs	1597 vs	8b	
45	1612.5 P 1618.0 Q (A) 1622.0 R	9.5	1632 ms	1627 w	8a	
46	1705.0 P (1709.0) (B) 1713.0 R	8	1702 s	1689 s 1702 m	(6a)(9b)=1701	-8
47	1718.0 P 1720.0 Q (A) 1726.0 R	8	-	1717 m	100, (12) <sub>2</sub> =1710	-10
48	1729.5 P 1734.0 Q (A) 1738.0 R	8.5	-	-	(10a) <sub>2</sub> =1728	-6
49	-	-	1786 m	1791 w		
50	-	-	1914 ms	1919 m	(6b)(3)=1924	10
51	-	-	2059 w	2054 w	(17b)(13)=2062.5	3.5
52	-	-	2092 w	2098 w	(12)(13)=2083.5	-9.5
53	-	-	2162 w	2164 w		
54	-	-	2188 w	2188 w	(14)(12)=2176	-12
55	-	-	2242 w	-	(7a)(1)=2243	1
56	-	-	2275 w	-		
57	-	-	2310 w	-	(18a)(3)=2300	-10
58	-	-	2397 w	-	(7a)(9a)=2388	-9
59	-	-	2452 m	2452 w		
60	-	-	2526 w	2526 w		
61	-	-	2531 w	2536 vw	(3)(7a)=2530	-1

Contd ---

Table 5.2 contd

1	2	3	4	5	6	7
62	2605.0 P (2608.0) (B) 2612.0 R	7	2610 m	2615 w	(1)(8b)=2604	-4
63	2734.0 P (2738.0) (B) 2741.5 R	7.5	2742 ms	-	(7a)(19b)=2744	6
64	2773.0 P (2777.0) (B) 2781.0 R	8	-	-	(9b)(8b)=2780	3
65	2790.5 P 2794.0 Q (A) 2799.0 R	8.5	2794 m	2799 w	(8a)(9b)=2796	2
66	2824.5 P (2829.0) (B) 2832.0 R	7.5	2831 ms	2829 m	$\nu_{\text{CH}}$ (CHO group)	1
67	-	-	2852 m	2854 w	(7a)(8b)=2843	-9
68	-	-	2868 w	2868 vw	(7a)(8a)=2859	-9
69	2936.0 P 2942.0 Q (A) 2946.0 R	10	-	-	(8a)(14)=2939	-3
70	2952.0 P 2956.0 Q (B) 2960.0 R	8	-	-	-	-
71	2978.0 P (2982.0) (B) 2986.0 R	-	-	-	-	-
72	2992.0 P 2996.0 Q (A) 3000.0 R	8	-	-	(19b) <sub>2</sub> =3006	10
73	3015.0 P (3018.0) (B) 3022.5 R	7.5	3013 w	3016 vw	7b	-
74	3053.0 P 3059.0 Q (A) 3061.0 R	8	3067 w	3069 w	2	-
75	3088.0 P (3092.0) (B) 3096.0 R	8	3087 ms	3087 ms	20b	-
76	-	-	3120 m	3117 w	20a	-

\*Values are from ref. (15)

TABLE 5.3

OBSERVED AND CALCULATED VALUES OF FUNDAMENTAL MODES OF PARA-  
FLUOROPHENOL AND PARA FLUOROBENZALDEHYDE

Symmetry	Designation	Description	Fundamental Frequency (cm <sup>-1</sup> )			
			Para fluorophenol		Para fluorobenzaldehyde	
			Obs.	Cal.	Obs.	Cal.
1	2	3	4	5	6	7
<u>a<sub>1</sub></u>	6a	X-sensitive	523	472	523	496
	12	X-sensitive	748.5	749	855	980
	1	ring	949	1019	1002	994
	18a	$\beta$ CH	1169	1132	1011	1094
	9a	$\beta$ CH	1200	1163	1147	1135
	7a	$\nu$ CO	1263	1249	1241( $\nu$ CO)	1212
	19a	$\nu$ CC	1514	1493	1420	1483
	8a	$\nu$ CC	1610	1604	1618	1595
	13	$\nu$ CF	1318		1228.5	
	2	$\nu$ CH	3038	3087	3059	3086
	20a	$\nu$ CH	3092	3100	3120	3137
		$\beta$ OH	1231	1220		
		$\nu$ OH	3650	3673		
	18b	X-sensitive	395 <sup>a</sup>	458	329 <sup>d</sup>	182
	6b	ring	640*	640	635	634
<u>b<sub>2</sub></u>	15	$\beta$ CF	385 <sup>a</sup>	344	418	395
	9b	$\beta$ CH	1086	1104	1200	1148
	3	$\beta$ CH	1292	1271	1289	1248
	14	$\nu$ CC	1338	1308	1321	1268
	19b	$\nu$ CC	1436	1416	1503	1400
	8b	$\nu$ CC	1592	1551	1602	1538

Contd



Table 5.3 contd

262

1	2	3	4	5	6	7
	7b	$\nu_{CH}$	3007	3084	3018	3084
	20b	$\nu_{CH}$	3070	3096	3092	3120
$b_1$	11	X-sensitive	280 <sup>(c)</sup>	324	329 <sup>(d)</sup>	333
	16b	X-sensitive	503		499	496
	4	$\tau_{CC}$	695 <sup>(a)</sup>	713	720	
	10b	$\nu_{CF}$	754 <sup>(a)</sup>	741	754	731
	17b	CF	829	877	834	781
	5	$\nu_{CH}$	923	926	959	913
		$\tau_{CO}$	350 <sup>(a)</sup>	363		
$a_2$	16a	$\tau_{CC}$	435 <sup>(b)</sup>	397	381 <sup>(a)</sup>	364
	10a	$\nu_{CH}$	810 <sup>(b)</sup>	886	864 <sup>(b)</sup>	818
	17a	$\nu_{CH}$	1015 <sup>(b)</sup>	1037	970 <sup>(e)</sup>	1000
CHO group vibrations of Para fluorobenzaldehyde						
	CHO rock				691	
	$\omega_{HCO}$				1383	1362
	$\nu_{CO}$				1720	
	$\nu_{CH}$				2829	2975
a	$\tau_{CHO}$				93.5 <sup>(d)</sup>	168
	$\nu_{CHO}$				592	

(a) IR liquid, (b) solid at INT, (c) in  $CCl_4$  solution, (d) reference (15)  
(e) reference (18)

TABLE 5.4

CALCULATED ROTATIONAL PARAMETERS (a) AND PR SEPARATIONS AT 300°K FOR  
INFRARED BAND CONTOURS OF PARA-FLUOROPHENOL AND PARA-FLUOROBENZALDEHYDE

Molecules	$A$ MC/sec	$B$ MC/sec	$C$ MC/sec	$\bar{B}$ MC/sec	$\bar{B}$	$S(\bar{\beta})$	PR Separations		
							$A(11)$	$B(1)$	$C(1)$
Para-fluorophenol	5606.2640	1438.9011	1145.0206	1291.9608	3.3393	1.1912	10.09	8.47	15.14
Para fluoro-benzaldehyde	5058.5941	965.0261	810.422	887.724	4.6983	1.1546	8.11	7.02	12.16

(a) The rotational constants and the parameters  $\bar{B}, \bar{\beta}, S(\bar{\beta})$  along with  $\Delta\nu_{PR}$  values for IR bend contours are defined earlier (cf Chap. III & IV).

TABLE 5.5

ASSUMED GEOMETRY FOR PARAFLUOROPHENOL AND  
PARAFLUOROBENZALDEHYDE

Parameters	Parafluorophenol	Parafluorobenzaldehyde
$R(C_1-H_1)$	1.0840 Å	1.0840 Å
$R(C_1-C_2)$	1.3965	1.3965
$R(C_3-F)$	1.3181	1.3181
$R(C-O)$	1.358 ( $C_6O$ )	1.241 ( $C_7O$ )
$R(C-CHO)$	-	1.489
$R(O-H)$	0.944 ( $OH_5$ )	-
$R(C-H)$	-	1.084
$\angle C_1C_2C_3$	119.94°	120.21°
$\angle C_1C_2H_2$	119.58	119.58
$\angle C_2C_3C_4$	120.0	120.0
$\angle C_2C_3F$	119.58	119.26
$\angle C_5C_6C_1$	119.88	119.58
$\angle H_5OC_6$	114.70	119.0
$\angle OCH$	-	119.0 $\angle OC_7H_5$

THE DEFINITIONS OF THE INTERNAL COORDINATES FOR PARAFLUOROPHENOL  
AND PARAFLUOROBENZALDEHYDE

Internal Coordinate	Description		Internal Coordinate	Description	
	Parafluoro- phenol	Parafluoro- benzaldehyde		Parafluoro- phenol	Parafluoro- benzalde- hyde
S1	$\nu C_1 C_2$	$\nu C_1 C_2$	S26	$\alpha C_4 C_5 C_6$	$\beta H_3 C_4 C_5$
S2	$\nu C_2 C_3$	$\nu C_2 C_3$	S27	$\beta C_4 C_5 H_4$	$\alpha C_4 C_5 C_6$
S3	$\nu C_3 C_4$	$\nu C_3 C_4$	S28	$\beta H_4 C_5 C_6$	$\beta C_4 C_5 H_4$
S4	$\nu C_4 C_5$	$\nu C_4 C_5$	S29	$\alpha C_5 C_6 C_1$	$\beta H_4 C_5 C_6$
S5	$\nu C_5 C_6$	$\nu C_5 C_6$	S30	$\beta C_5 C_6 O$	$\alpha C_5 C_6 C_1$
S6	$\nu C_6 C_1$	$\nu C_6 C_1$	S31	$\beta O C_6 C_1$	$\beta C_5 C_6 C_7$
S7	$\nu C_1 H_1$	$\nu C_1 H_1$	S32	$\beta H_5 O C_6$	$\beta C_7 C_6 C_1$
S8	$\nu C_2 H_2$	$\nu C_2 H_2$	S33	$\gamma C_1 H_1$	$\beta O C_7 C_6$
S9	$\nu C_3 F$	$\nu C_3 F$	S34	$\gamma C_2 H_2$	$\beta O C_7 H_6$
S10	$\nu C_4 H_3$	$\nu C_4 H_3$	S35	$\gamma C_3 F$	$\beta H_5 C_7 C_6$
S11	$\nu C_5 H_4$	$\nu C_5 H_4$	S36	$\gamma C_4 H_3$	$\beta C_1 H_1$
S12	$\nu C_6 O$	$\nu C_6 C_7$	S37	$\gamma C_5 H_4$	$\gamma C_2 H_2$
S13	$\nu O H_5$	$\nu C_7 O$	S38	$\gamma C_6 O$	$\gamma C_3 F$
S14	$\alpha C_6 C_1 C_2$	$\nu C_7 H_5$	S39	$\gamma O H_5$	$\gamma C_4 H_3$
S15	$\beta H_1 C_1 C_6$	$\alpha C_6 C_1 C_2$	S40	$\tau C_1 C_2$	$\gamma C_5 H_4$
S16	$\beta H_1 C_1 C_2$	$\beta H_1 C_1 C_6$	S41	$\tau C_2 C_3$	$\gamma C_6 C_7$
S17	$\alpha C_1 C_2 C_3$	$\beta H_1 C_1 C_2$	S42	$\tau C_3 C_4$	$\gamma C_7 O$
S18	$\beta H_2 C_2 C_1$	$\alpha C_1 C_2 C_3$	S43	$\tau C_4 C_5$	$\gamma C_7 H_5$
S19	$\beta H_2 C_2 C_3$	$\beta H_2 C_2 C_1$	S44	$\tau C_5 C_6$	$\tau C_1 C_2$
S20	$\alpha C_2 C_3 C_4$	$\beta H_2 C_2 C_3$	S45	$\tau C_6 C_1$	$\tau C_2 C_3$
S21	$\beta C_2 C_3 F$	$\alpha C_2 C_3 C_4$	S46	$\tau C_6 O$	$\tau C_3 C_4$
S22	$\beta F C_3 C_4$	$\beta C_2 C_3 F$	S47	=	$\tau C_4 C_5$
S23	$\alpha C_3 C_4 C_5$	$\beta F C_3 C_4$	S48	=	$\tau C_5 C_6$
S24	$\beta C_3 C_4 H_3$	$\alpha C_3 C_4 C_5$	S49	=	$\tau C_6 C_1$
S25	$\beta H_3 C_4 C_5$	$\beta C_3 C_4 H_3$	S50	=	$\tau C_6 C_7$

The running suffixes with the internal coordinates (S) show their identifying number while the suffixes with atoms represent their positions (Cf. Fig. 5.6.)

TABLE 5.7

REFINED UREY-BRADLEY FORCE-CONSTANTS FOR PLANAR AND NON-PLANAR  
VIBRATIONS OF PARA FLUOROPHENOL AND PARAFLUOROBENZALDEHYDE

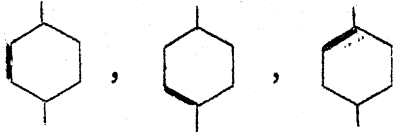
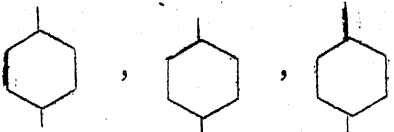
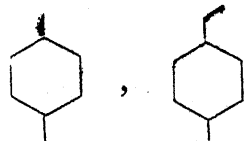
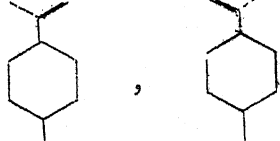
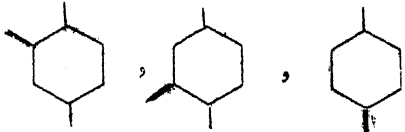
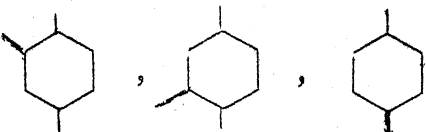
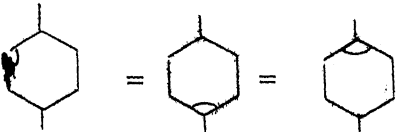
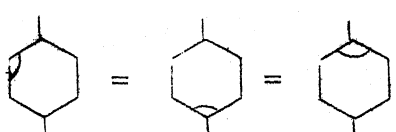
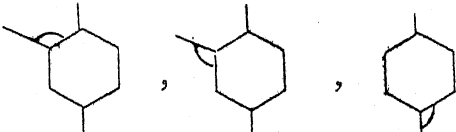
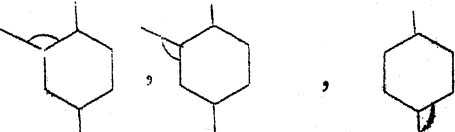
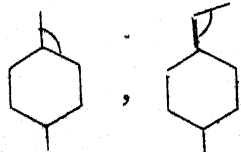
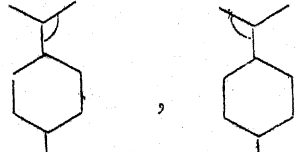
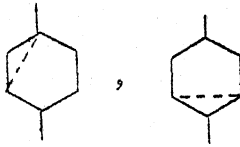
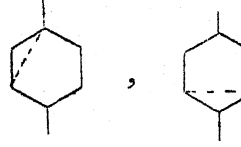
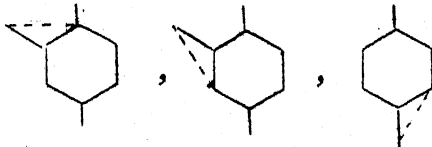
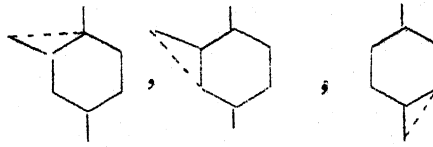
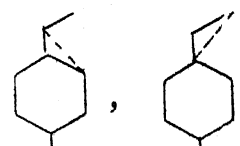
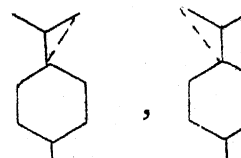
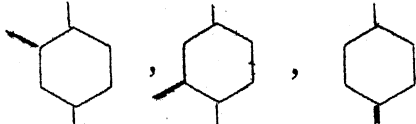
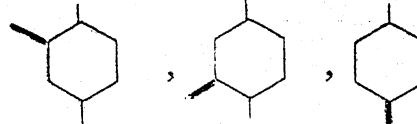
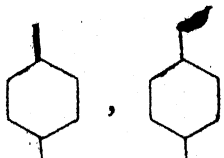
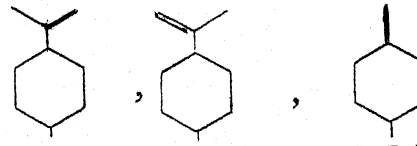
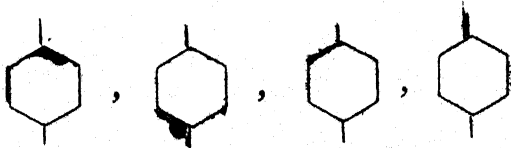
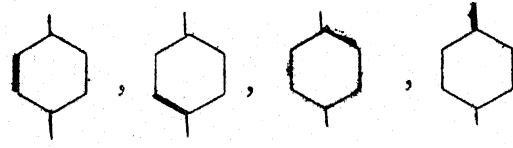
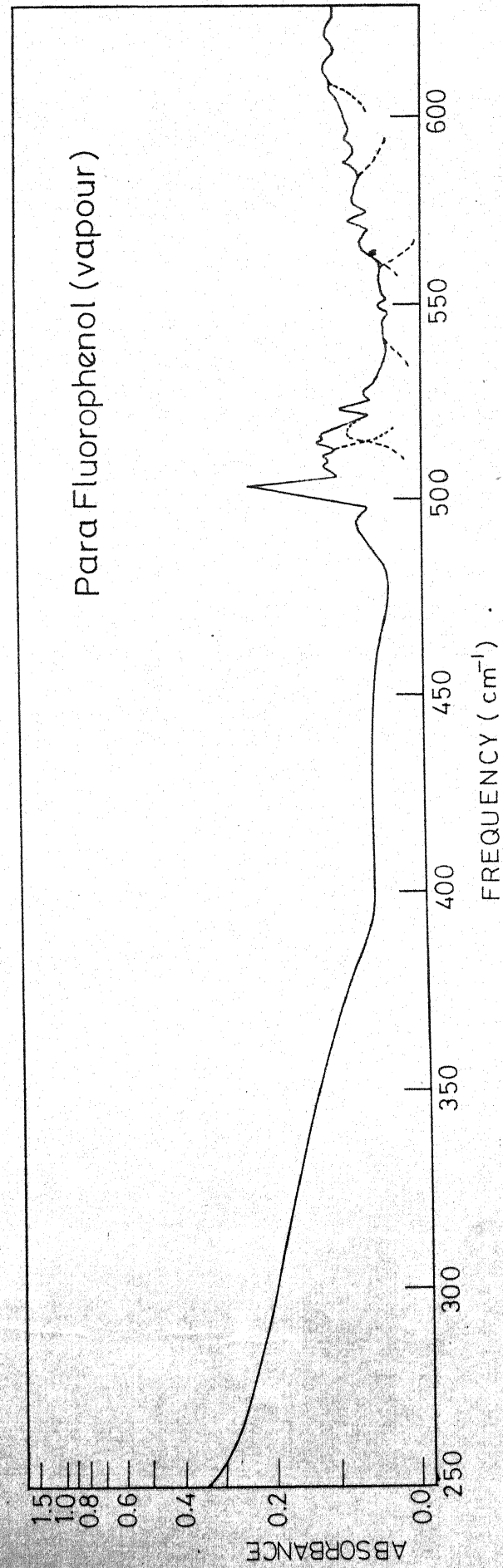
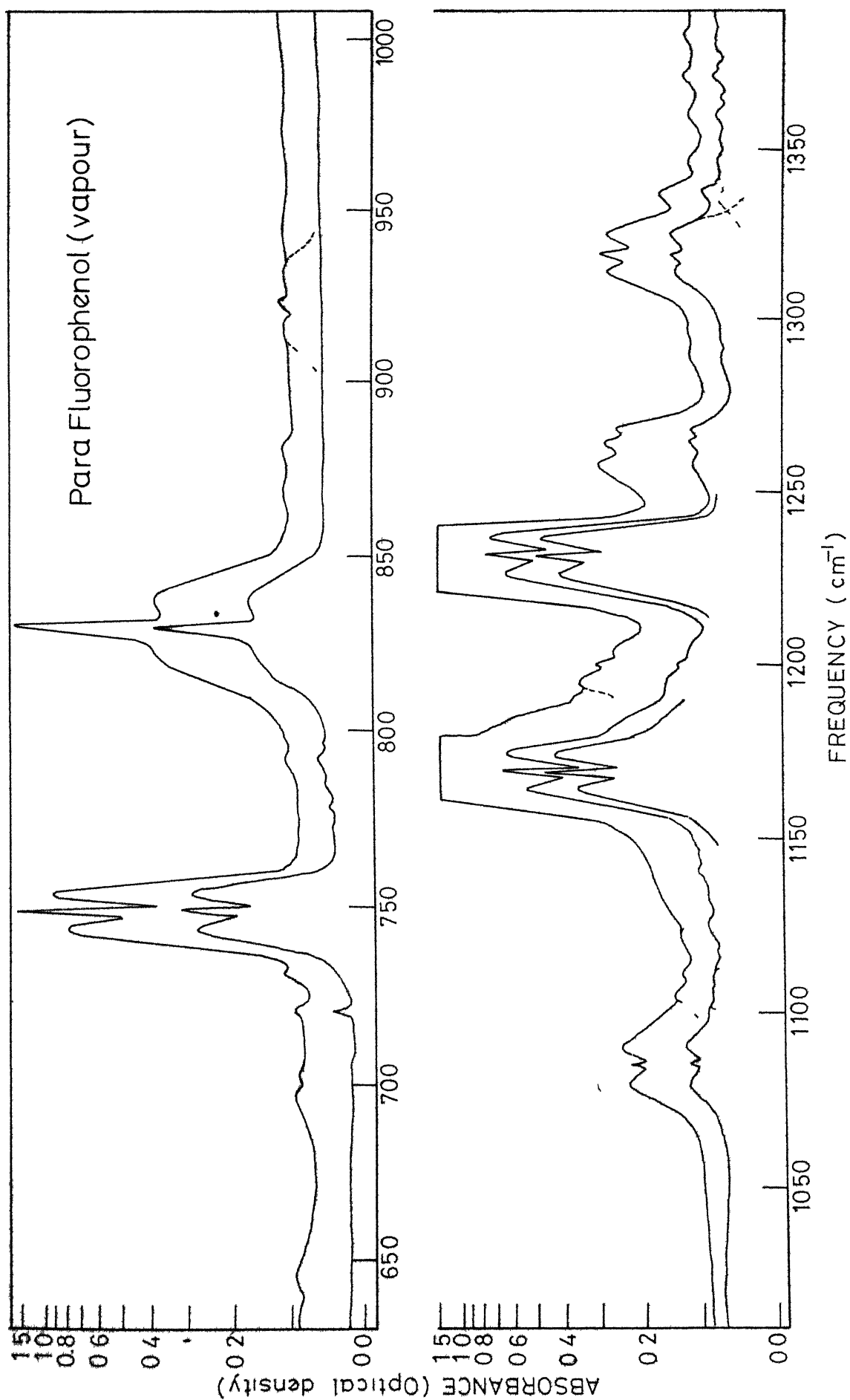
	Parafluorophenol	Parafluorobenzaldehyde
$K_{CC}$	 5.15    5.00    4.100	 5.51    4.100    4.100
$K_{CO}, K_{OH}$	 4.100    7.355	 3.83    3.83 ( $K_{CH}$ )
$K_{CH}, K_{CF}$	 4.745    4.785    3.845 ( $K_{CF}$ )	 4.745    4.865    3.850 ( $K_{CF}$ )
$H_{CC}$	 0.645	 0.645
$H_{CH}$	 0.233    0.395    0.258 ( $H_{CF}$ )	 0.233    0.345    0.260 ( $H_{CF}$ )
$H_{CO}, H_{OH}$	 0.408    0.516	 0.258    0.345 ( $H_{CH}$ )

Table 5. (contd.)

	Parafluorophenol	Parafluorobenzaldehyde
$F_{CC}$	 0.7057   0.8033	 0.7057   0.8033
$F_{CH}, F_{CF}$	 0.4395   0.3395   0.9226( $F_{CF}$ )	 0.4395   0.3395   0.9215( $F_{CF}$ )
$F_{CO}, F_{OH}$	 0.9226   0.350	 0.260   0.255( $F_{CH}$ )
$\gamma_{CO}, \gamma_{OH}$	 0.165   0.205   0.750( $\gamma_{CF}$ )	 0.165   0.205   0.755
$\gamma_{CO}, \gamma_{OH}$	 0.725   0.009( $\gamma_{OH}$ )	 0.385   0.195( $\gamma_{CH}$ )   0.725( $\gamma_{CC}$ )
$\tau_{CC}$	 0.112, 0.1345, 0.152, 0.0092( $\tau_{CO}$ )	 0.085, 0.1135, 0.152, 0.0093( $\tau_{CC}$ )

Units: K in m dynes/Å, H, F, C,  $\gamma$  and  $\tau$  in  $10^{-11}$  erg/rad.<sup>2</sup>







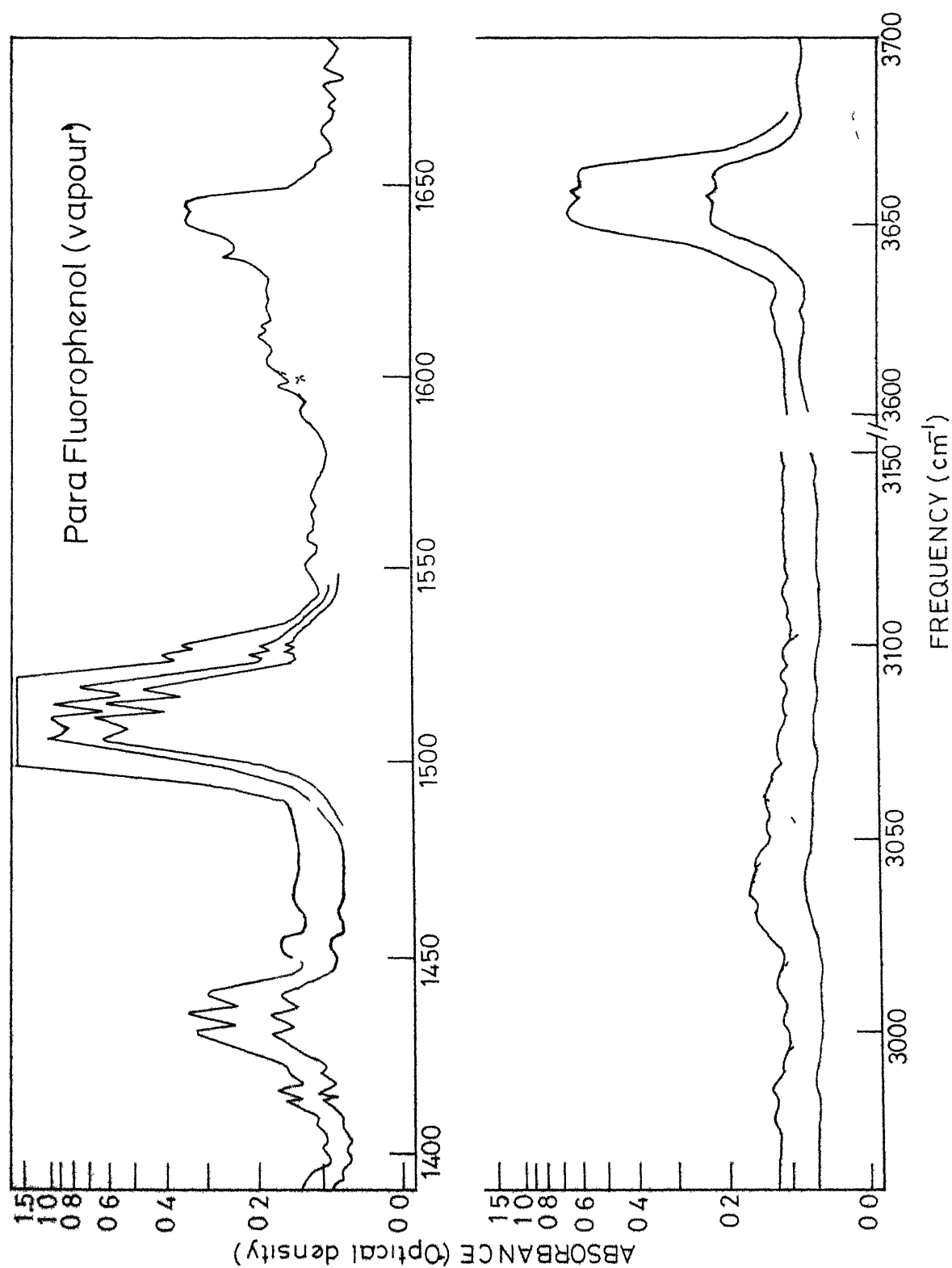


Fig 5 1 The infrared spectra of Para Fluorophenol at low pressure and four meter path length

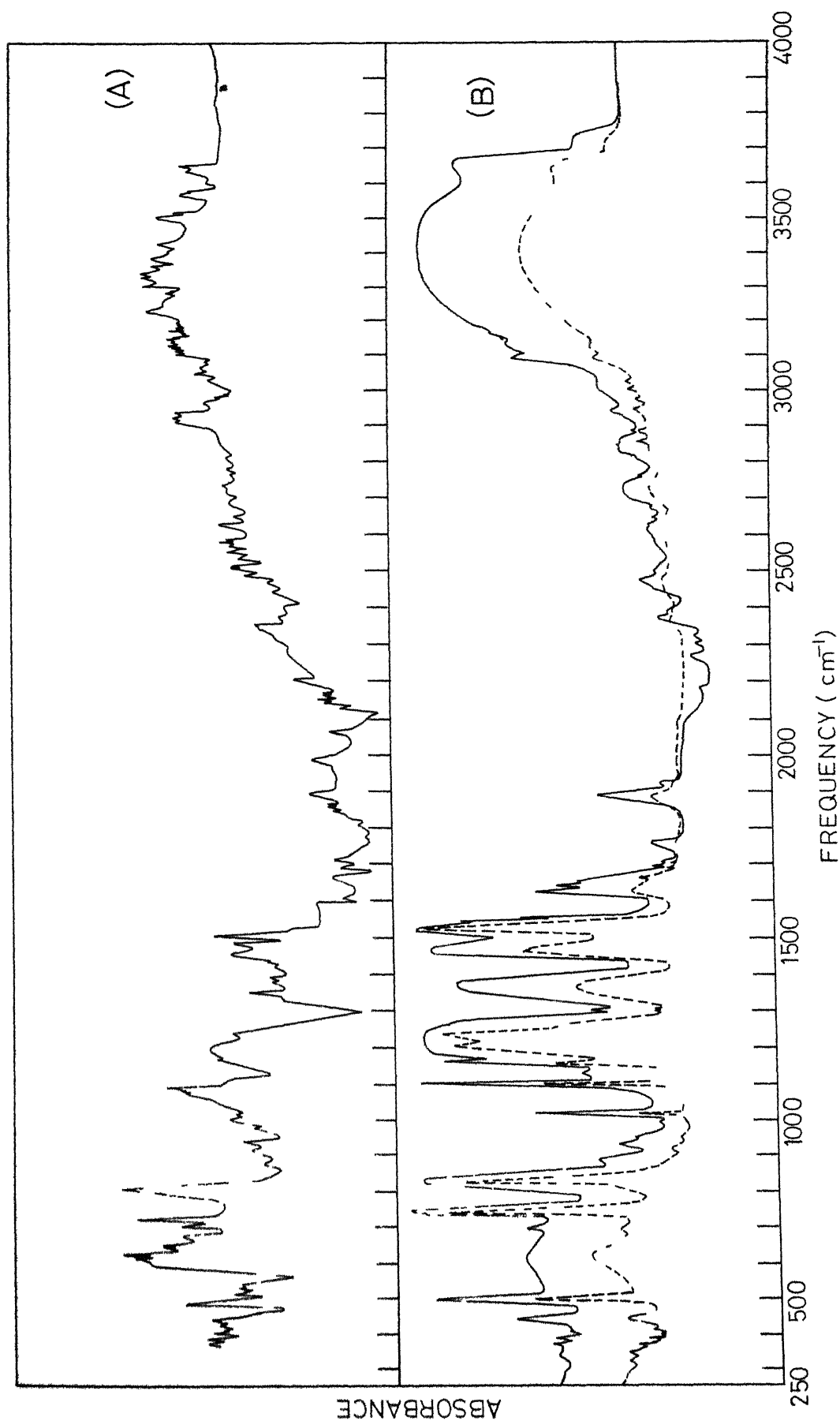


Fig 5 2 The infrared spectra of Para-Fluorophenol (A) at liquid nitrogen temperature (B) at room temperature with thin film denoted by ---- and thick film by —— using CsBr cells

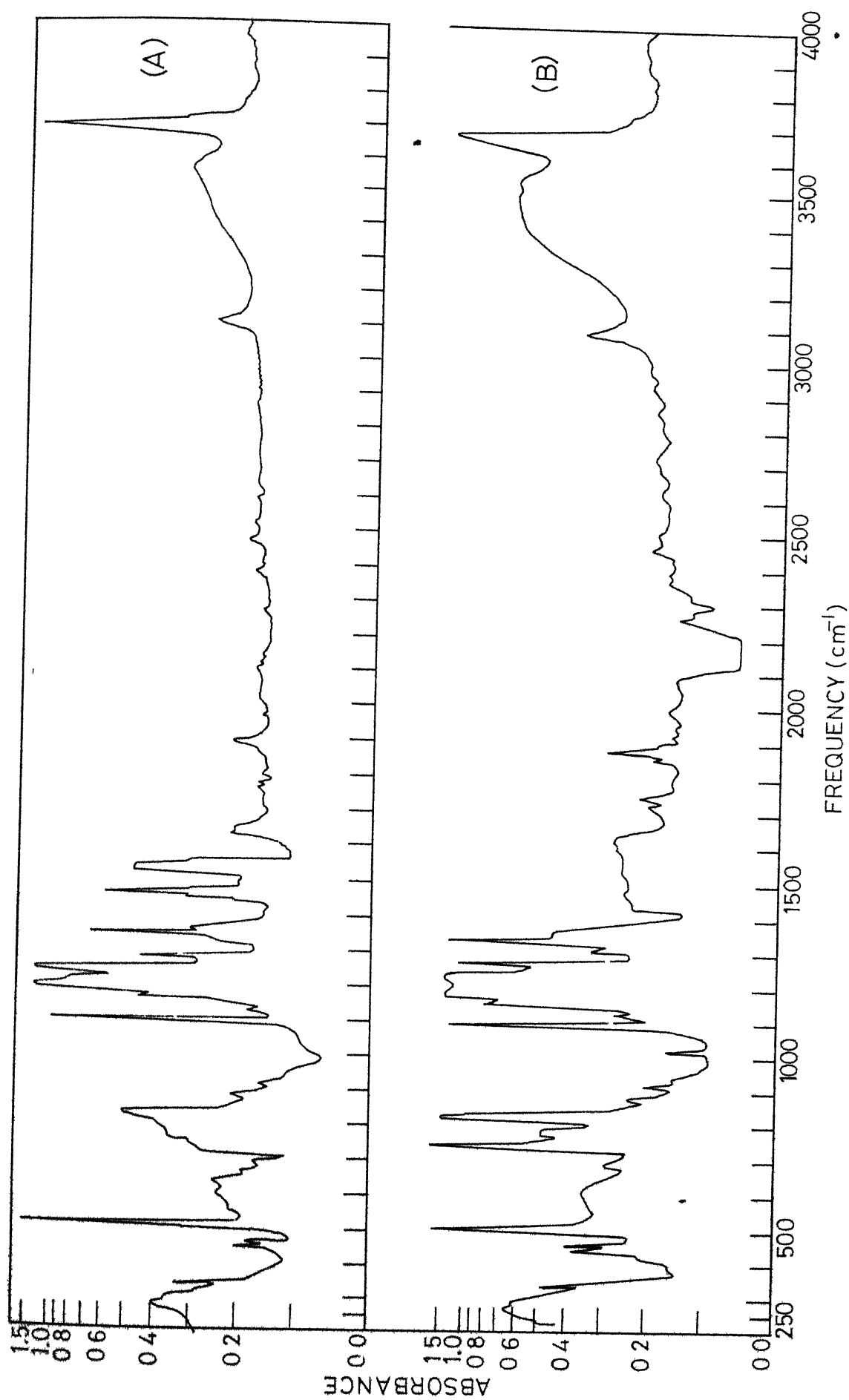
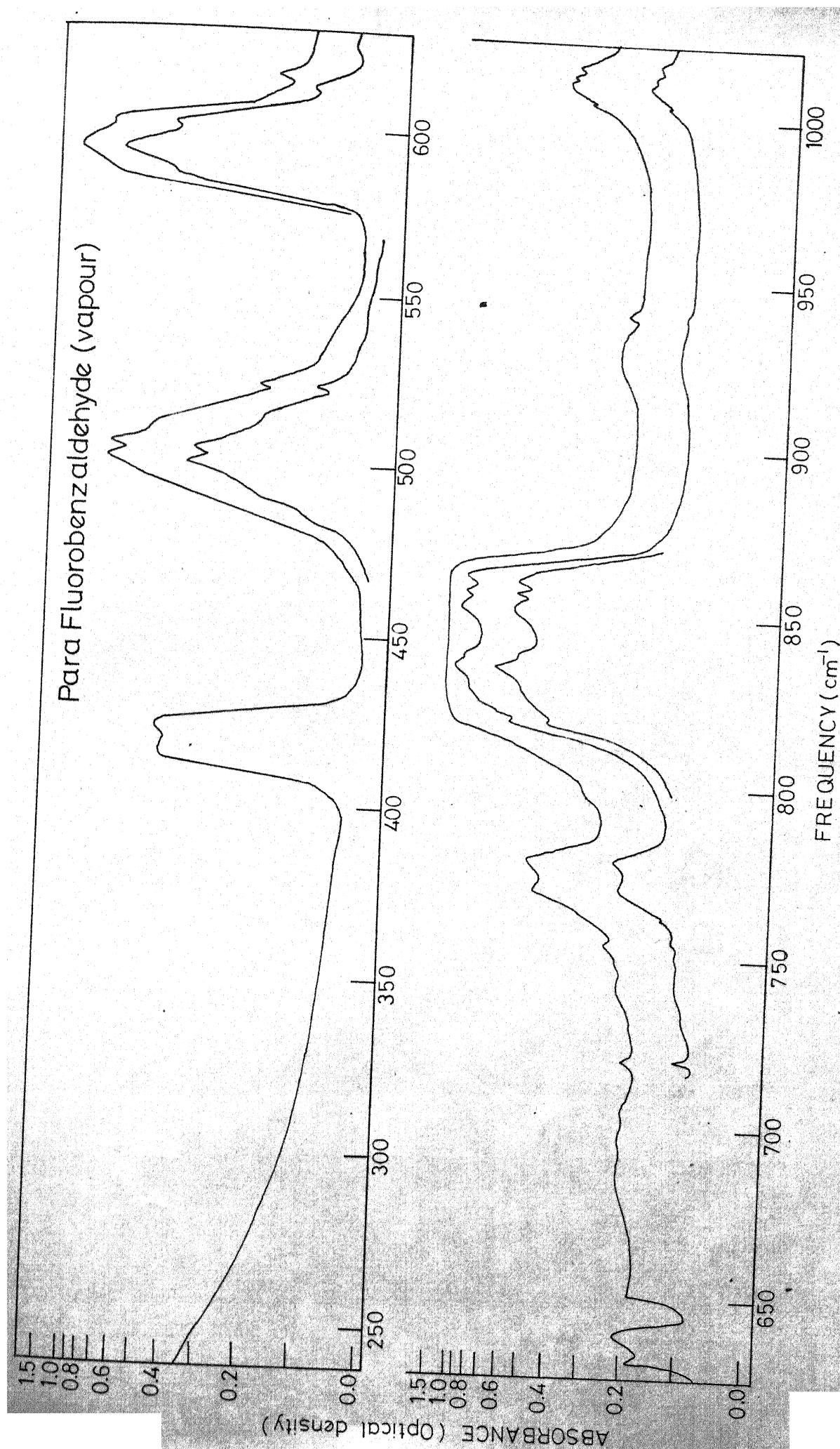
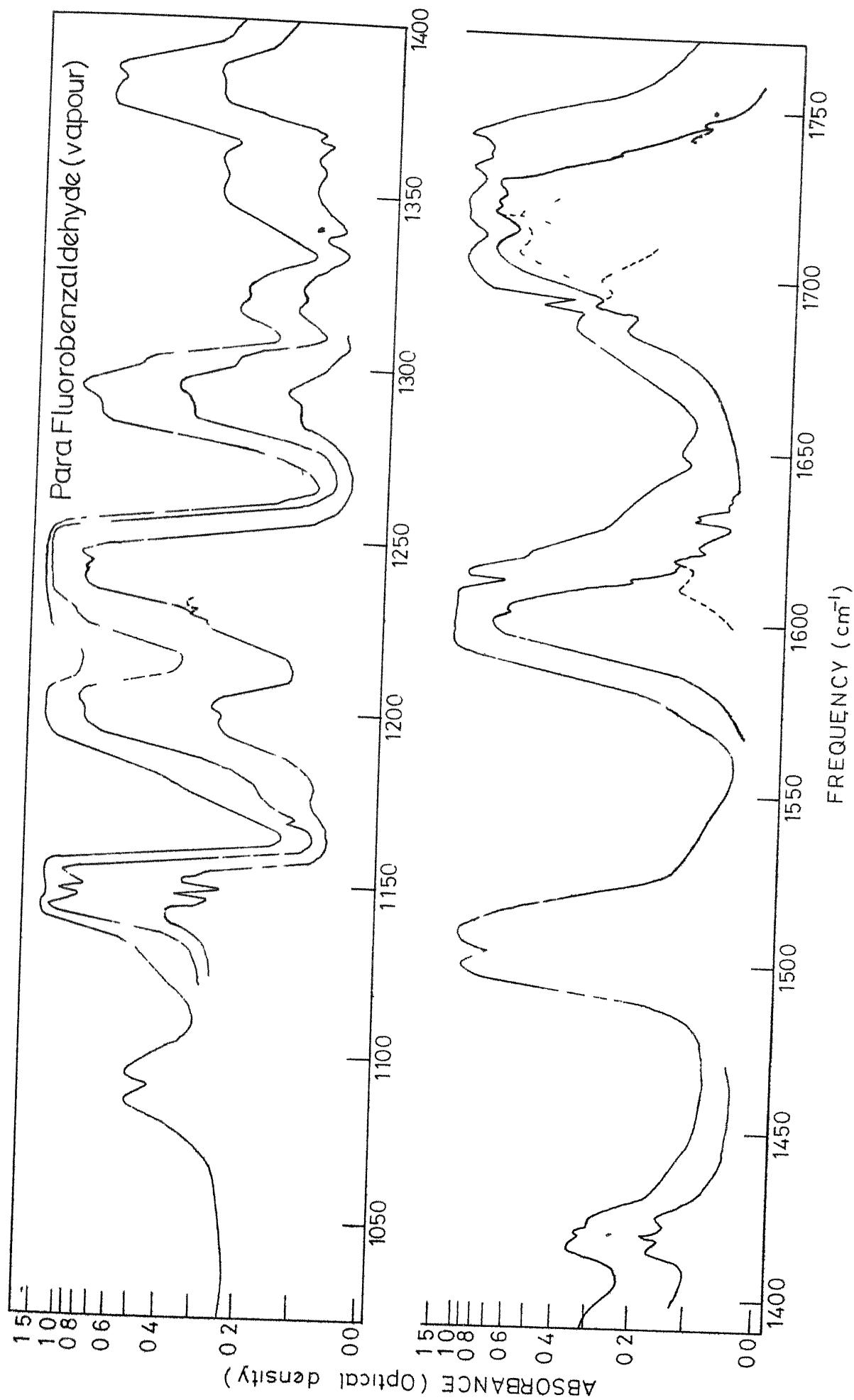


Fig 5 3 The infrared spectra of ParaFluorophenol (A) in  $\text{CCl}_4$  solution (B) in  $\text{CS}_2$  solution using 0.5 mm cell.





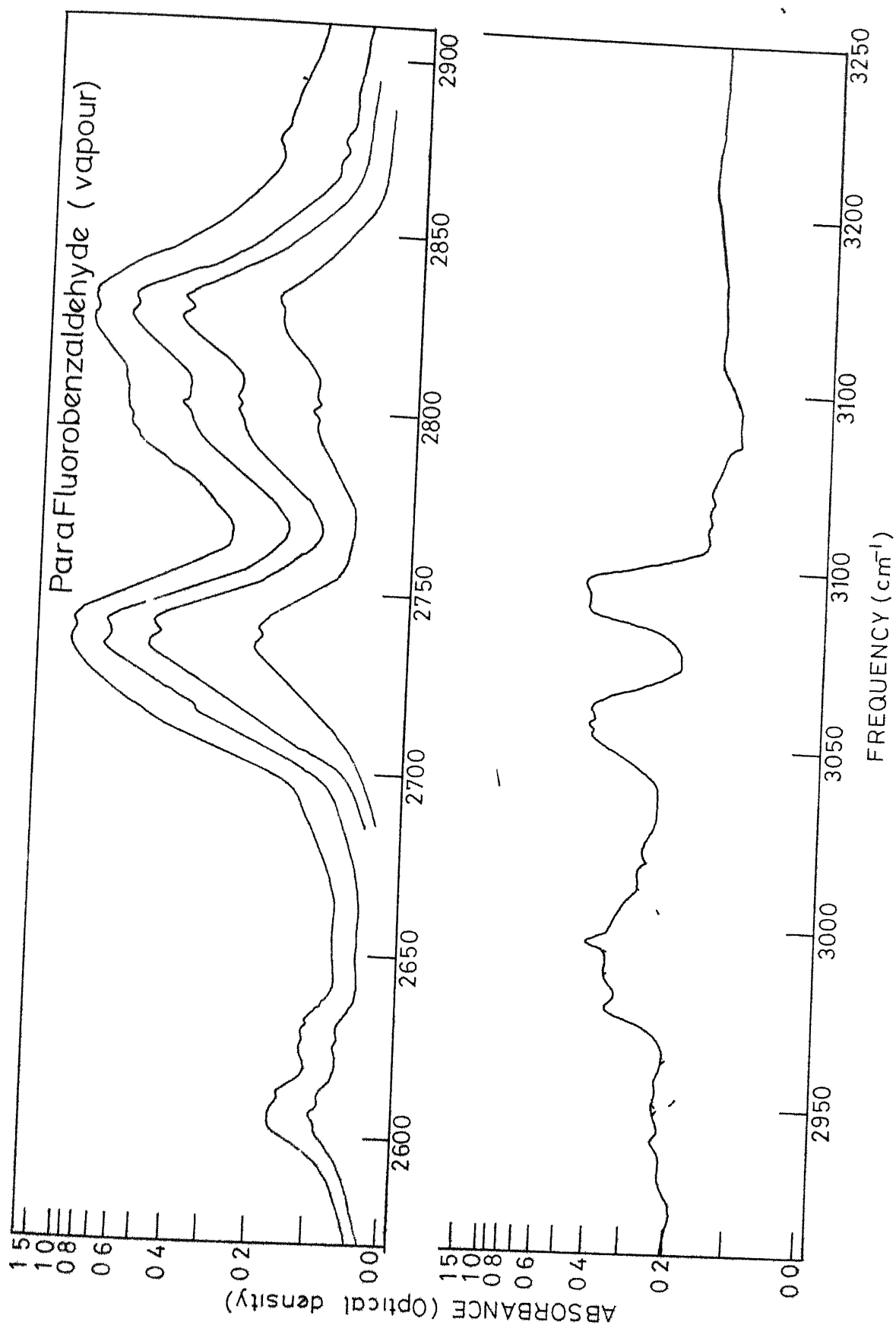


Fig 5 4 The infrared spectra of Para Fluorobenzaldehyde at low pressure and four meter path length

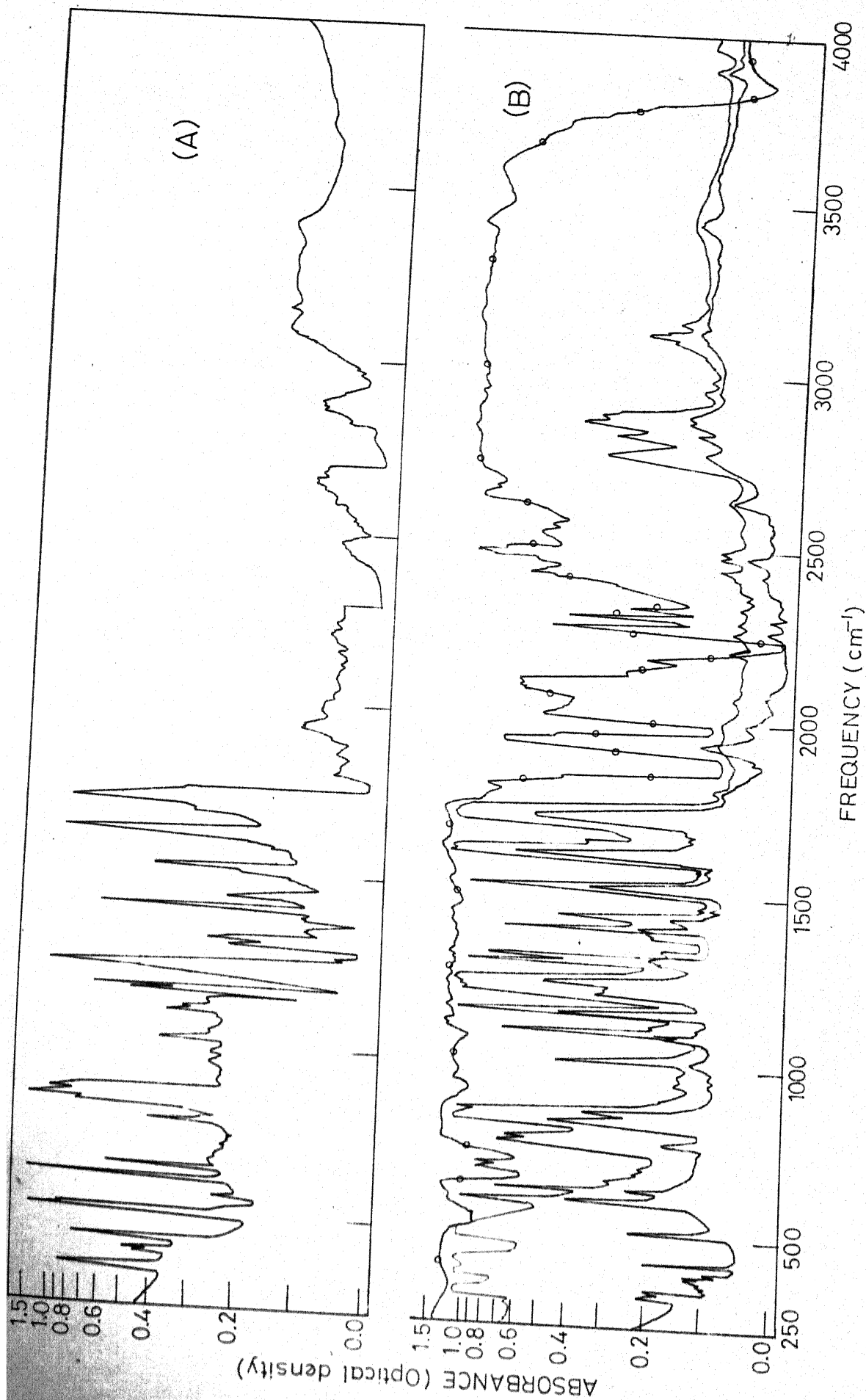


Fig. 5.5 The infrared spectra of ParaFluorobenzaldehyde (A) at liquid nitrogen temperature (B) at room temperature, using 0.5mm cell denoted by  $\bullet$ — $\bullet$  0.025mm and thin film by \_\_\_\_\_

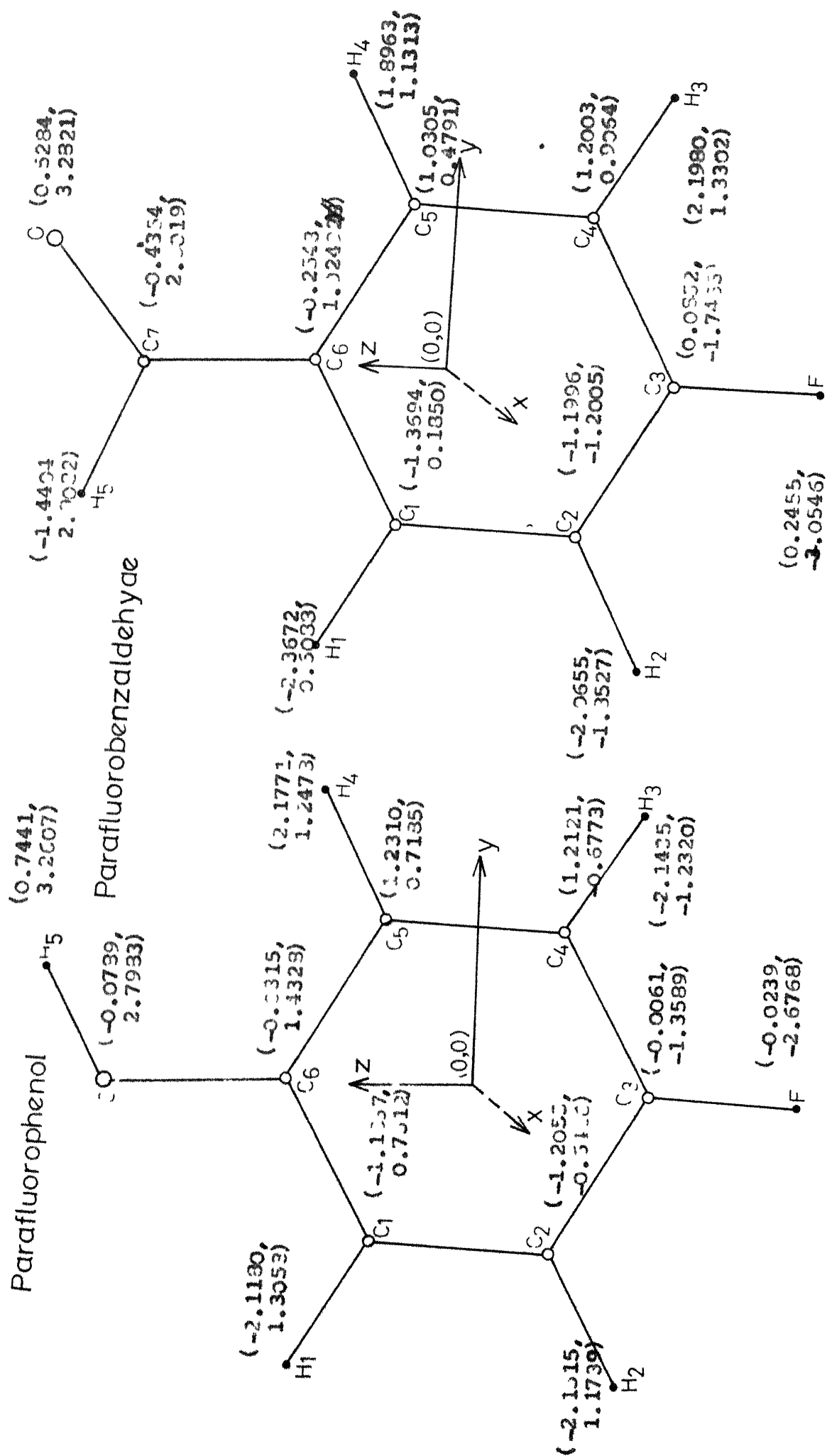


Fig 5 6 Vapour phase geometry of parafluorophenol and parafluorobenzaldehyde in ground state The number in parentheses denotes z, y coordinates (in Å units) of the atoms with respect to origin (0,0)



CHAPTER VITHE IDEAL GAS THERMODYNAMIC PROPERTIES OF  
CERTAIN POLYATOMIC MOLECULESABSTRACT

The vibrational vapour-phase frequencies and moments of inertia, discussed in Chapters III, IV and V have been used for computing the ideal gas thermodynamic properties of one mole gas of Pyridine N-oxide,  $\alpha$ -,  $\beta$ -, and  $\gamma$ -Picolines, Parafluorophenol and Parafluorobenzaldehyde at 1 atmosphere pressure in the temperature range 100-1500K for the first time.

## 6.0 INTRODUCTION

The ideal gas thermodynamic properties for Pyridine N-oxide,  $\alpha$ -,  $\beta$ -, and  $\gamma$ -Picolines, Parafluorophenol and Parafluorobenzaldehyde are not reported in the literature as yet. This is because of the non-availability of the complete vibrational frequencies and the molecular parameters for these molecules. As discussed in Chapters III, IV and V we now have the complete sets of fundamental frequencies and the molecular parameters for these molecules, hence it was possible to calculate the ideal gas thermodynamic properties for these molecules.

In this chapter, the ideal gas thermodynamic properties: Heat capacity at constant pressure ( $C_p^0$ ), entropy ( $S^0$ ), enthalpy ( $H^0 - H_0^0$ ), the Gibbs energy function  $[-(G^0 - H_0^0)/T]$  have been computed with great precision for above molecules. The enthalpy of formation ( $\Delta H_f^0$ ), Gibbs energy of formation ( $\Delta G_f^0$ ), and logarithm of equilibrium constant of formation ( $\log K_f$ ) for  $\alpha$ -,  $\beta$ -, and  $\gamma$ -Picolines have been evaluated. For this the statistical thermodynamic method based on a rigid rotor harmonic-oscillator approximation (1,2) has been employed. These properties are tabulated at temperatures from 100 to 1500K and at a pressure of one atmosphere. In these calculations most recent values of the fundamental constants (3) were used. The currently approved atomic weights used in these calculations

are carbon = 12.011, hydrogen = 1.008, fluorine = 18.9984, nitrogen = 14.0067, oxygen = 15.9994(4).

### 6.1 PYRIDINE N-OXIDE

Thermodynamics of Protonation of Pyridine N-oxide and its methyl substituted derivatives were measured spectrophotometrically by Klofular et al (5). However, the thermodynamic properties for Pyridine N-oxide vapour have been computed for the first time using (a) the precise vapour-phase fundamental frequencies (6,7) discussed in Chapter III (cf Appendix 6.1) (b) the three moments of inertia (8) (cf Appendix 6.2) and (c) the symmetry number one for overall rotation. The calculated values of thermodynamic properties are listed in Table 6.1.

### 6.2 $\alpha$ -, $\beta$ -, and $\gamma$ -PICOLINES

The thermodynamic properties of  $\alpha$ -,  $\beta$ -, and  $\gamma$ -Picoline have been computed for the first time. The quantities have been computed using (a) the precise vapour phase fundamental frequencies (cf Chapter IV, Appendix 6.1) (b) the three observed moments of inertia for  $\gamma$ -picoline (9) and computed moments of inertia for  $\alpha$ -, and  $\beta$ -picoline (cf Appendix 6.2), and (c) the symmetry number 'one' for overall rotation and 'three' for internal rotation. The contribution of the restricted rotation due to the presence of  $\text{CH}_3$ -group has been evaluated from the tables of Pitzer and Gwinn (10). The

enthalpy, the Gibbs energy and the equilibrium constant of formation from 100-1500K were calculated for  $\alpha$ -,  $\beta$ -, and  $\gamma$ -Picolines using the computed thermal functions and the enthalpies of formation at 298.15K from the literature (11).

$$\text{Hf}^\circ (\text{g}, \alpha\text{-picoline}) = 23.70 \text{ Kcal/mole}$$

$$\text{Hf}^\circ (\text{g}, \beta\text{-picoline}) = 25.42 \text{ Kcal/mole}$$

$$\text{Hf}^\circ (\text{g}, \gamma\text{-picoline}) = 24.41 \text{ Kcal/mole}$$

The enthalpy and Gibbs energy of C (12), H<sub>2</sub> (12) and N<sub>2</sub> (13) in their reference states were used.

The computed thermodynamic functions have been listed in Tables 6.2, 6.3 and 6.4 for  $\alpha$ -,  $\beta$ -, and  $\gamma$ -Picolines respectively.

### 6.3 PARAFLUOROPHENOL AND PARAFLUOROBENZALDEHYDE

The thermodynamic properties of Parafluorophenol and Parafluorobenzaldehyde have neither been determined experimentally nor computed from spectroscopic data in the past. These quantities have been evaluated for the first time using (a) the precise vapour phase fundamental frequencies discussed in Chapter V (cf Appendix 6.1) (b) the three computed moments of inertia using the correct geometry of the molecules (cf Appendix 6.2) and (c) the symmetry number 'one' for overall rotation and 'two' for internal rotation. The restricted rotational contributions due to OH and CHO group in Parafluorophenol and Parafluorobenzaldehyde respectively have been evaluated from the Tables of Pitzer and Gwinn (10). These computed thermodynamic properties have been listed in Table 6.5 and 6.6 for Parafluorophenol and Parafluorobenzaldehyde respectively.

TABLE 6.1

THE MOLAL THERMODYNAMIC PROPERTIES OF PYRIDINE N-OXIDE  
IN THE IDEAL GAS STATE

TEMP DEG. K	$C_p^\circ$	$S^\circ$	$-(G^\circ - H^\circ_O)/T$	$(H^\circ - H^\circ_O)$
		Cal/Deg. Mole		KCal/mole
0	0.0000	0.0000	0.0000	0.0000
100.00	9.251	56.640	8.376	0.826
150.00	11.577	60.796	51.844	1.343
200.00	14.783	64.548	54.554	1.999
273.15	20.312	69.959	57.954	3.279
298.15	22.267	71.822	59.039	3.811
300.00	22.412	71.960	59.118	3.853
400.00	29.772	79.440	63.264	6.470
500.00	35.862	86.763	67.236	9.763
600.00	40.680	93.745	71.078	13.600
700.00	44.502	100.314	74.790	17.866
800.00	47.593	106.465	78.370	22.476
900.00	50.136	112.222	81.815	27.367
1000.00	52.258	117.618	85.128	32.490
1100.00	54.046	122.685	88.314	37.807
1200.00	55.564	127.454	91.379	43.290
1300.00	56.861	131.954	94.329	48.913
1400.00	57.974	136.210	97.170	54.656
1500.00	58.935	140.243	99.908	60.502

TABLE 6.2

THE MOLAL THERMODYNAMIC PROPERTIES OF  $\alpha$ -PICOLINE IN THE  
IDEAL GAS STATE

TEMP Deg. K	$C_p^0$	$S^0$ Cal/Deg. Mole	$-(G^0-H^0)/T$	$\Delta H_f^0$ KCal/Mole	$\Delta G_f^0$	$\log K_f$
0	0.0000	0.0000	0.0000	28.583	28.583	Infinite
100.00	11.141	59.059	45.332	26.799	31.474	-58.73572
150.00	13.863	64.074	53.870	26.071	33.965	-49.48654
200.00	17.103	68.494	56.580	25.271	36.720	-40.12589
273.15	22.641	74.626	60.889	24.083	41.092	-32.37773
298.15	24.645	76.695	62.127	23.700	42.674	-37.28097
300.00	24.754	76.648	62.218	23.672	42.796	-31.17676
400.00	32.634	85.069	66.905	22.287	49.391	-26.98525
500.00	39.475	93.109	71.345	21.193	56.292	-24.60503
600.00	45.117	100.822	75.621	20.363	63.394	-23.09102
700.00	49.743	108.136	79.749	19.749	70.620	-22.04862
800.00	53.575	115.036	83.733	19.320	77.922	-21.28733
900.00	56.784	121.537	87.575	19.052	85.264	-20.70484
1000.00	59.494	127.664	91.281	18.939	92.660	-20.25074
1100.00	61.799	133.445	94.854	18.945	99.954	-19.85907
1200.00	63.767	138.909	98.300	19.029	107.375	-19.55553
1300.00	65.455	144.081	101.624	19.176	114.718	-19.28586
1400.00	66.908	148.987	104.833	19.380	122.130	-19.06527
1500.00	68.165	153.647	107.934	19.628	129.432	-18.83813

TABLE 6.3

THE MOLAL THERMODYNAMIC PROPERTIES OF  $\beta$ -PICOLINE IN THE IDEAL GAS STATE

Temp Deg. K	$C_p^\circ$	$C_p^\circ$ Cal/Deg Mole	$-(G^\circ - H^\circ_0)/T$	$(H^\circ - H^\circ_0)$ KCal/Mole	$\Delta H_f$ KCal/Mole	$\Delta G_f$	log K <sub>f</sub>
0	0.0000	0.0000	0.0000	0.0000	30.666	30.666	Infinite
100.00	11.243	75.220	50.190	0.909	28.484	33.135	-72.41937
150.00	14.079	64.362	54.092	1.541	27.764	35.615	-31.89032
200.00	17.319	63.846	57.228	2.324	26.975	38.354	-41.91129
273.15	22.775	75.032	61.173	3.786	25.800	42.698	-34.16260
298.15	24.755	77.112	62.422	4.480	25.420	44.270	-82.45053
300.00	24.902	77.266	62.513	4.425	25.392	44.390	-32.33836
400.00	32.680	85.509	67.234	7.310	24.015	50.943	-27.83397
500.00	39.495	93.555	71.698	10.929	22.923	57.799	-25.26390
600.00	45.129	101.271	75.989	15.169	22.095	64.856	-23.62376
700.00	49.754	108.587	80.129	19.921	21.482	72.038	-22.49120
800.00	53.586	115.488	84.121	25.093	21.054	79.295	-21.66225
900.00	56.797	121.991	87.971	30.617	20.788	86.591	-21.02709
1000.00	59.509	128.119	91.683	36.436	20.676	93.941	-20.53084
1100.00	61.815	133.902	95.261	42.506	20.683	101.191	-20.10464
1200.00	63.783	139.367	98.710	48.788	20.769	108.565	-19.77231
1300.00	65.471	144.541	102.039	55.253	20.918	115.863	-19.47825
1400.00	66.925	149.447	105.251	61.874	21.123	123.228	-19.23874
1500.00	68.181	154.109	108.354	58.531	21.373	130.484	-19.01144

TABLE 6.4

THE MOLAL THERMODYNAMIC PROPERTIES OF  $\gamma$ -PICOLINE IN THE IDEAL GAS STATE

Temp Deg. K	$C_P^\circ$	$S^\circ$ Cal/Deg Mole	$-(G^\circ - H_0^\circ)/T$	$(H^\circ - H_0^\circ)$	$\Delta H_f$ KCal/Mole	$\Delta G_f$	log K <sub>f</sub>
0	0.0000	0.0000	0.0000	0.0000	29.736	29.735	Infinite
100.00	11.565	56.581	49.938	0.864	27.509	32.232	-70.44227
150.00	13.550	63.433	53.647	1.468	26.762	34.751	-50.63269
200.00	17.157	67.830	56.649	2.236	25.958	37.540	-41.02165
273.15	22.361	74.020	60.475	3.700	24.784	41.958	-33.57108
298.15	25.045	76.120	61.698	4.300	24.410	43.556	-31.92701
300.00	25.200	76.276	61.788	4.346	24.383	43.673	-31.81939
400.00	33.333	84.655	66.459	7.371	33.054	50.320	-27.49520
500.00	40.404	92.877	70.924	10.976	22.041	57.256	-25.02653
600.00	45.193	100.774	75.247	15.316	21.313	64.372	-23.44739
700.00	50.388	108.260	79.433	20.179	20.810	71.595	-22.35286
800.00	54.729	115.314	83.482	25.466	20.496	78.877	-21.54800
900.00	57.908	121.959	87.391	31.102	20.343	86.183	-20.92312
1000.00	59.564	128.192	91.162	37.030	20.339	93.532	-20.44138
1100.00	62.802	134.072	94.798	43.201	20.449	100.769	-20.02088
1200.00	64.700	139.620	98.305	49.579	20.630	108.122	-19.69165
1300.00	66.318	144.865	101.686	56.132	20.867	115.391	-19.39893
1400.00	67.704	149.831	104.949	62.835	21.153	122.721	-19.15754
1500.00	68.898	154.544	108.100	69.666	21.478	129.936	-16.93184



TABLE 6.5

THE MOLAL THERMODYNAMIC PROPERTIES OF PARAFLUOROPHENOL  
IN THE IDEAL GAS STATE

Temp Deg. K	$C_p^0$	$S^0$	$-(G^0-H^0_o)/T$	$(H^0-H^0_o)$
		Cal/Deg Mole		KCal/Mole
0	0.0000	0.0000	0.0000	0.0000
100.00	9.634	59.703	51.420	0.828
150.00	13.048	64.220	54.946	1.391
200.00	17.097	68.519	57.803	2.143
273.15	23.341	74.769	61.510	3.622
208.15	17.784	69.216	58.236	2.285
300.00	25.611	77.063	62.799	4.279
400.00	33.442	85.531	67.427	7.242
500.00	39.900	93.714	71.873	10.921
600.00	45.019	101.460	76.165	15.177
700.00	49.082	108.716	80.303	19.889
800.00	52.357	115.492	84.283	24.967
900.00	55.045	121.818	88.106	30.341
1000.00	57.282	120.737	91.776	35.961
1100.00	59.165	133.288	95.300	41.786
1200.00	60.763	138.506	98.686	47.784
1300.00	62.128	143.425	101.940	53.931
1400.00	63.302	148.073	105.071	60.204
1500.00	64.316	152.476	108.085	66.586

TABLE 6.6

THE MOLAL THERMODYNAMIC PROPERTIES OF PRAFLUORO BENZALDEHYDE  
IN THE IDEAL GAS STATE

Temp Deg. K	$C_p^0$	$S^0$	$-(G^0 - H_0^0)/T$	$(H^0 - H_0^0)$
		Cal/Deg Mole		KCal/mole
0	0.0000	0.0000	0.0000	0.0000
100.00	11.954	62.760	53.268	0.949
150.00	15.141	68.189	57.362	1.624
200.00	18.871	73.045	60.683	2.472
273.15	24.911	79.809	64.904	4.071
208.15	19.520	73.811	61.182	2.629
300.00	27.168	82.249	66.347	4.771
400.00	35.120	91.178	71.445	7.893
500.00	41.850	99.762	76.256	11.753
600.00	47.296	107.892	80.858	16.220
700.00	51.682	115.524	85.271	21.177
800.00	55.247	122.666	89.504	26.529
900.00	58.178	129.348	93.564	32.205
1000.00	60.613	135.607	97.459	38.148
1100.00	62.653	141.483	101.197	44.315
1200.00	64.374	147.010	104.786	50.668
1300.00	65.836	152.222	108.237	57.181
1400.00	67.086	157.148	111.556	63.828
1500.00	68.160	161.814	114.753	70.592

APPENDIX 6.1VAPOUR PHASE FUNDAMENTAL VIBRATIONAL FREQUENCIES in  $\text{cm}^{-1}$ 

Mode	Pyridine N-oxide	$\alpha$ -Picoline	$\beta$ -Picoline	$\gamma$ -Picoline	PF Phenol	PF Benzal- dehyde
6a	540.3	545.5	534.0	513.0	523.0	523.0
12	842.8	735.0	751.0	801.0	748.5	855.0
1	1013.0	976.0	986.0	996.5	949.0	1002.0
18a	1044.8	1032.0	1049.0	1073.5	1169.0	1011.0
9a	1164.8	1147.5	1192.0	1192.0	1200.0	1147.0
7a	1303.0	1297.0	1230.0	1223.5	1263.0	1241.0
19a	1460.4	1477.0	1481.0	1498.0	1514.0	1420.0
8a	1609.3	1594.0	1601.5	1608.0	1610.0	1618.0
13	3045.0	-	-	-	1318.0 (vCF)	1228.5 (vCF)
2	3076.0	3024.0	3006.0	3002.0	3038.0	3059.0
20a	3099.0	3076.0	3069.0	3076.0	3092.0	3120.0
18b	469.3	358.0	340.0	376.0	395.0	329.0
6b	637.6	633.0	632.0	678.0	640.0	635.0
15	1068.5	1050.5	1030.5	1094.0	385.0 (vCF)	418.0 (vCF)
9b	1148.9	-	-	-	1086.0	1200.0
3	1184.5	1238.0	1243.0	1276.0	1292.0	1289.0
14	1244.1	1354.0	1340.0	1348.0	1338.0	1321.0
19b	1327.3	1435.0	1423.0	1420.0	1436.0	1503.0
8b	1595.3	1570.0	1583.0	1578.0	1592.0	1602.0
7b	3003.0	3024.0	3022.0	3039.0	3007.0	3018.0

contd

20b	3059	3094	3100	3072	3070	3092
11	230.5	213.0	218.0	219.0	280.0	329.0
16b	510.5	468.5	400.0	484.5	503	499.0
4	671.7	751.5	713.0	731.5	695.0	720.0
10b	758.5	797.0	785.5	796.5	754.0	754.0
17b	881.7	930.0	922.5	871.0	829.0	834.0
5	973.0	-	-	-	923.0	939.0
16a	415.0	401.0	418.0	388.0	435.0	381.0
10a	834.9	884.0	944.0	871.0	810.0	864.0
17a	989.6	930.0	1002.0	988.0	1015.0	970.0
$\alpha$ HCH( $a_1$ )	-	1382.0	1387.0	1381.0	-	-
$\nu$ CH( $a_1$ )	-	2940.0	2971.0	2938.0	-	-
$\alpha$ HCH( $b_2$ )	-	1103.0	1102.5	1108.0	-	-
$\alpha$ HCH( $b_2$ )	-	1453.0	1460.0	1458.0	-	-
$\nu$ CH( $b_2$ )	-	2968.0	2941.0	2967.0	-	-
$\gamma$ CH <sub>3</sub> ( $b_1$ )	-	1115.0	1060.0	1044.5	-	-
$\alpha$ HCH( $b_1$ )	-	1453.0	1460.0	1420.0	-	-
$\nu$ CH( $b_1$ )	-	2968.0	2941.0	2967.0	-	-
$\tau$ CH <sub>3</sub> ( $a_2$ )	-	125	125	125	-	-
$\beta$ OH	-	-	-	-	1231	-
$\nu$ OH	-	-	-	-	3650	-
CHO(rock)-	-	-	-	-	-	691.0
$\alpha$ HCO	-	-	-	-	-	1383.0
$\nu$ CO	-	-	-	-	-	1720.0
$\nu$ CH	-	-	-	-	-	2829.0
$\tau$ CHO	-	-	-	-	-	93.5
$\gamma$ CHO	-	-	-	-	-	592.0

APPENDIX 6.2ROTATIONAL CONSTANTS OF THE MOLECULES

	Pyridine N-oxide	$\alpha$ -Picoline	$\beta$ -Picoline	$\gamma$ -Picoline	Parafluoro- phneol	Parafluoro- to benzal- dehyde
$I_A$	85.661	83.913	89.711	83.117	89.524	99.189
$I_B$	180.840	174.129	187.068	200.222	348.738	519.944
$I_C$	266.512	255.245	274.030	283.370	438.262	619.133